Distribution Agreement

In presenting this thesis or dissertation as a partial fulfillment of the requirements for an advanced degree from Emory University, I hereby grant to Emory University and its agents the non-exclusive license to archive, make accessible, and display my thesis or dissertation in whole or in part in all forms of media, now or hereafter known, including display on the world wide web. I understand that I may select some access restrictions as part of the online submission of this thesis or dissertation. I retain all ownership rights to the copyright of the thesis or dissertation. I also retain the right to use in future works (such as articles or books) all or part of this thesis or dissertation.

Signature:

_____   _____
Jarred M Whitlock   Date

Anoctamin/TMEM16 Proteins in Lipid Scrambling and Membrane Signaling

1

By:

Jarred M Whitlock
Doctorate of Philosophy
Graduate Division of Biological and Biomedical Science
Biochemistry, Cell, and Development Biology

_____
H. Criss Hartzell, Jr., PhD
Advisor

_____
Guy Benian, PhD
Committee Member

_____
Victor Faundez, MD, PhD
Committee Member

_____
Michael H Koval, PhD
Committee Member

_____
Nael A McCarty, PhD
Committee Member

Accepted:

_____
Lisa A. Tedesco, Ph.D.
Dean of the James T. Laney School of Graduate Studies

_____
Date

Anoctamin/TMEM16 Proteins in Lipid Scrambling and Membrane Signaling

By

Jarred M. Whitlock
B.S., Anderson University, 2013

Advisor: H. Criss Hartzell, Jr, PhD

An abstract of
A dissertation submitted to the Faculty of the
James T. Laney School of Graduate Studies of Emory University
in partial fulfillment of the requirements for the degree of
Doctor of Philosophy.
in Graduate Division of Biological and Biomedical Science
Biochemistry, Cell, and Development Biology

2018

Abstract

Anoctamin/TMEM16 Proteins in Lipid Scrambling and Membrane Signaling
By Jarred M. Whitlock

The asymmetric organization of membrane lipids is a hallmark of the eukaryotic plasma membrane and is vital for proper cell function. This asymmetry arises from the organization of membrane lipids according to their headgroups via a system of membrane resident lipid transporters and typically results in an extracellular leaflet enriched in phosphatidylcholine and sphingomyelin and a cytosolic leaflet that retains phosphatidylethanolamine and phosphatidylserine. For >35 years it has been recognized that many cells possess the ability to rapidly break down this lipid asymmetry in a Ca^{2+}-dependent manner as a signaling process dubbed phospholipid scrambling. This membrane scrambling exposes cytosolic lipid headgroups (e.g. phosphatidylserine) to the extracellular face, where some are recognized as ligands in cell-cell signaling processes. Recently, members of the anoctamin family of membrane proteins have been recognized for their putative roles in this process. Here I summarize my contribution to the recognition of some anoctamin proteins as phospholipid scramblases, the understanding of how the structure of anoctamins facilitate lipid scrambling, and to the understanding of how anoctamin scramblases regulate biological processes.

Anoctamin/TMEM16 Proteins in Lipid Scrambling and Membrane Signaling

By

Jarred M Whitlock
B.S., Anderson University, 2013

Advisor: H. Criss Hartzell, Jr., PhD

A dissertation submitted to the Faculty of the
James T. Laney School of Graduate Studies of Emory University
in partial fulfillment of the requirements for the degree of
Doctor of Philosophy
in Graduate Division of Biological and Biomedical Science
Biochemistry, Cell, and Development Biology

2018

Table of Contents

Figure Index

11

Preface

The follow manuscript explores my dissertation work investigating the role of anoctamin/TMEM16 (ANO) proteins in the process of Ca^{2+}-dependent phospholipid scrambling (Ca^{2+}-PLS). Eukaryotic plasma membranes are made up of a phospholipid bilayer with an exofacial leaflet of membrane lipids enriched in phosphatidylcholine and sphingomyelin while the cytofacial leaflet is enriched in phosphatidylethanolamine and almost exclusively retains charged lipids like phosphatidylserine. Ca^{2+}-PLS scrambling is a process by which the asymmetric organization of plasma membrane lipids is lost, leading to the exposure of many lipid headgroups that are typically not exposed on the exofacial membrane. Exposure of cytosolic lipid headgroups to the extracellular environment functions as a means of cell-cell communication for the coordination of complex biological processes within tissues. The goal of my work has been to test the hypothesis that some ANO proteins act as Ca^{2+}-PLSases, and that this ANO function has biological consequences for cell function.

While testing the general hypothesis that some act as Ca^{2+}-PLSases, and that this ANO function has biological consequences, I have arrived at a number of discoveries that have significantly increased our understanding of ANO function and the role of Ca^{2+}-PLS in regulating cell processes. These discoveries include:

1. ANO5 and ANO6 elicit Ca^{2+}-PLS, while the Ca^{2+}-activated Cl^- channel ANO1 does not.

2. ANO5 and ANO6 possess a discrete domain necessary and sufficient for Ca^{2+}-PLS in ANO proteins.

3. ANO5 and ANO6 Ca^{2+}-PLS is associated with non-selective ionic conductance that is likely a consequence of lipid movement during phospholipid scrambling.

4. ANO5 is responsible for coordinating Ca^{2+}-PLS in muscle progenitor cells essential for proper skeletal muscle repair.

In my dissertation work I have focused primarily on the Ca^{2+}-PLS function of ANO5 and ANO6 and the role of ANO5-dependent Ca^{2+}-PLS in primary skeletal muscle repair. These two areas of focus address the role of ANO proteins as PLSases and the consequences of this activity in biologically relevant processes but have required different expertise and address different fields of study. In order to best represent this work, I would like to highlight the two areas of focus that are addressed in my dissertation. The first (Chapters I-IV) reviews the ANO literature and evaluates the function of ANO6 as a PLSase. The second section (Chapters V-VII) reviews the role of muscle progenitor cells and Ca^{2+}-PLS in skeletal muscle maintenance/repair and investigates the role of ANO5 in native skeletal muscle repair and Ca^{2+}-PLS. Chapters I-IV deal broadly with the function of ANO proteins and present work characterizing the function of ANO6. To introduce these topics, in Chapter I, I review the current state of the ANO literature. In Chapter II, I discuss the physiological role of Ca^{2+}-PLS in membrane signaling between cells and highlight evidence that some ANOs function as Ca^{2+}-PLSases. In Chapter III, I present a hypothesis for how ANO PLSases may have evolve to develop Ca^{2+}-activated Cl- channel function associated with ANO1. Finally in Chapter IV, I present my work supporting that ANO6 is a Ca^{2+}-PLSase, that the ion channel function of ANO6 is simply a consequence of PLS, and identifying a domain in ANO6 both essential for its PLSase function and sufficient to confer this activity to the Ca^{2+}-activated Cl- channel ANO1. This initial portion of my thesis supports the hypothesis that some ANO proteins function as Ca^{2+}-PLSases.

In Chapters V-VII, I address the role of Ca^{2+}-PLS in skeletal muscle maintenance/repair and present a role for ANO5-dependent Ca^{2+}-PLS in coordinating muscle progenitor cell fusion. In Chapter V, I review the role of active repair processes in the life-long maintenance of skeletal muscle and highlight how Ca^{2+}-PLS works to coordinate the fusion of mononucleated muscle progenitor cells to produce multinucleated muscle

fibers. In Chapter VI, I introduce a muscular dystrophy caused by mutations in *ANO5* and present work characterizing an Ano5 murine model we employed to study the physiological role of Ano5 in skeletal muscle. Moreover, in this chapter I also discover that the loss of Ano5 expression in primary murine progenitor cells results in perturbed fusion of these cells, producing muscle fibers with significantly reduced numbers of myonuclei. The efficient fusion of muscle progenitor cells is essential for proper muscle progenitor cell-dependent skeletal muscle repair. Finally in Chapter VII, I present my work in characterizing ANO5 Ca^{2+}-PLSase function and the role of ANO5 in coordinating the fusion of primary muscle progenitor cells by facilitating phosphatidylserine exposure during Ca^{2+}-PLS. This work demonstrates a novel role for ANO-dependent Ca^{2+}-PLS in regulating a physiologically relevant biologically process.

After presenting my work testing the hypothesis that some ANO proteins act as Ca^{2+}-PLSases, and that this ANO function has biological consequences for cell function, I conclude this dissertation by revisiting the aims and contributions of my thesis work.

Chapter 1

Anoctamins: A decade at light-speed.

It has been a decade since three independent groups identified Anoctamin 1 (ANO1) as a bona fide, Ca^{2+}-activated Cl^- channel (CaCC). In this time ANOs have been linked to a variety of human illnesses including: cancer, febrile seizures, ataxia, schizophrenia, bipolar disorder, muscular dystrophy, bone disease, and a bleeding disorder [1-8]. These diverse disease states affecting tissues throughout the body likely stem from perturbations in the many recognized ANO physiological roles such as: regulation of membrane excitability, olfactory transduction, smooth muscle tone, insulin secretion, nociception, coagulation, initiation of innate immune response, regulation of cell-cell fusion, and many others [9]. Here we review the ANO literature from the initial discovery to the current recognition of many ANOs as Ca^{2+}-activated phospholipid scramblases (Ca^{2+}-PLSases). The following chapter revisits early work exploring the role of ANO1 in malignancies, highlights seminal work identifying ANO1 and ANO2 as Ca^{2+}-activated Cl^- channels, and summarizes the body of work that has now established that many ANO proteins are Ca^{2+}-activated phospholipid scramblases (Ca^{2+}-PLSases).

ANO1/TMEM16A: FROM TUMOR FACTOR TO Cl^- CHANNEL.

ANO1 promotes cell proliferation and metastasis.

ANO1 was first recognized for its overexpression in malignancies long before it was functionally characterized. The initial description of ANO1, also TMEM16A (TransMEMbrane protein 16) (See Table 1), began when ANO1 was identified as a component of the 11q13 amplicon, a region of chromosome 11 frequently amplified in a variety of tumors [10, 11]. Since these early descriptions, ANO1 has been evaluated for its contribution to the development, progression, and metastasis of human cancers. ANO1 was found to be greatly over expressed in >80% of gastrointestinal stromal tumors, in head and neck squamous carcinomas, and in nearly 50% of oral squamous cell carcinomas [12-14]. Because of the significant upregulation and surface expression

19

of ANO1 in various cancers, antibodies were raised to the protein and are seen as diagnostic tools of choice for a variety of human cancers [12, 15-26]. Interestingly, although many other factors in the 11q13 amplicon have been recognized for their potential roles in driving the tumorigenesis, ANO1 overexpression in human carcinomas is also found independent of amplification of the 11q13 amplicon core [13]. This suggests that ANO1 may be sufficient to elicit some of the features of the malignancies associated with 11q13 amplification.

The role of ANO1 in cell proliferation

Despite its long history of association with cancers, the mechanistic role of ANO1 in these diseases remains unclear. ANO1 upregulation is associated with altered cell proliferation [27-29]. Loss of *Ano1* was associated with reduced proliferation in interstitial cells of Cajal *in vivo* (evaluated for their high, endogenous expression of *Ano1*) early in its physiological characterization. Moreover, generic Cl^- channel blockers' ability to suppress the proliferation of these cells supported ANO1's involvement in cell proliferation prior to the development of specific inhibitors [30]. Subsequently, *Ano1* knockdown has been found to reduce or eliminate growth in prostate, breast, and lung tumors [31-33]. Putatively, investigators have considered the channel activity of ANO1 responsible for its proliferative role in cancer cells, but few investigators have directly tested this hypothesis. Mazzone *et al.* treated interstitial cells of Cajal with $T16A_{inh}$-A01 (an ANO1 channel inhibitor) and demonstrated that CaCC currents and cell proliferation were significantly inhibited [29]. Others have demonstrated that ANO1 acts through the ERK signaling pathway to elicit its tumorigenic proliferation role, and that $T16A_{inh}$-A01 inhibits ERK signaling and proliferation *in vivo,*

HUGO Gene	Alternative Nomenclature
Anoctamin 1	TMEM16A, DOG1, *ORAOV2, TAOS2, FLJ10261*
Anoctamin 2	TMEM16B
Anoctamin 3	TMEM16C
Anoctamin 4	TMEM16D
Anoctamin 5	TMEM16E, GDD1
Anoctamin 6	TMEM16F
Anoctamin 7	TMEM16G, NGEP, *D-TMPP*
Anoctamin 8	TMEM16H
Anoctamin 9	TMEM16J
Anoctamin 10	TMEM16K

Table 1: Anoctamins are commonly described using diverse, non-official nomenclature. Alternative nomenclature of Anoctamins following HUGO recognized nomenclature. Italicized names represent historical nomenclature, non-italicized names are currently used in field-specific publications. (Primary effort on figure Whitlock, JM)

supporting ANO1 conductance's role in stimulating this pathway [34]. In contrast to data

strongly supporting the role of ANO1 ion conductance in regulating cell proliferation,

the Wasylyk group claim that ANO1 overexpression in HEp-2 cells alters cell migration

but does not affect proliferation [35]. However, proliferation was evaluated indirectly via

cell metabolism using a reagent that is known to be toxic to some epithelial cells-making

interpreting these data in the context of the body of work supporting the role of ANO1 in

regulating cell proliferation difficult [36]. Beyond the Wasylyk group, other lines of

investigation have produced conflicting conclusions concerning the effect of ANO1 on

cell proliferation (see Table 1 [37]), suggesting that ANO1's role in proliferation is quite

complicated and may not be consistent between tissues/cell types. However, the

consensus seems to be that ANO1 overexpression is associated with increased cell

proliferation.

ANO1 regulates embryonic development, potentially through its role in primary cilia.

ANO1 expression in murine development

ANO1 has continually piqued interest due to its association with tissue development. A

year prior to its characterization as a CaCC, ANO1 was identified in an unbiased screen

characterizing limb developmental regulation. Rock *et al*. sorted cells from the zone of

polarizing activity (ZPA), the developmental organizing center from which morphogenic

gradients regulate limb tissue development, and from other cells in embryonic murine

limb buds. Comparison of gene expression from these two cellular pools demonstrated

that ANO1 was overexpressed 40-fold in the ZPA as compared to the surrounding limb

bud [38]. Rock *et al.* went on to demonstrate that ANO1 is essential for pre- and

postnatal development of the limb and other tissues, and have highlighted the high

expression profiles of a number of ANO paralogs during embryonic and post-natal

development [39-42].

22

Loss of ANO1 expression results in perinatal lethality in mice. Rock *et al.* first demonstrated that ANO1 is an essential regulator of epithelial and smooth muscle organization, and that ANO1 knockout results in lethal tracheomalacia, or the pathological collapse of the upper airways [41]. More recently, these phenotypes have been associated with defects in the elongation of the primary cilium in this tissue [43].

ANO1 is associated with the primary cilium and ciliogenesis

Our lab demonstrated that ANO1 is essential for proper primary cilia formation [44] – a subcellular organelle that regulates embryonic tissue development. The primary cilium is a subcellular, organellular appendage that emanates from the apical surface of diverse cell types. The primary cilium is well recognized as a major regulator of embryonic, postnatal, and adult tissue development and morphology, akin to a sort of cellular antenna emitting and receiving diverse cellular signals (reviewed [45]). Ruppersburg and Hartzell demonstrated that ANO1 occupies an annular structure enriched in many ciliary proteins that is both spatially and temporally associated with the initial development of the primary cilium (i.e. ciliogenesis) [44]. Knock-down of ANO1 or inhibition of its CaCC current severely inhibits ciliogenesis resulting in both a diminished fraction of ciliated cells and retarded length [44].

In our initial discovery of ANO1's link to ciliogenesis, Ruppersburg suggested that ANO1 function might set cytoplasmic Cl^- homeostasis that regulated some vital step in the development of this organelle. Recently, the Jan laboratory has presented data supporting this hypothesis. This group demonstrates that Cl^- alterations elicit PM remodeling essential for epithelial morphogenesis, a potential mechanism for the role of ANO1 in regulating tissue development [43]. Moreover, this membrane remodeling, tied to cytoplasmic Cl^- levels regulated by ANO1, may play some role in supporting the early stages of ciliogenesis [43].

ANO1 is far from the only ANO homolog associated with proper tissue development. Loss of *Ano6* leads to the reduction of skeleton size and causes skeletal abnormalities [46]. These defects are thought to be the result of perturbed bone mineralization caused by defects in osteoclast function, however, the overall mechanism behind the functional role of ANO6 in this process is unclear. Although non-essential for embryonic/postnatal development, ANO5 is cited for its roles in proper sperm maturation and adult muscle regeneration [47, 48]. Many other ANOs' are expressed during development [40], however their requirement and functions during these processes remain to be determined.

ANO1 and ANO2 are bona fide CaCCs.

Shortly following the initial discovery of ANO1's link to various malignancies and pre/postnatal development, ANO1 and ANO2 were identified as functional CaCCs [49-51]. Many cell types including: neurons; many epithelial cells; olfactory and photo-receptors; cardiac, smooth, and skeletal muscle; Sertoli cells; mast cells; neutrophils; lymphocytes; brown fat adipocytes; hepatocytes; insulin-secreting beta cells; mammary, salivary, and sweat glands; *Vicia faba* guard cells; and *Xenopus* oocytes exhibit Cl^- currents when stimulated by increased intracellular $[Ca^{2+}]$ (reviewed [52]). These Ca^{2+}-activated Cl^- currents ($I_{Cl.Ca}$) were first described in *Xenopus* oocytes and *Axolotl* solitary rod inner segments within the retina [53-55]. The biophysical characteristics of the classical $I_{Cl.Ca}$ observed in *Xenopus*, *Axolotl*, and many mammalian secretory epithelial cells were well defined during the 26 years between description of the classical $I_{Cl.Ca}$ and the identification of the ANO/TMEM16 family members as the CaCCs responsible for this $I_{Cl.Ca}$.

Review of classical $I_{Cl.Ca}$ biophysical characteristics

For the sake of illustration, assuming the intracellular $[Cl^-]$ is ~10-fold lower than the interstitial soundings the equilibrium potential of Cl^- (E_{cl}) will be quite negative. The

24

resting membrane potential of many cells is also negative. So when active, I_{Cl} is directed outside of these cells, which in-turn depolarizes the plasma membrane (PM). In this sort of system, classical $I_{Cl \cdot Ca}$ has a variety of biophysical characteristics, but perhaps 6 main attributes define it: 1) $I_{Cl \cdot Ca}$ is activated by at $[Ca^{2+}]$ around 0.1-5μM; 2) at low $[Ca^{2+}]$ (<0.6 μM) $I_{Cl \cdot Ca}$ is strongly outwardly rectifying, but at higher $[Ca^{2+}]$ (>1 µM) $I_{Cl \cdot Ca}$ has a linear current:voltage relationship (I/V); 3) at significantly high $[Ca^{2+}]$ (>10 μM) $I_{Cl \cdot Ca}$ is actually inhibited by Ca^{2+} and runs down with time; 4) $I_{Cl \cdot Ca}$ is a Cl^- selective channel, but its Cl^- selectivity over Na^+ is fairly weak compared to typical cation channels ($I_{Cl \cdot Ca}$ is ~10-fold more selective for Cl^- vs Na^+, or P_{na}/P_{cl}= 0.1); 5) $I_{Cl \cdot Ca}$ exhibits a characteristic selectivity for anions in the sequence of $SCN^- > NO_3^- > I^- > BR^- > Cl^- > F^-$; and 6) $I_{Cl \cdot Ca}$ is inhibited by the non-selective Cl^- inhibitors niflumic acid (NFA) and 4,4'-diisothiocyanato-stilvene-2/2'-disulfonic acid (DIDS), among others.

Discovery of ANO CaCC function

In 2008 three independent groups converged on the discovery that ANO1 was the CaCC responsible for classical $I_{Cl \cdot Ca}$ [49-51]. Each group used complementary methods for elucidating the identity of the elusive CaCC. The Galietta group took advantage of their previous discovery that long-term treatment of bronchial epithelial cells with interleukin-4 strongly increases $I_{Cl \cdot Ca}$ [56]. This group evaluated upregulated mRNA coding putative membrane proteins with unknown functions via RNAi, and identified hANO1 as the CaCC upregulated in the system [49]. Employing expression cloning in *Axolotl* oocytes, which lack native $I_{Cl \cdot Ca}$ and regularly exhibit polyspermy [57], the Jan group employed expression cloning to evaluate a *Xenopus* oocyte cDNA library and identified xANO1 and further characterized mANO1 and mANO2 as CaCC subunits [50]. Finally, the Oh group identified mANO1 via directed *in silico* searches for uncharacterized transmembrane proteins and characterized the protein via many biophysical approaches

[51]. All efforts demonstrated that ANO1 was most likely a CaCC, but most the

convincing biophysical demonstration that ANO1 was in fact responsible for classical

$I_{Cl \cdot Ca}$ came from the Oh group. Beyond demonstrating that ANO1 is activated by

increased intracellular Ca^{2+} and exhibits Cl^- selectivity, Yang *et al.* found that ANO1

current is: 1) outwardly rectifying at nM $[Ca^{2+}]$, 2) displays a linear *I/V* at low μM $[Ca^{2+}]$,

and 3) is inhibited by >10μM $[Ca^{2+}]$; 4) ANO1 is Cl^- selective, where $P_{Na}/P_{Cl} = 0.03$; 5)

ANO1 current exhibits a relative monovalent anion selectivity of $NO_3^- > I^- > Br^- > Cl^- > F^-$;

and 6) ANO1 is strongly inhibited by both NFA and DIDS. These findings fulfilled all the

biophysical and pharmacological attributes of $I_{Cl \cdot Ca}$ discussed above. In addition, the Oh

group demonstrated that mutation of charged residues in the putative ANO1 pore alters

its Cl^- selectivity >30-fold, many murine tissues with strong endogenous classical $I_{Cl \cdot Ca}$

stained positively with a novel ANO1 antibody, and finally, *Ano1* siRNA injection strongly

inhibits salivary secretion, a physiological process driven by classical $I_{Cl \cdot Ca}$ in acinar cells

of the salivary glands. Many candidates were propose as the CaCC responsible for $I_{Cl \cdot Ca}$

before the identification of ANO1 (reviewed extensively [52, 58]), but ANO1 was

demonstrated, unequivocally as the CaCC responsible for classical $I_{Cl \cdot Ca}$.

ANOs are homodimers with two independent conduction pathways.

Like most ion channels [59], it was quickly demonstrated that ANO1 exhibits oligomeric

organization. Our lab and others have demonstrated–using a variety of biochemical and

live cell FRET-based approaches–that ANO1 forms a homodimer [60, 61]. Moreover,

recent scanning transmission electron microscopy investigation of ANO1 oligomerization

has demonstrated that ANO1 exists exclusively as a dimer within the PM of intact cells

[62]. Whether each subunit of the ANO1 dimer contained an independent pore or the two

formed a common conduction pathway remained an open question for some time.

Recently the Chen and Dutzler groups both demonstrated that ANO1 subunits contain

26

independent ion conducting pores, which activate independently by direct Ca^{2+} binding

and exhibit distinct biophysical characteristics [63, 64]. ANO2 and ANO6, in addition to

more distant ANO homologs Ist2, afTMEM16, and nhTMEM16, also exhibit dimerization

[65-68]. Based on the sequence similarity within the ANO family, it is likely that all full

length ANOs form dimers, however this assumption remains to be tested empirically.

Early biochemical investigations of ANO1 and ANO2 and a crystal structure of the fungal

scramblase nhTMEM16 suggested a role for the cytosolic termini in ANO protein

dimerization [68, 69]. Recently several independent high resolution structures of mANO1

dimers have been solved [70-72]. These mANO1 structures demonstrate unequivocally

that ANO1 dimerizes exclusively via contact sites within TMD10 (transmembrane

domain 10). However, the resolution of TMD10 precludes precise assignment of the

residues responsible for dimerization. ANO1's sole reliance on TMD10 differs from the

contribution of contact sites observed between the N- and C-termini of nhTMEM16

subunits in addition to contact along TMD10. The discrepancies in how ANO1 and

nhTMEM16 dimerize put forth an important question: do differences in how ANOs

dimerize have functional consequences?

First hints some ANOs are not CaCCs.

Quickly after the identification of ANO1 and ANO2, many questioned whether the other 8

mammalian ANOs might also function as CaCCs or perhaps Cl- channels activated by

other stimuli [58, 73, 74]. Just over a year after the identification of ANO1 and ANO2 as

CaCCs, Schreiber *et al.* claimed that all ANOs traffick to the PM, and several

demonstrated classical I_{Cl-Ca} exogenously expressed. Despite these claims the

investigators did not present data evaluating the trafficking of ANO3, ANO4, and ANO8.

More concerning, ANOs (besides 1 and 2) appeared predominantly–if not entirely–

cytoplasmic in the data presented. Additionally, the investigators found significant CaCC

activity for a short, 192aa, isoform of ANO7 that completely lacks TMDs, making the

27

data presented difficult to evaluate [75]. In our lab, ANOs 3-7 did not exhibit $I_{Cl.Ca}$, and

ANOs 3-7 and 10 did not obviously traffic to the PM when exogenously expressed in

several different cell lines [76]. Several other groups have reported similar observations.

Improvements in expression and characterization in other cell models have led to

progress in the elucidation of the function of several ANOs. ANO3 has since been

described as a β-subunit of the Na^+-activated K^+ channel, SLACK [77]. The *S.*

cerevisiae, IST2, has been characterized as a major PM/ER tethering factor, responsible

for regulating the cortical ER in yeast [78, 79]. Recently, many ANO proteins were found

to be Ca^{2+}-dependent phospholipid scramblases (Ca-PLSases) or to at least support this

activity in cells (reviewed [80]). In fact, more ANOs are now associated with Ca^{2+}-

dependent phospholipid scrambling than are CaCCs. The only additional ANO

homologue found to function as a CaCC is *D. melanogaster's* Subdued, which

biophysically exhibits a number of classical $I_{Cl.Ca}$ hallmarks [81]. In the decade following

the flurry of excitement around the identification as the ANOs as the long sought after

CaCCs, one thing has become abundantly clear–most ANOs are not CaCCs.

Most ANOs may elicit Ca^{2+}-dependent phospholipid scrambling (Ca^{2+}-PLS), not Cl^- conductance.

Lipid Bilayers: From oily coat, to asymmetric lipid bilayer.

Over 100 years ago Charles Overton suggested that cells should be defined by a "fatty

oil" boundary [82]. Pioneering work by Gorter and Grendel in the 1920s demonstrated

that the PM is a semi-permeable membrane created by a closely juxtaposed lipid bilayer

[83]. Nearly 50 years passed before the discovery that each side of most eukaryotic

bilayers is unique, with a specially segregated lipid repertoire [84], and around this same

period Singer and Nicolson elevated our thinking of the solvent-like properties of cellular

delimitations [85]. Despite the many advances in characterizing the makeup, physical

characteristics, and signaling properties of membranes over the last 50 years, many major questions concerning the dynamic signaling processes in native bilayers remain. Below we discuss recent advances in the understanding of bidirectional lipid mixing at the PM and how this process functions as a means of cell-cell communication, regulating a variety of biological processes.

PM lipid organization

Due to its increased accessibility, the PM is the best characterized eukaryotic membrane. In its simplest conceptualization, the PM is ~30 Å thick cellular delimitation with barrier properties similar to a thin layer of liquid hydrocarbon [86, 87]. The PM of eukaryotic cells is enriched in cholesterol and consists of an exofacial/extracellular leaflet rich in neutral lipid species [e.g. phosphatidylcholine (PC) and sphingolipids (SLs)] and a cytofacial/cytoplasmic leaflet enriched in diverse minor lipid species [e.g. phosphoinositides (PIPs), phosphatidylethanolamine (PE), and phosphatidylserine (PS)] that play many regulatory roles within the cell (reviewed [88]). Most intracellular membranes are more poorly characterized, but it is generally accepted that they exhibit an inverted organization compared to the PM, with PIPs, PE, and PS enriched in the cytoplasmic face–while PC and SLs are enriched in the luminal face. The post-ER organization of lipid asymmetry is thought to be maintained in order to preserve bilayer organization along the secretory pathway. This organization allows membrane cargo to exchange along the secretory pathway without altering the sidedness of the lipids at receiving membranes. One notable exception to this general organization is the ER, which exhibits a nearly symmetrical lipid bilayer due to constitutive lipid mixing via a process that remains to be elucidated [89].

The asymmetry of the PM is a vital hallmark of eukaryotic cells with a cytofacial leaflet that retains many charged lipid species (e.g. PIPs and PS) that play important roles in regulating the activity of many PM associated proteins. Membrane lipids themselves

exhibit a near inability to exchange between membrane leaflets due to their amphiphilic

design ($T_{1/2}$ = hours to days [90]). By virtue of the hydrophobic effect, the hydrophilic

head groups of lipids orient toward the polar environments of the extracellular face and

the cytosol, leaving the hydrophobic fatty acid tails to form a barrier within the bilayer

core. This hydrophobic core is highly resistant to the movement of polar/charged

molecules creating an energy barrier for the spontaneous movement of lipid

headgroups. Therefore, membrane asymmetry is created by a tightly regulated network

of ATP-dependent transporters that flip and flop lipids along hydrophilic clefts that

facilitate the movement of polar lipid headgroups through the membrane's hydrophobic

core[91]. The precise orientation of the lipids on the exo- or cytofacial leaflet is

determined by the selectivity of this transporter network that functions to set the

asymmetric orientation of the membrane. Flippases are a family of type IV P-type

ATPases that translocate lipid headgroups toward the cytosol. Floppases orient lipid

head groups away from the cytosol. Despite the enormous amount of energy expended

to maintain basal membrane asymmetry, many cells retain the ability to completely mix,

or "scramble" their PMs in a matter of minutes.

Phospholipid scrambling (PLS): a dynamic cell-cell signaling phenomenon.

The loss of PM lipid asymmetry occurs via a dynamic signaling process known as PLS.

Eukaryotic cells exhibit two separate pathways that elicit the complete loss of lipid

asymmetry–resulting in a symmetric lipid distribution at the PM [7, 92]. These membrane

scrambling pathways consist of a caspase-dependent pathway that is nearly ubiquitous

in cells and facilitates the removal of apoptotic cells [93, 94] and a Ca^{2+}-dependent

pathway employed in specialized cell-cell signaling processes [7, 95]. Although the rate

of lipid movement is probably identical in both pathways following PLSase activation

[92], generally the effective rate (from initial stimulation to activation of the PLSase) of

30

apoptotic scrambling is much slower (hours) than ligand stimulated Ca^{2+}-dependent scrambling (minutes). This likely stems from the multiple rate limiting steps involved in intrinsic apoptotic signaling [e.g. apoptotic induction, transcriptional regulation, release of cytochrome c, caspase cleavage cascade, etc.] [96-98].

There are a variety of biophysical consequences to the loss of membrane asymmetry, one of which is the exofacial exposure of many cytofacial lipids the cell has worked agonizingly to restrict from the exofacial surface of the PM. The headgroups of some of these lipids–namely PS and PE–are readily recognized by a range of effectors. These effectors–both membrane bound and soluble–recognize headgroup exposure as a ligand that initiates a host of downstream responses from the cell to system levels (reviewed [80]). A classic example of this scrambling initiated signaling process is the assembly of clotting factors for the efficient conversion of prothrombin to thrombin during the coagulation response. During hemostasis, the endothelial lining of the circulatory system is breached so that the circulating cells and factors are exposed to collagen matrix and tissue factor within the subendothelial layer. Collagen and tissue factor act as ligands that rapidly (mins) stimulate Ca^{2+}-activated phospholipid scrambling (Ca^{2+}-PLS), exposing PS exofacially. Exofacial PS acts as an assembly platform for the prothrombinase complex and results in a roughly 150,000-fold enhancement of conversion of prothrombin to thrombin (reviewed Lentz 2003). This burst of thrombin activates platelets and fibrin to build a clot, rapidly plugging the site of injury. Robust Ca^{2+}-PLS is essential for proper hemostasis following a breach of the circulatory system, as loss of Ca^{2+}-PLS results in the congenital bleeding disorder Scott's syndrome [99].

Ca^{2+}-PLS: A common membrane signaling phenomenon lacking a molecular identity.

Prior to 2010, several candidates for the molecular identity of the putative Ca^{2+}-PLS were proposed, but none truly fit the bill of a PLSase. In 2010, Suzuki *et al.* identified

31

ANO6 as an elicitor of Ca^{2+}-PLS in an unbiased expression screen. This group

accomplished this task by successively sorting a small population of cells that exhibited

high Ca^{2+}-PLS while slowly lowering the level of Ca^{2+} stimulation applied to the cells.

This resulted in a cell line that exhibited Ca^{2+}-PLS activated by native cytosolic Ca^{2+}

concentrations. By employing expression cloning utilizing the parental cell line with

minimal Ca^{2+}-PLS activity, Suzuki and colleagues identified that the increased activity

from the sorted cells was confered by ANO6. Moreover, they demonstrated that a

mutation in *ANO6* segregated with the inheritance of Scott's syndrome, a bleeding

disorder resulting from a loss of Ca^{2+}-PLS activity in patient platelets [7]. Shortly after,

two *Ano6* KO murine models were created, and cells from these animals exhibited

significantly perturbed Ca^{2+}-PLS [100, 101]. These initial descriptions of ANO elicitation

of Ca^{2+}-PLS have led to the intense, recent investigation of the ANO protein family for its

role in Ca^{2+}-PLS.

ANO scramblases

Many ANO proteins are now recognized as PLSases, however the empirical data

supporting the Ca^{2+}-PLS role of these ANOs varies. The initial identification of ANO6's

ability to activate PLS in Ba/F3 cells highlighted ANO6 as a PLSase candidate [7]. The

loss of ANO6 in Scott's syndrome patients elevated this candidacy [102-104], as the

extremely rare bleeding disorder has long been held as a Ca^{2+}-PLS model [105]. Others

have suggested that ANO6 is simply a cation channel that regulates an unidentified

PLSase and that exogenous ANO6 itself cannot confer Ca^{2+}-PLS [100]. We found that

not only can exogenous ANO6 confer Ca^{2+}-PLS, but also that ANO6-dependent Ca^{2+}-

PLS and ion conductance occur simultaneously [106]. Moreover, the ANO6-associated

ionic current is very non-selective (P_{Na}/P_{Cl}=1.6). These data suggest that ANO6-

dependent ionic current is simply a consequence of the disturbance of membrane

integrity associated with Ca^{2+}-PLS. Additionally, we found that just 34 amino acids from

32

ANO6 could confer Ca^{2+}-PLS competence to ANO1, despite the absence of the remainder of the ANO6 protein [106]. This gain of function in ANO1 conferred by this small insertion demonstrates that ANO6 does not simply upregulate an unidentified PLSase. Unfortunately, ANO6 has not been purified at this time, precluding reconstitution experiments to definitively demonstrate ANO6's PLSase sufficiency. In lieu of purified ANO6, two fungal ANO homologs, afTMEM16 and nhTMEM16, have both been purified, reconstituted in liposomes, and are sufficient to scramble diverse lipid species [66, 68].

Ca^{2+}-PLS is associated with simultaneous development of ion conductance that is a consequence of PLS. ANO6, afTMEM16, and nhTMEM16 exhibit PLS-associated ionic conductance that develops along with lipid movement [66, 107]. Like ANO6 currents, fungal PLS-associated currents exhibit nearly non-selective among monovalent ions. Taken together these data strongly support the hypothesis that some ANOs are Ca^{2+}-PLSases, and that PLS-associated ion conductance is a consequence rather than a regulator of PLS.

Curiously, both reconstituted afTMEM16 and nhTMEM16 exhibit a basal PLSase activity in the absence of Ca^{2+} stimulation [66, 68]. Since both proteins were purified in the presence of mM Ca^{2+}, one could dismiss this basal activity as an artifact of the purification process. However, basal ANO PLSase activity may carry some biological relevance that is yet unrealized. One would not immediately expect to detect basal PLS in cells because of the rapid activity of the PM flippase network. Flippases, which are responsible for restricting PS to cytosolic facing leaflets, do not work against PLS following Ca^{2+} stimulation because they are inhibited by increased intracellular Ca^{2+} (e.g. as little as 20 μM) (Bitbol 87). However, inhibition of PS flippases is not sufficient for lipid scrambling, as spontaneous exposure of PS occurs on the order of hours to days [108].

Perhaps Ca^{2+}-independent PLS of ANO homologs will be evaluated in the future by purifying and evaluating ANOs with mutations precluding Ca^{2+} binding.

Currently more ANO homologs are linked to Ca^{2+}-PLS than to Cl^- conductance. As mentioned above, ANO6 along with two fungal ANO homologs function as Ca^{2+}-PLSases. Murine ANOs 2, 3, 7, and 9 were found to rescue the Ca^{2+}-PLS competence of a ANO6 knock-out cell line [93]. Although, none of these ANOs have been evaluated for their sufficiency to confer Ca^{2+}-PLS to cell lines with nominal, endogenous Ca^{2+}-PLS. ANOH-1, an ANO homolog in *C. elegans*, was recently found to regulate PS exposure in cells within that organism, however this link is currently a simple observation and highlights the need for further evaluation of ANOH-1 function [109]. DdTMEM16, an ANO homolog from *D. discoideum*, was found to confer Ca^{2+}-PLS to HEK293 cells [110]. *Amoebozoa* diverged from metazoans long before fungi, making the scrambling DdTMEM16 the most evolutionarily divergent ANO evaluated to date. Additionally, we recently demonstrated the Ca^{2+}-PLS activity of ANO5 (Under Revision). Moreover, we find that loss of *Ano5* perturbs Ca^{2+}-PLS dependent PS exposure required for skeletal muscle fusion. The ever-growing list of scrambling ANOs strongly suggests that the CaCC ANO subgroup represents a more recently developed role for a small subset of the family.

The general mechanism of ANO PLS

Despite their recent discovery, much has been learned in the last few years concerning the mechanism by which ANO scramblases ferry lipid headgroups across the PM. PLS at the PM happens in a rapid, ATP-independent, bi-directional manner and appears to facilitate the movement of all phospholipids examined to date [95]. Early models predicted PLS preceded along a membrane exposed, hydrophilic cleft that would allow for the rapid diffusion of headgroups between leaflets in an unbiased manner, while the hydrophobic tails remained buried in the membrane core [111]. In the simplest

description, this is how flippases and floppases transport lipids, although specific

interactions between the lipid headgroups and the transporter at the entrance site of the

cleft determines the selectivity of these transporters [112]. Moreover, the hydrolysis of

ATP facilitates the opening and closing of gates at both entrances of the pathway-

producing directionality in the system and driving head groups against their

concentration gradients [113]. Similarly, ANO scramblases facilitate lipid exchange

between leaflets along a hydrophilic cleft–the aqueduct–,but they appear to do so with

the absence of a selectivity module or alternating gates. Therefore, the lipid transporter

network harnesses the hydrolysis of ATP to organize lipids against their concentration

gradients within the PM, effectively "charging" a sort of oily battery. The opening of this

pathway allows for lipid headgroups to diffuse along the ANO aqueduct, harnessing the

energy built into the membrane via the concentration gradient of headgroups exhausting

this oily battery-all while avoiding the extreme energy penalty of removing the fatty acid

tails of lipids from their preferred, hydrophobic environment.

Atomistic molecular dynamics simulations have elucidated the basic mechanism by

which lipids traverse the ANO aqueduct. Typically, the hydrophilic core of membrane

proteins is thought to occupy a space similar to the width of the lipid bilayer (~30 Å),

however it appears that ANO proteins thin the PM along their hydrophobic interface to a

minimum at the PLSase aqueduct (Fig. 1). In the case of nhTMEM16, simulations

predict that the minimal path between leaflets is actually offset with either leaflet

minimum at the complementary opening of the nhTMEM16 aqueduct creating a minimal

bilayer headgroup distance of ~18 Å along the aqueduct [114]. This distortion of the

membrane when combined with the hydrophilic nature of the aqueduct lowers the

energy barrier for lipid exchange between leaflets from >50 Kcal/mol (spontaneous

flipping of PC) to an estimate of ~ 1 Kcal/mol [114]. Our lab evaluated the occupancy of

the nhTMEM16 aqueduct by lipids in molecular dynamics simulations and found that in

35

lieu of a true "lipid binding site", the aqueduct contains three points where the lipids spend the majority of their time. Additionally, the headgroups of lipids are coordinated by a variety of electrostatic interactions via aqueduct residues at these sites [115]. These sites are spread along the aqueduct, with one at the cytosolic opening (S_{int}), one near the extracellular opening (S_{ext}), and one at the center of the aqueduct (S_{Cnt}). Our lab hypothesized that these sites help to coordinate the movement of headgroups along the aqueduct in the single file pattern observed in these simulations. Using structure function analysis, our lab not only demonstrated that critical residues at these aqueduct sites were essential for nhTMEM16 PLS, but also demonstrated that the corresponding residues were essential for TMEM16F PLS and sufficient to confer PLS activity to ANO1 with a single point mutation [115]. Perhaps the most interesting of these sites is S_{int}. Much of S_{int} is contributed by residues analogous to the region of TMDs 4 and 5 within the SCRD (scrambling domain) we identified in ANO6 previously [106]. This SCRD is highly divergent between PLS ANOs and CaCC ANOs, as discussed previously. Additionally, this site is aligned in the z-plane with one of the bound Ca^{2+} ions activating nhTMEM16. A critical residue in S_{int} that interacts electrostatically with lipid headgroups in our simulations, R505 (TM7), rests between two negatively charged residues responsible for coordinating that Ca^{2+} (E506 and D503) [115]. Removing the charge of this residue greatly reduced the PLS-dependent exposure of PS (R505Q). These findings further highlight the importance of the ANO SCRD in Ca^{2+}-PLS and suggest that R505 and the aqueduct S_{int} where it resides may play essential roles in the Ca^{2+}-activation of ANO PLSases.

Conclusion

Much has been elucidated concerning ANO function over the decade following the designation of ANO1 and ANO2 as CaCCs, but many recent findings have produced novel, complicated questions concerning the biological roles of ANO family proteins. A

36
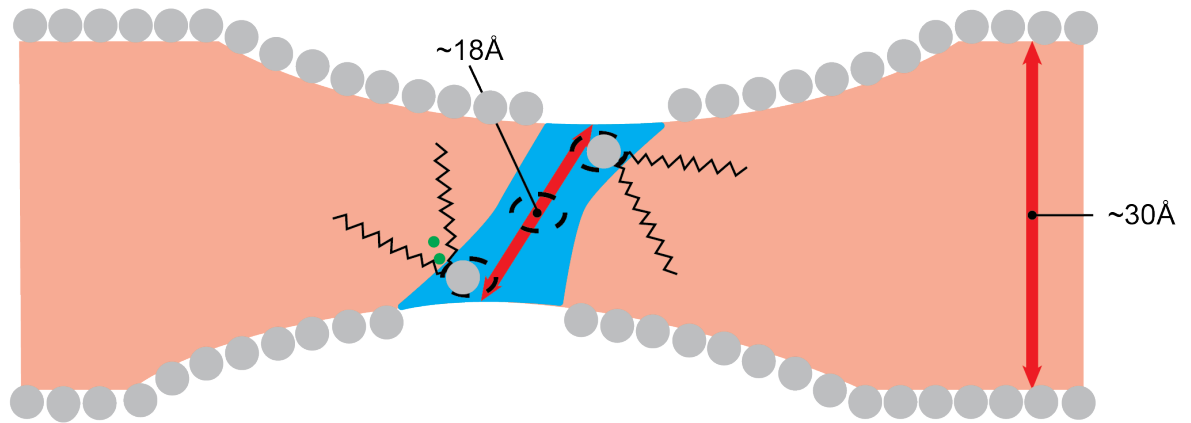
Figure 1: ANO PLSases thin membranes and create an energetically feasible pathway for lipid scrambling. Cartoon depiction of molecular dynamics and structural data from nhTMEM16. Blue denotes the hydrophilic nhTMEM16 aqueduct, peach represents the hydrophobic membrane core, grey spheres symbolize the headgroups of various membrane lipids, and green spheres depict where Ca^{2+} is expected if bound to the ANO protein. (Primary effort on figure Whitlock, JM)

quick check of ANO expression profiles using data from common repositories demonstrates that most cells/tissues express several ANO proteins [116, 117]. Despite the many advances in the understanding of ANO biology in the last decade, the consequence of the expression of multiple ANOs within the same cell is still completely unknown. To this point, ANO1 and ANO2 can heterodimerize, while ANO1 and ANO6 do not [69]. In the future it will be important to characterize fully which ANOs can heterooligomerize, as this may have major consequences for their functions and explain the diversity of ANO proteins in a given cell.

Perhaps the evaluation of the physiological consequences of ANO heterooligomerization will lead to the elucidation of a second outstanding question-what is the purpose of PLSase diversity within cells? We have demonstrated that ANO5 and ANO6 elicit Ca^{2+}-PLS and are both highly expressed in skeletal muscle (Under Revision). Loss of ANO5 appears to significantly perturb Ca^{2+}-PLS, despite the high expression of ANO6 in the same cell. These findings seem to suggest that although ANO elicitors of Ca^{2+}-PLS may have similar roles, they are not functionally redundant. Understanding the precise cellular roles of diverse ANO PLSases and how these roles might be divided or shared between multiple ANO PLSases expressed in the same cells are important aims to study as ANOs speed into their second decade of prominence.

Finally, ANO Ca^{2+}-PLS seems to be commonly associated with non-selective ionic current. Although all evidence points to these currents being a consequence of PLS, this does not discount the potential for ANO PLS-associated ionic current to contribute to modulating PLS or play a regulatory role in other physiological processes associated with Ca^{2+}-PLS. Understanding the roles of these currents will be an important future goal, however the inability to separate these two functions makes this a challenging task.

Chapter 2

Anoctamins/TMEM16 Proteins: Chloride channels flirting with lipids and extracellular vesicles

Prelude to "Anoctamins/TMEM16 Proteins: Chloride Channels Flirting with

Lipids and Extracellular Vesicles."

Much of my contribution to the anoctamin/TMEM16 field has focused on elucidating how ANOs elicit Ca^{2+}-PLS and characterizing how this ANO-associated membrane signaling process regulates biological function. In the following review Criss and I discuss the current mechanistic understanding of how phospholipid scramblases (PLSases) elicit loss of plasma membrane lipid asymmetry and the data that support that some ANO homologs function as Ca^{2+}-PLSases. Additionally, we briefly review the cellular functions associated with Ca^{2+}-PLS including: PLS-associated ion transport, alterations in membrane biophysical characteristics, exposure of intracellular leaflet lipids and the receptors in neighboring cells that recognize them, the scaffolding function of exposed anionic lipids, the production of extracellular vesicles as a means of cell-cell signaling, and the role of PLS in membrane fusion.

Summary

Anoctamin/TMEM16 proteins exhibit diverse functions in cells throughout the body and are implicated in several human diseases. Although the founding members ANO1 (TMEM16A) and ANO2 (TMEM16B) are Ca^{2+}-activated Cl^- channels, most ANO paralogs are Ca^{2+}-dependent phospholipid scramblases that serve as channels facilitating the movement (scrambling) of phospholipids between leaflets of the membrane bilayer. Phospholipid scrambling significantly alters the physical properties of the membrane and its landscape and has vast downstream signaling consequences. In particular, phosphatidylserine exposed on the external leaflet of the plasma membrane functions as a ligand for receptors vital for cell-cell communication. A major consequence of Ca^{2+}-dependent scrambling is the release of extracellular vesicles that function as intercellular messengers by delivering signaling proteins and noncoding RNAs to alter target cell function. We discuss the physiological implications of Ca^{2+}-dependent phospholipid scrambling, the extracellular vesicles associated with this activity, and the roles of ANOs in these processes.

41

Introduction

The uncertainty that abounded in the field of Ca^{2+}-activated Cl^- channels (CaCCs) 10 years ago was encapsulated in a review titled, "Calcium-activated chloride channels: (un)known, (un)loved?" [52, 118]. The mood in the field changed dramatically in 2008 when it was shown unambiguously that Anoctamin-1 (ANO1) [also known as transmembrane protein 16A (TMEM16A)] and ANO2 (TMEM16B) encode CaCCs [49-51]. Since 2008, there have been nearly 400 papers published on ANO1/TMEM16A, and it has become apparent that these two founding members of the family have functions as diverse as the tissues in which they are expressed. Classical functions of ANO1 and ANO2 include roles in membrane excitability in the nervous system and cardiac muscle, olfactory transduction, smooth muscle tone in blood vessels and other tissues, gut myoepithelial cell contractility, and phototransduction. In addition, ANO1 functions have recently expanded to include novel roles in cancer, hearing, primary ciliogenesis, insulin secretion, inhibitory neurotransmission, and nociception. Unexpectedly, the field has been upended by the discovery that many, maybe most, ANO paralogs are not Cl^- channels but are phospholipid scramblases, a type of lipid transporter.

CaCC: Ca^{2+}-activated Cl^- channel

ANO: anoctamin or TMEM16

Because the ANO literature has been well reviewed [119-125], we have chosen to focus on one narrow aspect of the field. We believe that the key to understanding all of the ANOs, both Cl^- channels and lipid transporters, is dependent on understanding the relationships of ANOs with lipids. We develop the idea that ANO-dependent phospholipid scrambling (PLS) alters the biophysical properties of the plasma membrane (PM) in a way that favors both membrane fusion and fission events that play important roles in cellular physiology.

PLS: phospholipid scrambling

PM: plasma membrane

MOST ANOCTAMINS ARE PHOSPHOLIPID SCRAMBLASES, NOT CHLORIDE CHANNELS

The ANO family is widely expressed in eukaryotes, and many ANOs are linked to human disease (Figure 1). ANOs are most highly represented in the Chordates, where each species typically has 10 ANO paralogs, although fish may have 12. Nonchordate species generally have fewer ANO genes, with fungi and plants often having only one or two, whereas Caenorhabditis elegans has two, and Drosophila has five ANO genes [122, 126].

When ANO1 and ANO2 were first discovered to be CaCCs, it was expected that all ANOs would encode Cl^- channels because of their high sequence similarity. Comparing only transmembrane domains (TMDs), the sequence identity of mouse ANO1 is 82% to ANO2, 51--59% to ANOs3 through 7, 46% to ANO9, and 25% to ANO8 and ANO10. However, when expressed in HEK cells, most of the other ANOs unexpectedly either did not produce Cl^- currents and/or did not traffic to the PM [75, 76]. The puzzle was solved in 2010 when the Nagata lab discovered that ANO6 is essential for Ca^{2+}-dependent PLS (Ca^{2+}-PLS) [7]. Mutations in ANO6 are linked to a congenital bleeding disorder stemming from perturbed Ca^{2+}-PLS in both humans (Scott syndrome) [7] and dogs [103]. Disruption of Ano6 in mouse phenocopies Scott syndrome and perturbs Ca^{2+}-PLS in cells isolated from these animals [7, 100, 127, 128]. Subsequently, it has been shown that ANOs 3, 4, 5, 6, 7, and 9 are also linked to Ca^{2+}-PLS [47, 129]. If at first the proposal that some ANOs are scramblases was greeted with some reservation, the

43

a

Ascomycetes

IST2

afTMEM16   nhTMEM16

Basidiomycetes

Streptophytes

Invertebrate
ANO5

CG6938

ANO2   ANO1

Invertebrate
ANO1

CG10353

SUBDUED

AXS

ANO10

ANO7

ANO3

ANO4

CG15270

anoh-2

ANO8

anoh-1

ANO6

ANO5   ANO9

0.13

Annelid
Arthropod
Ascomycete
Basidiomycete
Chordate
Cnidaria
Echinoderm
Mollusc
Nematode
Platyhelminth
Porifera
Streptophyte

b

ANO3
Febrile seizures

ANO10
Ataxia

ANO2
Olfactory function

ANO4
Schizophrenia?
Bipolar disorder?

ANO1
Cancers
Respiratory and
gut development

ANO5
LGMD2L
GDD1
Infertility

ANO6
Scott syndrome
Bone mineralization

ANO7
Prostate biomarker

Figure 1 Anoctamins are diverse and cause human disease. (*a*) The anoctamin

protein family tree, with branches colored according to phylum. Chordate ANO1--

10 are colored in two shades of green to differentiate between adjacent families.

Individual ANOs of note are labeled: *Caenorhabditis elegans* anoh-1 and anoh-

2; *Drosophila* SUBDUED, AXS, CG10352, CG6938, CG15270; fungal

nhTMEM16 and afTMEM16; and yeast IST2. The tree was generated as follows:

4,131 anoctamin protein sequences were obtained from Uniprot. After removing

duplicates, fragments, sequences lacking the initial methionine, sequences <600

amino acids, and sequences having sequencing or assembling errors, 1,066

sequences remained. One species was chosen to represent each phylogenetic

order, leaving 392 sequences. These were aligned using MUSCLE with 16

iterations. The N and C termini were then deleted to leave only the predicted

transmembrane domains TMD1--TMD10 with 50--100 flanking amino acids.

Phylogenetic trees were constructed using a neighbor-joining Kimura protein

algorithm in CLC Main workbench 7.7. (*b*) An illustration of tissues in which

anoctamins have been associated with disease. Human diseases resulting from

ANO mutations are in red, and abnormalities resulting from disruption of the ANO

gene in murine models are in blue. (Primary effort on figure: (a) Hartzell, HC; (b)

Whitlock, JM)

uncertainty was abandoned when fungal ANO homologs were purified and shown to mediate Ca^{2+}-PLS when reconstituted into liposomes [66, 68]. These fungal homologs have ~25% sequence identity to human ANOs in their TMDs, their transmembrane topology closely matches that predicted for the human ANOs, and the residues that coordinate Ca^{2+} are highly conserved. Despite the founding members of the ANO family being Cl^- channels, to date only ANO1 and ANO2 have been shown unambiguously to be CaCCs.

Ca^{2+}-PLS: Ca^{2+}-dependent phospholipid scrambling

TMDs: transmembrane domains

PHOSPHOLIPID SCRAMBLING IS A UBIQUITOUS CELLULAR SIGNALING MECHANISM

Phospholipids Are Organized Asymmetrically in the Plasma Membrane

Cell membranes are a 5--10 nm-thick layer of proteins and amphipathic lipids. The lipids are highly polymorphic (thousands of structures), each having a hydrophilic head group attached to one or more hydrophobic hydrocarbon chains through a glycerol or sphingoid backbone (Figure 2a--d). In our simplest conceptualization, membrane lipids are organized as two molecular monolayers (leaflets) with head groups facing the aqueous medium on either side and hydrocarbon chains forming the hydrophobic core of the membrane [88]. This arrangement results in a large energy barrier for head groups to flip through the hydrocarbon layer between leaflets (15--50 kcal/mol). Before PLS, the head groups and hydrophobic tails repel equally, and the bilayer is held together mainly by the hydrophobic effect at the interface between the head groups and the tails. After PLS, intermolecular interaction between lipids becomes unbalanced between the head groups and the tails. This alters the biophysical properties of the membrane by changing

the electrostatics and lipid packing to produce stress curvature that leads to production

of extracellular vesicles.
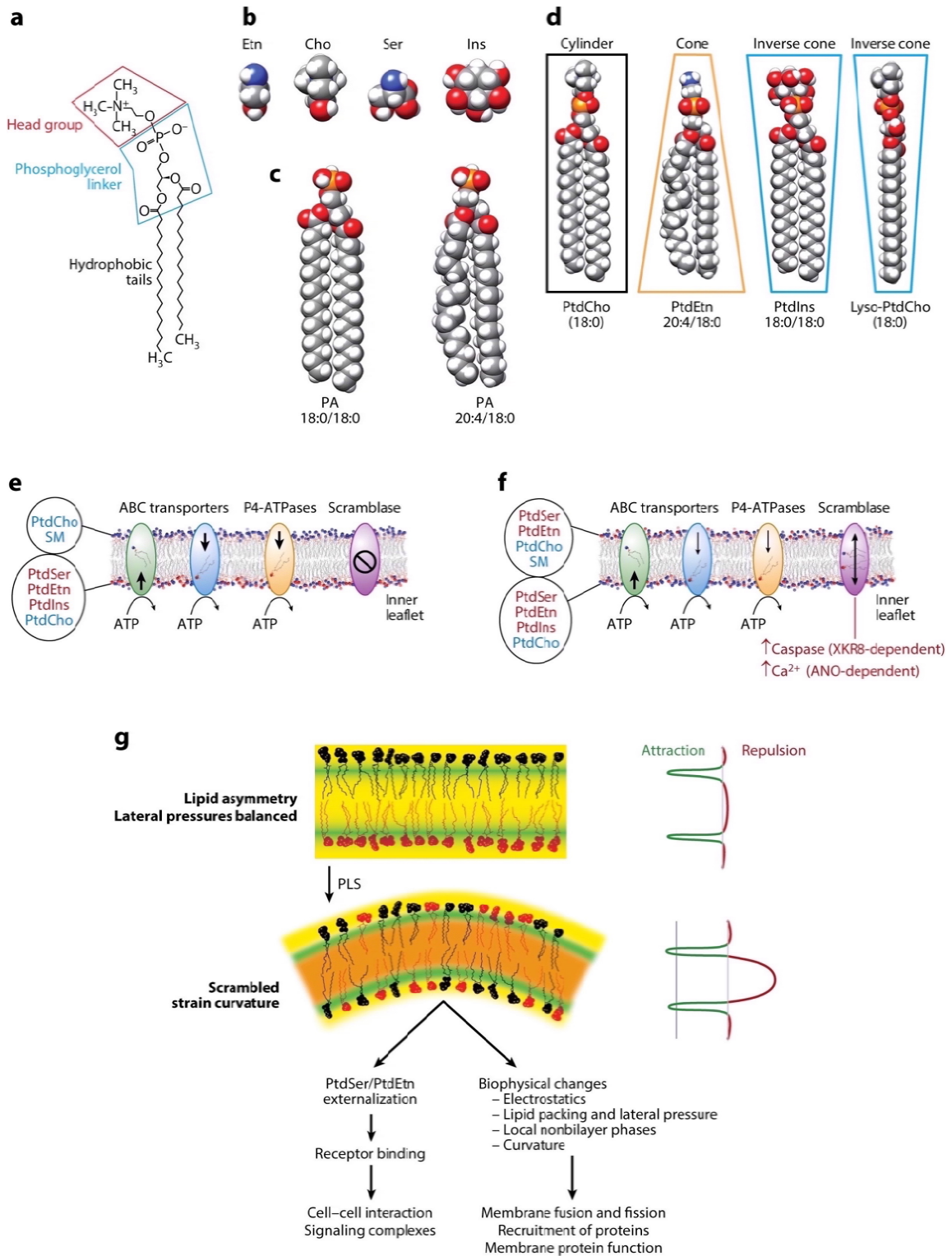
Figure 2 Phospholipids have different shapes that determine membrane curvature,

which is altered during PLS. (*a*) The structural formula of PtdCho, illustrating that phospholipids are constructed from three modules: the hydrophilic head group, a linker (either phosphoglycerol or sphingoid base) , and one or more hydrophobic fatty acid chains (tails). (*b*) Space-filling models of major phospholipid head groups to illustrate variations in size: ethanolamine (Etn), choline (Cho), serine (Ser), and inositol (Ins). (*c*) The structure of PA, composed of a phosphoglycerol linker and two hydrophobic acyl chains. Hydrocarbon chains differ in length and saturation. Unsaturated double bonds are kinked and occupy more space than saturated chains. PA 18:0/18:0 shows two saturated 18-carbon chains linked to phosphoglycerol. PA 20:4/18:0 shows one unsaturated 20-carbon chain (*left*, with four double bonds) and one saturated 18-carbon chain (*right*). These images are somewhat misleading, because in the membrane the hydrocarbon tails are quite flexible, and they assume a wide variety of conformations. (*d*) Examples of different glycerol phospholipids illustrating that their shapes vary from cylindrical (*open rectangle*) to cone-shaped (*brown wedge*) and inverted cone-shaped (*blue wedges*). Lyso-PtdCho has only one fatty acid chain. (*e*) ABC transporters and P4-ATPases establish phospholipid asymmetry in the plasma membrane in an ATP-dependent manner. The model membrane here is composed of PtdCho (head group nitrogen, *blue dots*) and PtdSer (head group nitrogen, *red dots*). (*f*) Elevation of cytosolic Ca^{2+} or activation of caspases activates phospholipid scramblase enzymes that passively allow lipids to equilibrate across the bilayer. In addition, under some circumstances inhibition of ATPases may facilitate PLS. (*g*) The consequences of PLS include receptor binding and changes in membrane biophysics. The top panel shows a lipid bilayer with lipid species distributed asymmetrically, and the bottom panel shows the membrane after PLS has occurred. Interaction between adjacent phospholipids in each panel is depicted in the corresponding graph on the right and in the background

49

shading with green representing attraction and longer wavelengths indicating repulsion.

(Primary effort on figure: Hartzell, HC)

Extracellular vesicles play important roles in physiological responses by serving as scaffolds for signaling complexes and as vehicles for delivering signaling machinery, including both mRNA and noncoding RNAs, such as microRNAs, and various signaling proteins. When anionic lipids are externalized, they can be recognized by soluble and cellular receptors.

In model bilayers, lipid flip-flop occurs on a time scale of hours to days. Typically, the outer leaflet of the PM of eukaryotic cells is enriched in phosphatidylcholine (PtdCho) and sphingomyelin (SM), whereas the inner leaflet is enriched in phosphatidylserine (PtdSer), phosphatidylinositol (PtdIns), and phosphatidylethanolamine (PtdEtn). This lipid asymmetry comes about because adenosine triphosphate (ATP)-dependent flippases actively transport certain lipids to the cytoplasmic leaflet while ATP-dependent floppases transport others to the outer leaflet [111, 130-132] (Figure 2e). In addition, certain lipids can be trapped in one leaflet or the other by binding to other lipids or proteins.

PtdCho: phosphatidylcholine

SM: sphingomyelin

PtdSer: phosphatidylserine

PtdIns: phosphatidylinositol

PtdEtn: phosphatidylethanolamine

Externalization of Phosphatidylserine and Phosphatidylethanolamine to the Extracellular Leaflet Is Regulated

In opposition to ATP-dependent transporters that segregate lipids, phospholipid scramblases are thought to be lipid channels that lower the energy barrier for passive movement of lipids between leaflets (Figure 2f). Two major PLS pathways have been identified [95]. One is activated by a process that involves caspase activation and XKR8 proteins [93]. Most notably, caspase-dependent PLS marks apoptotic cells and cell

fragments for phagocytosis [94, 133, 134]. The other pathway involves elevation of cytosolic Ca^{2+} and the ANO scramblases [7, 129]. These two PLS pathways are formally independent of one another because ANO6 disruption abolishes Ca^{2+}-PLS while leaving caspase-PLS intact [7]. However, physiologically the two pathways likely interact because cytosolic $[Ca^{2+}]$ increases during apoptosis, and a Ca^{2+} requirement for caspase-dependent PLS has been shown by some investigators [135-137]. Ca^{2+}-PLS is now recognized as a ubiquitous membrane signaling mechanism [95]. There are two major consequences of PLS (Figure 2g). First, phospholipids that are normally sequestered in the cytoplasmic leaflet in unstimulated cells are exposed to the external environment. These externalized phospholipids, mainly PtdSer and PtdEtn, are recognized by soluble and cellular receptors that orchestrate various signaling cascades. Second, PLS changes the physical properties of the membrane by altering lipid packing, the lateral pressure between lipids, and membrane electrostatics, and by forming local nonbilayer phases. This has several important sequelae that include changes in membrane curvature that favor membrane fusion or fission events, effects on the function of integral membrane proteins, and the recruitment of new proteins to the membrane.

MECHANISMS OF PHOSPHOLIPID SCRAMBLING

Phospholipid Scramblases Are a Type of Channel for Lipid Head Groups

Initial ideas about the mechanism behind PLS suggested that it was caused by Ca^{2+}-binding to membrane lipids like PIP2, and did not invoke a scramblase enzyme, but in 1995 Williamson *et al.* [138] demonstrated that Ca^{2+}-PLS required a specific protein. The first candidate scramblase was PLSCR1, which was able to elicit Ca^{2+}-PLS in reconstituted liposomes. However, these experiments are now suspect because <8% lipids were scrambled over several hours, whereas the reconstituted ANOs can

scramble a significant portion of the liposome lipids in minutes [66]. Because knockouts

of PLSCR1 and its paralogs have little effect on PLS, PLSCRs are unlikely to be

scramblases, but they may play a role in regulating Ca^{2+}-PLS [95].

nhTMEM16: Nectria haematococca TMEM16

The structure of the fungal ANO nhTMEM16 has provided important insights into the

mechanisms of PLS. But long before this structure was available, Pomorski & Mennon

[111] imagined scramblases as proteins having a hydrophilic groove along their surface

to provide a pathway so that lipid hydrophilic head groups could translocate between

leaflets while the hydrocarbon tails remained in the hydrophobic phase of the bilayer

(Figure 3a,b). The structure of nhTMEM16 has validated this model [68]. Phospholipid

scramblases are essentially ion channels except that, instead of being structured like the

funnel of a classic ion channel, they are like a bobsled run, with lipids being conducted

with their head groups as sleds and their acyl chains as scarves blowing in the wind. The

nhTMEM16 protein has 10 membrane helices with a hydrophilic furrow connecting the

cytosolic and extracellular sides of the membrane. This furrow, bordered by helices 4

and 6, faces the lipid bilayer and is ideally suited for lipid transport from one leaflet to the

other. Mark Samson's group has performed molecular dynamics simulations of

nhTMEM16 in a PtdCho bilayer

(http://sbcb.bioch.ox.ac.uk/memprotmd/beta/protein/pdbid/4WIS) and has shown that

lipid head groups are predicted to populate this furrow, as expected if the furrow was the

phospholipid conduit across the membrane (Figure 3c). Homology models of ANO6

have a similar hydrophilic furrow [139]; one side of the furrow is lined by the scramblase

domain we recently identified in ANO6 [106].

The mechanism of PLS activation by Ca^{2+} is likely to be the same for ANO scramblases

as it is for ANO Cl^- channels,direct binding of Ca^{2+} to the ANO protein [100, 140-142]. All

ANOs share highly conserved acidic amino acids in TMDs 6, 7, and 8.
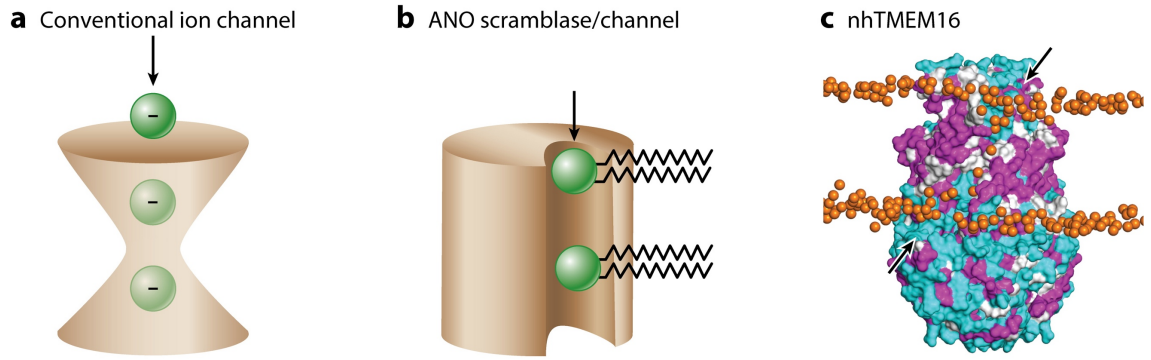
53

Figure 3 The passive diffusion model of ANO-scramblase function. (*a*) Classic ion channels are represented in schematic form as funnel-shaped structures where the ion conductance pathway is completely surrounded by protein. (*b*) Phospholipid scramblases are envisioned as membrane proteins that have a slot facing the lipid phase of the membrane. The slot is hydrophilic so that lipid head groups can move through it while the hydrophobic tails remain in the hydrophobic phase of the lipid. (*c*) Crystal structure of nhTMEM16 showing a molecular dynamics simulation of PtdCho moving through the hydrophilic furrow. Head group nitrogen atoms are blue. The nhTMEM16 surface is colored to indicate hydrophobicity (*cyan*, hydrophilic; *magenta*, hydrophobic). Note the deformation of the lipid bilayer by nhTMEM16. Arrows indicate the hydrophilic furrow. (Primary effort on figure: Hartzell, HC)

These amino acids coordinate Ca^{2+} in the nhTMEM16 structure and control its PLS

activity [68]. They also play a role in Ca^{2+} gating of ANO1 [140, 141] and regulate

scramblase activity of afTMEM16 [66]. Intriguingly, although mutations of the conserved

Ca^{2+} binding residues nearly abolish PLS, reconstituted afTMEM16 and nhTMEM16

scramble lipids significantly in the absence of Ca^{2+}. This raises questions whether the

purified scramblase may be missing a subunit.

afTMEM16: Aspergillus fumigatus TMEM16

Phospholipid scramblases are generally believed to be nonselective for lipids [95].

Although different rates of scrambling have been reported for different lipids, these

differences generally are small and not always consistent. ANO6 has been shown to

scramble PtdSer, PtdCho, PtdEtn, and SM [7] with slightly different kinetics. Likewise,

the reconstituted fungal ANOs exhibit little selectivity among different lipids tested and

are capable of scrambling PtdCho, PtdSer, PtdEtn, glucosylceramide, and DOTAP [66,

68]. However, quantitative comparisons between different lipids remain technically

problematic and represent a major issue that needs to be resolved. In addition, the

question whether PLS depends on the length or saturation of the acyl chains remains

unanswered.

Relationship of Ion Transport and Phospholipid Scrambling

Another important question concerns the relationship between PLS and ion transport in

the ANO superfamily. Although ANO6 and afTMEM16 scramblases exhibit ionic currents

as well as PLS, the significance of these currents remains uncertain. Yang *et al.* [100]

suggested that Ca^{2+} influx through ANO6 might play a role in regulating PLS via another

unidentified protein that is the true scramblase, but this seems unlikely in light of the

demonstration that the fungal ANOs are bona fide scramblases. It seems more likely that

ion transport by ANO scramblases is an (inconsistent) by-product of PLS [139].

nhTMEM16 has no convincing ion channel activity, whereas that of afTMEM16 depends

on the lipid composition of the membrane and is nonselective for ions [66], and ANO6

conductance has variable ionic selectivity that activates concurrently with PLS [106,

139]. To date, there is no evidence that ion transport by phospholipid scramblases has a

physiological function. Cl⁻ transport does not seem to be required for PLS because Cl⁻

channel blockers and the substitution of extracellular Cl⁻ with large organic anions have

no effect on Ca^{2+}-PLS [143]. PLS by reconstituted afTMEM16 is independent of the ions

present and is unaffected by inhibiting ion transport [66]. Whether ion transport by

phospholipid scramblases has a physiological function remains to be determined,

however, one can imagine that if scramblases conduct Ca^{2+}, this would serve as a

positive feedback mechanism for PLS.

The idea that ion transport by scramblases is a by-product of PLS suggests that the

pathways of ion and lipid transport are the same or they at least structurally overlap. If

so, this implies that the Cl⁻ conduction pathway of ANO1 is structurally homologous to

the lipid transport pathway of ANO scramblases [139]. Mutagenesis of ANO1 has shown

that residues involved in ion conduction and ionic selectivity are located in a region of

the protein that is homologous to the hydrophilic furrow in nhTMEM16 [139]. That ANO1

and ANO2 seem to form an out-group of the ANO superfamily (Figure 1a) is consistent

with the idea that ANO Cl⁻ channels evolved from ancestral lipid scramblases. The

bobsled run structure of the hydrophilic furrow may seem incompatible with ion transport

because the permeant Cl⁻ ion would be exposed on one side to the lipid bilayer.

However, we speculate that the membrane adjacent to ANO1 is a nonbilayer structure

with phospholipid head groups oriented toward the furrow. We imagine that Cl⁻ ions are

conducted across the membrane between the protein and lipid head groups. An

alternative model entertained by Brunner *at al.* [68] is that the Cl⁻ channels and

scramblases may differ in how they dimerize. In scramblases, the hydrophilic furrow is

56

located on the surface of each monomer opposite to the dimerization surface so that each dimer contains two furrows. Brunner *et al.* suggest that in ANO1 Cl⁻ channels the dimer might be rearranged so that the interface is formed by the furrow surfaces to form a single enclosed Cl⁻ conduction pathway.

RECOGNITION OF ANIONIC PHOSPHOLIPIDS BY RECEPTORS

Externalized Anionic Phospholipids Are Recognized by Soluble and Cell-Surface Receptors

Multiple receptors for PtdSer have been identified (Figure 4). Cell surface receptors include stabilins, TIM1, TIM4, BAI1, and members of the CD300 family [133, 144]. Soluble receptors include MFG-E8 that bridges the exposed PtdSer to αVβ5 integrins and Protein-S and Gas6 that bridge PtdSer to TAM receptors. The physiological endpoint for PtdSer and PtdEtn externalization may depend to a large extent on the receptors available to bind them. For example, different CD300 receptors can either suppress or support phagocytosis [145, 146]. Furthermore, there is evidence that different receptors may mediate alternative steps in the phagocytic process [147]. Exposure of PtdSer alone is not sufficient to mark a cell for phagocytosis because cells expressing a constitutively active form of ANO6 have a comparable amount of PtdSer externalized butare not engulfed by macrophages [148]. However, these cells are capable of being phagocytosed when they are treated with the apoptotic Fas ligand. Receptors recognize externalized anionic lipids by several different mechanisms. One mechanism is simply electrostatic: Receptors having a stretch of cationic amino acids interact with the negative surface charge of membranes enriched in anionic phospholipids. In addition, certain proteins bind specifically (and sometimes stereospecifically) to PtdSer or PtdEtn head groups.

57

a

Soluble receptors

	Lipid preference	Engulfment
Gas6 — Gla – EGF 2 3 4 – Laminin G – 2	PtdSer	Promotes
Protein-S — Gla – EGF 2 3 4 – Laminin G – 2	PtdSer	Promotes
MFG-E8 — EGF – C2-like – 2	oxPtdSer, PtdSer, PtdEtn	Promotes
DEL1 — EGF 2 3 – C2-like – 2	PtdSer not PtdEtn	Promotes
ANXA5 — Annexin 2 3 4 ILxCxxDE	PtdSer	Inhibits
Factor X lc — Gla EGF 1	PtdSer and PtdEtn	Promotes
Factor V hc — A3 – C2-like – 2	PtdSer and PtdEtn	Promotes

Membrane-bound receptors

	Lipid preference	Engulfment
CD300a — Ig – TM – Inhibitory ITIMs	PtdSer and PtdEtn	Inhibits
CD300b — Ig – TM – Grb2	PtdSer not PtdEtn	Promotes
CD300f — Ig – TM – Inhibitory ITIMs	PtdSer	Inhibits
TIM1 — Ig – Thr-rich – TM	PtdSer not PtdEtn	Promotes
TIM4 — Ig – Thr-rich – Ser-rich – TM	PtdSer not PtdEtn	Promotes
BAI1 — Thrombospondin repeats	PtdSer not PtdEtn	Promotes

100 amino acids

b

Unstimulated cell

Multivesicular body

PLS →

Exocytosis

Budding

Soluble receptors

Extracellular vesicles

Cellular receptors

Adapter

Integrins/co-receptor

PtdSer receptor

Vesicular binding and fusion

Figure 4 PtdSer receptors and the role of PLS in cell-cell signaling. (*a*) PtdSer binding proteins. Soluble proteins are on top, and membrane-bound receptors are below. Regions that bind PtdSer in a Ca^{2+}-dependent manner are colored yellow to red

as follows: orange, immunoglobulin-like; magenta, epidermal growth factor-like; yellow,

glutamic acid--rich γ-carboxyglutamic acid; red, C2-like; purple, thrombospondin. Other

domains shown are: white, transmembrane, blue, protein-specific domains. Lipid

preference indicates the preference of the receptor to bind PtdSer or PtdEtn. Engulfment

indicates whether the receptor has been shown to promote or inhibit phagocytic

engulfment. (*b*) Consequences of PLS. An unstimulated cell on the left has an

asymmetric plasma membrane (*blue*, PtdCho and SM; *red*, PtdSer and PtdEtn) and

contains MVBs. PLS scrambles the plasma membrane and stimulates release of

exosomes by exocytosis of MVBs and ectosomes by budding of the plasma membrane.

Externalized PtdSer and PtdEtn on the plasma membrane and on released EVs are

recognized by soluble receptors and by cell-bound receptors that bind directly or

indirectly to the externalized phospholipid. EVs deliver cargo by binding and/or fusion to

target cells. (Primary effort on figure: (a) Whitlock, JM; (b) Hartzell, HC and Whitlock,

JM)

PtdSer receptors are better understood than PtdEtn receptors [133, 144]. Domains that have been identified to be important in PtdSer binding include Ca^{2+}-dependent C2 domains, Ca^{2+}-independent discoidin C2 domains, poly-γ-carboxylglutamic acid (Gla) domains, and WxND motifs. PtdEtn receptors are much less well characterized, but recently it has been shown that CD300a receptors bind PtdEtn preferentially to PtdSer via WxND motifs [146, 149]. PtdEtn binding proteins 1--4 (PEBP1--4) are ubiquitously expressed, but their functions remain poorly understood.

Exposed Anionic Phospholipids Function as a Signaling Platform

Externalized PtdSer not only serves as a ligand that brings two cells together (e.g., phagocytosis), but it may also serve as a scaffold to organize soluble proteins into signaling complexes. For example, when platelets are exposed to collagen and trace amounts of thrombin during vascular damage, cytosolic Ca^{2+} rises and stimulates ANO6-mediated Ca^{2+}-PLS. The externalized PtdSer serves as a surface for assembly of plasma-borne coagulation factors that stereospecifically bind to PtdSer to form the prothrombinase complex that generates the quantities of active thrombin necessary to catalyze coagulation. This binding surface increases the local concentration of the enzymes, cofactors, and substrates necessary for clotting and physically juxtaposes them. By constraining diffusion of the reactants, scaffolding further optimizes multistep reactions resulting in a >105-fold increase in the rate of thrombin formation [95].

PHOSPHOLIPID SCRAMBLING REGULATES MEMBRANE CURVATURE

The externalization of PtdSer and PtdEtn also changes lipid packing in the membrane. As shown in Figure 2, membrane phospholipids are highly polymorphic, being composed of head group modules of different sizes and electrostatic charge and acyl chain modules of varying lengths and saturation. Intermolecular interactions between these

polymorphic lipids establish a lateral pressure in the membrane [87, 150]. Acyl chains

repel one another because of entropic and steric interactions, whereas head groups

repel one another electrostatically, entropically, and sterically (Figure 2g). The bilayer is

held together by a strong attractive force at the interface between the head groups and

the acyl chains that is created by the hydrophobic effect which is caused by the large

energetic cost of exposing the acyl chains to a hydrophilic environment. Some lipids in

isolation (e.g., PtdCho) energetically favor bilayer structures because the lateral

pressures in the head group and acyl chain regions are balanced. Other lipids that are

charged (e.g., PtdSer) or have small (e.g., PtdEtn) or large (e.g., PtdIns) head groups

relative to the acyl chains energetically prefer nonbilayer structures such as micelles or

inverse hexagonal phases. When nonbilayer lipids are mixed with bilayer-promoting

lipids, they cause strain in the monolayer due to an imbalance in lateral pressures. The

membrane will then bend, depending on the sum of strains in the two monolayers [151].

Thus, when the distribution of different lipids in the two monolayers changes during PLS,

the lateral pressure in the membrane will be disrupted, and the curvature of the

membrane will very likely change. Proteins also play an important role in determining

membrane curvature [151, 152], but they do so in concert with membrane lipids.

The necessity of redistributing membrane lipids during formation of membrane vesicles

may be appreciated by comparing the geometries of the PM of a 10 μm--diameter cell

(essentially flat) and a ~50 nm--diameter synaptic vesicle (marked curvature). Assuming

that the membrane is ~5 nm thick, the area of the outer surface of the vesicle is $4\pi r2 =$

7,854 nm2, whereas the area of the inner surface is 20% smaller, 6,362 nm2. Although

this difference could be accounted for by fewer lipids in the inner monolayer, this would

come at a large energetic cost if all the lipids were essentially cylindrical in shape

because the high curvature of the membrane would tend to expose the hydrophobic core

of the membrane to the hydrophilic environment. The differences in the radius of

curvature between monolayers would impose a significant lateral strain in the membrane. Changes in membrane curvature are essential for processes such as endocytosis or exocytosis [151, 153]. This membrane trafficking is brought about partly by the redistribution of lipids between bilayers and by insertion of membrane proteins that disrupt the packing of lipids in the bilayer to change the lateral pressure profile in the membrane.

Not only does membrane curvature affect lipids, but it also affects the function of integral membrane proteins, because membrane proteins are coupled to the surrounding lipid bilayer by their hydrophobic membrane-spanning domains [87, 154]. Conformational changes in proteins will be affected by the energetics of lipid-protein interactions that will be affected by the lateral pressure between lipids. In addition, the change in membrane electrostatics and curvature can affect the association of proteins with the membrane. For example, BAR-domain proteins that stabilize/induce membrane curvature are recruited to the membrane by specific membrane curvatures [152].

CHANGES IN MEMBRANE CURVATURE LEAD TO EXTRACELLULAR VESICLE PRODUCTION

The earliest descriptions of PLS were accompanied by observations that PLS is accompanied by the release of EVs into the medium [155-157]. In fact, >25% of the procoagulant activity associated with activated platelets is actually elicited by platelet-derived EVs released during activation that expose PtdSer and assemble the prothrombinase complex [157, 158]. Because PLS alters membrane curvature, and membrane curvature is an essential step in vesicle formation, a reasonable hypothesis is that PLS is necessary for and precedes EV membrane shedding by promoting budding and lowering the energy required for vesicle scission. EVs have now been shown to be released from most cell types and are found in every fluid in the human body examined

thus far. EVs are typically loaded with precious cargo that includes both coding and noncoding RNAs and signaling proteins. There is growing evidence that EVs mediate diverse intercellular signaling functions [159-167]. Although more may be known about the role of PtdSer in regulating membrane dynamics, PtdEtn plays a central role in recruiting proteins to membrane compartments, both in vesicular/organellar fusion and fission and in the production of extracellular vesicles (EVs) [162, 167-171]

EV: extracellular vesicle (both exosomes and ectosomes)

Extracellular Vesicle Nomenclature, Definition, and Biogenesis

EVs are typically divided into two flavors, exosomes and etcosomes (also microparticles). A key distinction is that exosomes are released by exocytosis of multivesicular bodies (MVBs, also called multivesicular endosomes), whereas ectosomes are formed by outward budding of the PM. However, in practice, EVs are often characterized by their size, sedimentation properties, and the presence of certain molecular markers. Ectosomes are typically larger (50 nm--1 μm in diameter) than exosomes (30--100 nm), but because isolation procedures are not standardized, and because there is significant overlap in size distributions and the presence of molecular markers, it is frequently difficult to evaluate the extent of cross-contamination in different EV preparations. Another problem is that whereas conventional fluorescence-activated cell sorting is often used to separate exosomes and ectosomes, this technique cannot reliably separate particles in the 30--200 nm range, which is near or below the diffraction limit of visible light.

Exosomes are expelled into the extracellular space by the Ca^{2+}-dependent exocytosis of MVBs [165]. MVBs form from late endosomes by the inward budding of the membrane to form intraluminal vesicles (ILVs). ILVs are filled with various protein and nucleic acid cargo from the cytoplasm that have been positioned near sites of vesicle budding.

Cargos may vary depending on cell type and physiological condition. ILV formation can occur by several mechanisms, but the best studied utilizes the ESCRT (endosomal sorting complex required for transport) machinery, but ESCRT-independent mechanisms have also been described (reviewed in [161]). Exosome release is regulated by small GTPases and likely involves SNARE fusion machinery. Released exosomes are capable of eliciting a variety of changes in target cells, suggesting that they play important intercellular signaling functions (reviewed in [160]).

ILV: intraluminal vesicle

Ectosomes are, on average, larger than exosomes (100--1,000 nm) and include apoptotic bodies. They are shed into the extracellular environment by blebbing from the PM itself and can be released seconds after cell stimulation, in contrast to exosomes that are released more slowly. Although ectosomes bud from the PM itself and do not rely on exocytosis for release, many components of the ESCRT complex seem to be required for ectosome budding.

Topologically, neither ectosomes nor exosomes would be expected to have PtdSer externalized because the cytoplasmic leaflet of the membrane is oriented toward the lumen in both cases. However, many EVs typically have PtdSer and/or PtdEtn exposed on the extracellular surface, suggesting that phospholipid scramblases are involved in the biogenesis or release of EVs. Platelet EVs have been reported to be diverse with regard to externalization of anionic phospholipids [168]. Although many papers indicate that both exosomes and ectosomes (often identified on the basis of size alone) have externalized PtdSer, relatively few studies have carefully examined both exosomes and ectosomes at the same time. Two studies suggest that exosomes have much less externalized PtdSer than ectosomes [157, 172].

ANO6 Regulates Extracellular Vesicle Release Associated with Phospholipid Scrambling

Although EV release and PLS occur concurrently, until recently it was unknown whether these two processes are mechanistically linked or simply occur in parallel. The first clue that Ca^{2+}-PLS regulates EV release came when investigators recognized that Scott syndrome patients also exhibited defective EV release [173-175]. Moreover, cells from ANO6 knockout mice exhibit both perturbed Ca^{2+}-PLS and EV release [101, 176]. Although EV release from platelets is disrupted in both Scott syndrome patients and Ano6 knockout mice, exocytosis appears unaffected because release of α-granules and dense granules is normal. Although the role of ANO6 in MVB exocytosis and exosome release has not been directly investigated, the finding that Scott syndrome platelets release α-granules, which are a type of MVB that often contain some exosomes, suggests that ANO6 may be involved in the shedding of ectosomes but not in the exocytosis of MVBs and release of exosomes. Because ANO5 is closely related to ANO6, we suspect that ANO5 also plays a large role in EV formation in cell types, such as muscle, that express it.

Extracellular Vesicles Have Two Major Functions: Scaffolding and Communication

As discussed above, in blood clotting, platelet-derived EVs serve as catalytic surfaces for the assembly of the prothrombinase complex. Additionally, specialized EVs called matrix vesicles (MVs) are also essential in the mineralization of bone, where PtdSer plays an essential role in the scaffolding of factors required for mineral nucleation. MVs, 50--200 nm in diameter, bud from PM domains on osteoblasts and chondrocytes to mineralize collagen deposits and form bone [177]. PtdSer plays an essential role in nucleating crystals of inorganic phosphate and calcium, in the form of hydroxyapatite necessary for mineralization, within the MV lumen. The role of PLS in MV biogenesis

and function remains unclear. In MVs, PtdEtn is externalized, but PtdSer remains luminal, likely anchored by PtdSer binding proteins required for hydroxyapatite nucleation (reviewed in [178]). Interestingly, Ano6$^{-/-}$ mice exhibit major defects in bone mineralization during development, and osteoblasts from these mice exhibit perturbed C Ca^{2+}-PLS [127]. The loss of ANO6 in Scott syndrome causes impaired EV release, suggesting that MV biogenesis may be dependent on ANO6 and that defective MV production is to blame for defective bone mineralization.

MV: matrix vesicle

In addition to their scaffolding function, EVs are capable of stimulating antigen-specific IgG production in B cells, inducing angiogenesis, regulating endothelial cells, and stimulating neutrophils; they can also contribute to the invasiveness of certain types of cancers [178-182]. It has become increasingly clear that EVs perform a fundamental role in intercellular communication by fusing with target cells to deliver microRNAs, lipid, and protein cargo. Recent investigation has demonstrated a role for EV signaling in many cell types, including EV regulation of myogenesis in myoblasts, sperm maturation, and osteoclast precursor differentiation. EVs may also regulate trophoblast fusion, suggesting that the signaling role of EVs is a general cellular phenomenon [164, 169, 183, 184].

THE ROLE OF PHOSPHOLIPID SCRAMBLING IN MEMBRANE FUSION

Although most eukaryotic cells are mononucleated, there are several notable exceptions: skeletal and cardiac muscle, osteoclasts, syncytiotrophoblasts, and giant multinucleated cells that form by the fusion of mononucleated cells to make a multinucleated syncytium. Cell-cell fusion involves multiple steps, numerous transcription factors, adhesion/migration proteins, and signaling proteins, but cellular fusion exhibits

66

many common themes in diverse cell types [123, 185]. One common theme is the reorganization of the lipid component of the PM. Many aspects of bilayer structure and lipid physical properties are thought to contribute to membrane fusion, including lipid packing, changes in membrane fluidity, formation of local nonbilayer phases, and alterations in bilayer curvature.

Myoblast Fusion Involves PtdSer Exposure

Almost 20 years ago, van den Eijnde and coworkers observed exposure of PtdSer on the outer leaflet of the PM in differentiating muscle *in vivo* [186]. At first, this was interpreted as indicative of apoptosis, however, subsequent observations suggest a more sophisticated scenario. PtdSer is exposed on the surface of myoblasts around the same time they begin fusing to form myotubes. PtdSer exposure is transient, localizes to sites of cell-cell contact, and diminishes as myotubes form [187]. The idea that PtdSer exposure is required for fusion is provided by observations that prolonged exposure to Annexin-V (see sidebar, Annexins are PtdSer-binding Proteins) or a PtdSer-antibody during myoblast fusion significantly inhibits the myotube formation [187, 188] and that liposomes of PtdSer, but not PtdCho, stimulate myoblast fusion [187, 188]. Recently it has been reported that the PtdSer receptors BAI1 and BAI3 play roles in myoblast fusion [189, 190]. For example, BAI1 overexpression increases myoblast fusion through the ELMO/Dock180/Rac1 pathway. These investigators suggest that PtdSer exposure occurs in a subset of apoptotic myoblasts that promote fusion but do not actually fuse themselves because myoblast fusion is impaired by caspase inhibitors [190]. While this model is intriguing, the effect of caspase inhibitors conflicts with earlier studies [187].

Topic Sidebar: Annexins in PtdSer signaling

Annexins are an important class of Ca^{2+}- and PtdSer-binding proteins that have opposing functions. For example, whereas Annexin-V blocks

67

myoblast fusion, Annexin-I clearly promotes myoblast fusion [191, 192].

This illustrates an important aspect of PtdSer exposure, namely, that

different PtdSer receptors promote different outcomes. Annexins bind

PtdSer in a Ca^{2+}-dependent manner with Ca^{2+} bridging annexin carbonyl

and carboxyl groups and PtdSer phosphoryl groups [193]. Annexin-V and

Annexin-I, however, differ in important ways. Annexin-I forms a

symmetrical bivalent heterotetramer with two Annexin phospholipid

binding domains connected by an S100 dimer [194]. In contrast, Annexin-

V does not form a bivalent structure because it has a short N terminus. In

the presence of membranes, Annexin-V self-assembles into trimers that

form a two-dimensional (2D) lattice. Consistent with these structural data,

Annexin-I aggregates PtdSer vesicles or chromaffin granules, whereas

Annexin-V does not [195, 196]. This also explains why Annexin-V plays

an anticoagulant role in the blood: The 2D lattice of Annexin-V essentially

masks PtdSer that may be externalized at low levels on cells. Annexin-V

also inhibits phagocytosis of apoptotic cells while Annexin-I supports

phagocytosis.

ANO5 Knockout Mice Suggest That Phospholipid Scrambling May Be Important in Muscle Regeneration

Myoblast fusion is important not only for muscle development during embryogenesis but also for muscle regeneration after damage. Adult muscle tissue is populated with mononucleated muscle progenitor cells (satellite cells) that play a role throughout adulthood to regenerate injured muscle fibers [197]. Recently, it has been shown that mutations in ANO5 are linked to a spectrum of myopathies that might be explained by defective membrane repair and muscle regeneration [8, 198-200]. These disorders

range from severe muscle weakness and atrophy to exercise-induced muscle pain

associated with elevated serum creatine kinase indicative of "leaky" muscle cells.

Dominant ANO5 mutations cause a different disorder, gnathodiaphyseal dysplasia

(GDD1), a skeletal syndrome characterized by bone fragility and thickening [201]. ANO5

is likely to be a phospholipid scramblase because it is 65% identical to ANO6 in the

TMDs, and it contains a scramblase domain nearly identical to the one we described in

ANO6 [47, 106]. Knockout of ANO5 in mice phenocopies human limb girdle muscular

dystrophy type 2L (LGMD2L) [202]. *Ano5*-deficient mice exhibit delayed regeneration of

muscle after cardiotoxin injury. This is at least partly explained by a defect in the ability

of myoblasts to fuse, because for myoblasts in culture, the fusion index (the percentage

of cells with >1 nucleus) was 35% less for ANO5$^{-/-}$ myoblasts than for wild-type

myoblasts. In addition, the number of nuclei per myotube was greatly reduced in Ano5$^{-/-}$

cells [202]. Because humans with ANO5 myopathies and Ano5 knockout mice have no

obvious muscle phenotypes at birth, this suggests that ANO5 may not play a significant

role in myoblast fusion during embryogenesis but may be more important in satellite cell

fusion in the adult. Two other groups have reported that Ano5 knockout mice have no

muscle phenotype [47, 203]. This may be related to genetic background or to the way in

which the knockouts were constructed. The Xu *et al.* [204] and Gyobu *et al.* [47] mice

may be true nulls, with knockout constructs inserted in exons 1 or 2, whereas the Griffin

et al. [202] mice may express residual truncated transcript, as stop codons are inserted

after exon 8. This may mimic more closely the LGMD2L founder mutation (c.190dupA) in

exon5 that is predicted to cause a frameshift and premature stop.

Membrane Repair Involves Phosphatidylserine

Membrane damage occurs during ordinary activity, and cells have evolved complex

repair mechanisms to deal with it. Membrane repair by active resealing requires

extracellular Ca^{2+} and is thought to involve formation of a patch at the site of injury [205-207]. After membrane damage, increases in intracellular Ca^{2+} trigger endocytosis of damaged PM that relies on ESCRT function, similar to EV biogenesis [205, 207-209]. These endocytosed vesicles then fuse with lysosome-like organelles that are transported to the site of damage and fuse with the PM by an exocytosis-like process to patch the lesion [207, 210, 211]. Membrane repair is complex and involves a myriad of proteins, but a common feature is the requirement for C2 domain-containing proteins that bind Ca^{2+} and PtdSer to induce a positive curvature strain that destabilizes the membrane to promote fusion [203, 212-215]. In nonmuscle cells, fusion of repair vesicles is mediated by the C2-domain-containing synaptotagmin-7 and SNARE proteins [208, 216]. In muscle, dysferlin, a C2-domain protein, serves the same purpose as a Ca^{2+} sensor and/or a fusogenic protein. Dysferlin is a member of the ferlin family that is involved in a range of membrane fusion events. Dysferlin along with other Ca^{2+}- and PtdSer-binding proteins, including annexins A1, A2, and A6 (see sidebar, Annexins are PtdSer-binding Proteins), promote membrane repair via Ca^{2+}-dependent fusion of vesicles with the sarcolemma [217-220]. When membrane damage occurs, dysferlin-containing PM is endocytosed. These endosomes fuse with other endolysosomal organelles to form larger vesicles that undergo a process similar to exocytosis to patch the lesion. The damage-induced recruitment of dysferlin concentrates PtdSer at the lesion, forming a PtdSer-rich platform for assembly of other components.

The Role of ANO5 in Membrane Repair

In many muscular dystrophies, the cellular lesions are caused by a breach of sarcolemmal integrity. In the most common muscular dystrophies (e.g., Duchenne) mutations in the dystrophin-glycoprotein complex connecting the extracellular matrix and the actin cytoskeleton render the PM more susceptible to mechanical damage [221]. In

70

contrast, dysferlin mutations associated with dysferlinopathies affect the ability of the muscle to repair normal physiological damage [218, 222]. ANO5-linked muscular dystrophies share features with dysferlinopathies at the histological, fine-structural, and clinical levels [8, 223, 224]. Mutations in both dysferlin and ANO5 are associated with elevated serum creatine kinase levels, weakness in both proximal and distal musculature, disruptions of the sarcolemma, defects in sarcolemmal repair, and amyloid deposits [225]. This similarity of ANO5-myopathies to dysferlinopathies has led to the suggestion that ANO5, like dysferlin, participates in membrane repair processes. This idea is supported by observations that muscles from ANO5-myopathy patients have sarcolemmal lesions at the electron-microscope level [8] and that fibroblasts from MMD3 patients fail to repair wounded membranes [8, 223]. Repair of muscle fibers damaged by a laser pulse is defective in ANO5 knockout mice, suggesting that ANO5 plays a role in membrane fusion [202].

Sperm-Egg Interaction

Sperm-egg fusion is one of the iconic examples of cell-cell fusion, but the role of PtdSer externalization in fertilization is unclear. Mammalian spermatozoa are unable to fertilize the egg immediately after leaving the male reproductive tract; they must first undergo capacitation to become capable of executing the acrosome reaction and to develop the high motility necessary for fertilization. Capacitation involves a number of physiological changes, one of which includes changes in membrane lipids such as the loss of cholesterol and exposure of PtdSer [226, 227]. The acrosome reaction involves the exocytosis of the acrosome, a large lysosome-like organelle. This exocytotic event may produce significant alterations in the composition of the PM. Fertilization requires the PtdSer binding protein MFG-E8 [228]. As with other cell-cell fusion processes, one might expect MFG-E8 to bridge PtdSer on the sperm to a receptor on the egg. In addition, the

71

exocytosis of the acrosome releases swarms of EVs formed by the fusion of the PM and the acrosomal membrane [164, 229]. Recently it was shown that Ano5 knockout mice exhibit reduced male fertility and sperm motility, but otherwise the sperm appeared normal. Gyobu *et al.* It remains unclear whether Ano5 functions as a phospholipid scramblase in sperm, because the Ano5 knockout sperm underwent capacitation normally including externalization of PtdSer [47].

Osteoclasts and Multinucleated Giant Cells

The fusion of cells of the monocyte/macrophage lineage is required to form osteoclasts that are involved in bone reabsorption and to generate multinucleated giant cells that are found in a variety of inflammatory conditions [230]. In these cells it has been observed that PtdSer is locally externalized and that fusion is blocked by Annexin-V or by PtdSer-containing liposomes [231]. Although ANO5 and Ano6 mutations affect bone development [127, 201], it remains unknown whether osteoclast function is affected.

Syncytiotrophoblast Fusion Depends on PtdSer Externalization

During implantation of an embryo in the uterus, trophoblast cells surrounding the inner cell mass of the blastocyst fuse to form a multinucleated syncytium called the syncytiotrophoblast. PtdSer externalization is associated with this fusion event [232, 233]. The finding that antibodies to PtdSer inhibit fusion supports the essential role for PLS in trophoblast fusion [234]. However, it remains unsettled which phospholipid scramblase pathway is activated and whether PLS is mediated by a phospholipid scramblase or an ATP-dependent transporter [235]. Interestingly, in antiphospholipid syndrome, a disease linked to an increased risk of thrombosis and recurrent pregnancy loss, the serum of patients frequently contains antibodies to phosphatidylserine and Annexin-V [236, 237]. Although there is no evidence that the ANOs play a role in

syncytiotrophoblast fusion, ANO6 is expressed in human placenta

(http://www.bioGPS.org).

LOOSE ENDS: IST2 AND Endoplasmic Reticulum-Plasma Membrane Junctions

The yeast Saccharomyces cerevisiae has one ANO homolog called IST2. The encoded

protein, Ist2p, plays a key role in the formation of specific contact sites between the

endoplasmic reticulum (ER) and the PM that are important for communication between

these two cellular compartments. Deletion of IST2 in yeast results in separation of the

cortical ER and PM [78, 79], and the overexpression of IST2 in mammalian cells induces

the formation of ER-PM contact sites [238]. Ist2p brings the ER and PM membranes to

within 30 nm of one another because its C terminus binds to the PM while the TMDs are

embedded in the ER membrane [239]. The C terminus binds to the PM because it

contains an amphipathic α-helix and a cluster of basic amino acids called the cortical

sorting signal that associates with PtdIns(4,5)P2 in the PM [240]. IST2 is most closely

related to Chordate ANO10 (39% similar) and nhTMEM16 and afTMEM16 (44% similar).

However, the finding that reconstituted Ist2p does not support PLS [66] raises questions

concerning exactly how it fits into the ANO story.

ER: endoplasmic reticulum

Intriguingly, ER-PM junctions are involved in lipid and cholesterol trafficking [241]. The

main site of phospholipid, ceramide, and cholesterol biosynthesis in the cell is the ER

[88]. From the site of synthesis, lipids are transported to the plasma membrane by both

vesicular and nonvesicular routes. One of the nonvesicular routes involves ER-PM

junctions where lipids are exchanged between membranes by various mechanisms,

including diffusion of lipids (either free or bound to transfer proteins) across the 10--30

nm gap between the ER and PM, exchange of lipids during direct membrane contact,

and transient bilayer hemifusion. If Ist2p is not a lipid scramblase, this raises an

73

intriguing possibility that one role of ANOs may be to bring membranes into apposition to facilitate membrane fusion, fission, or lipid transfer. If so, perhaps PLS is a more intricate process than an enzyme that facilitates free lipid diffusion between membrane leaflets and instead involves the exchange of lipids between membranes that promotes membrane scrambling at these sites of membrane mixing. Considering that PLS can be induced by a variety of chemicals and peptides as well as proteins, PLS caused by ANOs in reconstituted systems might simply be a consequence of a protein-lipid interaction that is more complex in the physiological context. In other words, is PLS the trigger for production of EVs, or is PLS the consequence of vesicular/lipid trafficking?

CONCLUSION

The realization that many ANOs function as Ca^{2+}-dependent phospholipid scramblases has reinvigorated both the fields of phospholipid transport and Cl^- channel physiology. Now that the proteins responsible for phospholipid scrambling have been identified, a host of issues have become accessible to investigation. Major questions that will be addressed in the coming years include the following: Is direct Ca^{2+}-binding essential/sufficient for ANO-PLS, or are there other activators or regulatory factors involved? The pertinence of this question is emphasized by the finding that ANO6-associated ionic currents activate very quickly in excised patches but very slowly in whole-cell recordings [100, 106] and that there is significant scrambling activity of the fungal ANOs in the absence of Ca^{2+} [66, 68]. Are subunits of an ANO6 complex lost in excised patches and reconstituted systems? What are the roles of ANOs and PLS in the production of EVs? Are these parallel processes or linked mechanisms, and if the latter, is PLS essential for all vesicle release or just for ectosome release? Does membrane trafficking play a role in the actual mechanism of scrambling itself in cells? Do any of the ANOs exhibit specificity among different phospholipid head groups or acyl chains? Are

74

Ca^{2+}- and caspase-PLS truly separate processes? Does caspase-dependent PLS operate in the absence of all ANOs? What is the structure of the ANO1 Cl$^-$ channel pore and is there a role for lipids (39)? Is the pathway for Cl$^-$ transport homologous to the pathway for lipid transport? There is much to be learned that will likely expand our understanding of cellular physiology.

SUMMARY POINTS

1. Most anoctamin/TMEM16 proteins are scramblases; the Cl$^-$ channel members probably evolved from scramblases.
2. ANO-mediated PLS elicits major physical and chemical alterations in the membrane and is associated with the release of EVs that play crucial roles in cell signalling.
3. A major cellular effect of scrambling is the exposure of PtdSer and PtdEtn that function as a ligands for numerous receptors that function in cell-cell communication.
4. PLS is a major mechanism of cell-cell communication in tissues as diverse as skeletal muscle and gametes.
5. Membrane trafficking is an integral component of PLS.

FUTURE ISSUES

1. What is the substrate specificity of ANO phospholipid scramblases for lipids?
2. Do ANO scramblases have accessory subunits?
3. What is the function of the ionic leak of ANO scramblases?
4. What is the function of PLSCR1 in ANO-mediated PLS?
5. How do Ca^{2+}-dependent and caspase-dependent phospholipid scrambling interact?

What is the precise mechanism of ANOs in EV production?

Chapter III

A Pore Idea: The ion conduction pathway of TMEM16/ANO proteins is composed partly of lipid.

Prelude to "A Pore Idea: the ion conduction pathway of TMEM16/ANO proteins is composed partly of lipid."

The discovery of ANO PLSases has led many, including Criss and I, to suggest that the ANO family's ancient function is likely Ca^{2+}-PLS. This leads to the curious question of how ANO CaCCs fit into the family? In the manuscript below Criss and I review the ANO CaCC literature and conclude that previous structure/function data suggest that the ANO CaCC ion conductance pathway is simply a modified ANO Ca^{2+}-PLS lipid pathway. We employ a homology modeling approach to evaluate the pathway by which ANO6 facilitates PLS and find that the residues that form the lipid pathway align with residues that have been identified over the last decade as residents of the ANO1, ion conducting pore. Moreover, we hypothesized that while the CaCC ANO1 does not facilitate Ca^{2+}-activated lipid exchange between membrane leaflets, the ANO1 ion pore is partially composed of lipid head groups. Prior to the recent ANO1 cryo-EM structures, we believed that this model explained a number of phenomena discussed in the ANO1 literature. As I will outline following the review, our model that the ANO1 ion channel pore is partially composed of lipid headgroups is controversial and has been challenged by recent cryo-EM structures of the ANO1 pore. Although current cryo-EM structures of ANO1 have suggested that the ANO1 pore is closed, restricting lipid access along the majority of the membrane spanning region, current ANO1 atomic structures likely represent inactivated, closed ANO1 ion pores. With this in mind, it is difficult to precisely predict the association of an open ANO1 ion pore with the lipids that surround it. Based on our current structural understanding, it is likely that lipids do not line the entire ion pore, but their headgroups may line a portion of the pore and contribute to ANO1's biophysical function.

Summary

Since their first descriptions, ion channels have been conceived as proteinaceous conduits that facilitate the passage of ionic cargo between segregated environments. This concept is reinforced by crystallographic structures of cation channels depicting ion conductance pathways completely lined by protein. Although lipids are sometimes present in fenestrations near the pore or may be involved in channel gating, there is little or no evidence lipids inhabit the ion conduction pathway. Indeed, the presence of lipid acyl chains in the conductance pathway would curse the design of the channel's aqueous pore. Here we make a speculative proposal that anion channels in the TMEM16/ANO superfamily have ion conductance pathways composed partly of lipids. Our reasoning is based on the idea that TMEM16 ion channels evolved from a kind of lipid transporter that scrambles lipids between leaflets of the membrane bilayer and the modelled structural similarity between TMEM16 lipid scramblases and TMEM16 anion channels. This novel view of the TMEM16 pore offers explanation for the biophysical and pharmacological oddness of TMEM16A. We build upon the recent x-ray structure of nhTMEM16 and develop models of both TMEM16 ion channels and lipid scramblases to bolster our proposal. It is our hope that this model of the TMEM16 pore will foster innovative investigation into TMEM16 function.

Introduction.

Lipid membranes are energy barriers that charged ions must cross to enter or exit cellular compartments. The major component of this barrier is the energy associated with moving the ion from an aqueous medium of high dielectric constant (ε = 80) into a greasy, hydrophobic one composed of lipid acyl chains having a low dielectric constant ($\varepsilon \sim 4$). Ion channels lower this energy barrier by forming a high dielectric ("aqueous") conduit through the acyl chains. This principle is illustrated beautifully by the structure of KcsA, the first ion channel to have its atomic structure determined by X-ray crystallography in 1998 by the McKinnon lab [242]. At the mouth of the pore, the K^+ ion loses its bound waters and, then as it passes into the selectivity filter, is stabilized by electronegative carbonyl oxygen atoms of the protein backbone. These carbonyl oxygens act essentially as surrogate water molecules that surround the K^+ ion to provide a hydrophilic environment for the K^+ ion to traverse the membrane. Since then, KcsA has served as a conceptual icon for ion permeation through proteinaceous pores. Although variations on this theme abound, the idea that ion channels rely entirely on protein-lined pores to facilitate ion passage through the hydrophobic core of the membrane is strongly rooted in our collective concepts of ion channels.

In contrast to our clear understanding of cation channels like KcsA, anion channels remain somewhat enigmatic. For example, prior to the availability of Cl^- channel crystal structures, approaches to identify the selectivity filters of the ClC, bestrophin, CFTR, and TMEM16 chloride channels by mutagenesis yielded results that were more ambiguous than those we came to expect from K^+ channels. Although more clarity has been achieved as some Cl^- channel crystal structures have become available, many questions about how Cl^- moves through the channel still remain.

The TMEM16 family

TMEM16 proteins are found in all eukaryotes (Figure 1A). In vertebrates, the family consists of ten genes (TMEM16A – TMEM16K with 16I skipped) (Figure 1B). Although the HUGO approved name of the family is ANO ("Anoctamin" derived from ANion + OCTA=8 transmembrane domains), most investigators prefer the TMEM16 terminology because many TMEM16 proteins are not anion channels, and they have ten, not eight, transmembrane domains. After TMEM16A and TMEM16B were discovered to be *bona fide* Ca^{2+}-activated Cl^- channels (CaCCs) in 2008 [124, 243-245], it was fully expected that all - or most - of the TMEM16 genes would encode CaCCs because of their high sequence similarity (Figure 1B). The first clue that things might not be so simple came when we were unable to find Cl^- currents when we expressed TMEM16C – TMEM16K in HEK cells [246]. This surprising result was soon resolved by the revelation that some TMEM16s are not CaCCs, but are phospholipid scramblases that transport lipids between the two leaflets of the membrane bilayer [7, 68]. This unexpected and exciting discovery that the TMEM16 family is functionally split raises very interesting questions about the evolutionary relationships of TMEM16 channels and scramblases. Below, we will briefly discuss some of the properties of the TMEM16 proteins. This summary is highly selective, and reader is encouraged to consult several excellent, more balanced reviews [124, 244, 245, 247]. The goal of this article is to develop the *hypothesis* that (1) TMEM16A evolved from an ancestral lipid scramblase, (2) the TMEM16A pore shares structural similarity to ancestral TMEM16 lipid channels, and (3) the Cl^--selective pore of TMEM16A is formed - not of pure protein - but is partly composed of lipids. We will then show how this hypothesis explains a number of enigmatic features of TMEM16A currents. Our hypothesis about the TMEM16A pore draws on a new interpretation of TMEM16F structure-function. Although TMEM16F has been shown to be a phospholipid scramblase, it also conducts ions.

81
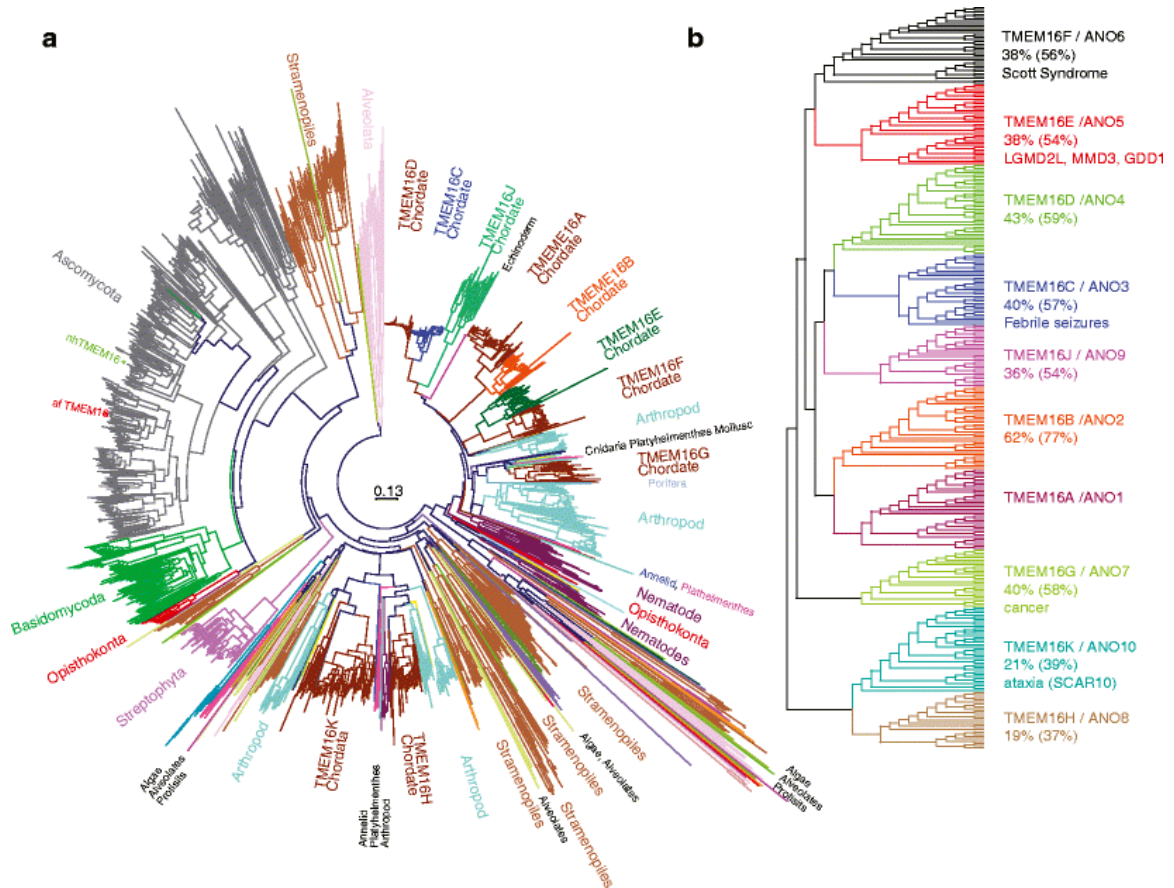
Figure 1 The TMEM16/Anoctamin (ANO) family tree. a A phylogenetic tree generated from 1650 TMEM16 sequences in Uniprot. Non-redundant sequences were aligned by MUSCLE [248] and columns containing >50 % gaps were removed with TrimAl [249]. Phylogenetic trees were constructed by CLCBIO Main Workbench 6.9 using Kimura Neighbor-Joining. The fungal TMEM16 proteins afTMEM16 and nhTMEM16 are indicated. **b** A subset of vertebrate TMEM16 proteins identified by Uniprot were assembled and curated to remove splice variants and duplicate sequences. The sequences were truncated by deleting (~50) variable N-terminal amino acids. Trees were displayed using Dendroscope (http://dendroscope.org/). Percent identity and (similarity) refer to human proteins compared to human TMEM16A. Brief description of known disease relevance follows sequence alignments. (Primary effort on figure Hartzell, HC)

We will review the TMEM16F literature to develop the idea that the TMEM16F ion conduction pathway is physically the same as the lipid conduction pathway. We then suggest that the homologous pathway in TMEM16A has evolved to conduct ions but not lipids.

Phospholipid Scrambling (PLS)

The lipid composition of cell membranes varies, but characteristically the outer leaflet of the eukaryotic plasma membrane is enriched in phosphatidylcholine (PtdCho) and sphingomyelin (SM), while phosphatidylethanolamine (PtdEt), phosphatidylserine (PtdSer), and phosphatidylinositides are almost exclusively retained in the inner leaflet [132, 250-253] (Figure 2). The asymmetric organization of lipid species between leaflets contributes to the physical properties of the membrane, regulates protein function, controls membrane permeability and membrane trafficking, and determines membrane curvature [88, 111, 254-257]. Cells can disrupt this asymmetry by redistributing lipid species between membrane leaflets by phospholipid scrambling (PLS) [111]. At least two independent pathways activate PLS: one is dependent on caspase activity and the other on Ca^{2+} signaling [258-262]. One important consequence of lipid scrambling is the exposure of negatively charged lipid species like PtdSer on the external leaflet of the membrane [260, 262]. Exposed PtdSer acts as a platform for assembly of signaling complexes and plays an essential role in a variety of cellular functions including apoptotic cell recognition by phagocytes [259], the activation of blood platelets where it serves as a catalytic scaffold for the assembly of coagulation factors [258, 263, 264], and the fusion of progenitor cell types to produce multinucleated cells (e.g. muscle fibers [187, 188, 190]) (Figure 2).

83
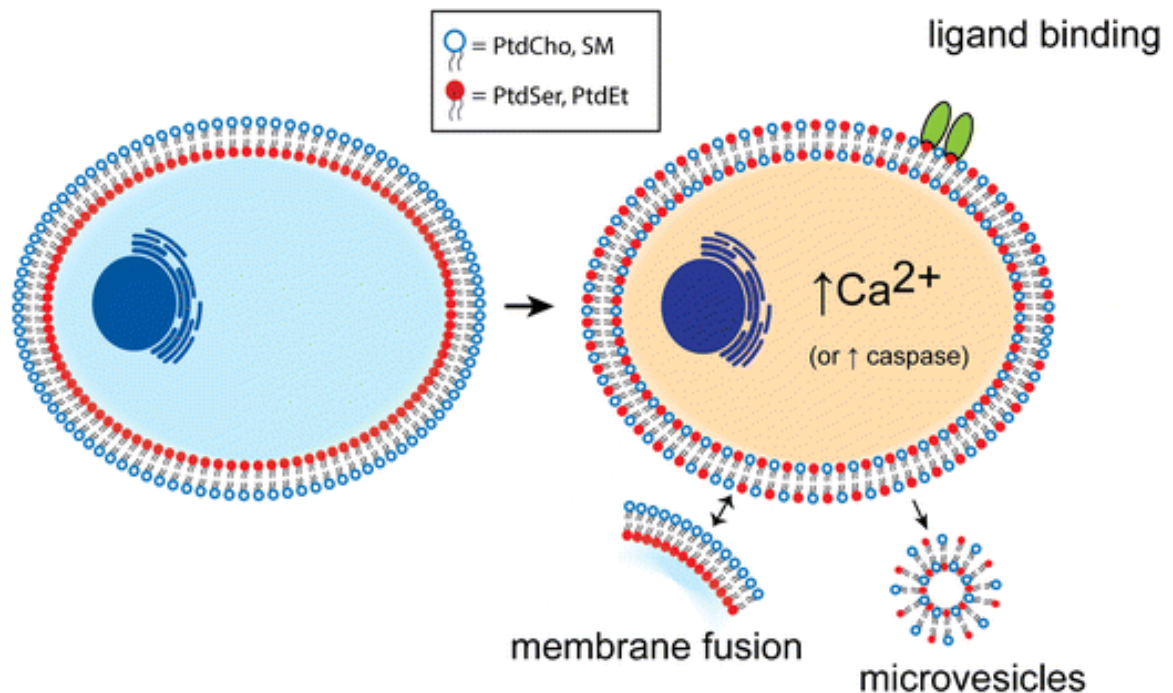
Figure 2 Phospholipid scrambling is a ubiquitous cell signaling process. *Left:* Phospholipids are asymmetrically distributed between the two leaflets of the plasma membrane. PtdCho and sphingomyelin (open blue circles) are concentrated in the outer leaflet while PtdEtn and PtdSer (*solid red circles*) are concentrated in the inner leaflet. *Right:* Phospholipid scrambling stimulated by elevation of cytosolic Ca^{2+} or by apoptotic caspase activation results lipid mixing that exposes PtdSer and PtdEtn on the external leaflet. PtdSer and PtdEt exposure results in assembly of various macromolecular complexes (ligand binding) and membrane trafficking events associated with cell fusion and production of microvesicles [94, 187, 188, 190, 230, 235] (Primary effort on figure Whitlock, JM)

TMEM16 proteins have diverse functions and many are linked to PLS.

Although it was initially assumed that all TMEM16s were CaCCs because of their high sequence similarity and predicted transmembrane topologies, so far only TMEM16A and TMEM16B have been unambiguously shown to be CaCCs [124, 265]. Although it is possible that other TMEM16s may function as CaCCs, possibly in intracellular locations [246], there is growing appreciation for the diverse molecular functions of the TMEM16 family. TMEM16C (57% similarity to TMEM16A) has been identified as a β-subunit of the K^+-activated sodium channel SLACK and has been linked to febrile seizures but elicits no ion channel activity on its own [2, 77]. TMEM16E (54% similarity to TMEM16A) has been linked to several types of muscular dystrophy [8, 198, 266, 267] and bone disease [268], but the molecular function of TMEM16E has not yet been identified. TMEM16F (56% similarity to TMEM16A) elicits Ca^{2+}-activated phospholipid scrambling (Ca^{2+}-PLS) and mutations in the protein cause the congenital bleeding disorder Scott's Syndrome [7, 105, 106]. TMEM16G (58% similarity to TMEM16A) has been suggested to be a cell-cell junction protein in prostate tissue and has been recognized for its potential as a prostate cancer biomarker and immunotherapy target, but its function remains in question [269-271]. TMEM16K (39% similarity to TMEM16A) mutations cause a type of spinocerebellar ataxia (SCAR10) associated with coenzyme Q10 deficiency, but the exact function of this protein remains to be elucidated [272].

There is now growing suspicion that Ca^{2+}-PLS might be a common theme underlying the diverse functions of the TMEM16 proteins. TMEM16C, D, F, G, or J have been reported to elicit Ca^{2+}-PLS [129], suggesting that many of the mammalian TMEM16s may be phospholipid scramblases. Recent studies on TMEM16 homologs in evolutionarily distant species that have only one or two TMEM16 genes have bolstered the idea that a unifying feature of the TMEM16s may be their relationship to lipids. Specifically, the purified and reconstituted solitary TMEM16s from the saprophytic fungi *Nectria haematococca* and

Aspergillis fumigatus both function as phospholipid scramblases [68, 273]. The yeast *Saccharomyces cerevisiae* has one TMEM16, IST2, that is essential for the formation of cortical ER, a structure that plays vital roles in the trafficking of lipids from the endoplasmic reticulum to the plasma membrane [78, 79, 274]. The nematode *C. elegans* has two TMEM16s, one of which is implicated in PLS [109]. The observation that a common function of TMEM16s, especially in "lower" eukaryotes, is lipid-related suggests the possibility that lipid transport may have evolutionarily preceded ion channel function in TMEM16s. In any case, the finding that TMEM16s expressed in such evolutionarily diverse species as human, worm, and fungi function as lipid scramblases suggests the possibility that the entire TMEM16 family - regardless whether they are scramblases or Cl^- channels - may have a specific relationship with lipids.

Phospholipid Scrambling by TMEM16F and homologs.

TMEM16F was identified for its essential role in Ca^{2+}-PLS in an expression-cloning strategy aimed at identifying proteins essential for PLS [7]. Mutations in TMEM16F have been identified as the cause of Scott's Syndrome [7, 102], a congenital bleeding disorder caused by the loss of Ca^{2+}-PLS [105]. Knockout of TMEM16F expression in mice recapitulates the suppression of platelet activation and increased bleeding time observed in Scott's Syndrome patients [100], and primary cells isolated from TMEM16F$^{-/-}$ mice lack Ca^{2+}-PLS [129]. Exogenous expression of TMEM16 C, D, F, G, or J rescues Ca^{2+}-PLS in cells isolated from TMEM16F$^{-/-}$ mice but expression of TMEM16 A, B, E, H, or K does not [129]. Further support for the hypothesis that TMEM16F is a scramblase was provided by our identification of a scramblase domain (SCRD) in TMEM16F that when mutated abolishes Ca^{2+}-PLS [106]. Replacing the homologous sequence of TMEM16A with the corresponding SCRD of TMEM16F causes TMEM16A to elicit Ca^{2+}-PLS.

86

There is not, however, universal agreement that TMEM16F is a phospholipid scramblase. Some investigators maintain that TMEM16F is an ion channel [100, 275-277]. Further, Yang et al. [100] were unable to elicit PLS in HEK cells transfected with TMEM16F, in contrast to our results [106]. We also have been somewhat reluctant to conclude definitively that TMEM16F is the scramblase enzyme, because we found a weak correlation between TMEM16F expression level and PLS activity [106]. However, with the demonstration that purified fungal TMEM16s function as phospholipid scramblases in reconstituted systems [68, 273], it seems hard to avoid the conclusion that certain TMEM16s are phospholipid scramblases.

The mechanism by which lipids traverse the plasma membrane remains an outstanding question. Ca^{2+}-PLS does not require ATP, unlike the flippase and floppase P4-ATPases and ABC transporters that do [278, 279]. Rather, phospholipid scrambling is thought to be driven by downhill flux of lipid from high concentration in one leaflet to low concentration in the other. Scramblases must work differently than ion channel pores, because the permeant molecule (lipid) is amphipathic rather than purely hydrophilic: the routes taken by the hydrophobic acyl chains and the hydrophilic head groups must be environmentally different. Thus, the conduction pathway must somehow accommodate the amphipathic nature of its cargo. One solution would be a hydrophilic furrow in the protein that would allow the head groups to translocate from one side of the membrane to another while the acyl chains remain in the hydrophobic phase of the membrane. Such a model was proposed in 2006 by Pomorski and Menon [111].

Recently, crystallization of a fungal TMEM16 lipid scramblase has provided validation of this model [68] (Figure 3). The protein has a hydrophilic furrow facing the lipid bilayer that is bordered by helices 4 and 6 and connects the cytosolic and extracellular nhTMEM16 domains (Figure 3A, middle panel). Intuitively, this furrow is well-suited for transport of lipids from one leaflet to the other.

87
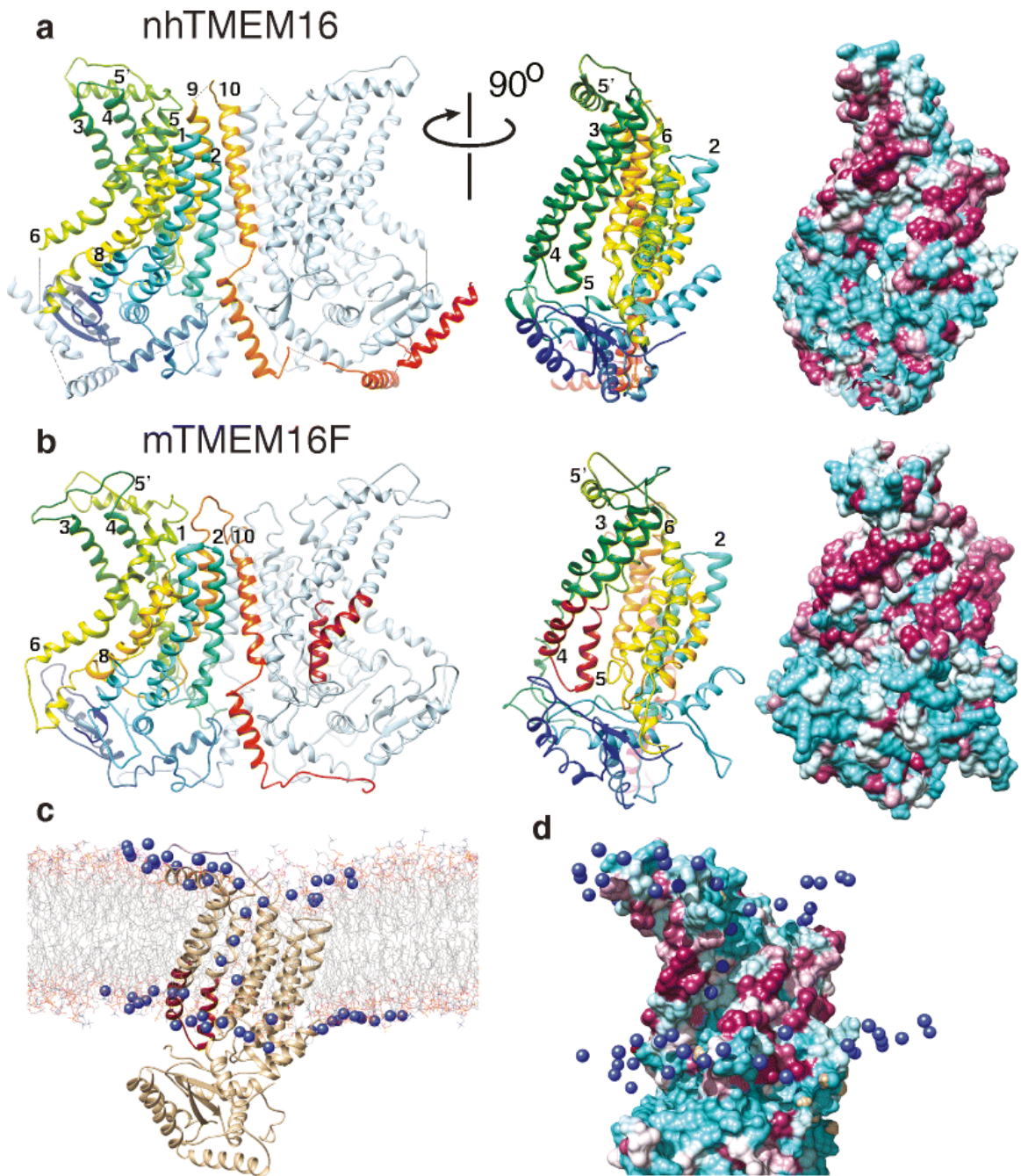
Figure 3 Phospholipid scrambling by TMEM16 proteins. a Crystal structure of

nhTMEM16 [68] (4WIS) and **b** a homology model of TMEM16F based on the

nhTMEM16 structure using Phyre2 [280]. One monomer is colored rainbow (*blue* is N-

terminus, *red* is C-terminus) and the other is *grey- light blue*. Helices are

numbered. *Left panels*: dimer viewed from the plane of the membrane. *Middle panels*:

one monomer rotated 90° around the *y*-axis. The scrambling (SCRD) domain in TMEM16F in B is colored *firebrick red. Right panels:* molecular surfaces of the same view as the middle panel. *Cyan* = hydrophilic (−4.5, Kyte-Doolittle scale). *Magenta* = hydrophobic (4.5). **c** Molecular dynamics simulation of interaction of lipids with nhTMEM16 (http://sbcb.bioch.ox.ac.uk/memprotmd/beta/protein/pdbid/4WIS). A bilayer-embedded model was produced from the nhTMEM16 crystal structure through the MemProtMD protocol [281]. Lipids are shown in wire representation and the nitrogens of the choline headgroups of PtdCho molecules near the protein are shown as *blue spheres*. PtdCho molecules can be seen in the hydrophilic furrow and clustering near the SCRD. **d** Molecular surface of a close-up view of the hydrophilic furrow. The orientation is the same as **c**. Only the N of the PtdCho choline head groups is shown. Images were created using UCSF Chimera v. 1.10. (Primary effort on figure Hartzell, HC)

Mark Samson's laboratory has performed molecular dynamics simulations of nhTMEM16 in a PtdCho bilayer (http://sbcb.bioch.ox.ac.uk/memprotmd/beta/protein/pdbid/4WIS) and has shown that lipid head groups are predicted to populate this furrow, as one would expect if this were a phospholipid conduit across the membrane (Figure 3C,D). Homology models of TMEM16F show a similar hydrophilic furrow (Figure 3B). One side of this furrow is lined by the SCRD we recently identified [106].

TMEM16A may have evolved from phospholipid scramblases.

We hypothesize that the TMEM16A Cl$^-$ channel evolved from an ancestral phospholipid scramblase. The TMEM16 family is functionally split, with TMEM16A and TMEM16B being Cl$^-$ channels and TMEM16C, D, F, and J being scramblases (Figure 1). This functional duplicity is reminiscent of other anion channels that apparently evolved from transporters. CFTR (cystic fibrosis transmembrane conductance regulator) is a Cl$^-$ channel that evolved from ABC transporters [282-284], and the CLC chloride channels CLC-1, CLC-2, CLC-Ka, and CLC-Kb are members of a 9-gene family that includes five H$^+$-Cl$^-$ exchangers [285, 286]. It seems reasonable to speculate that the primordial TMEM16 was a phospholipid scramblase and that "broken" versions of the lipid pathway evolved to become Cl$^-$ channels. Another piece of evidence supporting the idea that PLS is an ancient function of TMEM16s is the finding that the solitary TMEM16 gene in two different fungi encodes phospholipid scramblases [68, 273].

Regardless whether TMEM16 Cl$^-$ channels evolved from lipid scramblases or scramblases evolved from Cl$^-$ channels, the sequence similarity of these proteins suggests that both channels and scramblases interact with lipids in particular ways. Within their transmembrane domains (which would be the likely sites of protein-lipid interaction) the Cl$^-$ channel TMEM16A is 51% *identical* to the phospholipid scramblase TMEM16F. Moreover, the finding that we can convert TMEM16A into a scramblase by replacing ~15

90

amino acids of TMEM16A with aligned amino acids of TMEM16F [106] emphasizes that the architectures of the two proteins are likely very similar.

The proteolipidic pore hypothesis.

If the architectures of TMEM16A and TMEM16F are alike, their interactions with lipid are probably similar, even though TMEM16A does not appear to transport lipids. From mutagenesis experiments on mammalian TMEM16F [106] and the x-ray structure of the *N. haematococca* TMEM16 phospholipid scramblase [68], there is good reason to believe that lipid scrambling occurs by a flipping of lipid head groups through the hydrophilic furrow running between the cytosolic and extracellular domains of the TMEM16 protein. As described in more detail below, ionic currents that have been associated with TMEM16F are likely leak currents flowing through this furrow concurrent with phospholipid movement. We suggest that in TMEM16A, the Cl^- permeation pathway is structurally cognate to the hydrophilic furrow in TMEM16F. This idea is illustrated in Figure 4 which shows how we imagine ions and lipids move in TMEM16F and TMEM16A. We suggest that TMEM16 Cl^- channels might have evolved from scramblases if lipid scrambling activity were lost while the ionic leak pathway were retained in some form. This could have occurred in several ways. The hydrophilic furrow could have folded over and narrowed, essentially converting the furrow into a pore that only ions but not lipids could pass. However, formation of an enclosed aqueous channel would presumably require major structural rearrangements. Alternatively, less drastic molecular rearrangements might have conspired to create an aqueous pore if lipid head groups were included as part of the ion conduction pathway. We propose that the TMEM16A protein stabilizes a non-bilayer phase in the membrane so that the two leaflets are continuous (⊃) where they interact with the protein. However, the furrow in TMEM16A is partially obstructed, disallowing the lipids to move through the furrow. The lipid head groups would then provide a hydrophilic environment forming half of the pore and ions could move across the

91

membrane in the "channel" formed between the protein and the lipid head groups. Just as the ionic currents flowing during lipid scrambling in TMEM16F likely represent leak of ions around the lipid-protein interface, the ions would flow through TMEM16A in the analogous space with the lipids playing a structural role. This proposed pore structure explains a number of unusual features of the TMEM16A currents, especially their pharmacology and ionic selectivity.

TMEM16F conductance is a non-selective leak through the hydrophilic furrow.

Our reasoning that the TMEM16A ionic current occurs through a proteolipidic pore is partly inspired by the conclusion that ionic currents in TMEM16F represent leak of ions through the space between the scrambling lipid and the protein. The nature of the TMEM16F ionic current has been a matter of considerable confusion in the literature. It has been reported to be a non-selective cation channel [100, 287], a swelling-activated Cl⁻ channel [288], an outwardly-rectifying Cl⁻ channel [276], a CaCC [277, 289, 290], and a CaCC of delayed activation [275]. We think that this diversity of opinion is explained partly by the parable of six blind men describing an elephant: overall, the data support the conclusion that TMEM16F has a non-selective pore. But, additionally, this diversity may be explained if the TMEM16F pore can exist in multiple open conformations – a restricted conformation and a dilated conformation. In the dilated conformation, the pore is likely to accommodate ions as large as NMDG$^+$ and aspartate having a minimum diameter of ~6 Å. Such dilation might be more easily accomplished in a channel with a flexible relationship with lipids than in a proteinaceous pore that is constrained by the secondary and tertiary structure of the protein. There is precedent for this idea: certain TRP channels have been shown to have at least two distinct open states, a restricted and a dilated state (e.g., [291]). The restricted state is a non-selective cation channel, whereas the dilated state allows flux of much larger molecules (MW>500).

TMEM16F conducts anions. Studies that have concluded that TMEM16F is a Cl⁻ channel

show clearly that it conducts anions, but cation permeability was not rigorously examined. For example, Martins et al. [276] suppose that TMEM16F is a Cl^- channel because the current is blocked by classical anion channel blockers and because a mutation (Y405F) in the putative pore domain shifts the IV curve as if the relative cation:anion permeability increased. However, the authors do not test whether the E_{rev} of the wild type TMEM16F current changes with $[Cl^-]$ [288] according to the GHK equation nor do they analyze quantitatively how the Y405F mutation alters cation:anion permeability. Shimizu et al. [277] argue that TMEM16F is Cl^--selective because switching from Na^+ to $NMDG^+$ does not alter E_{rev}. However, this conclusion depends on the assumption that $NMDG^+$ is impermeant, which other authors contest (see below). Grubb et al. [275] assume that TMEM16F is an anion channel, despite their finding that $P_{Na}:P_{Cl} = 0.3$, because they believe that Na^+ does not utilize the same pore as anions. They reason that Na^+ takes a different path than anions because TMEM16F exhibits selectivity among anions: selectivity follows the Eisenman type 1 sequence $SCN^- > I^- > Br^- > Cl^-$. They assume that such a selectivity filter would likely exclude cations. In Eisenman's theory [292], selectivity sequences are the result of two competing phenomena, the attraction of the ion into a charged binding site and the energetic dehydration penalty for entering the binding site. The type 1 series implies that permeability is dominated by the second of these phenomena – the relative energetic ease with which waters are removed from the ion. While such a mechanism may explain anion selectivity, it does not rule out cations permeating by the same pathway. Indeed, because the ionic radius of Na^+ is about half that of Cl^- (1.0 Å vs 1.8 Å) it is even possible that Na^+ could permeate the channel in a partially hydrated state.

TMEM16F also exhibits significant cation permeability. Although TMEM16F may exhibit selectivity among anions, four different labs that have examined cation permeability conclude that TMEM16F also conducts cations, although there is considerable

disagreement quantitatively. P_{Na}:P_{Cl} has been measured to be 0.3 [275], ~0.5 [293], 1.4 [106], and 6.7 [100]. Indeed, Yang et al. [100] labeled TMEM16F a Ca^{2+}-activated non-selective cation channel because the reversal potential does not shift when NaCl is replaced with Na-MES, but this conclusion depends on the assumption that MES^- is impermeant, which, as discussed below, may be untrue. In any case, the 20-fold range in P_{Na}:P_{Cl} ratios reported in the literature suggests that TMEM16F has a highly variable personality. We contend that one explanation for this may be related to the lipid composition of the membrane. Because the ionic current activates coincidently with phospholipid scrambling [106], the biophysical features of the current may depend on which lipids happen to be scrambling and the charge of the lipid head groups that are engaged.

TMEM16F has a large pore. Two labs have found that $NMDG^+$ is permeant through TMEM16F channels: Yu et al. [106] find P_{NMDG}:P_{Cl} = 0.5, while Yang et al. [100] report P_{NMDG}:P_{Cl} ~ 2. $NMDG^+$ has dimensions of 5.5 Å × 6.0 Å × 11.7 Å and an estimated minimum diameter of 6 Å [291]. Furthermore, two labs report that the channel is significantly permeable to aspartate (P_{Asp}:P_{Cl} = 0.5), which has an estimated minimum diameter of 5.1 Å [275, 277]. If TMEM16F is permeable to $NMDG^+$, it is likely also permeable to MES^-, which has the same molecular mass. If MES^- is permeant, this might explain why Yang et al. [100] conclude TMEM16F is a cation channel. In contrast, Grubb et al. (2013) propose that $NMDG^+$ is impermeant, because E_{rev} = E_{Cl} with 100 mM Cs-aspartate + 40 mM CsCl inside and 140 NMDG-Cl outside and the IV curve is described by the GHK equation [275]. However, the conclusion might be compromised if $NMDG^+$ and Cs^+ are also permeable. Our review of the literature leads us to conclude that TMEM16F is relatively ion non-selective and that the pore diameter may be >6 Å. This argument leads us to propose that TMEM16F ionic currents are caused by a leak that occurs while lipids are being transported (Figure 4A).

94
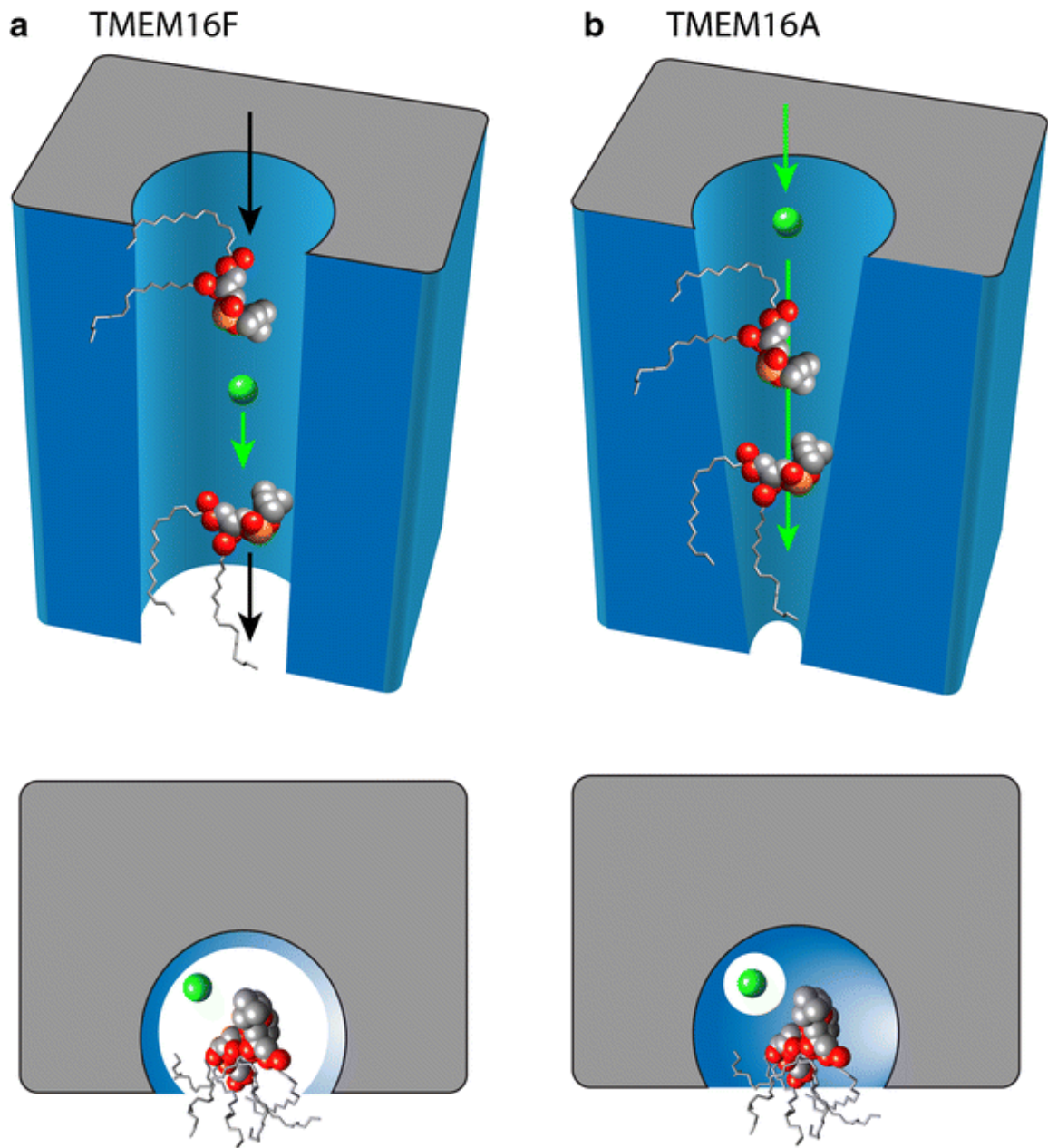
Figure 4 Hypothesis for evolution of a Cl⁻ channel from a phospholipid

scramblase. As discussed in the text, we believe that PLS mediated by TMEM16F is

associated with leakage of ions through the lipid scrambling pathway (the hydrophilic

furrow) between the protein and the scrambling lipid head groups. Structural changes

in the phospholipid scrambling pathway during evolution may have produced a

Cl⁻ selective channel by decreasing phospholipid mobility in the furrow while still

retaining the association of the head groups with the protein as a structural component. In this case, ions would still be capable of flowing between the lipid head groups and the protein. Ionic selectivity would be determined by both the protein and cognate phospholipids. **a** Cartoon of the scrambling furrow showing TMEM16F scramblase. *Top panel* is viewed in perspective from the plane of the membrane. *Bottom panel* is a view down the furrow from the extracellular space. Two PtdCho molecules are shown moving through furrow along with a Cl$^-$ ion. The phospholipids are shown with their acyl tails in stick representation projecting into the hydrophobic bilayer. The polar head group atoms are shown as spheres with the atoms colored by element (*grey* = carbon, *red* = oxygen, *orange* = phosphorous). **b** Cartoon of TMEM16A. Two PtdCho molecules are lodged in the furrow because it is too narrow for them to move. However, Cl$^-$ ions can slip between the lipid head groups and the protein. The effective diameter of the "pore" is imagined as smaller in TMEM16A than TMEM16F as seen in the lower panels. Although only 2 phospholipid molecules are shown, we calculate that the furrow is filled with 4–5 phospholipid molecules creating a monolayer that joins the outer and inner leaflets. (Primary effort on figure Hartzell, HC)

As reviewed above, lipid transport in nhTMEM16 is thought to occur via the hydrophilic furrow that is bordered by TMD4 and TMD6. We propose that ions also flow through this pathway coincident with lipid movement.

Fungal afTMEM16 has a large, lipid-dependent, non-selective ion conductance.

afTMEM16 reconstituted into lipid bilayers exhibits a single channel conductance of ~300pS and is poorly ion-selective (P_K:P_{Cl} = 1.5). The estimated pore diameter is 8 - 13 Å [273]. Malvezzi et al. suggest that afTMEM16 has separate pathways for ions and lipid because they can separate PLS and ionic currents. For example, ionic currents were not observed when afTMEM16 was reconstituted with a lipid mixture of POPE:POPG (3:1), whereas currents were observed in more complex lipid mixtures containing *E. coli* polar lipids. In contrast, PLS was similar regardless of lipid composition. These studies further showed that PLS was not dependent on ionic current by replacing K^+ with presumably impermeant $NMDG^+$. This ability to separate ionic currents from PLS suggests that the ions and lipids take different pathways. However, an equally probable explanation is that, depending on the species of lipid present, the conformational packing of the protein and lipid differs in a manner that essentially seals the lipid transport pathway so that ionic leak is minimized. In contrast to afTMEM16, Brunner et al. report that nhTMEM16 does not exhibit ionic currents when reconstituted in *E. coli* polar lipids and egg PtdCho [68]. One possible explanation of this result is that the lipids chosen for reconstitution may have not been the "correct" ones that support nhTMEM16 ionic currents. Brunner et al. also were unable to find currents when they expressed nhTMEM16 in HEK cells, but the protein did not appear to traffic well to the plasma membrane.

Cl^- conduction through TMEM16A occurs via the hydrophilic furrow.

We constructed a homology model of TMEM16A based on the fungal nhTMEM16 structure. Although the extracellular and intracellular domains are not well modeled, the

transmembrane domains are modeled with high confidence [106]. These models show that TMEM16A has a hydrophilic furrow that resembles nhTMEM16 (and our TMEM16F homology model) with the exception of the presence of a hydrophobic patch at the cytoplasmic end of the furrow (Figure 5A, B). This patch might explain why TMEM16A is not a scramblase, because these hydrophobic amino acids might provide a barrier for movement of the hydrophilic head groups through the furrow.

Mutagenesis of TMEM16A has revealed a number of amino acids that participate in the Cl⁻ conduction pathway. Below we summarize these data and show that it is likely that these residues are located along the hydrophilic furrow. Using cysteine accessibility mutagenesis, we identified a number of amino acids between G628 and Q637 in TMEM16A that we predicted comprise the vestibule of the pore [141]. We considered that these amino acids were located in the vestibule because cysteine-reactive MTS reagents were able to alter current density and anionic selectivity in cysteine-substituted TMEM16A channels. In addition, Peters et al. [294] identified 4 basic residues equivalent to R515, K603, R621, and R788 that alter anion selectivity similarly to those we found in the vestibule. The mutations also change the sensitivity of TMEM16A to two newly-described blockers, NTTP and 1PBC, that block the channel in a weakly voltage dependent manner (δ ~ 0.1). When mapped onto an TMEM16A homology model based on the nhTMEM16 structure, all of these amino acids cluster at the top of the hydrophilic furrow that is analogous to the presumptive lipid transport furrow in nhTMEM16 (Figure 5C, D, orange spheres). These data strongly indicate that the Cl⁻ conduction pathway of TMEM16A includes the hydrophilic furrow.

Another residue that has been implicated in TMEM16A ionic selectivity is K588 [100]. This amino acid is located at the N-terminus of the SCRD-homology domain that we identified and lies in the hydrophilic furrow [106] (Figure 5C,D, dark blue spheres). The K588Q

mutation almost doubles the relative Na$^+$ permeability (P_{Na}:P_{Cl} increases from 0.14 to 0.24).
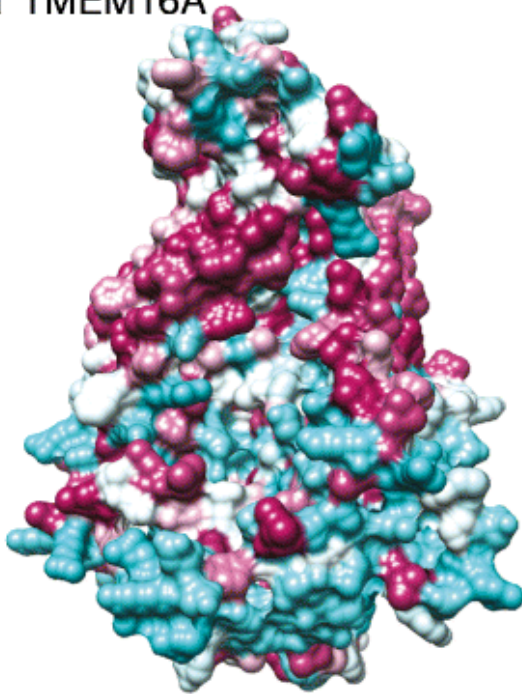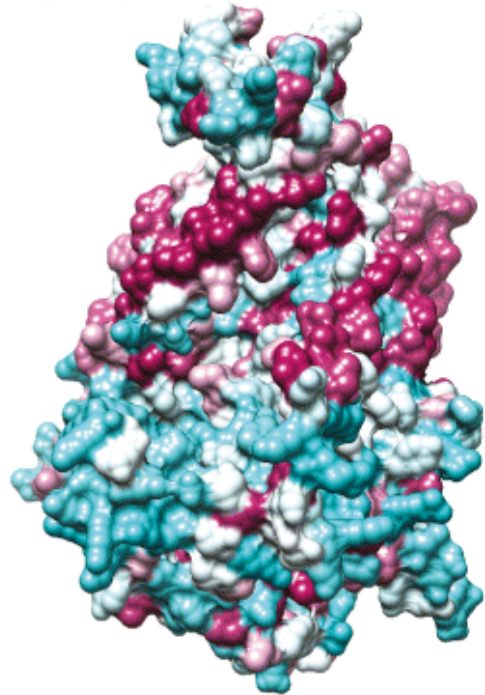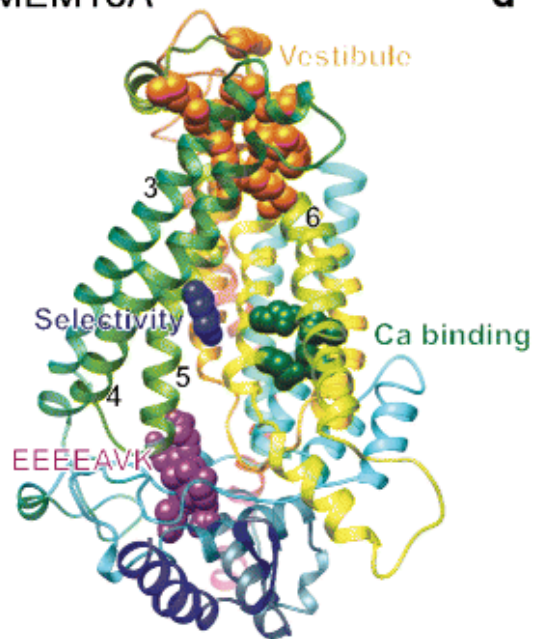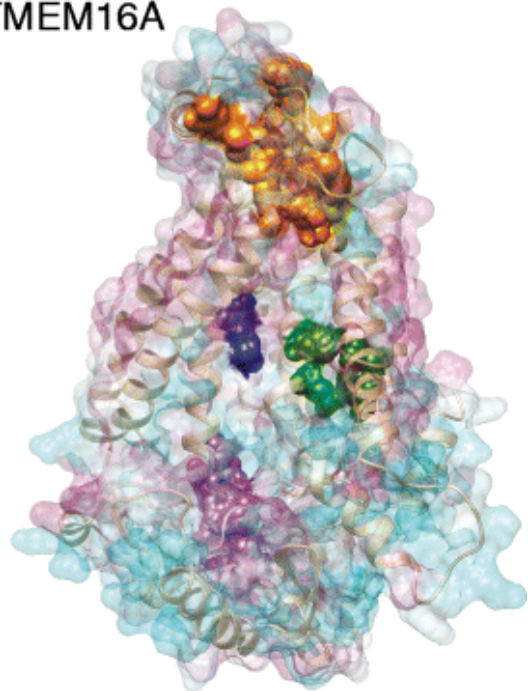
Figure 5 The TMEM16A furrow likely forms the conduction pathway for Cl⁻.

Molecular surface of homology models of **a** TMEM16A and **b** TMEM16F. Homology models were made from nhTMEM16 structure (4WIS) using Phyre2 [280]. *Cyan* = hydrophilic (−4.5, Kyte-Doolittle scale). *Magenta* = hydrophobic (4.5). Note hydrophobic region at the base of the furrow in TMEM16A that is hydrophilic in TMEM16F. **c** Functional residues of TMEM16A. Homology model of TMEM16A with functional amino acids identified by mutagenesis shown as spheres. *Orange*: vestibule [141, 294]. *Blue*: selectivity [100]. *Green*: Ca^{2+} binding [100, 141]. *Magenta*: gating modifier EEEEEAVK [295]. Transmembrane helices are colored as in Fig. 3. **d** Model of TMEM16A with a superimposed surface colored by hydrophobicity showing the relationship of the functional residues to the hydrophilic cleft. (Primary effort on figure Hartzell, HC)

The Ca^{2+} binding site that is responsible for activation of TMEM16A is also located at one side of the hydrophilic furrow [106, 140] (Figure 5C, D, green spheres). This suggests that Ca^{2+} may gain access to its binding site by entering the hydrophilic furrow from the cytosolic side. This may explain why the current is outwardly-rectifying at low Ca^{2+} concentrations: negative voltages may effectively pull Ca^{2+} from its binding site. In any case, the location of the Ca^{2+} binding site in the hydrophilic furrow supports the idea that this is a hydrophilic environment that is energetically favorable for occupation by ions.

Finally, we showed that the EEEEEAVK sequence in the first intracellular loop between TMD2 and TMD3 is involved in allosterically regulating channel gating and Ca^{2+} sensitivity [296]. A similar conclusion was reported by Ferrera et al. [297]. This sequence is located at the cytosolic end of the hydrophilic furrow (Figure 5C, D, magenta spheres).

Taken together, these functional residues define the hydrophilic furrow and suggest that Cl^- ions traverse the membrane by way of this furrow. However, this suggestion raises a conundrum because the furrow is essentially a hemi-channel with its open side facing the core of the membrane. If the core of the membrane is composed of hydrophobic lipid acyl chains, as would be the case if the lipid is structured as a bilayer, it is not clear how the furrow would provide a sufficiently hydrophilic environment for Cl^- ions to move. To solve this problem, we propose that the open side of the furrow is filled with hydrophilic lipid head groups that have their acyl chains oriented approximately parallel to the membrane (rather than perpendicular to the membrane as in a phospholipid bilayer). In TMEM16F, we imagine that movement of lipids from one leaflet to the other involves a lipid head groups slipping along the hydrophilic furrow in tight association with one another. In effect, we think that the lipids form a continuous monolayer connecting the inner and outer

101

leaflets with no gaps. The head groups are oriented towards the protein in the furrow while the acyl chains dangle in the hydrophobic phase. In TMEM16A, we imagine that the lipid head groups occupy equivalent locations, but they do not exhibit net movement (scrambling does not occur) due to the inability of the furrow to dilate sufficiently to allow the passage of lipid head groups from one leaflet to another. In our conceptualization, for this furrow to function as a proteolipidic Cl^- selective pore, the lipid head groups must be well ordered, tightly juxtaposed to one another, and in close association. In other words, the polar head groups must completely fill the open face of the furrow, as any gaps would expose permeant ions to the hydrophobic acyl chains that occupy the inner membrane space. Indeed, the amphipathic nature of phospholipids is perfectly suited to form a hydrophilic channel in the lipid bilayer with little energetic penalty for the ion passing along the polar head groups. Despite the restricted dilation of TMEM16A that disallows the exchange of lipid head groups between leaflets, we fancy that there is enough space for Cl^- ions to slip between the protein and the lipid head groups to traverse the membrane (Figure 4B).

We have played with this whim by asking whether it might be possible to construct a TMEM16A pore that is partly composed of lipid. We began by superimposing the homology model of TMEM16A on the molecular dynamics simulation of nhTMEM in a phospholipid bilayer (introduced in Figure 3C, D). In this pseudo-simulation, the lipids that populate the hydrophilic furrow in nhTMEM16 are found along the analogous structure in TMEM16A (Figure 6A, B). Interestingly, there is just sufficient space for a Cl^- ion to fit between TMEM16A and the lipid head groups located in the furrow. Furthermore, even $C(CN)_3$, which we have shown can permeate TMEM16A CaCC channels [298], fits in this space (Figure 6C). When we superimpose the TMEM16F homology model on the MD simulation, we see that the space between the lipids and the furrow in TMEM16F is even larger than it is in TMEM16A. In TMEM16F, this space allows for $NMDG^+$ to fit (Figure 6D),

102

which is consistent with the lesser selectivity of TMEM16F compared to TMEM16A. These

manipulations by no means provide a test of our hypothesis, but simply illustrate the
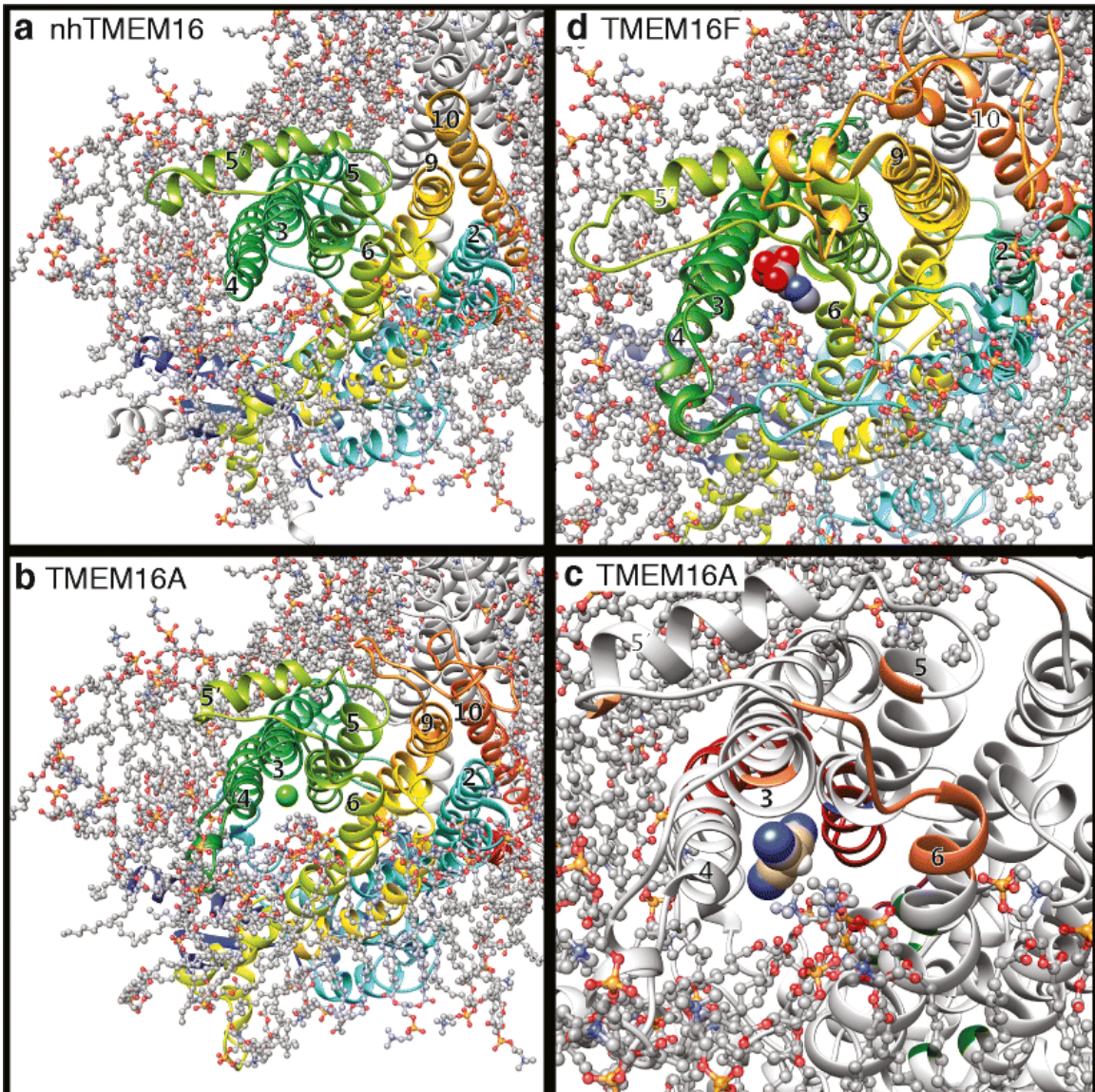
Figure 6 Lipid head groups may form part of the Cl⁻ conductance pathway in

TMEM16A. a Molecular dynamics simulation of nhTMEM16 in a PtdCho bilayer,

viewed from the extracellular space looking down the hydrophilic furrow formed by

transmembrane helices α3, α4, α5, and α6. PtdCho molecules are shown in ball-and-

stick representation colored by element (C=*grey*, *blue*=N, P=*orange*, O=*red*). Lipid

head groups are seen in the furrow. Helices are numbered and colored as in Fig. 3. **b–d** Fantasy models of how ions may permeate TMEM16A and TMEM16F. **b** An homology model of TMEM16A was placed in register with nhTMEM16 using MatchMaker in UCSF Chimera with the Needleman-Wunsch alignment algorithm. The lipids were kept in the same absolute position as in A. The vestibule residues are *red* [129] and *orange* [86]. The Cl⁻ ion (*green*) was added to scale to show that it can fit between the lipid head groups and the protein. **c** Tricyanomethanide ($C(CN_3)$) was positioned manually in the TMEM16A homology model. Functional residues are colored as in Fig. 4: the SCRD-homology domain [130] formed by α4 and α5 is *red* and the vestibule residues are *orange*. Although largely obscured by other regions of the protein, the selectivity filter is *blue*, the EEEEAVK sequence is *magenta*, and the Ca^{2+} binding residues are *green*. **d** $NMDG^+$ was placed manually in the pore of the TMEM16F homology model. (Primary effort on figure Hartzell, HC)

possibility that hydrophilic head groups of lipids could form one side of the TMEM16A pore.

In nhTMEM16 and the TMEM16A and TMEM16F homology models, there are no obvious ion conduction pathways other than this one along the furrow. Although there is a large cavity at the dimer interface formed by TMD 3, 5, and 9 on monomer A and TMD 10 of monomer B viewed from the extracellular side of the membrane, this cavity is highly hydrophobic, suggesting that it is unlikely to be the ion conducting pore.

One potential glitch to this interpretation is our observation that a chimeric protein composed of TMEM16A with the 35-amino acids scrambling domain of TMEM16F can exhibit both Cl⁻ selective currents like TMEM16A and non-selective currents like TMEM16F [106]. At low [Ca^{2+}] this chimera exhibits Cl⁻ selective currents similar to TMEM16A, but as [Ca^{2+}] is increased further and Ca-PLS is activated, the currents become non-selective like TMEM16F currents. This finding suggests that the chimeric TMEM16A/F pore can exist in different conformations that allow passage of different sized cargo (Cl⁻ ion vs lipid head group). We surmise that the conformation associated with lipid exchange between leaflets involves dilation of the furrow to allow the passage of a wide range of ionic cargo. In contrast, TMEM16A is unable to dilate sufficiently to allow lipid head group passage but is dilated sufficiently to allow the passage of Cl⁻ and possibly some larger ions.

TMEM16A has low ionic selectivity.

One might expect that a proteolipidic pore constructed in such a way would have relatively low selectivity. Although TMEM16A is colloquially called a Cl⁻ channel, in seems that it is often not especially selective. We have previously shown that CaCC channels encoded by TMEM16A are permeable to virtually all monovalent anions >6 Å in diameter, which

includes organic anions as large as tricyanomethanide, $C(CN)_3$. The relative anionic permeability is related to the energetic penalty of dehydrating the ion [298]. Furthermore, the cation permeability of the channel is relatively large ($P_{Na}:P_{Cl}$ = 0.1) and the channel is measurably, although weakly, permeant to $NMDG^+$ ($P_{NMDG}:P_{Cl}$ = 0.06). We have modeled the pore as a dielectric tunnel with ε = 21 that exhibits some charge selectivity. These data reinforce the idea that the TMEM16A pore has features qualitatively similar to TMEM16F and that Cl^- ions traverse the evolutionary remnants of the phospholipid pathway. Interestingly, TMEM16A reconstituted into liposomes composed of *E. coli* polar lipids and PtdCho exhibits very high selectivity to Cl^- relative to K^+ [299]. Although these authors did not examine the relative permeability to various cations quantitatively, it appears that the reconstituted channel has different selectivity properties than the channel expressed in HEK cells. Whether this is related to the lipid composition or is some feature of the protein or its potential accessory subunits remains to be seen. Although there is the possibility that some of the cation permeability of TMEM16A/B observed in cells could be explained by contaminating currents carried by endogenous channels, this is not obviously supported by any data.

TMEM16A has multiple conducting conformations.

Another important feature of TMEM16A channels is that their permeability ratio changes with time after initiating whole-cell recording and with different [Ca^{2+}], as if the channel has multiple open states [100, 300]. For example, $P_I:P_{Cl}$ = 11 immediately after raising cytosolic Ca^{2+}, but decreases to 7.6 at later times. Furthermore, the relative ion permeabilities are dependent on Ca^{2+} concentration. For example, $P_{SCN}:P_{Cl}$ decreases from ~12 at 400 nM Ca^{2+}, to <6 at 1.7 µM Ca^{2+}. Similar results have been obtained with TMEM16B [301, 302]. Therefore, it appears that the TMEM16A channel has restricted and dilated conducting states. The presence of multiple conducting states with different biophysical properties could explain why different labs report quantitatively different anion permeability ratios for

TMEM16A. If the channel exists in multiple conducting states, it suggests that the pore is rather flexible. Such flexibility might be facilitated by a proteolipidic pore.

One of the most intriguing aspects of CaCCs is that their biophysical properties are dependent on the Ca^{2+} concentrations used to activate them [303]. At low Ca^{2+} concentrations, the currents strongly rectify outwardly and exhibit voltage- and time-dependence, while they are essentially voltage-independent at higher Ca^{2+} concentrations. So striking is this plasticity that, when we first began studying these channels in the mid-1990's, we and others wondered whether CaCCs were comprised of two channels – one channel activated at low Ca^{2+} and another that became active at higher Ca^{2+} [300, 304-306]. In addition to the different biophysical properties of currents activated by different Ca^{2+} concentrations, the pharmacological properties (sensitivity to A9C) and regulation by PKC was reported to be Ca^{2+}-dependent (see [303]). It is likely that this gating behavior is allosterically related to pore dilation. Interestingly, the crystal structure of nhTMEM16 reveals 2 Ca^{2+} ions in each monomer binding site [68]. We have previously shown that the Hill coefficient for current activation by Ca^{2+} increases from 1 at negative potentials to 2 or greater at positive potentials [296, 298]. This raises the possibility that the different conducting/gating states of the channel are related to the number of liganded Ca^{2+} ions.

Although other channels also have multiple conducting conformations, TMEM16A is unusual in the qualitative differences in current properties at different Ca^{2+} concentrations. For example, the conformational changes that occur during KcsA gating are very modest, largely because the way the protein is constructed and anchored in the membrane makes the selectivity filter relatively rigid. This assures that the backbone carbonyl oxygens are positioned at optimal distances to stabilize the permeant K^+ ion. However, the selectivity filter of TMEM16A appears to be much more flexible.

107

NFA

1PBC

NPPB

T16Ainh-A01

Benzbromarone

CaCCinh-01

MONNA

DIDS

Tannic acid

A9C

108
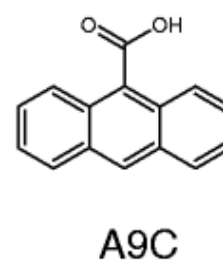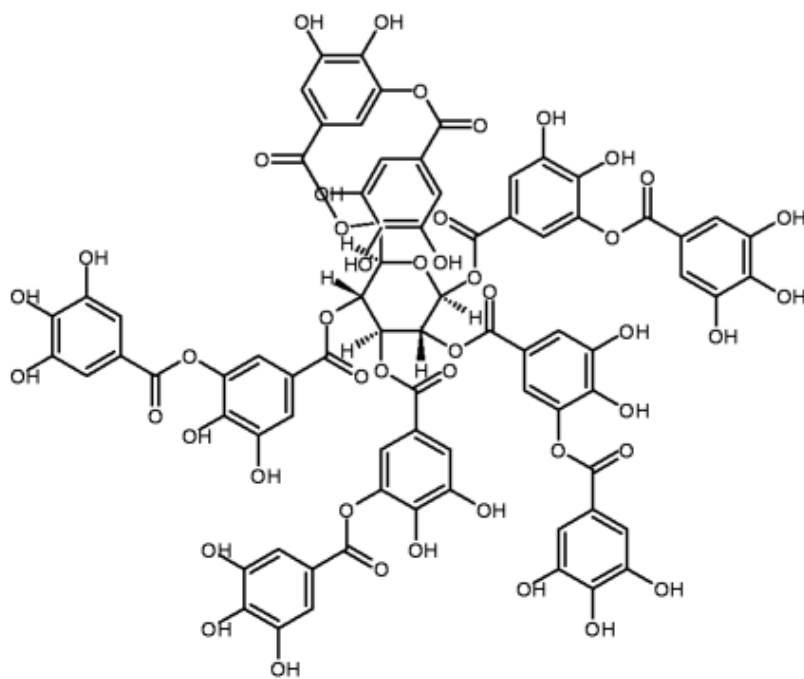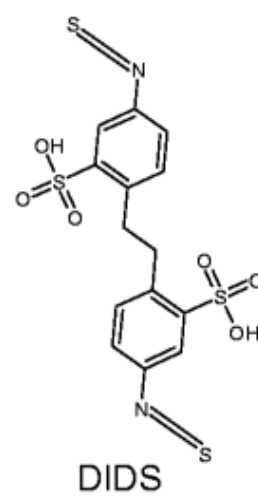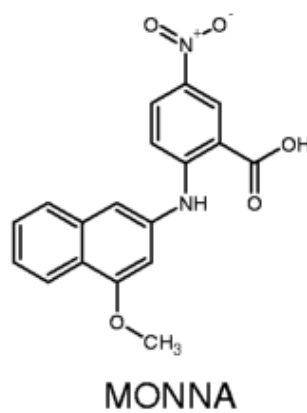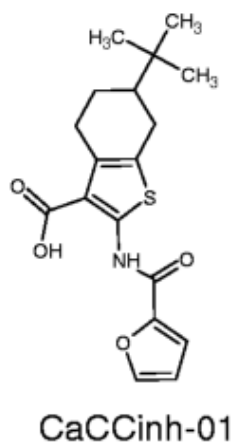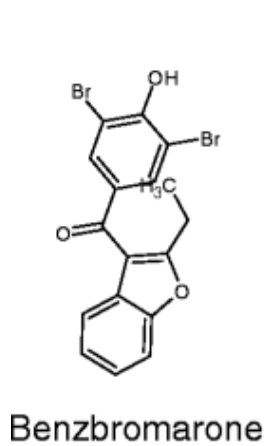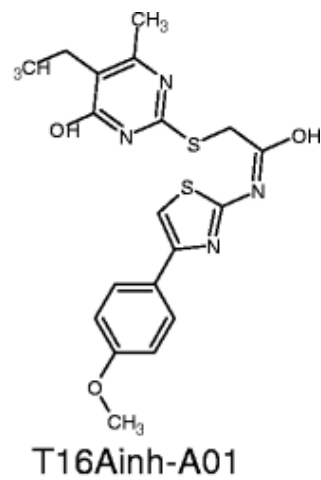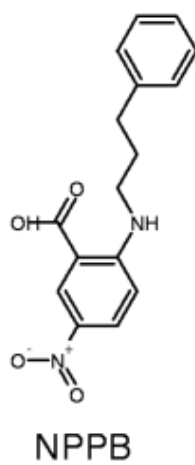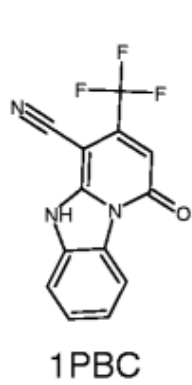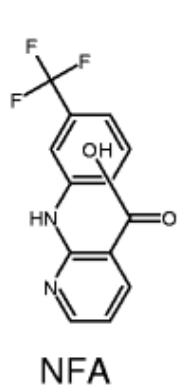
Figure 7 TMEM16A blockers are hydrophobic molecules. The structures include the classical TMEM16A blockers niflumic acid (NFA), anthacene-9-carboxylic acid (A9C), 4,4′-diisothiocyanostilbene-2,2′-disulfonic acid (DIDS), and 5-nitro-2-(3-phenylpropylamino)benzoic acid (NPPB) [52], and more recently identified inhibitors 1PBC [294], T16A$_{inh}$-A01 [307], benzbromarone [121], CaCC$_{inh}$-A01 [308], MONNA [309], and tannic acid [310]. Other blockers not shown are also hydrophobic structures with aromatic rings. (Primary effort on figure Hartzell, HC)

TMEM16A blockers are hydrophobic and a little weird.

Figure 7 shows the structures of some of the most common drugs used to block TMEM16A currents. In all cases, these compounds have at least two aromatic rings and are quite hydrophobic. Although this is a common feature of blockers of all Cl$^-$ channels, not just TMEM16A channels, this suggests that these drugs act in a very hydrophobic domain of the protein, or alternatively, associated lipid. In general these blockers have IC$_{50}$'s in the tens of micromolar range. Blockers that have a potency in the low micromolar range seem to be only partly effective [311]. These large IC$_{50}$'s suggest that the drugs do not have a high affinity binding site in the protein. The mechanisms of channel block have not been unambiguously elucidated for any of these compounds, and it remains unclear whether they block by acting in the permeation pathway or allosterically.

In cases where the pharmacology has been investigated in detail, these blockers have peculiar properties and do not behave like the classical cation channel blockers that we have come to love. For example, although A9C applied to the bath of whole-cells behaves as a classic open pore blocker with voltage- and time- dependence, it paradoxically also blocks at apparently the same site when applied from the cytosolic side in inside-out patches [312]. The same is true of DPC. This suggests that although these drugs do not permeate the channel appreciably, they have access to the blocking site regardless of the side to which they are applied. The classic CaCC blocker NFA is even more weird. It blocks from either the outside or inside with little or no voltage dependence. This would seem to suggest that it blocks allosterically rather than by lodging in the pore. However, block by NFA is reduced by occupancy of the pore by permeating anions [313], which is characteristic of a blocker that competes with the permeant ion in the conduction pathway. Therefore, how does NFA access its binding site from both sides of the membrane and also compete with the permeant ion? Moreover, it has been reported that NFA and A9C

have different effects on inward and outward currents. While NFA blocks outward currents, it slows the voltage-dependent inward deactivating inward tail currents [314].

Perhaps the most puzzling blockers are polyphenols like tannic acid [310, 315]. These very hydrophobic molecules are much too large to enter the pore of the channel. Although they could sit on top of the permeation pathway, it remains uncertain how the hydrophobic tannins would dock on the hydrophilic surface of the channel. More likely, the tannins are binding to lipids. It is known that tannins have both stabilizing and destabilizing effects on model phospholipids and cellular membranes [316]. For example, tannins destabilize phospholipid bicelles by increasing the hydrophobic volume and reducing positive curvature to promote bicelle-to-hexagonal transition [317].

The explanations of these strange effects are not clear, but they challenge the idea that these compounds have a single specific binding site in the TMEM16A protein. The difficulty in interpretation is augmented by the fact that there appears to be serious quantitative disagreement in the literature about the potency of various blockers. The quantitative discrepancies can be illustrated with NFA. NFA has been reported to block native TMEM16A currents with Ki's of 3 – 50 µM. Although these differences might be explained by splice variants or animal species, this is not the whole story. One possible explanation is that these drugs inhibit the channel, not by interacting *only* with protein, but by interacting with lipid. If these blockers act on lipids at sites of lipid-protein interaction, variations in drug efficacy and potency might be explained by differing membrane lipid compositions.

TMEM16A single channels are not well characterized.

Studies in native tissue (*Xenopus* oocytes and arterial smooth muscle) indicate that TMEM16A single channel conductance (γ) is ~ 3 pS with subconductance states [243, 318, 319]. The single channel conductance of recombinant TMEM16A is γ = 3.5 pS measured either by single-channel recording [320] or by noise analysis [287]. These

111

reports conflict with Yang et al. who reported that γ = 8 pS [321]. However, none of these published data on TMEM16A single channels are compelling. There have been no studies showing that mutations in TMEM16A affect single channel conductance or gating; therefore, it remains an open question whether these single channels are actually encoded by TMEM16A or possibly are encoded by upregulated endogenous channels. We made a serious effort over several years to record TMEM16A single channels, and our impression is that the channels exhibit multiple low conductance states (0.5 – 3 pS) that are hard to resolve as discrete opening events and often look like noise. When we found discrete single channels, these were also present in native untransfected HEK cells. The published single channel traces confirm our experience: the traces are generally noisy (not surprising given the low single channel conductance) with multiple sub-conductance states [320]. Although amplitude histograms reveal discrete peaks, these histograms were apparently obtained from idealized traces or records filtered at a considerably lower frequency than the representative traces shown. Data from noise analysis are not convincing [287] because the variance vs. current amplitude plot does not reach a clear maximum, a requirement for extracting γ, and an observation we confirm. The paucity of data on TMEM16A single channel behavior is another limitation in understanding how these channels operate.

The Role of Lipids in Ion Channel Pores

Although the role of lipids in ion channel structure and function is becoming more widely appreciated [322-328], the participation of lipids in the conduction pathway has not been previously suggested to our knowledge. However, the idea that lipids can participate in forming hydrophilic pores in lipid membranes is well-known. Pure lipid membranes can form hydrophilic pores, especially near lipid phase transition temperatures. This can be facilitated by membrane proteins that are unable by themselves to form channels [329, 330]. Pure lipidic pores can exhibit quantized single channel currents that are very similar

112

to ion channel protein single channel currents, except that the lipid pore conductances are frequently much larger. Interestingly, these channels observed in membranes made of cationic lipids are often anion-selective. One way that lipid pores are thought to occur is by formation of non-lamellar structures in the membrane.

Many small pore-forming peptides (PFPs) form aqueous pores by deforming the membrane to elicit the fusion of the inner and outer leaflets creating a proteolipidic channel (reviewed in [331]). These structures are known to form both 'matrix-type' toroidal pores formed by interspersed polypeptide chains and lipids or 'arc-type' pores where one half of the pore is formed by peptide and the other half is complemented by a toroidal arrangement of lipid head groups [332-335]. The formation of toroidal pores is a major function of many antimicrobial peptides in combating bacteria, but it is now recognized that the amphipathic regions of many cellular proteins can also insert into and deform membranes resulting in toroidal pore formation in a manner analogous to the mechanism of pore formation in pure lipid membranes elicited by electrical charge or detergents [336, 337]. Many toroidal pores exhibit anionic selectivity. However, changes in the lipid composition of the membrane can greatly alter the ion selectivity of these structures, in some cases from anion- to cation-selective [338-341]. Interestingly, many descriptions of toroidal pores are accompanied by observations of PLS occurring concurrently with ion conductance [332, 339, 342-344].

We are not suggesting that TMEM16s form toroidal pores, but we believe there are many parallels that can be drawn from the function of these proteolipidic structures and the hydrophilic furrow in TMEM16 proteins. If lipid head groups compose part of the TMEM16 pore, this suggests that the abundance of different lipid species in the protein's resident membrane may contribute to ion selectivity. This could explain the variability observed in TMEM16A ion selectivity from different laboratories, as lipid head groups of various

diameters would likely stabilize alternative dilation states of the TMEM16A pore discussed earlier.

Conclusion.

The ionic selectivity of ion channels is a macroscopic manifestation of the competing interactions between dissolved ions, water, and larger molecular units. In general, our understanding of how anions interact in this context remains less well-developed than that of cations. It may be a truism to say that Cl^- ions have different physicochemical properties than cations, but the differences extend beyond simple electronegativity. The electron affinities of anions are less than those of comparable cations or neutrals [345, 346] and the Cl^- ion is considerably larger than its cation counterparts that are relevant in biology (Na^+, K^+, Mg^{2+}, and Ca^{2+}). Not only does this mean that the pore diameter of Cl^- channels is likely to be larger, the lower charge density of a Cl^- ion is likely to make electrostatic interactions less influential. To overly simplify this point, a single charge distributed over the surface of Na^+ ion of radius 1 Å will have a surface charge density ~3-times greater than a Cl^- ion with a radius of 1.8 Å. This opens the door to selectivity filter designs that operate in ways that differ from those we have come to expect from some cation channels. The reader may decide that our proteolipid pore hypothesis is a very pore idea. However, we believe that this idea is tenable, based on the *in flagrante* liason of lipids with many TMEM16 proteins and what we know about the conductance pathways of TMEM16A and TMEM16F. Furthermore, this proposal may help explain some of the enigmatic features of CaCC currents that have plagued us since early days. Understanding the relation of TMEM16s to lipids and the architecture of their resident membranes is essential to the elucidation of the mechanistic function of CaCCs and should be a major focus of future TMEM16 investigation.

Disclaimer.

Some of the generalizations made here do not take into consideration differences between (1) species, (2) splice variants, (3) native vs. cloned channels. It was assumed that native CaCC currents, like those in *Xenopus* oocytes are encoded by homomeric TMEM16A. All numbering is adjusted to mouse TMEM16A(a,c) sequence, even if experiments were performed on other splice variants or species with different numbering.

Abbreviations.

PLS, phospholipid scrambling; Ca^{2+}-PLS, Ca^{2+}-dependent phospholipid scrambling; PtdSer, phosphatidyl serine; PtdCho, phosphatidyl choline; $NMDG^{+}$, N-methyl_D-glucamine; NFA, niflumic acid; A9C, anthracene 9-carboxylic acid;

Additional Developments

Following the development of our hypothesis that the TMEM16A ion conducting pore is partially composed of lipid head groups, three manuscripts have elucidated the structure of TMEM16A using cryo-electron microscopy. These manuscripts demonstrate a number of characteristics of the TMEM16A CaCC that differ from the nhTMEM16 structure solved previously, however the most obvert difference is that TMD 6, which lines outer porting of the nhTMEM16 scramblase cleft, is in close contact with TMD 4, closing 2/3rd of the TMEM16 ion conducting pore and occluding access to the membrane [70-72]. This closure of the TMEM16A pore is observed in both the Ca^{2+}-bound and Ca^{2+}-free structures solved by two independent groups, strongly suggesting that the TMEM16A pore is not lined by lipid headgroups along its entire length. However, the majority of the predicted ion pore in all the cryo-EM structures of ANO1 to date is too small to allow the permeation of Cl^- or I^-, two anions know to permeate the ANO1 pore from empirical study. Interestingly even in these closed ANO1 structures, the intracellularly facing 1/3rd of the ANO1 ion pore does appear to be open to lipid access by virtue of a gap between TMDs 4 and 6, and investigators did observe distortions in the density associated with the detergent micelle in the structures. An analogous gap is observed in the nhTMEM16 structure that is thought to play a major role in membrane bending that has been implicated in the mechanism of Ca^{2+}-PLS in recent molecular dynamics simulations. Additionally, it is of note that this ANO1 gap is adjacent to the scrambling domain we have identified in TMEM16F and E that is capable of conferring Ca^{2+}-PLS to ANO1. The ability to predict and evaluate the association of lipid headgroups with the ion conducting pore of ANO1 is an active area of investigation in our lab, and the lab is currently employing a variety of molecular dynamics simulations and structure function studies to better characterize the partial occupancy and biophysical consequences of lipid headgroups lining the ANO1 ion conduction pore.

Chapter IV

Identification of a lipid scrambling domain in ANO6/TMEM16F

Summary

Phospholipid scrambling (PLS) is a ubiquitous cellular mechanism involving the regulated bidirectional transport of phospholipids down their concentration gradient between membrane leaflets. Recently, ANO6/TMEM16F has been shown to be essential for Ca^{2+}-dependent PLS, but there is controversy surrounding whether ANO6 is a phospholipid scramblase or an ion channel like other ANO/TMEM16 family members. Combining patch clamp recording with measurement of PLS, we show that ANO6 elicits robust Ca^{2+}-dependent PLS coinciding with ionic currents that are explained by ionic leak during phospholipid translocation. By analyzing ANO1-ANO6 chimeric proteins, we identify a domain in ANO6 necessary for PLS and sufficient to confer this function on ANO1, which normally does not scramble. Homology modeling shows that the scramblase domain forms an unusual hydrophilic cleft that faces the lipid bilayer and may function to facilitate the translocation of phospholipid between membrane leaflets. These findings provide a mechanistic framework for understanding PLS and how ANO6 functions in this process.

Introduction

The transbilayer asymmetric distribution of phospholipids in cell membranes is evolutionarily conserved and essential to cellular physiology. In eukaryotic plasma membranes, the outer leaflet is enriched in phosphatidylcholine (PtdCho) and sphingomyelin (SM) and the inner cytoplasmic-facing leaflet is rich in phosphatidylserine (PtdSer) and phosphatidylethanolamine (PtdEtn) [84, 132, 264, 347]. This asymmetry is established by ATP-dependent lipid flippases, most notably members of the P4 ATPase family [348] and ABC transporters [349], that actively transport phospholipids to one leaflet of the membrane and are important in membrane biogenesis. Phospholipid asymmetry plays critical roles in membrane function in two ways. (1) Charges on the phospholipid head groups bind and regulate protein function. The best known examples may be the effects of phosphatidylinositol bisphosphate (PtdInsP$_2$) on ion channel proteins [350], but PtdSer and PtdEtn play equally important roles [133, 188, 351, 352]. (2) The different molecular shapes (e.g.; cylindrical or conical) of various lipids determine membrane curvature which is key to membrane trafficking and fusion [151, 152, 203, 353].

In opposition to ATP-dependent flippases, ATP-independent phospholipid scramblases (PLSases) facilitate the equilibration of phospholipid distribution between the two membrane leaflets. PLSases play essential roles in the synthesis of glycoconjugates, such as N-glycosylated proteins and GPI-anchored proteins in the endoplasmic reticulum [111]. Moreover, at the plasma membrane dissipation of phospholipid asymmetry by phospholipid scrambling (PLS) is a common cell signaling mechanism [260, 347]. For example, exposure of PtdSer on the external leaflet of the plasma membrane marks apoptotic cells for phagocytosis by macrophages and plays a key role in blood clotting [7, 94, 133, 259, 264, 354, 355]. PtdSer exposure that occurs when platelets sense tissue damage serves as a catalytic surface for assembly of plasma-

borne coagulation factors and a $>10^6$-fold increase in the rate of thrombin formation [278, 356, 357]. PtdSer exposure also plays important roles in developmental processes that involve fusion of mononucleated progenitor cells to form multinucleated cells such as skeletal muscle [188, 190], osteoclasts [123, 230, 358-360] and placental syncytiotrophoblasts [233, 361].

In the simplest conceptualization, PLS is mediated by phospholipid scramblases (PLSase) that are thought to provide, in a manner analogous to ion channels, an aqueous pathway for the hydrophilic phospholipid head groups to flip between the inner and outer leaflets [111, 362]. However, the molecular mechanisms of PLS have remained elusive partly because PLS can be catalyzed by a variety of unrelated proteins. PLS is stimulated by two pathways, a rapid one triggered by increases in intracellular $[Ca^{2+}]$ and a slow caspase-dependent pathway associated with apoptosis [363]. At least four different families of proteins have been implicated in PLS [260, 264, 278]. The first putative phospholipid scramblases (PLSCR1 – PLSCR4) were identified by their ability to stimulate Ca^{2+}-dependent PtdSer scrambling when incorporated into liposomes [364, 365], but the role of PLSCRs in PLS is controversial because these proteins are small calmodulin-like molecules whose disruption in mice, flies, and worms has little effect on PLS [260, 347, 366, 367]. More recently, the Xk-family protein Xkr8 has been shown to be necessary for caspase-dependent PtdSer scrambling that can be rescued by multiple Xkr8 paralogs [93, 261]. Unexpectedly, several G-protein coupled receptors including rhodopsin and the β-adrenergic receptor have also been shown to elicit PLS [368]. Although lipid-translocating ABC transporters and phospholipid synthesis may also play roles in PLS, these processes cannot fully explain PLS [347, 368].

Recently, it has been suggested that some members of the 10-gene Anoctamin (TMEM16) family are PLSases. Evidence supporting a role for ANO6 in PLS includes

120

the findings that (a) mutations in ANO6 produce Scott Syndrome, a blood clotting disorder where platelets fail to expose PtdSer in response to cytosolic Ca^{2+} increases [7, 143, 369], (b) knockout of ANO6 in mice abolishes the ability of cells to expose PtdSer and to scramble other lipid species in response to elevated cytosolic Ca^{2+} while PLS stimulated by the apoptotic Fas receptor is unaffected [7], and (c) over-expression of ANO6 in knockout cells rescues PLS [129]. However, the suggestion that ANO6 is a PLSase is confounded by the fact that other members of the anoctamin family, ANO1 and ANO2, encode the pore-forming subunits of Ca^{2+}-activated Cl^- channels (CaCCs) [44, 119, 124, 244, 321, 370, 371]. It was initially presumed that all ANOs are Cl^- channels because of the close sequence similarity between ANO family members (ANO1 is 38 - 45% identical to ANOs -3 to -7, >90% coverage), however, the requirement of ANO6 for Ca^{2+}-dependent PLS and the ability of ANOs 3, 4, 6, 7, and 9 to rescue this activity suggests functional divergence within the ANO family [7, 129]. Questions remain whether ANO6 is a PLSase itself and/or is an ion channel that regulates PLSase activity [124, 245, 247]. ANO6 has been reported to be a non-selective cation channel [287, 372], a swelling-activated Cl^- channel [288], an outwardly-rectifying Cl^- channel [276], a CaCC [277, 289, 290], and a CaCC of delayed activation [275]. Furthermore, in contrast to Suzuki et al. [7], Yang et al [369] conclude that ANO6 is a regulator of an endogenous PLSase because they find that expression of ANO6 in HEK cells does not cause PtdSer exposure. However, the suggestion that some ANOs are PLSases and are not simply regulators of endogenous PLSases is supported by recent reports that two fungal ANO homologs purified and incorporated into liposomes mediate Ca^{2+}-stimulated PLS [68, 273].

Here we address three questions. (1) Does expression of ANO6 stimulate Ca^{2+}-dependent PLS in HEK cells? We find that ANO6 expression in HEK cells induces robust Ca^{2+}-activated scramblase activity. (2) Is the ion channel activity of ANO6 related

121

to PLS? We find that ANO6 currents are non-selective among ions and are activated simultaneously with PLS. This suggests that ionic currents are a consequence of phospholipid translocation. Chimeric constructs that exhibit PLS also exhibit simultaneous non-selective currents. Furthermore, we find that drugs that block ANO1 currents do not block ANO6 currents or PLS. This is consistent with the idea that the ion conduction pathway associated with ANO6 is unlike the ANO1 pore. (3) What are the domains of ANO6 that are required for phospholipid scrambling? We find that mutating several amino acids in ANO6 between TMD4 and TMD5 eliminates both phospholipid scrambling and ion channel activity. Furthermore, replacing as few as 15 amino acids in ANO1 in the TMD4-TMD5 region with ANO6 sequence confers robust PLS activity on ANO1, which normally does not elicit PLS activity.

Results

ANO6 expression induces robust phospholipid scrambling in HEK cells. We first asked whether ANO6 when expressed heterologously induced PLS in HEK293 cells. Ca^{2+}-dependent PtdSer exposure on the outer leaflet of the plasma membrane was measured by confocal imaging of two PtdSer probes, either LactoglobulinC2 fused to Clover fluorescent protein ("LactC2") or Annexin-V conjugated to AlexaFluor-568 ("Annexin-V") [373-375]. Our initial experiments employed LactC2 with a clonal cell line stably transfected with mANO6-FLAG$_{3X}$. 100% of the cells express ANO6-FLAG$_{3X}$ as shown by staining with anti-FLAG antibody (Figure 1A). Intracellular Ca^{2+} was elevated by incubation of the cells in 10 μM A23187 in nominally zero Ca^{2+} solution followed by washout of A23187 and addition of 5 mM Ca^{2+} to initiate Ca^{2+}-dependent PLS. Twelve minutes after adding Ca^{2+}, ~92% of the cells (N = 404) showed LactC2 binding to the surface (Figure 1B,G). In contrast, little or no LactC2 binding was seen in the parental cell line (0.2% positive cells, N = 724) or in ANO1-FLAG$_{3X}$-expressing cells (8% positive cells, N = 316) (Figure 1D,E,G). The difference in PLS observed with ANO1 and ANO6

122

expressing cells was not explained by differences in expression as shown by western

blot (Figure 1F). These data show clearly that ANO6 expression facilitates PLS.

However, the finding that a small fraction (8%) of ANO6-FLAG$_{3X}$ expressing cells do not

exhibit PLS raises the possibility that ANO6 may not be sufficient for PLS and may

require additional components.

An advantage of LactC2 is that it does not require Ca^{2+} to bind PtdSer [373, 375], so we

were able to use it to test whether ANO6-elicited PtdSer exposure requires Ca^{2+}. ANO6-

FLAG$_{3X}$ cells exposed to A23187 without addition of Ca^{2+} exhibited no detectible LactC2

binding over 15 min, whereas subsequent addition of Ca^{2+} stimulated robust LactC2

binding (Figure 1E). Next, we compared LactC2 and Annexin-V as probes for PLS. The

percentage of cells stained with Annexin-V and LactC2 were the same, however, the

kinetics of binding of the two probes were markedly different. After elevating cytosolic

Ca^{2+}, Annexin-V fluorescence increased mono-exponentially with a mean $\tau = 143$ sec (7

separate experiments, χ^2 of fit = 0.03) and approached a plateau within less than 10 min

(Figure 1H). In contrast, the time course of LactC2 binding was significantly slower (5

separate experiments, $\tau = 433$ sec, χ^2 of fit = 0.02). LactC2 binding exhibited a lag period

of 1 – 2 min before binding was detectable. One potential explanation of the difference in

Annexin-V and LactC2 time courses may be related to the fact that LactC2 prefers

binding to oxidized PtdSer [376]. Because Annexin-V binds with more rapid kinetics, the

rest of the experiments shown here were performed using Annexin-V.

Because all of the cells in the clonal cell line express ANO6-FLAG$_{3X}$ at about the same

level, we turned to a polyclonal cell line stably expressing ANO6-EGFP to evaluate the
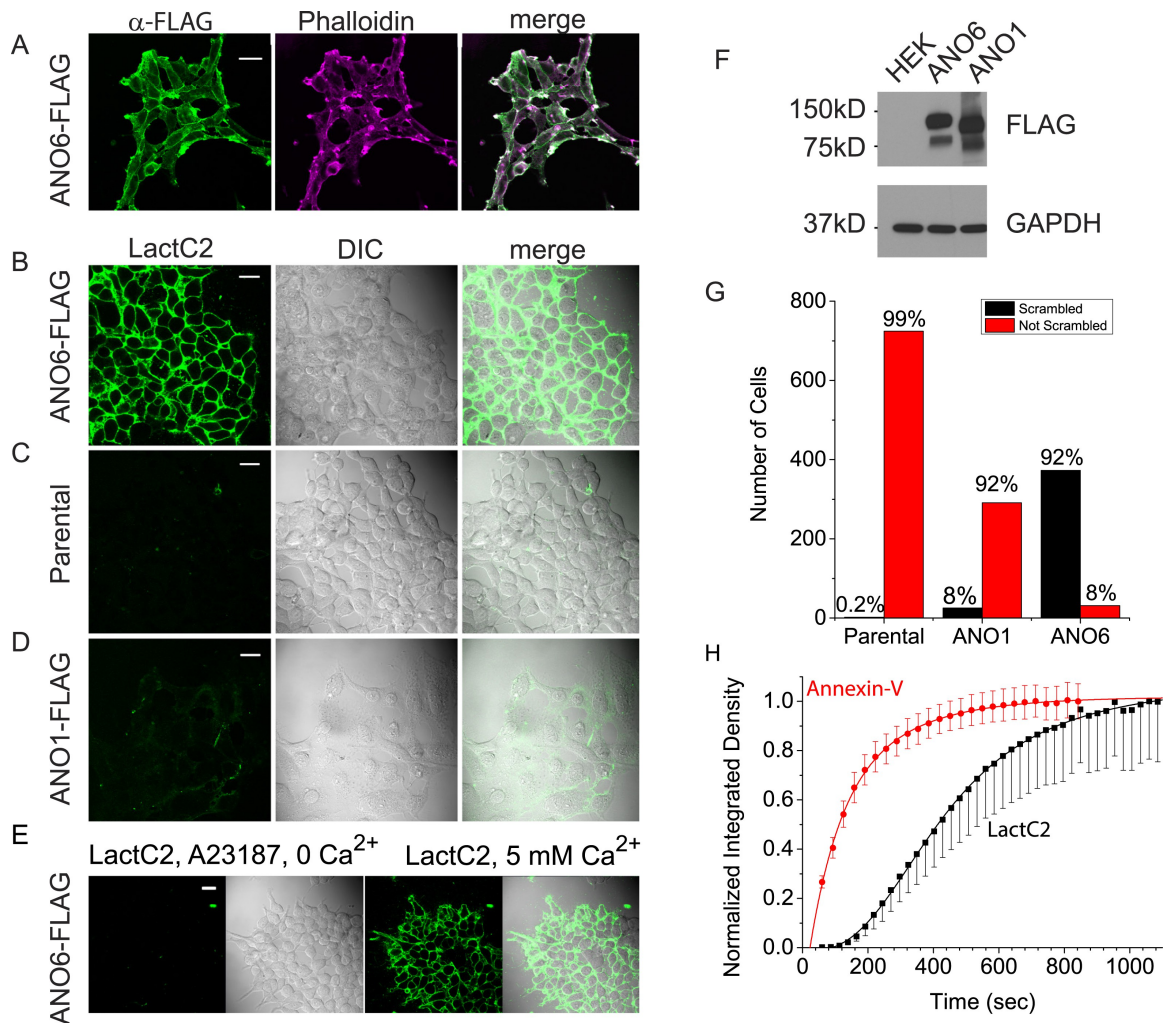
Figure 1 Expression of ANO6 in HEK cells stimulates Ca^{2+}-dependent phospholipid scrambling (PLS). (**A**) Images of HEK cells stably transfected with ANO6-FLAG$_{3X}$ fixed and stained with anti-FLAG (green) and phalloidin (magenta). (**B**–**D**) Images of live cells after exposure to 10 μM A23187 in zero-Ca^{2+} solution for 5 min followed by solution containing 5 mM Ca^{2+} and 3 μg/ml LactC2-Clover for 12 min as described in 'Materials and methods'. Green channel: LactC2-Clover. DIC channel: differential interference contrast. (**B**) HEK cells stably expressing ANO6-FLAG$_{3X}$. (**C**) Parental HEK cells not expressing ANO6. (**D**) HEK cells stably transfected with ANO1-FLAG$_{3X}$. (**E**) A23187 in zero Ca^{2+} does not stimulate LactC2 binding. The first two panels show LactC2-Clover binding in cells incubated in A23187 in zero Ca^{2+} containing LactC2

124

for 15 min. The second two panels show the same cells 10 min after adding 5 mM Ca^{2+}.

(**F**) Level of expression of ANO1 and ANO6 in stably expressing HEK cells. Extracts of cells in **B**–**D** were immunoblotted with anti-FLAG and anti-GAPDH to quantify protein expression. (**G**) Numbers of cells binding Annexin-V ('scrambled') or not binding Annexin-V ('not scrambled') for parental HEK cells, ANO6-FLAG$_{3X}$, and ANO1-FLAG$_{3X}$ expressing cells. (**H**) Time course of Annexin-V and LactC2 binding to HEK cells expressing ANO6-FLAG$_{3X}$. Images of the same field of 30–100 cells were acquired at ~20 s intervals. Annexin-V: mean ± SEM of seven independent experiments, LactC2: mean ± SEM of five independent experiments. Means at the end of the recordings were normalized to 1. Scale bars = 20 μm. (Primary effort on figure: (A-E and G) Whitlock, JM; (F) Yu, K; (H) Hartzell, HC and Whitlock, JM)

125

relationship of ANO6 expression to the rate and extent of Annexin-V binding (Figure 2). In the polyclonal line, ANO6-EGFP expression level was variable and 85% of ANO6-EGFP cells exhibited PLS (N = 180). This percentage may be lower than the ANO6-FLAG$_{3X}$ clonal line because some ANO6-EGFP positive cells may have lower expression than the ANO6-FLAG$_{3X}$ cells. There was a direct relationship between the level of ANO6-EGFP expression and the level of Annexin-V binding 10 min after elevating cytosolic Ca^{2+} (Pearson correlation coefficient = 0.84) (Figure 2C), however there was considerable variation around the fitted relationship, with some highly-expressing ANO6 cells showing little Annexin-V binding and low-expressing cells showing high levels of binding. The rate of Annexin-V binding was similar among cells (τ in this experiment ranged from 152 – 229 sec), but the plateau level of Annexin-V binding attained after 12 min varied markedly among cells. Neither the rate nor the plateau level of binding correlated with the level of ANO6-EGFP fluorescence. This lack of correlation may reflect an inability to distinguish between ANO6-EGFP located on vs. adjacent to the plasma membrane or may reflect heterogeneity in the expression of other components required for PLS.

ANO6 current activates in parallel with PLS. The next question that we sought to answer was whether the ionic current that has been associated with ANO6 [275-277, 288-290, 372, 377] is linked to PLS or is an independent function of the protein. We patch-clamped HEK cells transiently expressing ANO6-EGFP and recorded ANO6 currents while simultaneously imaging Annexin-V binding. A typical experiment is shown in Figure 3A with average results in Figure 3B-C. After establishing whole-cell recording, the time course of activation of membrane currents in ANO6-expressing cells was very slow even when the patch pipet solution contained high (200 µM) Ca^{2+}.

EGFP   Annexin   Merge w/DIC

A   ANO1-EGFP   ANO1   Annexin-V

B   ANO6-EGFP   ANO6   Annexin-V

C

D
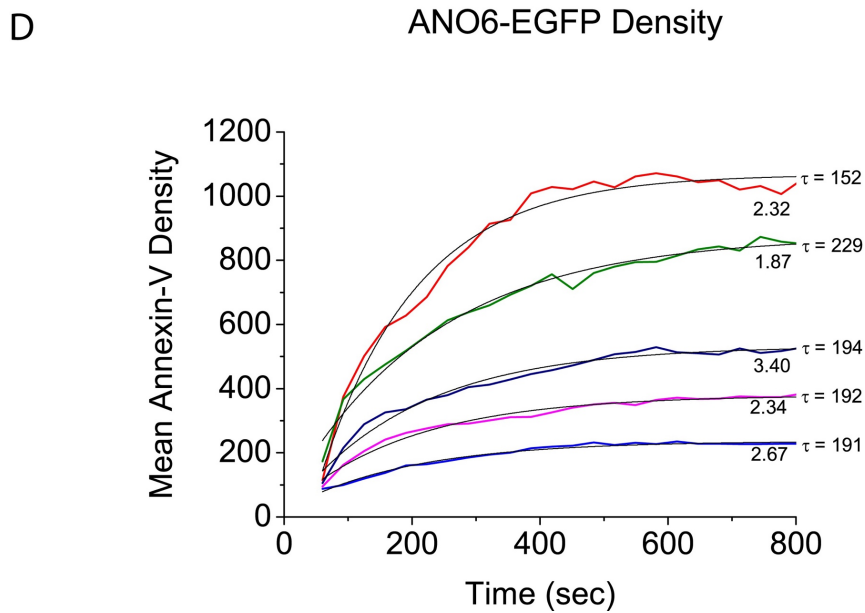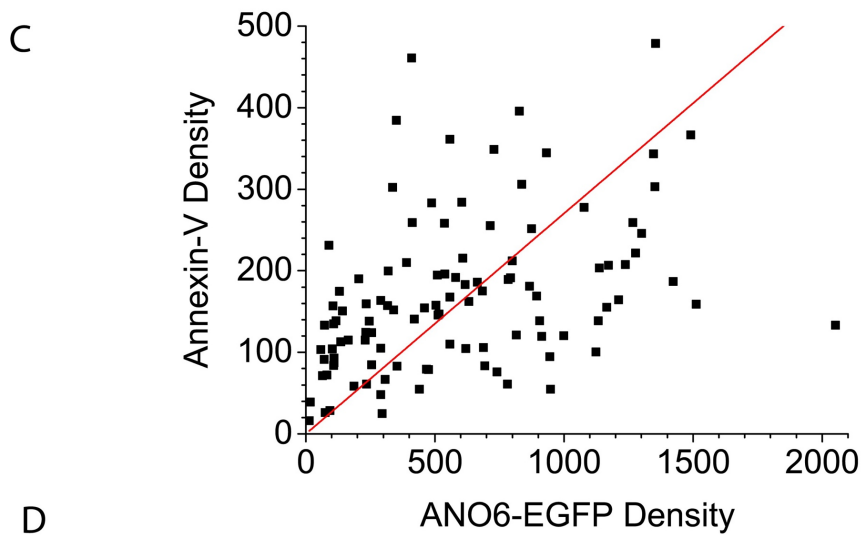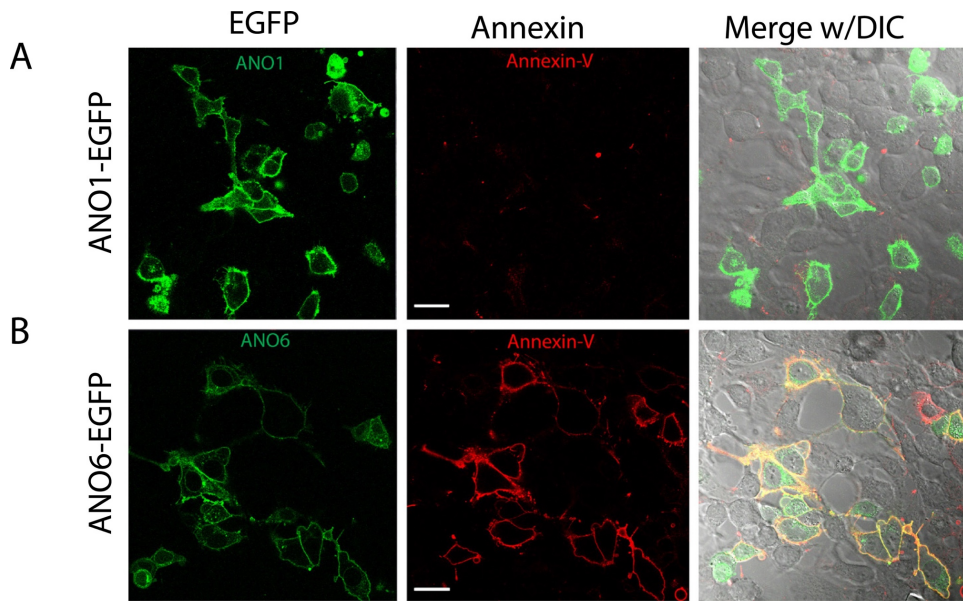
Figure 2 Characteristics of PLS linked to ANO6. Intracellular Ca^{2+} was elevated by A23187, as in Figure 1, in polyclonal lines of HEK cells expressing (**A**) ANO1-EGFP or (**B**) ANO6-EGFP. (**C**) The relationship between ANO6-EGFP expression (mean EGFP pixel density of each cell) and AnnexinV-Alexa568 binding (mean pixel density in the Annexin-V channel masked by the EGFP channel). The line is the best fit to a straight line with Pearson's correlation coefficient r = 0.84. (**D**) Examples of the time course of Annexin-V binding to five individual cells in a typical experiment. The numbers at the end of the trace represent the relative EGFP density of the cell and τ is the time constant of a mono-exponential fit (light black line) of the data. (Primary effort on figure: (A and B) Whitlock, JM; (C and D) Hartzell, HC and Whitlock, JM)

The currents typically began to increase 8 min after initiating whole cell recording, which is similar to that reported by others [275]. Annexin-V binding usually became detectable 2 - 3 min later (Figure 3B-C). The time courses of ANO6 current activation and Annexin-V binding were fit to the equation $y = A2 + (A1-A2)/1+exp[(t-t_0)/\tau]$. Although the time constants of the increases in Annexin-V binding (τ = 2.24 ± 0.15 min) and ANO6 current (τ = 2.31 ± 0.34 min) were the same, the time (t_0) at which Annexin-V fluorescence reached half of its maximal value [(A1+A2)/2] was delayed 3 min relative to the current. In contrast to ANO6, ANO1 currents activated quickly after initiating whole-cell recording and then ran down with time (Figure 2), as previously reported [142] and no Annexin-V binding was observed.

There are two explanations for the lag between ANO6 current activation and Annexin-V binding. One possibility is that current is required for PLS. However, we believe that the lag is partly explained by inherent differences in way the two events are measured. Patch clamp recording measures membrane conductance instantaneously, while detection of Annexin-V fluorescence requires the accumulation of Annexin-V on the membrane that is limited by its binding kinetics and the sensitivity of the fluorescence detection. Because Annexin binding to model bilayers is known to be slow and requires a threshold PtdSer concentration [373, 378] and the numerical aperture of the microscope objective was 0.6, we believe that currents and PLS occur contemporaneously. This correlation suggested the possibility that currents reflect transmembrane ion leakage associated with the process of phospholipid transport. The alternative hypothesis that ionic current through ANO6 somehow activates PLS is excluded by the finding that PLS occurs normally in ANO6-expressing cells under conditions where there is no ionic current (for example, cells voltage-clamped at 0 mV with identical intracellular and extracellular solutions where E_{rev} for every ion is 0 mV).
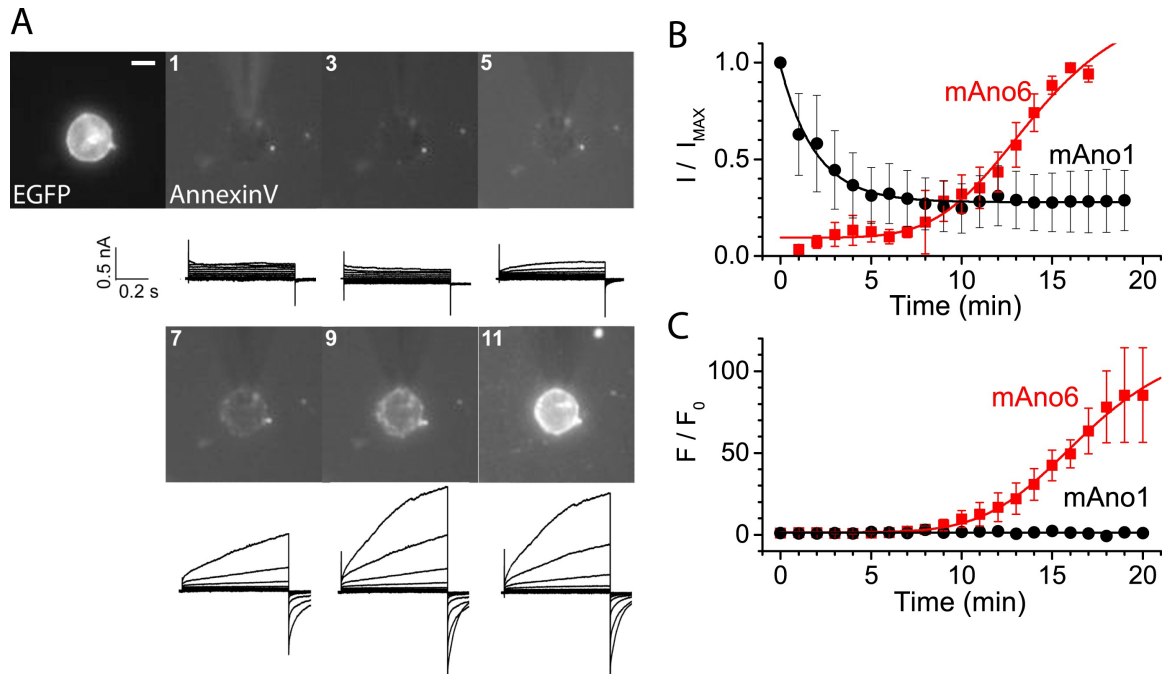
Figure 3 ANO6 current activates coincidently with PLS. HEK cells transiently expressing ANO6-EGFP were patch clamped in the presence of Annexin-V-Alexa-568 in the bath. The EGFP fluorescence image was obtained before establishing whole-cell recording and F_o was determined immediately after establishing whole-cell recording. Annexin-V fluorescence images were acquired immediately after obtaining each I-V curve by voltage clamp at 1 min intervals. The patch pipet contained 200 µM free Ca^{2+}. I-V curves were obtained by voltage steps from −100 mV to +100 mV in 20 mV increments. (**A**) Representative images and currents of one of 20 experiments. The first image shows ANO6-EGFP fluorescence. The patch pipet can be seen entering the field from 12 o'clock. Scale bar 10 µm. (**B**) Average current amplitudes normalized to maximum current for cells expressing ANO6 (red square) or ANO1 (black circles) plotted vs time after establishing whole-cell recording. (**C**) Average Annexin-V fluorescence normalized to maximum fluorescence for the same cells as in **B** (n = 6). (Primary effort on figure Yu, K)

130

ANO6 current and PLS require the same Ca^{2+} concentration for activation. If ANO6 current is a consequence of PLS and not a separate function of the protein, we would expect that current and PLS would require the same Ca^{2+} concentration for activation. Activation of ANO6 current requires >20 µM free Ca^{2+}_i and requires minutes to develop (Figure 4A,B). With 20 µM Ca^{2+}, neither PLS nor currents are observed even after 20 min of recording. Currents and PLS are consistently observed only with 200 µM Ca^{2+}. Although this finding does not exclude the possibility that ion conductance and PLS are separate functions of ANO6, it is consistent with the two functions being linked.

The ANO6 current is non-selective. If one accepts the proposal that ANO6 currents and Annexin-V binding occur simultaneously, this suggests that ANO6 currents may represent the flux of ions through micro-disruptions of the lipid membrane occurring during PLS rather than ions flowing through a defined aqueous pore defined by ANO6 protein. If ANO6 currents are a consequence of PLS, we would predict that their ionic selectivity would be very low. To explore the idea that ANO6 currents are essentially leak currents, we examined the ionic selectivity of the currents appearing after PLS was activated. In comparison to ANO1 currents, which exhibit robust anion:cation selectivity (P_{Na}/P_{Cl} = 0.03), the ANO6 current is highly non-selective (Figure 5). The ionic selectivity sequence was Na^+ > Cl^- > Cs^+ > $NMDG^+$ (P_{Na}/P_{Cl} = 1.38, P_{Cs}/P_{Cl} = 0.6, P_{NMDG}/P_{Cl} = 0.48). These data are consistent with the permeation pathway of ANO6 being relatively large and capable of passing $NMDG^+$ which has a mean diameter of ~7.3 Å. The finding that ANO6 currents have very low ionic selectivity and are activated contemporaneously with PLS over the same Ca^{2+} concentration range suggested that PLS and currents have the same underlying mechanism.

Identification of a protein domain required for scrambling. Because ANO1 has no scramblase activity while ANO6 does [68, 129, 273, 299], we hypothesized that ANO6 contains a domain responsible for PLS that is absent in ANO1.

131
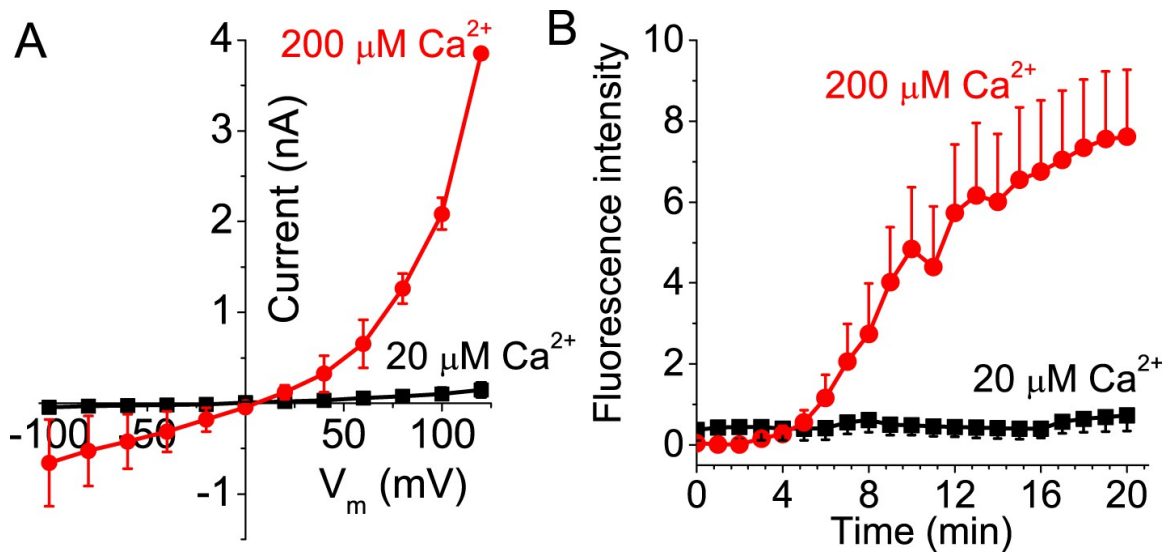
Figure 4 Activation of ANO6 current and PLS requires high intracellular Ca^{2+} concentrations. (**A**) Average current–voltage relationships of currents recorded ~20 min after establishing whole-cell recording in Ano6-expressing cells patched with 20 μM (black squares, N = 6) or 200 μM Ca^{2+} (red circles, N = 10) in the patch pipet. (**B**) Annexin-V binding in Ano6-expressing cells patched with 20 μM (black squares, N = 5) and 200 μM (red circles, N = 15) Ca^{2+} in the patch pipet. Error bars are S.E.M. (Primary effort on figure Yu, K)

We employed computational approaches to gain insights into sequence differences that could define this functional difference. We analyzed Type-I and Type-II divergence between mammalian ANO1 and ANO6 as an indication of the functional relevance of different amino acids [379]. Sequences used for the analysis are shown in Figure 6-figure supplement 1 and an alignment of ANO6 and ANO1 is shown in Figure 6 – figure supplement 2. Type I divergence occurs shortly after gene duplication and is characterized by amino acids that are highly conserved in one paralogous group of proteins and highly divergent in the other. Type II divergence occurs later when specific functions undergo positive selection within a paralogous group, resulting in conserved changes in amino acid properties. Type II divergence is exemplified by alignment positions that are identical within paralogous groups but have amino acids with radically different properties between paralogous groups. There are three major regions of Type-II divergence between ANO1 and ANO6 (Figure 6A). These regions are located in (a) intracellular loop 1, (b) TMD4 and TMD5 and the short intracellular loop between them, and (c) the C-terminus adjacent to the last transmembrane domain. To test the functional significance of these divergent amino acids, we made chimeric constructs of ANO1 and ANO6, named X-Y-X_*i-j*, where ANO paralog X has its amino acids *i-j* replaced with aligned amino acids from ANO paralog Y. The 1-6-1 chimeras, made by replacing short segments of ANO1 sequence with ANO6 sequence, were first screened by confocal microscopy of cultures.

Of twenty-six 1-6-1 chimeras, seventeen trafficked to the plasma membrane and generated Cl⁻ currents in patch clamp (Figure 6B, Figure 6 - figure supplement 3). Thirteen 1-6-1 chimeras did not exhibit PLS. However, 4 chimeras having ANO1 sequence replaced with ANO6 sequence in the region spanning TMD4 and TMD5 showed robust PLS activity (chimeras 1-6-1_D554-K588, 1-6-1_C559-F584, 1-6-1_S532-G558, and 1-6-1_D554-V569.

133

A. ANO6

EC: 150 CsCl   15 CsCl

+100
-100

1nA
0.2s

2

EC:150 mM CsCl
EC: 15 mM CsCl

nA

1

ΔE_{Cs} = -55.8

ΔE_{Cl}= 55.8

-50   0   50   mV

-1

-2

ΔE_{rev} = 15.7 mV

B. ANO1

EC: 150 CsCl   15 CsCl

+60
-60

1nA
0.4s

2

nA

1

-50   0   50 mV

-1

-2

ΔE_{rev} = 40.2 mV

C

Ano6
Ano1

40

E_{rev} (mV)

20

0

146 NaCl   15 NaCl   150 CsCl   15 CsCl   150 NMDG-Cl

D

Ano6
Ano1

1.8
1.5
1.2
0.9

P_X / P_{Cl}

0.6
0.3
0.0

Cs^+ Na^+ $NMDG^+$
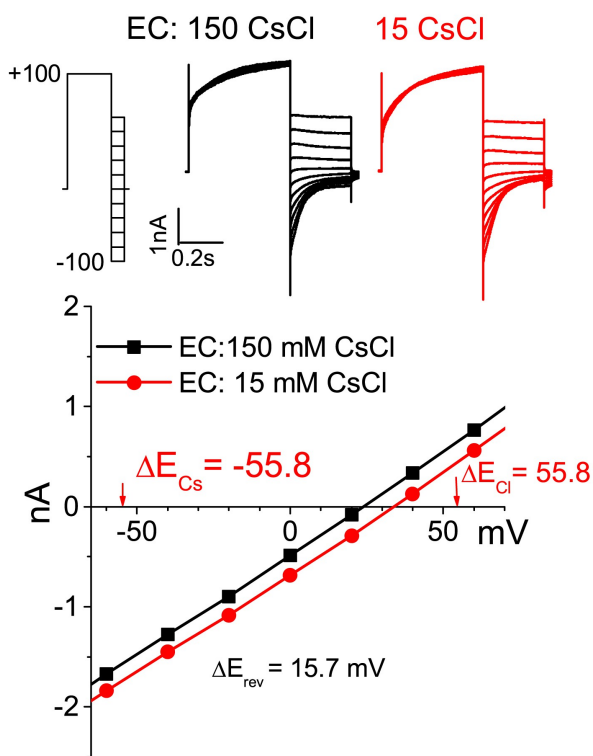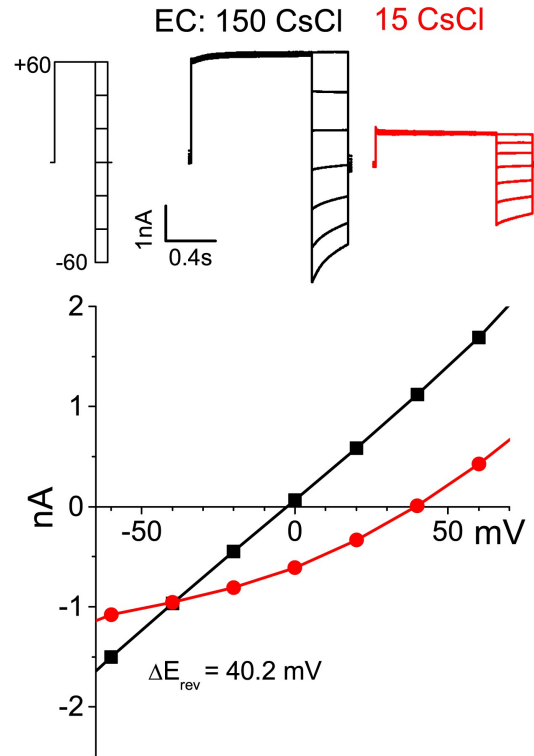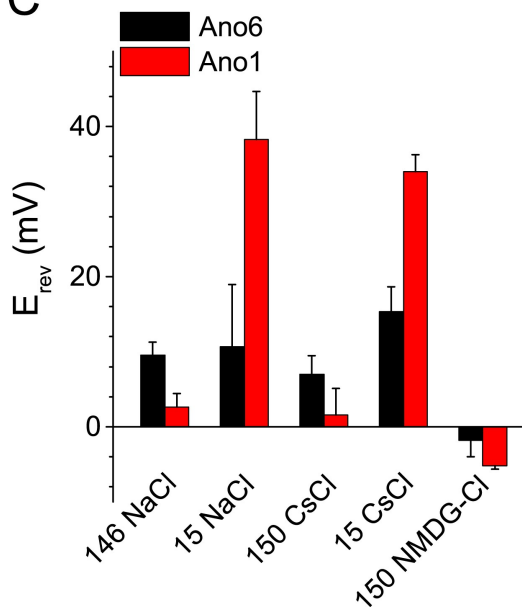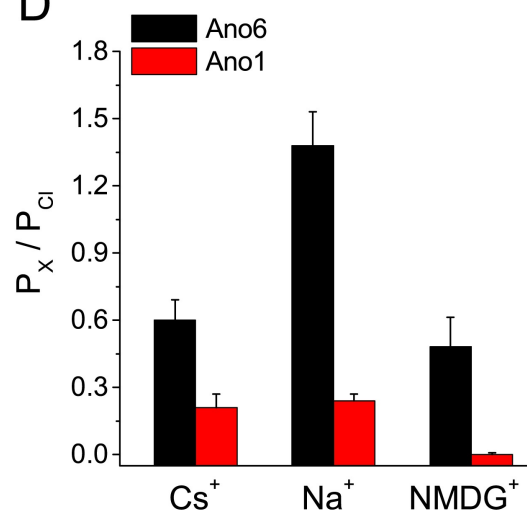
Figure 5 Ionic selectivity of ANO6 currents. Representative whole-cell patch-clamp recordings and current–voltage relationships from (**A**) ANO6 and (**B**) ANO1 expressing cells with 200 µM $[Ca^{2+}]_i$. Currents were recorded in 150 mM or 15 mM extracellular

134

CsCl. The reversal potentials (E_{rev}) shift very little with ANO6-expressing cells, while the shift is large for ANO1-expressing cells. (**C**) Average E_{rev} values for ANO6 or ANO1 expressing cells bathed in 146 NaCl, 150 CsCl, 15 NaCl, 15 CsCl, or 150 NMDG-Cl. (**D**) Relative permeabilities calculated from the Goldman-Hodgkin-Katz equation. N = 6–17. (Primary effort on figure Yu, K)
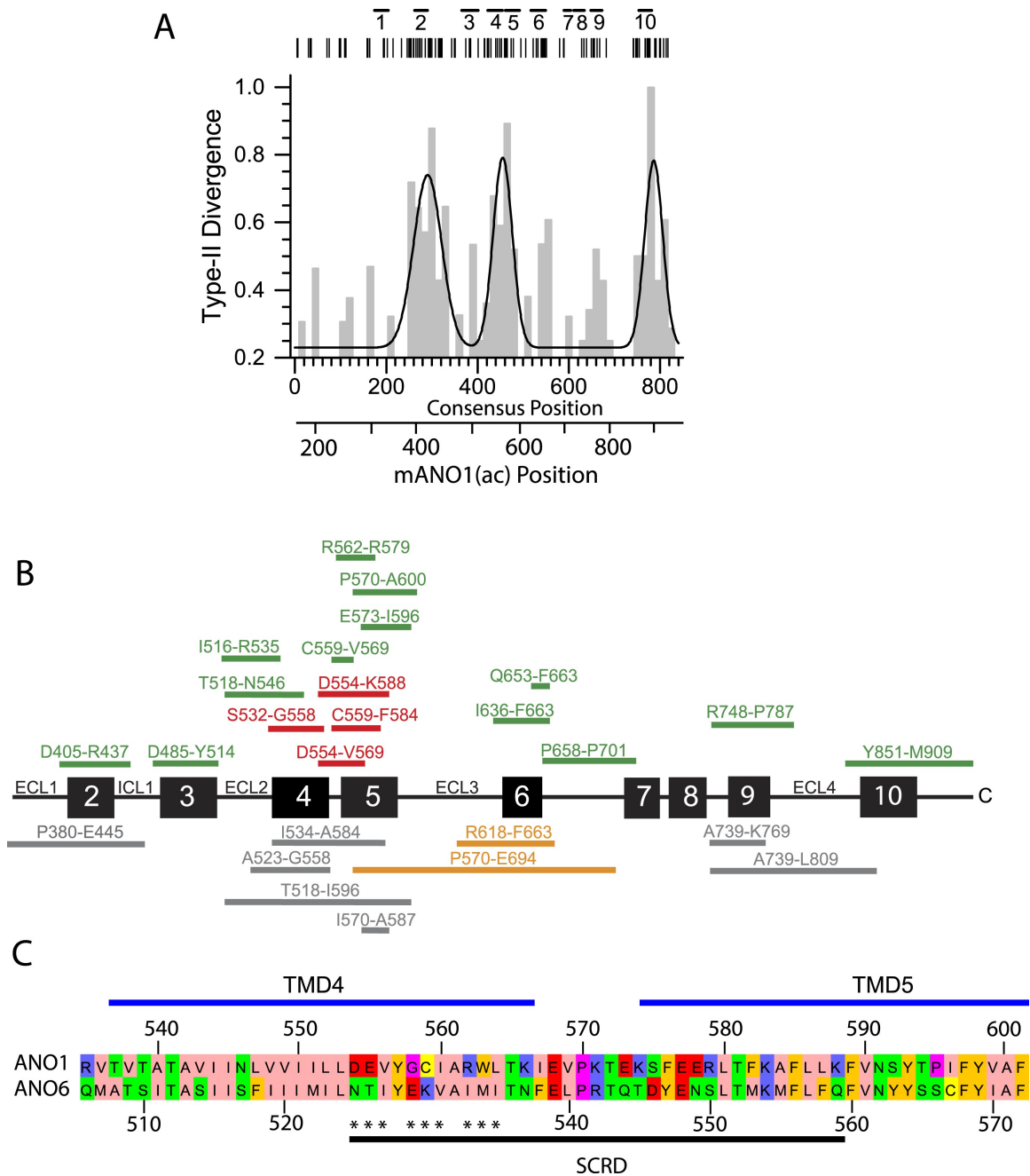
Figure 6 Identification of a PLS domain in ANO6. (**A**) Site-specific Type II divergence

scores were calculated by comparing ANO1 and ANO6 sequences from 24 mammalian

species, binned over a 15-amino acid window, and normalized to the maximum value.

Horizontal lines at top indicate transmembrane domains. Vertical lines indicate individual

amino acids with high Type II Divergence Scores. (**B**) Summary of 1-6-1 chimeras. Black

line represents ANO1 sequence with TMDs 2–10 labeled. Colored horizontal lines represent ANO1 sequence that was replaced with the corresponding ANO6 sequence. Numbers refer to ANO1 sequence. Green: ANO1-like currents, no scrambling. Red: scrambling. Grey: weak plasma membrane expression, but no currents or scrambling. Orange: some plasma membrane expression, no currents or scrambling. (**C**) Scrambling domain (SCRD). The sequences of ANO1 (535–601) and ANO6 (506–572) are aligned with TMD 4 and TMD5 indicated. Amino acids are colored according to Rasmol. SCRD shows region associated with PLS. Asterisks show amino acids that are essential for PLS in ANO6. Figure 6—figure supplement 1 lists sequence accession numbers used for Diverge analysis. Figure 6—figure supplement 2 shows alignment of mANO1 and mANO6 used for chimeric construction. Figure 6—figure supplement 3tabulates the properties of all of the 1-6-1 chimeras. Figure 6—figure supplement 4 shows a confocal image of scrambling by the 1-6-1_(554-588) chimera. Figure 6—figure supplement 5 summarizes properties of mutations in ANO6 SCRD. (Primary effort on figure: Hartzell, HC; Lee, K; Yu, K; Whitlock, JM)

The 1-6-1 chimera that scrambled having the smallest ANO6 sequence (1-6-1_D554-V569) had 15 amino acids of ANO1 replaced with amino acids 525-540 from ANO6. Additional constructs were made in which only pairs or triplet amino acids in ANO1 were mutated to the divergent amino acids from ANO6, but none of these chimeras exhibited PLS activity (Figure 6-figure supplement 4). We term this region of ANO6 between amino acids 525 – 559, capable of conferring PLS activity on ANO1, the scrambling domain (SCRD) (Figure 6C).

The ability of the SCRD to confer PLS activity on ANO1 does not necessarily prove that it is required for ANO6 PLS. To test this possibility, we mutated these amino acids in ANO6 to determine if they abolished ANO6-mediated PLS. Chimeras in which portions of the ANO6 SCRD were replaced with ANO1 sequence had greatly reduced PLS activity (Figure 6-figure supplement 5). Furthermore, mutation of several triplets of amino acids (525NTI, 529EKV, and 533IMI) between N525 and I535 abrogated ANO6 PLS activity.

Chimeras that trafficked to the plasma membrane, as judged by confocal microscopy, were then subjected to patch clamp analysis to measure ionic currents generated during PLS. Figure 7A,B shows the percentage of cells that bound Annexin-V after 15 min whole cell patch clamp recording using 200 µM Ca^{2+} in the patch pipet and the amplitude of the ionic current at +100 mV when Annexin-V binding had plateaued (see also Figure 6-figure supplements 3-5). Chimeras that support PLS invariably had ionic currents, while 6-1-6 chimeras that do not scramble (6-1-6_N525-Q559, 6-1-6_N525-I527, 6-1-6_E529-V531, and 6-1-6_N541-T662) exhibited very small or no currents. However, the amplitudes of the currents did not correlate with the percentage of cells that exhibited PLS, possibly because of differences in surface expression, which were not controlled (Figure 7A,B). The finding that mutations in ANO6 that abolished PLS also abolish ionic

138

currents suggests that ions and phospholipids are translocated by overlapping molecular machinery.

To investigate the properties of the chimeras in more detail, we selected the PLS-positive chimera 1-6-1_D554-K588 and the PLS-negative chimera 6-1-6_N525-I527 for analysis. We first examined PLS in intact cells after elevation of cytosolic $Ca^{2+}$with A23187. Like ANO6, 1-6-1_D554-K588 exhibited robust Annexin-V binding within 10 min (Figure 7C). In contrast, 6-1-6_N525-I527, which had 3 amino acids of ANO6 swapped with ANO1 sequence, did not exhibit PLS (Figure 7C). 96% of cells transfected with 1-6-1_D554-K588 (N = 178) of cells bound Annexin-V (Figure 7D). In contrast, only 15% of the cells (N = 127) transfected with 6-1-6_N525-I527 bound Annexin-V. The rate of Annexin-V binding was very similar for 1-6-1_D554-K588 and ANO6 (Figure 7E). On average, Annexin-V binding to ANO6-expressing cells occurred with т = 143 sec (Figure 2D), whereas Annexin-V binding in cells transfected with 1-6-1_D554-K588 occurred with т = 218 sec, χ^2 = 0.03). Although other 1-6-1 chimeras that exhibited PLS were not investigated at the same detail, the characteristics of PLS of these chimeras were qualitatively similar to 1-6-1_D554-K588.

Patch clamp analysis shows that the currents of chimeras exhibiting PLS have properties that are a hybrid of ANO1 and ANO6 (Figure 7-figure supplement 1). While no PLS and no currents were observed in cells transfected with 6-1-6_N525-I527 during 20 min using 200 μM Ca^{2+}_i, in cells transfected with 1-6-1_D554-K588, robust Annexin-V binding occurred even with 20 μM Ca^{2+}_i. Therefore, it seems that this chimera retains the Ca^{2+} sensitivity of ANO1. Moreover, the current was largest immediately upon establishing whole cell recording and then it ran down with time, similar to ANO1 currents (Figure 7-figure supplement 1). However, the rundown was not monotonic, but was interrupted by a transient increase in current.

139

A

% Cells binding Annexin-V

ANO6, ANO1, 1-6-1(532-558), 1-6-1(554-588), 1-6-1(554-555), 1-6-1(559-584), 1-6-1(570-587), 1-6-1(554-569), 1-6-1(562-579), 6-1-6(525-559), 6-1-6(541-662), 6-1-6(525-527), 6-1-6(529-531)

29, 17, 6, 18, 6, 9, 4, 9, 5, 5, 6, 5, 3

B

Current (nA)

ANO6, ANO1, 161(532-558), 161(554-588), 161(554-555), 161(559-584), 161(570-587), 161(554-569), 161(562-579), 616(525-559), 616(541-662), 616(525-527), 616(529-531)

C

EGFP_Chimera   Annexin-V

1-6-1_D554-K588

6-1-6_N525-I527

D

Number of Cells

Scrambled
Not scrambled

92%

96%

16%

ANO6, 1-6-1_D554-K588, 6-1-6_N525-I527

E

Integrated Density x 10^{-4}

1-6-1(D554-K588)

ANO6

Time (sec)

140

Figure 7 Properties of chimeras of ANO1 and ANO6. (**A**, **B**) Patch clamp analysis of

PLS (**A**) and ionic currents (**B**) in ANO1-ANO6 chimeras. Cells were patch clamped with

200 μM Ca^{2+} in the pipet and PLS was monitored by Annexin-V binding and currents

measured by voltage steps from 0 mV to +100 mV. (**C**) Confocal imaging of Annexin-V

binding to HEK cells transfected with the 1-6-1_D554-K588 or the 6-1-6_N525-I527

chimeras 10 min after elevating Ca^{2+} with A231187. (**D**) Number of cells binding

Annexin-V ('scrambled') or not binding Annexin-V ('not scrambled') 10 min after

elevation of Ca^{2+} with A23187 (N = 3 experiments each). (**E**) Time course of Annexin-V

binding to cells expressing the 1-6-1_D554-K588 chimera (red) compared to the time

course of Annexin binding to ANO1-expressing cells (black). (Primary effort on figure: (A

and B) Yu, K; (C and D) Whitlock, JM; (E) Hartzell, HC and Whitlock, JM)

We interpret these data to indicate that this chimera initially exhibits ANO1-like currents, and that as PLS begins, the current acquires the properties of ANO6. The nature of this current is investigated below.

Ionic currents associated with scrambling. We reasoned that if the pathway taken by ions is the same as the one taken by phospholipids, the two events might have similar pharmacology. Therefore, we tested the effects of MONNA, a small molecule that blocks ANO1 currents [309]. We find that although 10 µM MONNA blocks ANO1 currents ~90%, ANO6 currents are unaffected (Figure 8A). These data support the suggestion that the permeation pathway for Cl⁻ in ANO1 differs from the ion conduction pathway of ANO6. Furthermore, MONNA does not block currents of 1-6-1 chimeras that exhibit PLS activity (Figure 8A). This suggests that the structural determinants of PLS in the SCRD alter that pharmacology of ANO1.

We have previously shown that ANO1 currents can be activated by strong depolarizations in the absence of Ca^{2+} [296]. Because ANO6 does not exhibit such Ca^{2+}-independent currents, we asked whether we could detect Ca^{2+}-independent ANO1-like currents in 1-6-1_D554-K588 in zero Ca^{2+}. Like ANO1, 1-6-1_D554-K588 exhibits Ca^{2+}-independent currents at very positive potentials and these currents are blocked by MONNA (Figure 8B, blue triangles). This current is Cl⁻-selective ($P_{Cs}:P_{Cl} = 0.08$) (Figure 8C). Thus, in zero Ca^{2+} 1-6-1_D554-K588 currents resemble ANO1. However, after PLS has been activated by Ca^{2+}, the current is not blocked by MONNA (Figure 8B, red squares) and the current is >4-fold less Cl⁻-selective ($P_{Cs}:P_{Cl} = 0.39$) (Figure 8D). These data suggest that as PLS develops in response to elevated intracellular Ca^{2+}, the ionic conductance pathway changes from Cl⁻-selective to non-selective. In fact, this transition between MONNA-sensitive and MONNA-insensitive currents can be seen when MONNA is applied shortly after establishing whole-cell recording with Ca^{2+} in the pipet (Figure 8B, black open circles).

142
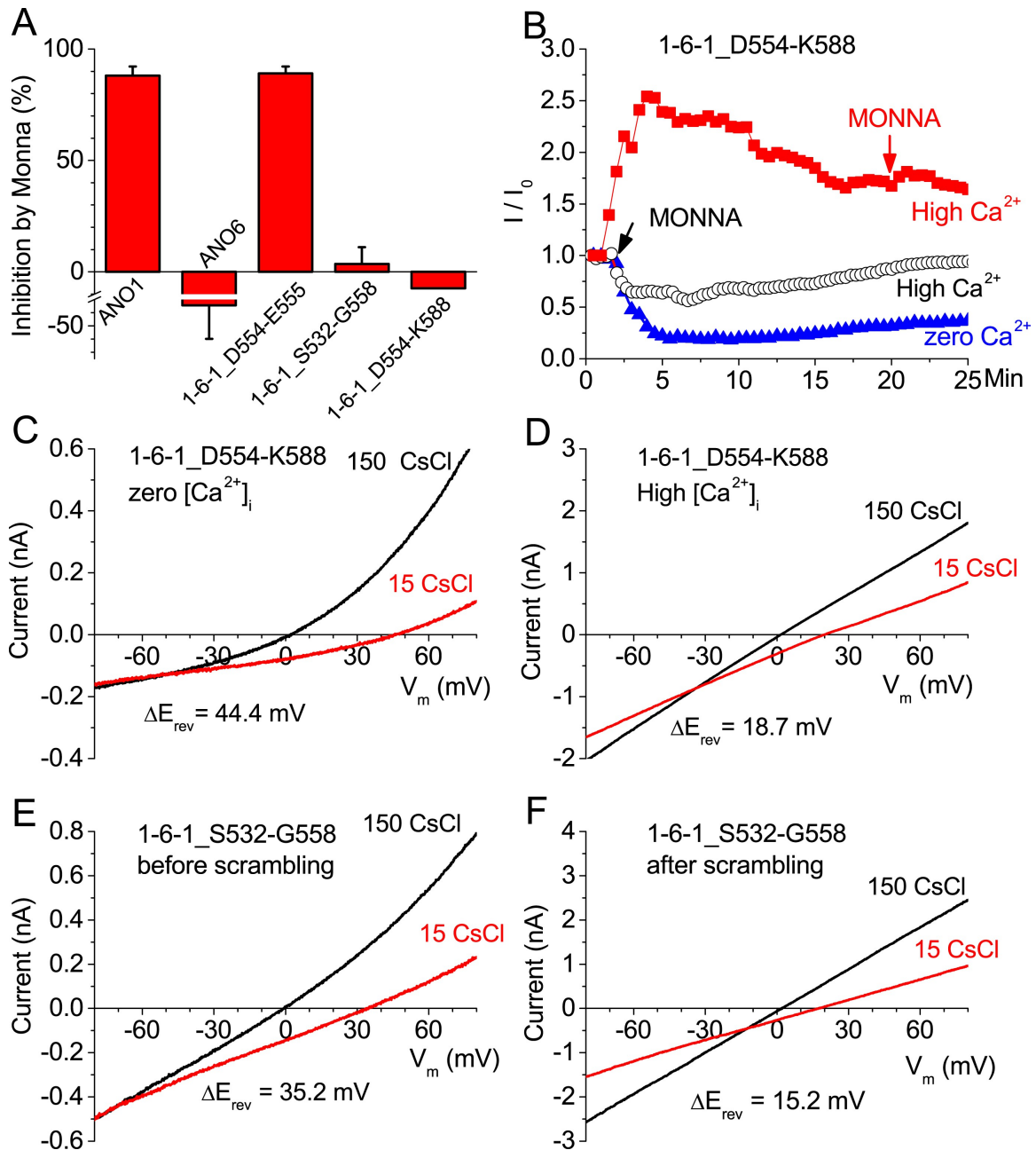
Figure 8 Ion channel properties of ANO1-ANO6 chimeras. (**A**) Inhibition of currents by MONNA. ANO1 is nearly completely blocked by 10 μM MONNA, while ANO6 and the 1-6-1 chimeras that scramble are not affected. (**B**) Effects of MONNA on currents associated with the 1-6-1_D554-K588 chimera. MONNA blocks the Ca^{2+}-independent current elicited by depolarization to +100 mV (blue triangles), but has no effect on the Ca^{2+}-activated current after scrambling has occurred (red squares). In contrast, before

scrambling has occurred, MONNA partially blocks the Ca^{2+}-activated current (open circles). (**C**–**F**) The ionic selectivity of currents associated with the 1-6-1_D554-K588 chimera (**C**–**D**) and the 1-6-1_S532-G558 chimera (**E**, **F**) were determined by the dilution method (see 'Materials and methods') by measuring reversal potentials with external solutions containing either 150 mM (black line) or 15 mM (red line) CsCl. (**C**) Ca^{2+}-independent (zero Ca2+iCai2+) and (**D**) Ca^{2+}-activated currents associated with the 1-6-1_S532-G558 chimera. Currents recorded (**E**) before and (**F**) after scrambling with the 1-6-1_S532-G558 chimera. N = 3–7. Error bar represents SEM. (Primary effort on figure: Yu, K)

The current is initially blocked partially by MONNA, but then the current begins to increase coincidently with development of PLS.

Because PLS of 1-6-1_D554-K588 develops quickly after establishing whole cell recording, it is difficult to compare the properties of the currents before and after PLS in the same cell. Therefore, we used the chimera 1-6-1_S532-G558 which activates PLS more slowly. About 5 min after establishing whole-cell recording before PLS was detectable, the current exhibited Cl^--selectivity as indicated by a 35 mV shift in E_{rev} upon switching from 150 mM CsCl to 15 CsCl (P_{Cs}:P_{Cl} = 0.15) (Figure 8E). In contrast, after scrambling had occurred, cation permeability was significantly increased, with an ΔE_{rev} shift of only 15 mV (P_{Cs}:P_{Cl} = 0.50) (Figure 8F). We cannot formally determine whether the Cl^--selective pathway in the absence of PLS and the non-selective PLS-linked pathway are the same, but the observation that MONNA blocks the Cl^--selective pathway but has no effect on the current after PLS develops suggests that the Cl^--selective pathway is no longer present after PLS occurs. This is consistent with the Cl^--selective pathway becoming less selective during scrambling.

Homology Model of ANO6. Recently, the X-ray structure of an ANO homolog from the fungus *Nectria haematococca* was published [68]. This protein, nhTMEM16, exhibits PLS activity when reconstituted into liposomes. Evidence for its channel activity is lacking, although the authors indicate that the lack of channel activity might be an artifact of the purification and reconstitution conditions. To gain insights into the structure-function relationships of the SCRD to protein structure, we created a homology model of ANO6 based on nhTMEM16 (Figure 9). This model shows that the SCRD forms a unique structure. Along with helices 3, 6, and 7, it forms what Brunner et al. [68] call the "subunit cavity," a hydrophilic crevice that faces the lipid membrane on the side of the

protein away from the dimer interface. Brunner et al. speculate that this region may be

involved in lipid transport.
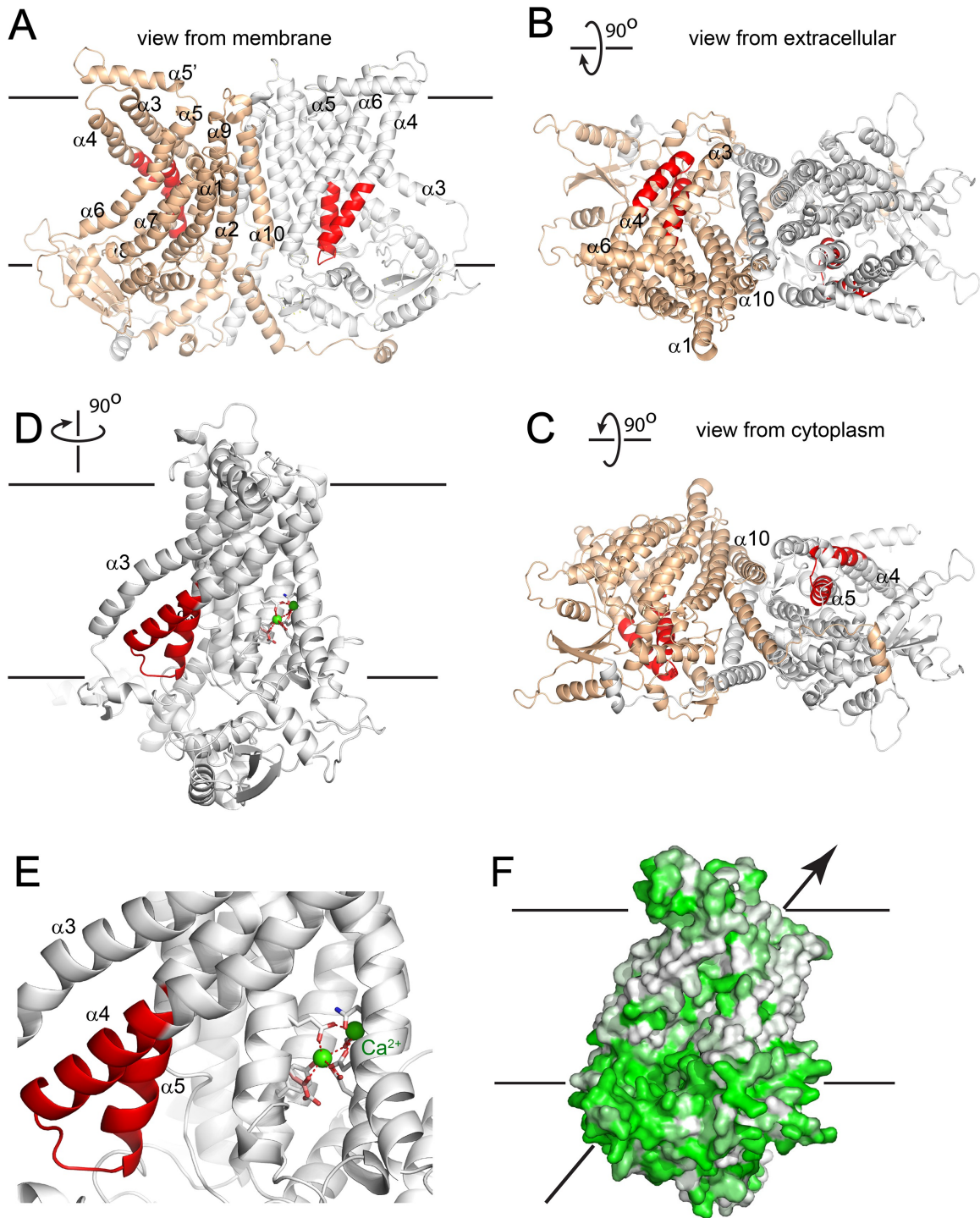
Figure 9 Homology model of ANO6. (**A**) Side view from the membrane. ANO6 is

shown as a dimer with the left subunit in gold and the right subunit in grey. The SCRD is

colored red. Transmembrane helices are numbered. (**B**) View from extracellular side. (**C**)

View from cytoplasm. (**D**) A view from the membrane looking towards the hydrophilic

cleft showing the SCRD in red and the Ca^{2+} binding site in stick representation. Residues conserved between ANO6 and TMEM16 that coordinate Ca^{2+} (green) are shown as white sticks (C = white, O = red). ANO6 contains GXXX (pink), which is a D503 in TMEM16. (**E**) Close-up view of **D**. (**F**) Same view as **D** with surface colored to show hydrophilicity. Green: hydrophilic. White: hydrophobic. (**Primary effort on figure:** Hartzell, HC and Ortlund, E)

Discussion.

The scrambling pathway of ANO6. Phospholipid scramblases are conceived to function in a fashion similar to ion channels by forming an aqueous pore for the polar head groups of the phospholipids to cross the hydrophobic center of the membrane [111, 362]. The recent 3-dimensional structure of nhTMEM16, which catalyzes phospholipid scrambling when incorporated into lipid vesicles, provides key insights into this process [68]. The authors noticed a peculiar hydrophilic cavity facing the hydrophobic bilayer that they propose may be involved in lipid scrambling, although no lipids were visualized in the structure. The idea that this cleft may be the phospholipid "channel" is supported by our ANO6 homology model that predicts that the SCRD forms one side of this cleft. Intriguingly, residues located in TMD7-TMD8 of ANO1, identified for their roles in Ca^{2+} binding and gating, make up the other side of this hydrophilic cavity [140, 141, 380] (Figure 9D,E). The Ca^{2+} binding site, therefore, is well situated to control structural rearrangements of the hydrophilic cleft to provide a potential pathway for phospholipid translocation.

Is ANO6 a PLSase? An important role of ANO6 in PLS seems well established [7, 129], although its identity as a PLSase has been contested [369]. This debate has attracted considerable attention [124, 143, 247, 377]. It is important to note that despite the motivation to conclude that ANO6 is a PLSase based on its similarity in structure to nhTMEM16, it remains a possibility that ANO6 is a regulator of another protein that is the PLSase. Our finding that only about 92% of cells expressing ANO6 exhibit PLS suggests that ANO6 is not sufficient for PLS. Further, the lack of correlation between ANO6 expression levels and PLS activity supports some skepticism. One must only recall that PLSCR1 incorporated into liposomes mediates PLS but that knockout of its gene does not have clear-cut effects on PLS to appreciate a need for caution [260, 347, 366, 367].

149

The ion conduction pathway. We propose that during scrambling ions pass through the same pathway that is occupied by the phospholipid. Ions might accompany the phospholipids as counterions or may simply flux independently through the same pathway. This suggestion is based on the observation that PLS and ionic currents activate contemporaneously and exhibit similar sensitivity to Ca^{2+}. Furthermore, the presence of non-selective, slowly-activating currents that are insensitive to the ANO1 inhibitor MONNA correlate with the ability of chimeras to scramble. Some support for this idea is provided by cysteine mutagenesis and accessibility experiments showing that amino acids that we believe form the vestibule of the Cl^- selective pore of ANO1 [141] are located at the extracellular surface of the hydrophilic cleft (Figure 9-figure supplement 1).

Evolution of the ANO/TMEM16 family. Our data add to the already growing awareness that the ANO family is functionally split with some of its members being anion-selective ion channels (ANO1 and ANO2) and other members having the ability to transport lipids between membrane leaflets. This functional duplicity is reminiscent of two other anion channels, CFTR and CLCs, which apparently evolved from transporters. CFTR (cystic fibrosis transmembrane conductance regulator) is a Cl^- channel that evolved from ABC transporters [282-284], and the CLC chloride channels CLC-1 and CLC-2 are members of a 9-gene family most of which are H^+-Cl^- exchangers [285, 286]. Additionally, the P4 ATPases that function as lipid flippases evolved from a family of ion transporters [113, 381]. One might speculate that the primordial ANO was a lipid transporter. During evolution, functional divergence likely occurred after gene duplication where the selective pressure for the major function (lipid transport) decreased, thus enabling the enhancement of the minor sub-function (ion transport). The finding that fungi have only one ANO gene, but that some fungal ANO homologs have PLS activity [68, 273], supports the idea that PLS is an ancient function of ANOs. Our data suggest that the

150

ionic currents carried by ANO6 are essentially flowing along with the scrambling lipids. Thus, the non-selective ion transport that occurs concomitantly with PLSase activity may have been a sub-function in the ancestral ANO. After gene duplication occurred, this sub-function may have evolved Cl⁻ ion specificity.

ANOs that have evolved into anion channels may be more Cl⁻ selective than the scrambling ANOs simply because the energy contour of the conduction pathway is altered by the absence of lipid substrate. Because Cl⁻ is more hydrophobic than its cationic cousins, it may be more suited to traverse the evolutionary remnants of the phospholipid pathway. Consistent with this idea is the fact that, compared to many voltage-gated cation channels, Cl⁻ channels are sadly non-selective: virtually all anions permeate and cations are often significantly permeable [120]. The pores of Cl⁻ channels are often modeled as large viaducts that provide selectivity based largely on ionic hydration energies [298, 382, 383]. This low selectivity is precisely what one might expect to evolve from a transporter that previously transported phospholipids. The finding that we can convert ANO1 into a protein capable of catalyzing PLS provides further support for this hypothesis for ANO1 evolution. Like the ClC family, where a single glutamic acid residue can determine whether a protein is a H^+-Cl⁻ transporter or a Cl⁻ channel, here we show that a few amino acids can convert ANO1 into a protein that supports PLS activity. However, we have not yet been able to convert ANO6 into a Cl⁻ selective ion channel. It is likely that additional changes outside the SCRD are required to confer Cl⁻ selectivity. This may be also be explained by epistasis, where evolutionary trajectories are blocked by the accumulation of neutral mutations that have no impact on the initial function (non-selective ion transport) but prevent acquisition of the new function (Cl⁻ selectivity) [384, 385]. Yang et al. (2011) have reported that mutations of the last amino acid in the SCRD (Q559 in ANO6, K588 in ANO1) alters the ionic selectivity, but the changes are only 2-3-fold and do not shift selectivity from cation to anion.

Intriguingly, the *Saccharomyces* ANO homolog, Ist2p, has been shown to play a role in tethering the cortical ER to the plasma membrane, but it is not known whether this protein also has PLSase or ion channel activity. However, one might speculate wildly that Ist2p may play a role in transport of lipids from the ER to the plasma membrane, because tethering of the ER to the plasma membrane is important for the proper function of non-vesicular lipid transport [255] and deletion of Ist2p along with other ER-plasma membrane tethering proteins results in aberrant phosphatidylinositol 4-phosphate levels and localization [78, 79, 274, 386].

Is ANO1 a PLSase? ANO1 is well established as the pore forming unit of Ca^{2+} activated Cl^- channels [321, 370, 371] and is incapable of rescuing PLS in cells with ANO6 disrupted [129]. However, our finding that the function of ANO1 can be converted by replacing a domain as small as 15 amino acids raises questions whether ANO1 might be a PLSase under appropriate conditions. Perhaps a missing subunit or regulatory enzyme could activate its PLSase activity. Alternatively, the SCRD may hold a vital interaction site for another component essential for this process or possess a key site of posttranscriptional modification required for activating this activity. In any case, it is clear that ANO1 function is intimately dependent on phospholipids [299] and understanding the relationships of the ANOs to membrane lipids is certain to be a major research goal for many laboratories in the coming years.

Materials and Methods

cDNAs. mANO1 (Uniprot Q8BHY3) and mANO6 (Uniprot Q6P9J9) tagged on the C-terminus with EGFP were provided by Dr. Uhtaek Oh, Seoul National University. For designing chimeras, mANO1 and mANO6 were aligned using MUSCLE [387]. Chimeras were constructed using overlap extension PCR [388]. Chimeras are named X-Y-X_*i-j*, where X is the ANO paralog template whose amino acids numbered *i-j* are replaced with the aligned amino acids from ANO paralog Y. The alignment is shown in Figure 5-figure

supplement 2. PCR primers were designed to engineer complementary overlapping sequences onto the junction-forming ends of PCR products that were subsequently assembled by PCR. PCR-based mutagenesis was used to generate mutations in one or a few amino acids. The protein coding region of all chimeras and mutants were sequenced.

Clover-(His)$_6$-LactC2. A cDNA construct consisting of Clover fluorescent protein followed by a hexa-histidine tag and lactadherin-C2 (Clover-(His)$_6$-LactC2) in the pET-28 bacterial expression vector was a generous gift from Dr. Leonid Chernomordik (NIH/NICHD). Rosetta2(DE3) BL21 *E.coli* (Novagen) were transformed with Clover-(His)$_6$-LactC2 in pET28, grown in TB medium at 37 ^{o}C in 50 µg/ml kanamycin and 30 µg/ml chloramphenicol until the culture reached A$_{600}$ = 1. After addition of 1 mM IPTG, the culture was grown for 3 hrs at 28 ^{o}C. Cells were lysed in B-Per (Thermo Scientific) containing lysozyme, benzoase, and protease inhibitor cocktail III (Calbiochem). After centrifugation at 20,000g 10 min, Clover-(His)$_6$-LactC2 was purified from the supernate on a 1-ml Talon cobalt affinity column (Clontech). Stock solutions of 1 -3 mg/ml were stored in the elution buffer (150 mM imidazole pH 7 plus 0.02% NaN$_3$) and were used at ~1 - 3 µg/ml.

Patch clamp electrophysiology. HEK293 cells were transfected with ~1 µg cDNA per 35 mm dish) using Fugene-9 (Roche Molecular Biochemicals, Indianapolis, IN). Single cells identified by EGFP fluorescence were patch clamped ~2 days after transfection. Transfected cells were identified on a Zeiss Axiovert microscope by EGFP fluorescence. Cells were voltage-clamped using conventional whole-cell patch-clamp techniques with an EPC-7 amplifier (HEKA). Fire-polished borosilicate glass patch pipettes were 3-5 MΩ. Experiments were conducted at ambient temperature (22-26°C). Because liquid junction potentials calculated using pClamp were predicted to be < 2 mV, no correction was made. The zero Ca^{2+} pipet (intracellular) solution contained (mM): 146 CsCl, 2 MgCl$_2$, 5

EGTA, 10 sucrose, 10 HEPES pH 7.3, adjusted with NMDG. The ~20 µM Ca^{2+} pipet

solution contained 5 mM Ca^{2+}-EGTA. The 0.2 mM Ca^{2+} solution was made by adding

additional 0.2 mM $CaCl_2$ to the 20 µM Ca^{2+} pipet solution. The standard extracellular

solution contained (mM): 140 NaCl, 5 KCl, 2 $CaCl_2$, 1 $MgCl_2$, 15 glucose, 10 HEPES pH

7.4. For determination of ionic selectivity, the external solution contained 2 $CaCl_2$, 1

$MgCl_2$, 15 glucose, 10 HEPES pH 7.4, and various concentrations of NaCl, CsCl, or

NMDG-Cl as indicated. The internal solution contained (mM): 150 NaCl (or CsCl), 1

$MgCl_2$, 5 Ca-EGTA plus 0.2 $CaCl_2$, and 10 HEPES pH 7.4. The osmolarity of each

solution was adjusted to 300 mOsm by addition of mannitol. Relative permeabilities of

cations (X) relative to Cl^- were determined by measuring the changes in zero-current E_{rev}

when the concentration of extracellular NaCl or CsCl was changed ("dilution potential"

method) as previously described [141, 389]. Relative permeabilities were calculated from

the shift in E_{rev} calculated using the Goldman-Hodgkin-Katz equation:

$\Delta E_{rev} = 25.7 \ln[(X_o + Cl_i * P_{Cl}/P_{Na}) / (X_i + Cl_o * P_{Cl}/P_{Na})]$, where X is the cation and ΔE_{rev} is

the difference between E_{rev} with the test solution XCl and that observed with symmetrical

solutions.

Phospholipid scrambling. Phospholipid scrambling (PLS) was assessed by live-cell

imaging of the binding of Annexin-V conjugated to Alexa Fluor-568 (Invitrogen, "Annexin-

V" diluted 1:200) or LactC2 fused to Clover fluorescent protein [356]. PLS was measured

in populations of intact HEK293 cells grown on glass coverslips mounted in Attofluor

chambers (Invitrogen) and imaged at ambient temperature with a Zeiss confocal

microscope using a 63X Plan-Aprochromat NA 1.4 objective. PtdSer exposure was

measured by binding of Annexin-V-AlexaFluor-568 (543nm excitation; 560 nm long pass

emission) or LactC2-Clover (488nm excitation, 500-530nm band pass emission). The

bath solution contained (mM) 140 NaCl, 10 $CaCl_2$, 10 Tris-HCl pH 7.4. PLS was

stimulated by elevation of intracellular Ca^{2+} using the Ca^{2+} ionophore A23187 (10 µM).

154

The most reproducible PLS was obtained by incubation of cells 5 min in A23187 in nominally zero-Ca^{2+} solution followed by washout of A23187 and addition of 5 mM Ca^{2+} to initiate PLS. We presume that the A23187 exposure in zero Ca^{2+} depletes internal stores and that the readdition of Ca^{2+} results in store-operated Ca^{2+} entry that is more rapid than Ca^{2+} entry through A23187 channels alone. In some experiments, PLS was stimulated by exposure to A23187 and Ca^{2+} simultaneously Sometimes SERCA inhibitors were included with no obvious effect. Scrambling was quantified by measuring the increase in Annexin-V fluorescence in EGFP-expressing cells by creating a binary mask from the EGFP channel for each Annexin-V-Alexa-568 frame in the time series using Fiji Image-J 1.49. The raw integrated density was then calculated by adding the intensity of all pixels in the unmasked area.

Binding of Annexin-V-AlexaFluor-568 to patch-clamped cells during voltage-clamp recording was imaged with a wide-field Zeiss Axiovert 100 microscope using a 40X NA 0.6 LD-Acroplan objective. Images were acquired with an Orca-FLASH 4.0 digital CMOS camera (C11440, Hamamatsu) controlled by Metamorph 7.8 software (Molecular Devices). Annexin-V-AlexaFluor-568 was added to the normal extracellular solution before patch clamping the cell. After whole-cell recording was established with an intracellular solution containing either zero, 20 μM, or 200 μM free Ca^{2+} the accumulation of Annexin-V on the plasma membrane was imaged at 1-min intervals synchronously with voltage clamp recording.

Immunostaining and Antibodies. Stable ANO6-FLAG$_{3X}$ cells were fixed on glass coverslips in 4% PFA for 10 min at room temperature, permeablized with 1.5% Tritonx-100 and stained with anti-FLAG M2 antibody (Sigma-Aldrich) for two hours at room temperature. Coverslips were washed and stained with anti-mouse-Alexa-488 secondary and Alexa-633 conjugated phalloidin (1:1000, Molecular Probes). Western blot analysis

155

was performed on protein lysates using anti-FLAG M2 antibody and anti-GAPDH (Millipore) followed by incubation with HRP conjugated anti-mouse secondary (BioRad).

Divergence Analysis. Type-II divergence was determined using DIVERGE 3.0 (http://xungulab.com/software.html) [379, 390]. Sequences used for the DIVERGE analysis are listed in Figure 5-figure supplement 1. Sequences were curated, divergent N-terminal and C-terminal sequences were deleted, and the sequences aligned using MUSCLE. For plotting, the site-specific posterior ratios for Type II divergence were binned across a window of 15 amino acids and normalized to the maximum value.

Homology Models. We created homology models of ANO6 based on nhTMEM16 [68]. mANO6 sequence was submitted to the Phyre2 Protein Fold Recognition Server [280]. mANO6 (truncated to 833 residues by deleting the extreme N- and C- termini) was aligned to the nhTMEM16 sequence extracted from PDB ID 4WIT (674 residues). These two sequences share 23% identity and 37.4% similarly (calculated by the BLSM62 algorithm). A total of 12 gaps were introduced, primarily at the N- and C-termini and in loops between secondary structural elements. Secondary structure prediction was incorporated into the alignment for Phyre2 (and all of the other modeling servers used for comparison including Swiss-Model and Tasser). There are no gaps in or near the SCRD, with the nearest gaps located in extracellular loops between helices 3 and 4 (2 residue gap 24 residues away) and between helices 4 and 5 (1 residue gap 22 residues away). While overall alignment and homology model generation would benefit from a template with greater sequence identity, all modeling servers reported high confidence in the generated models with no variation in the placement of the SCRD between models. Model geometry was minimized and the model subjected to 500 steps of geometry idealization and energy minimization using Phenix [391]. The overall RMSD of Cα atoms in the final alignment was 1.485 Å with a Q-score of 0.667 (calculated by UCSF Chimera).

156

Analysis of Data. Electrophysiological traces were analyzed with Clampfit 9 (Molecular Devices). Fluorescence intensity was analyzed with MetaMorph 7.8 and Fiji Image-J 1.49. Data are presented as mean ± SEM. Statistical difference between means was evaluated by two-tailed t-test. Statistical significance was assumed at $p<0.05$.

157

	ANO1	ANO6
Ochotona princeps	XP_004598328	XP_004597939
Mus musculus	XP_006508516	XP_006520292
Sorex araneus	XP_004618642	XP_004617125
Myotis brandtii	XP_005864562	XP_005881770
Rattus norvegicus	XP_006230838	XP_006242346
Cavia porcellus	XP_003468174	XP_003476132
Chinchilla lanigera	XP_005384296	XP_005406650
Octodon degus	XP_004627166	XP_004638701
Loxodonta africana	XP_003422667	XP_003405435
Otolemur garnettii	XP_003798337	XP_003793601
Homo sapiens	NP_060513	XP_005268763
Pan troglodytes	XP_003313240	XP_003313797
Tupaia chinensis	XP_006171411	XP_006168620
Camelus ferus	XP_006174720	XP_006190384
Mustela putorius furo	XP_004808701	XP_004808033
Canis lupus familiaris	XP_854489	XP_005637010
Orcinus orca	XP_004278099	XP_004274476
Ceratotherium simum simum	XP_004441181	XP_004428978
Pantholops hodgsonii	XP_005963680	XP_005963792
Capra hircus	XP_005700109	XP_005680114
Ovis aries	XP_004019998	XP_004007487
Bos taurus	NP_001179646	XP_002687401
Bos mutus	XP_005908980	XP_005902421

Figure 6-1 Genebank accession numbers of sequences of mammalian species ANO1 and ANO6 used for DIVERGE analysis.

158

ANO1_MOUSE MRVPEKYSTL PAEDRSSHIV NICAIRLGY LPSEGTLLNS LSVDPDAECK YGLYFRDGKR KVDYILVYHH KRASGSRTLA 80
ANO6_MOUSE ---------M QMMTHKS-LL NMELETDD- --EDGDIVLE NFDQTIVCPT FGSLENQQDF RTPEFEEFNG KPDSLFFTDG 67

ANO1_MOUSE RRGLQNDMVL GTRSVRQDQP LPGKGSPVDA GSPEVPMDYH EDDKRFREE VEGLLEAGE ELENDEDTKI HGVGFVKIHA 160
ANO6_MOUSE QRRIDFILVY EDESKKENNK ---KGT---- ---------N FKQKR-KPQA YESNLICHGL QLEATRSVSD DKLVFVKVHA 130

ANO1_MOUSE PWHVLLREAE FLKLKMPTKK VYHISETHGL LKTINSVLQK IIDPIQPKVA EHREQTTKRL SYPESREKQH LFDLTRDSF 240
ANO6_MOUSE PWEVLCTYAE IMHIKLPLKP --NDLKTRSP FGNLKW---- FIKVLRVNES VIKFEQ-EFF TAPTEKSRMN DFYILGRDSF 203

ANO1_MOUSE EDSKTRSTLV YELKETT-- CTKAKYSMGI TSLLANGVKS ARYPLHDG-- DYEGDNVEF- NDRKLLYEEW ASYGVFYKYQ 315
ANO6_MOUSE FNPATRSRIV YFILSEVKYQ VMNNVNKFGI NREVSSFIYK ARFLLPDCRF NYESEDISCP SERYLLYREV NHPRSIVKKQ 283

1
ANO1_MOUSE PIDLVRKYFG EKVGLYFAWL GAYTQMLIPA SIVGVIVFLY GCATVYENIP SMEMCDQRYN --ITMCPLCD KTCSYWKMSS 393
ANO6_MOUSE PLDLIGKNYG EKIGIYFAWL GYYTQMLLLA AVIGVACFLY GYLDQDNCTW SKEVGDPDIG GQILMCPQCD RLCPFWRLNI 363

2
ANO1_MOUSE ACATARASHL PFNPAIVFFS VFMALWAATF MEHWKRKQMR INERWDLTGF EEEEEAVKDH PRAEYEA--- --RVLEKSLR 468
ANO6_MOUSE TCESSKKLCI FDSFGTLIFA VFMGVVVTLF LEFWKRRQAE FEFEWDTVEL QQEEQAR--- F--FYFAQCN HVVINEITQE 438

3
ANO1_MOUSE KESRNKETDK VKLTWRDRFP AYETNLVSII FMIAVTFAIV FGVIYRISTA AAALMNSSS SVRS-NIRVT VTAFAVIINL 547
ANO6_MOUSE EERIPFTTCG KCIRVTLCAS KVFFWILLII ASVIGIIVYR ISWFLVFSTT LPKNPNGTDK IQKYLTPQMA TSITASLISF 518

4
ANO1_MOUSE VVIILDEVY GCIARWLTKI EVPKTEKSFE ERITFKALLL KEVNSYTPIF YVAIFKGREV RKSGLYMIF RSFRMEELAY 627
ANO6_MOUSE IIIMIENTIY EKVAIMITNF ELPRTQTDYE NSITMKMFLF QFVNYYSSCF YIAFFKGKFV GYPGDPVYLL GKYRSEECDP 598

5
ANO1_MOUSE GGCIMELCIQ LSIIMLSKQL IQNNLFEIGI PKMKKFIRYL KLRRQSPKDR EEYVKRKQRY EVDFNLEPFA GLTPEYMEMI 707
ANO6_MOUSE GGCILELTTQ LTIIMGGKA- IWNNIQEVLL PWVMNLIG-- RYKKVSGTEK ---ITPRWEQ DYHLQPMGKL GLFYEYLEMI 672

6 7
ANO1_MOUSE IQFGFVTLFV ASFPLAPLFA LLNNIIEIRL DAKKFVTELR RPVAIRAKDI GIWYNILRGV GKLAVIINAF VISFTSDFIP 787
ANO6_MOUSE IQFGFVTLFV ASFPLAPLLA LVNNILEIRV DAWKLTTQFR RMVPEKAQDI GAWQPIMQGI AILAVVTNAM IIAFTSDMIP 752

8
ANO1_MOUSE RLVYLYMYS- ------QNGT VHGFVNHTLS SFNVSDFQNG TAPNDPLDIG YEVQICRYKD YREPPWSEHK YDISKDFWAV 860
ANO6_MOUSE RLVYYWSFSI PPYGDHTYYT VDGYINNTLS VFNITDFKNT DKENPYIGLG -NYTLCRYRD FRNPPGHPQE YKHNIYYWHV 831

9 10
ANO1_MOUSE LAARLAFVIV FQNLVMFMSD FVDWVIPIP KDISQQLHKE KVLMVELFMR EEQGKQQLLD TWMEKSKPRD VPCNNHSYTT 940
ANO6_MOUSE IAAKLAFIIV MEHIIYSVKF FISYAIPEVS KITKSKIKRE KYLTQKL-LH ESHLKDLTKN MGIIAERIGG TVDNSVRPKL 910

ANO1_MOUSE HPEAGDGSPV PSYEYHGDAL 960
ANO6_MOUSE E--------- ---------- 911

Figure 6-2 MUSCLE alignment of mANO1(ac) and mANO6 used for constructing chimeras. Blue lines indicate membrane helices 1–10 determined by a homology model based on nhTMEM16. (Primary effort on figure: Hartzell, HC)

159

mANO1(ac) (960aa)	mANO6 (insert)	I_{+100mV} 20µM Ca^{2+}	N	I_{+200mV} Zero Ca^{2+}	N	PLS (% positive cells)
P380-E445	P350-Q415	0.16	4	<0.1	3	2
D485-Y514	G448-Y447	0.51	4	<0.1	3	2
T518-N546	V481-S517	1.19	2	<0.1	3	5
S532-G558	G495-E529	4.75	6	0.255	7	85
C559-V569	K530-L541	8.3	5	0.301	5	65
C559-F584	K530-F556	6.11	6	0.201	6	70
D554-E555	N525-T526	10.7	3	1.64	6	8
D554-K588	N525-Q559	2.21	6	4.7	6	90
P570-A600	P541-A571	0.45	5	0.10	4	3
E573-I596	Q544-C567	0.22	3	0.075	3	7
I636-F663	T608-L633	0.31	5	0.776	5	3
Q653-F663	F623-L633	4.5	4	0.209	4	3
R618-F663	G589-L633	0.05	4	0.222	3	5
P658-P701	P628-Y665	1.81	3			7
R748-P787	R713-P752	6.11	3	0.255	7	3
Y851-M909	Y822-L879	2.38	3			4
WT-ANO1		8.97	3	0.45	6	5

Figure 6-3 Properties of 1-6-1 chimeras that trafficked to the plasma membrane and generated ionic currents. Cells were transiently transfected with the indicated constructs in which the indicated amino acids of mANO1(ac) were replaced with the corresponding amino acids of mANO6 (as determined by the alignment shown in Figure 5—figure supplement 2). Currents were measured with 20 µM free Ca^{2+} in the patch pipet at +100 mV or with zero Ca^{2+} in the patch pipet at +200 mV. PLS was measured by Annexin-V-Alexa568 binding to cultures of cells 10 min after addition of 10 µM A23187 and 1 µM thapsigargin. PLS was assessed in >3 independent experiments, counting >100 cells. (Primary effort on figure: Yu, K)

ANO1	Replaced with ANO6	PLS (%positive cells)
D554-E555	N530-T531	4
D554-V556	N525-I527	3
G558-I560	E529-V531	7
R562-L564	I533-I535	5
K566-I567	N537-F538	5

Figure 6-4 Properties of 1-6-1 chimeras in which pairs or triplets of amino acids were mutated. None of these chimeras exhibited PLS. (Primary effort on figure: Yu, K)

ANO6	Replaced with ANO1	PLS (% positive cells)	Currents (pA at 100 mV)
N525-T526	D554-E555	12	
N525-I527	D554-V556	15	54 ± 24
E529-V531	G558-I560	7	77 ± 41
I533-I535	R562-L564	15	
N537-F538	K566-I567	78	
N525-Q559	D554-K588	5	71 ± 43
P541-L662	P570-A697	7	65 ± 50

Figure 6-5 Properties of ANO6 with mutations in the SCRD. Various mutations in the SCRD abolish PLS and ionic currents. (Primary effort on figure: Yu, K)

161

A 1-6-1_D554-K588

EGFP   Annexin-V >

B 6-1-6_(N525-I527)
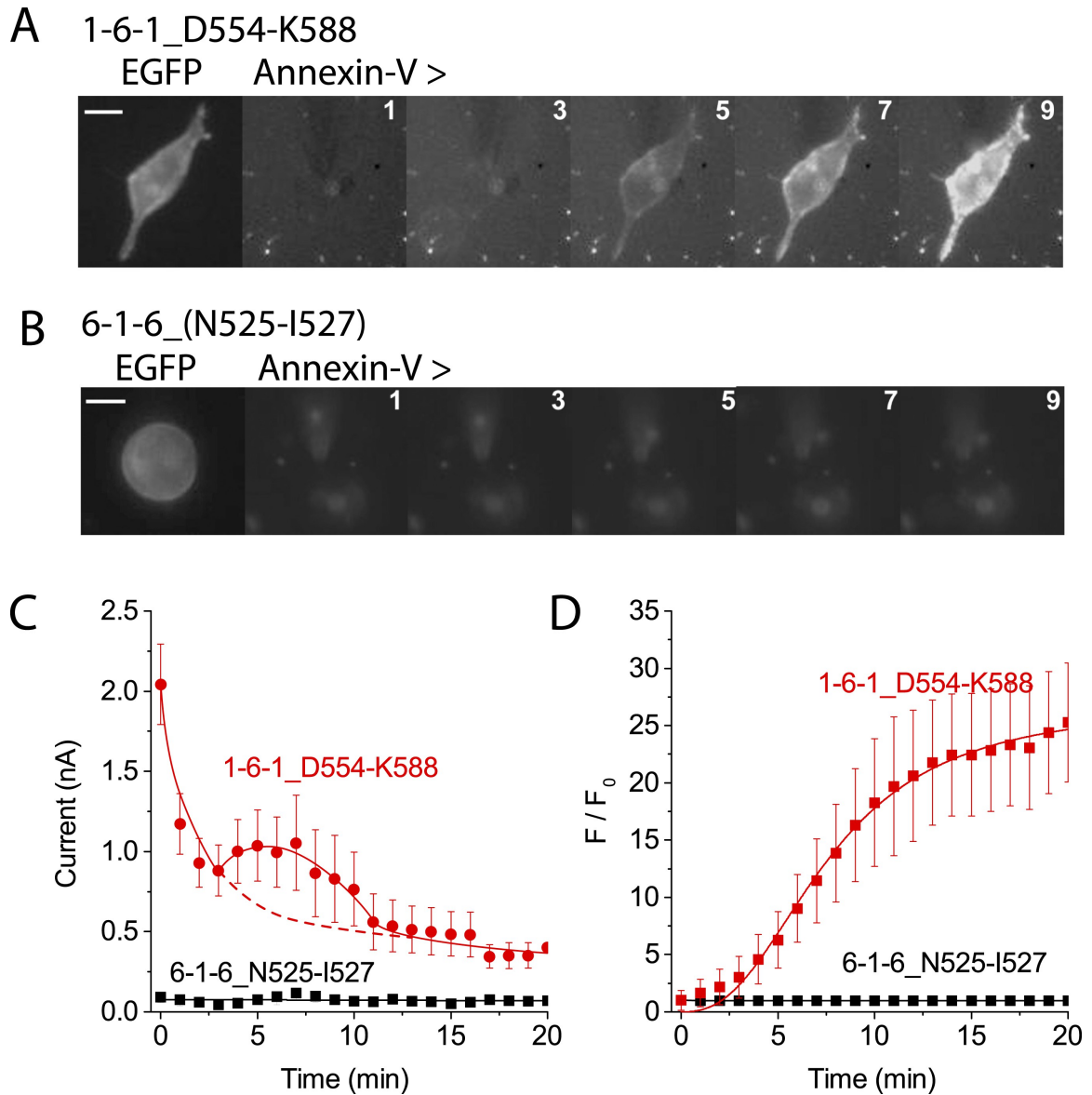
EGFP   Annexin-V >

Figure 7-1 Patch clamp analysis of ANO1-ANO6 chimeras. HEK cells expressing (**A**) 1-6-1_D554-K588 or (**B**) 6-1-6_N525-I527 were patch clamped in the presence of Annexin-V-Alexa-568 in the bath. The first image shows ANO6-EGFP fluorescence obtained before establishing whole-cell recording. F_o was determined immediately after establishing whole-cell recording. Annexin-V fluorescence images were acquired immediately after obtaining each I-V curve by voltage clamp at 1 min intervals. The patch pipet contained 20 µM free Ca^{2+} for 1-6-1_D554-K588 and 200 µM for 6-1-6_N525-

I527. I-V curves were obtained by voltage steps from −100 mV to +100 mV in 20 mV increments. Scale bars 10 μm. (**C**) Average current amplitudes ± SEM at +100 mV for 1-6-1_D554-K588 (red circles) and 6-1-6_N525-I527 (black squares) plotted vs time after establishing whole-cell recording. The red curve was drawn by hand as the sum of an exponential and a Gaussian with the dashed portion of the curve representing the exponential curve in the absence of the Gaussian component. (**D**) Average Annexin-V fluorescence divided by the initial fluorescence ± SEM for the same cells as in C (n = 5). (Primary effort on figure: Yu, K)
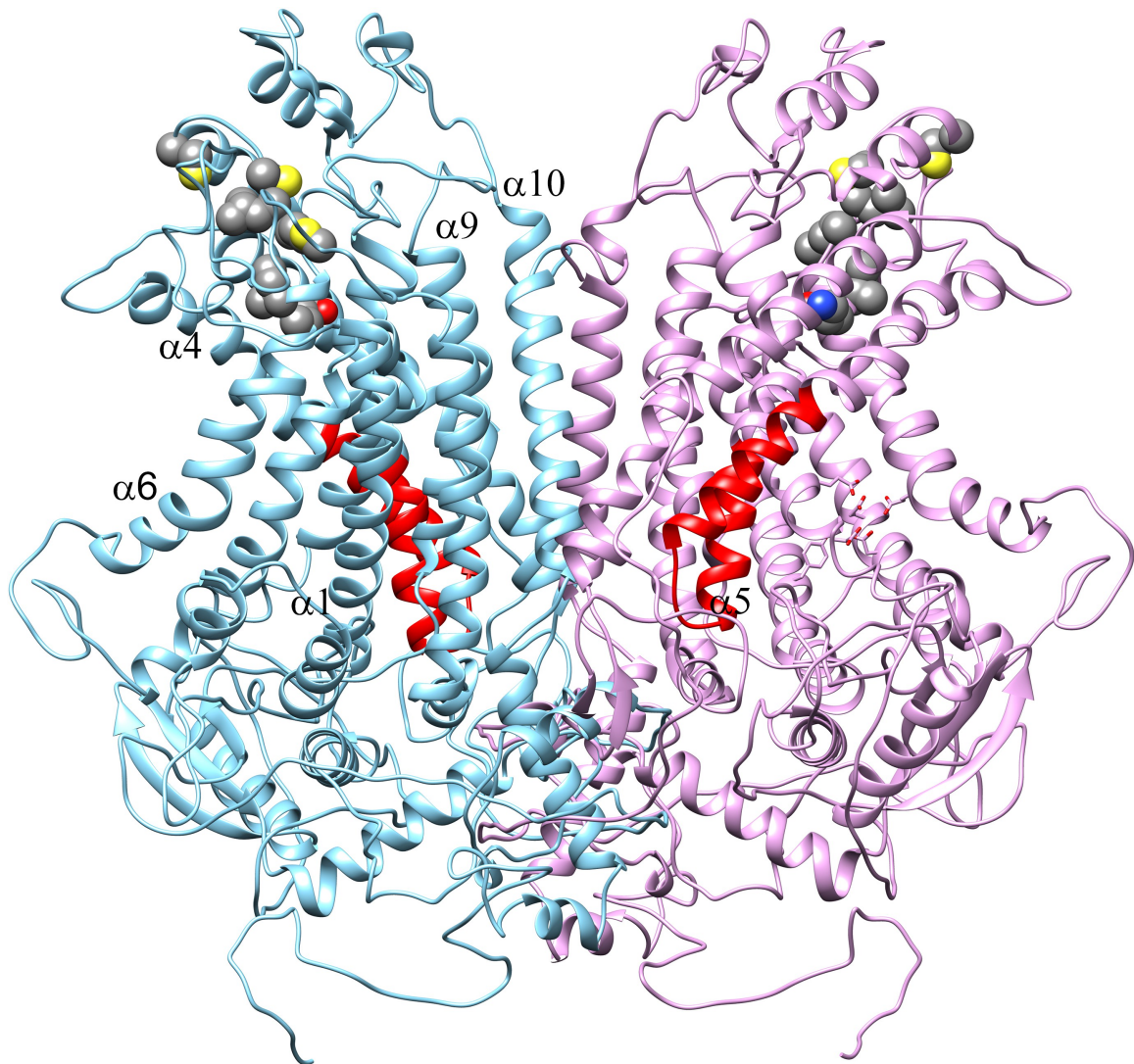
Figure 9-1 Homology model of ANO1 dimer. The SCRD homology domain is colored red. The Ca^{2+} binding site is shown in stick representation in the right monomer. Residues identified by <u>Yu et al. (2012)</u> as forming the vestibule of the ion conduction pathway of ANO1 are shown in spacefill (C625, G628-M632, I636-Q637). (Primary effort on figure: Hartzell, HC)

Chapter V

Muscle Progenitor Cell Fusion In The Maintenance Of Skeletal Muscle

Muscle fibers are the individual, cellular units comprising skeletal muscle tissues and represent a highly specialized cell type. Skeletal muscle tissue represents ~40% of the overall body mass and is essential for indispensable tasks such as the consumption of food and breathing [392]. Each muscle fiber is created by the fusion of hundreds to thousands of muscle progenitor cells during development to produce a single, continuous cell that can run up to 600 mm in length in humans [197, 393]. These fibers consist of a specialized plasma membrane, the sarcolemma (SL); a specialized cytoplasm, the scarcoplasm (SRM); a modified endoplasmic reticulum, the sarcoplasmic reticulum (SR); many sarcomeres, the basic actin/myosin based contractile unit of skeletal fibers, organized into long chains termed myofibrils; and hundreds to thousands of myonuclei, whose numbers are tightly maintained following pre- and postnatal development (Fig. 1a) [394, 395].

Much of the specialization surrounding muscle fibers revolves around their contractile role and the requirement that each muscle fiber must transduce electrical signals along their entire length, initiating from innervations at the neuro muscular junction (NMJ), to tightly coordinate Ca^{2+} signaling. The tight regulation of this Ca^{2+} signaling is essential for the coordination of sarcomere contraction along the length of the fiber in synchronization with neighboring fibers to produce a concerted contraction of the tissue. To coordinate this tightly regulated Ca^{2+} cascade invaginated SL, the transverse tubules, rapidly transmit action potentials to activate resident L-type Ca^{2+} channels. The activity of these L-type Ca^{2+} channels stimulates dihydropyridine receptors that elicit Ca^{2+} released from the SR. The specialized SR network, which winds through the entire fiber in a regulated pattern, quickly releases Ca^{2+} into the SRM that is filled largely with contractile units referred to as myofibrils [iterative collections of sarcomeres (Fig. 1b)]. This intracellular signaling cascade elicits the coordinated contraction of the myofibrils and converts a chemical signal elicited by the original electrical impulse at the NMJ into a

166
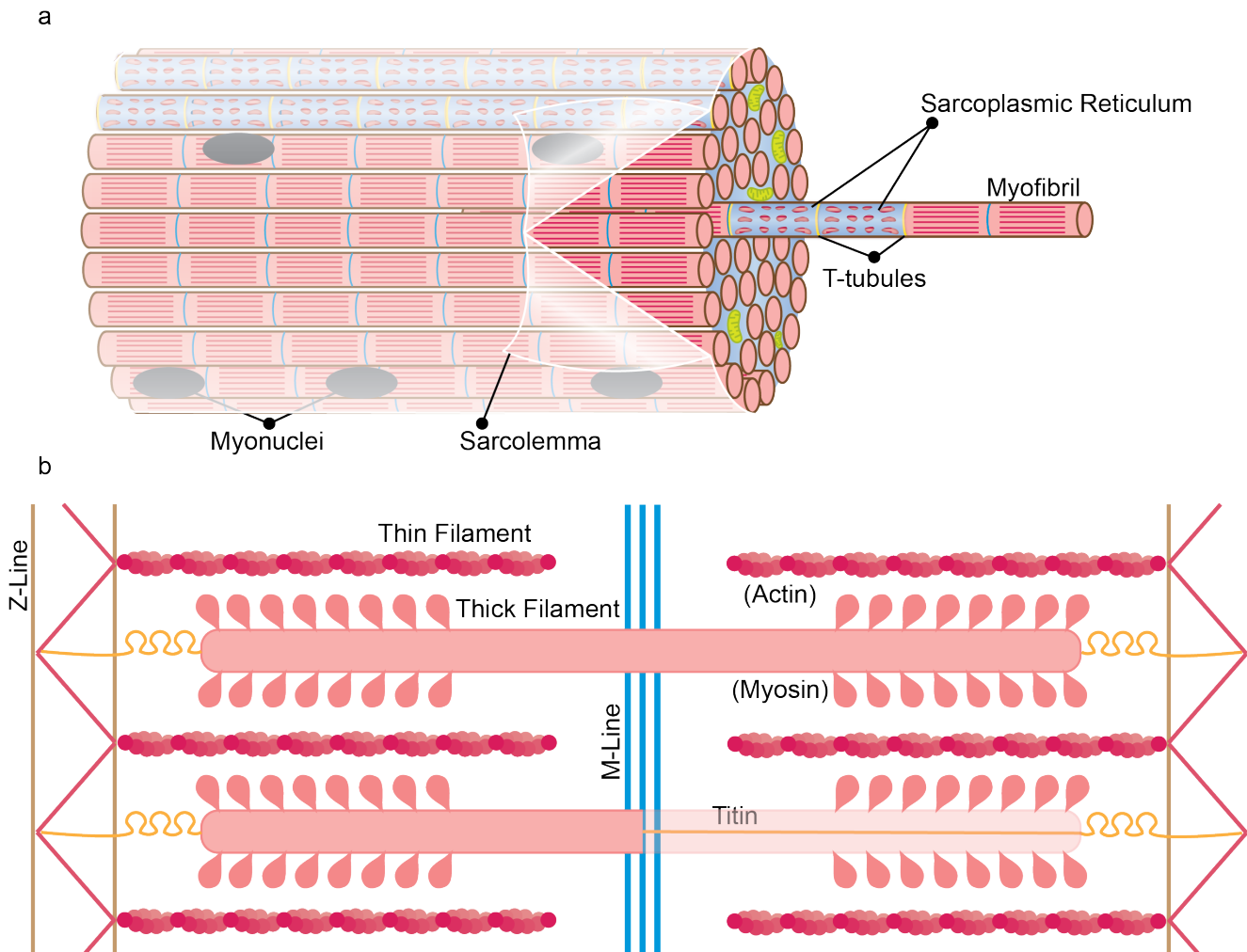
Figure 1 An illustrative representation of skeletal muscle cell ultrastructure. (**a**) Ultrastructure of a single skeletal muscle fiber along its longitudinal axis. (**b**) The general organization of a single sarcomere. (Primary effort on figure: Whitlock, JM)

physical action within skeletal muscle tissue (reviewed in greater detail [396]). Skeletal muscle is akin to a marvelous biological machine–however like any machine–this evolutionary marvel requires a system of repair processes that dynamically maintain its function.

SKELETAL MUSCLE REQUIRES RAPID REPAIR/REGENERATION MECHANSIMS FOR LIFELONG MAINTENANCE

Skeletal muscle relies on at least two essential repair processes that work to maintain its integrity and function. These processes include a membrane patch repair process, present in all mammalian cell types, and a specialized repair/regeneration mechanism that relies on a resident, mononucleated stem cell population. These processes work in parallel to maintain muscle function throughout life. Perturbations in either of these repair processes have been shown to lead to a variety of myopathies, primarily disorders that result in muscle weakness and wasting [muscular dystrophies (MDs)]. Here we will review these repair processes and what is known concerning their mechanisms.

Plasma membrane lesions undergo patching via Ca^{2+} regulated exocytic repair.

For more than half a century it has been well recognized that extracellular Ca^{2+} flux through plasma membrane lesions triggers the rapid (seconds) resealing of the membrane to avoid Ca^{2+} toxicity (reviewed [397]). If these injuries are small enough (a few nanometers) the lesions can be rapidly resealed by virtue of membrane lipids rearranging to avoid exposure of the hydrophobic membrane core to the outside, polar environment [398]. However if lesions exceed several nanometers, active repair processes are required to reinstate membrane integrity [399]. Active repair of membrane lesions often occurs through the rapid exocytosis of intracellular vesicles [400, 401]. The

resealing capability of this pathway is highlighted in classical experiments using

microneedle damage of echinoderm egg membrane, where these cells can employ

exocytic patch repair to reseal lesions of >2,000 μm^2 in <5 seconds [402]. Why cells go

to such great lengths to maintain the mechanism of membrane patch repair lies in the

propensity of this process to protect irreplaceable cell types (neurons) or those that are

of significant energetic value (skeletal muscle). The mechanistic intricacy of membrane

patch repair combined with its diversity of players in different cells types strongly

suggests that it has been governed by immense selective pressure during cellular

evolution.

General Membrane Patch Repair Mechanism

The general mechanism of membrane lesion patch repair is consistent throughout many

diverse cell types, however, the exact proteins regulating patch repair and the

membranes contributing to the patch continue to be hotly debated topics and likely differ

greatly between cell types and organisms. Much of the controversy surrounding this field

likely stems from the many associated processes that are stimulated by intracellular Ca^{2+}

flux, but may not be essential for membrane patch repair to restore PM barrier

competence. For instance, the fusion of exocytic vesicles during conventional exocytosis

associated with the secretory pathway is regulated by increases in Ca^{2+}, therefore,

damaging the PM might cause exocytic vesicles to fuse with the PM due to incidental

Ca^{2+} flux. This does not mean that these vesicles are necessarily important for

membrane repair or that their fusion machinery should also be considered patch repair

machinery. Moreover, because of the importance of closing membrane lesions to the

survival of the cell, the probability of built-in redundancy is high.

In short, upon elevated Ca^{2+} flux from the extracellular solution through the lesion site,

vesicular membranes are recruited to the site of membrane breach and rapid exocytic

processes elicit the fusion of intracellular vesicles with the lesion. Vesicle-vesicle fusion

169

produces a growing membrane patch, while fusion of these patch vesicles with the

lesion membrane restores membrane barrier competence [399]. This process is likely

regulated by exocytic machinery, of which syaptotagmin-7 and a variety of other SNARE

proteins have recently been highlighted for their roles in Ca^{2+} sensing and fusogenic

repair [403-406]. Because diverse intracellular vesicles are fusion competent and

vesicular fusion is regulated in part by elevated cytosolic Ca^{2+}, most vesicular

membranes are probably capable of contributing to membrane patch repair, although

some may be preferred. There are also a variety of non-vesicular repair pathways that

likely complement this process and may even be sufficient for lesion closure in some

special cases (reviewed elsewhere [397]).

Skeletal muscle fibers have a particular dependence on membrane patch repair, as up

to 30% of skeletal muscle fibers exhibit membrane wounding *in vivo* [407]. Muscle fibers

possess orders of magnitude more delimiting membrane than any other cell type and

this membrane is continuously subjected to immense mechanical stress that leads to SL

lesions [408]. Although considerable controversy exists over the precise mechanism of

skeletal muscle patch repair, a general consensus has been discovered following

decades of investigation. Following SL insult, dysferlin is thought to function as a Ca^{2+}

sensor and/or a fusogenic protein regulating membrane patch formation by virtue of its

C2 domains Ca^{2+}-dependent affinity for phospholipids containing. The C2 domains of

dysferlin and many other regulators of intracellular membrane fusion are essential for the

Ca^{2+}-dependent association of these proteins with membranes [409]. This is similar to

related ferlin proteins in other cell systems [210, 222, 410]. Recent investigation

suggests that when SL damage occurs, dysferlin-laden SL is endocytosed and fuses

along with endosomes and other endo-lysosomal organelles to form a membrane patch

[222]. In addition, dysferlin may remain at the membrane lesion and work to coordinate

the fusion of membrane patch vesicles in SL resealing. Strong evidence suggests that

170

the Ca^{2+}-dependent association of annexins with phosphatidylserine (PS) at the lesion membrane coordinates the action of dysferlin in SL resealing [218]. In parallel, MG53 oligomerizes on PS containing intracellular vesicles upon Ca^{2+} flux and works to recruit repair vesicles and patch repair machinery to the lesion site [411, 412]. Mutations and/or loss of any of these components leads to perturbations of muscle repair *in vivo*, and some of the genes encoding these proteins are linked to a variety of human MDs [191, 210, 411, 413].

Skeletal muscle employs a multipotent stem cell population in fiber repair/regeneration.

Because of the essential nature of maintaining proper musculature, muscle possesses a second major repair process that relies on a native, multipotent stem cell population. These stem cells are termed satellite cells because of their proximity to the muscle fiber, occupying a niche in the surrounding basal lamina [414]. Satellite cell dependent muscle repair/regeneration is essential for the lifelong maintenance and function of skeletal muscle [415, 416]. Upon fiber injury, satellite cells are activated and begin rampant proliferation of daughter cells that contribute to the repair of damaged skeletal muscle [417, 418]. Like developmental muscle precursors, their multipotent daughter cells proceed through a muscle developmental program (myogenesis), and undergo homotypic (progenitor cell-progenitor cell) and heterotypic fusion with the damaged fiber to restore the fiber [419]. Additionally, this muscle precursor population retains the ability to fuse and regenerate lost fibers *de novo* in order to restore damaged muscle lost to injury/disease [420-423].

Satellite cell dependent muscle repair: A trip back to development?

171

Myogenic progression in skeletal muscle progenitor cells

Our understanding of satellite cell dependent muscle repair is largely colored by the characterization of myogenic progression during development. Skeletal muscle develops from the dorsal portion of the somites, with the exception of many head muscles [424]. Embryonic myogenic specification is controlled primarily by the transcription factor PAX3, and to a lesser extent PAX7, which plays a sort of master regulatory role in the process of myogenic specification [425, 426]. Further commitment to differentiated muscle involves sequential activation of 4 myogenic regulatory factor (MRF) family transcription factors Myf5, MyoD, myogenin, and MRF4 (reviewed extensively [427]). Some controversy remains involving the hierarchy of these regulators, but the consensus is that Myf5–followed shortly by MyoD–act as determination factors, committing cells to a myogenic fate. Next myogenin and MRF4 expression increase and fulfill essential roles for terminal muscle differentiation. Largely, myogenic progression of resident muscle stem cells in adult tissue proceeds through a similar myogenic progression (i.e. myogenesis), however some differences exists in the mechanistic action of these general processes.

Satellite cells become activated and migrate to tissue damage upon muscle injury.

Following muscle injury, skeletal muscle stems cells must become activated and migrate to sites of fiber injury to participate in tissue repair, as illustrated in Figure 2. Adult skeletal muscle maintains a satellite stem cell population in the basal lamina surrounding the muscle fiber that play essential roles in myogenic repair/regeneration. These stem cells reside in a quiescent state with a high nuclear:cytoplasm ratio and very low transcriptional and metabolic activity at rest [428]. Resting satellite cells are very similar to undifferentiated muscle progenitors in development, however this stem cell population

172

displays an essential requirement for PAX7, which they express at very high levels in contrast to the high reliance on PAX3 developmentally [415, 416, 426, 429]. Upon muscle injury nitric oxide is near instantly generated and plays an essential role in the injury induced activation of satellite cells [430]. The extracellular matrix (ECM) of the basal lamina embeds satellite cells and insulates them from the influence of circulating growth factors. Nitric oxide strongly upregulates the production of matrix metalloproteinase that degrade the ECM environment of the satellite cell niche [431]. Upon ECM damage, satellite cells are exposed to and activated by a variety of circulating factors. One factor, FGF2, induces a rapid intracellular Ca^{2+} spike through TRPC channels, which activates NFATc and leads to cell cycle reentrance [432]. A similar activating role has also been ascribed to HGF [433, 434]. Cell cycle reentrance marks the initiation of satellite cell dependent muscle repair.

Following activation, satellite cells become highly mobile, and migrate to the site of muscle fiber injury where they proliferate, giving rise to a pool of highly fusogenic muscle precursor cells. Activation is first followed by rapid migration to the site of injury (267). Initial migration to the site of injury is essential, as activated satellite cells become less mobile following proliferation (142, 313). Injured muscle releases a variety of soluble chemoattractant molecules, illustrated by the ability of extract from crushed muscle to promote directional migration of isolated muscle progenitor cells [435]. The chemoattractant abilities of some soluble molecules within crush extracts have been recognized (e.g. TGF-β, HGF, FGF-2, and FGF-6) [436, 437], however the exact contributions of various factors to muscle progenitor chemotaxis remains an area of open investigation. Upon reaching the site of damage, activated satellite cells begin proliferating in order to produce a population of multipotent daughter cells capable of repairing the musculature.

Proliferation of myogenic daughter cells for contribution to the musculature.

At the site of muscle injury, activated satellite cells undergo successive rounds of proliferation producing many repair competent daughter cells while also maintaining an uncommitted stem cell population for future muscle maintenance. These satellite cell attributes were perhaps best highlighted by Collins *et al.* who evaluated satellite cell dependent muscle repair in irradiated murine hindlimbs [421]. Transplantation of a single muscle fiber with as few as 7 satellite cells was sufficient to repopulate irradiated muscle with >100 resident satellite cells and produce ~100 regenerated muscle fibers containing an estimated 25,000-30,000 differentiated myonuclei in 3 weeks post transplantation [421]. Moreover, the repopulated satellite cell population contributed to subsequent satellite cell dependent muscle repair when the muscles were injured with notexin injection, demonstrating that these repopulated cells were true repair competent satellite cells. Exactly how satellite cell proliferation gives rise to separate populations of committed progenitors and uncommitted stem cells has been extensively evaluated in recent years. Although these recent investigations have produced a basic understanding of satellite cell division and self-renewal, this is still a very active area of investigation. For some time, whether $PAX7^+$ satellite cells were true stem cells or whether they were dedifferentiated committed myoblasts was an open question. In 2007 the Rudnicki group demonstrated that ~10% of the total satellite cell pool were $PAX7^+$/ $Myf5^-$ and had never expressed the commitment factor Myf5 throughout the history of the cell [438]. This never committed $PAX7^+$/ $Myf5^-$ population expands to ~30% of the satellite cell pool following injury, suggesting a role for the expansion of satellite stem cells in muscle repair. These $PAX7^+$/ $Myf5^-$ cells are thought to represent the true, uncommitted stem cell population in skeletal muscle, however the precise origin of individual muscle stem
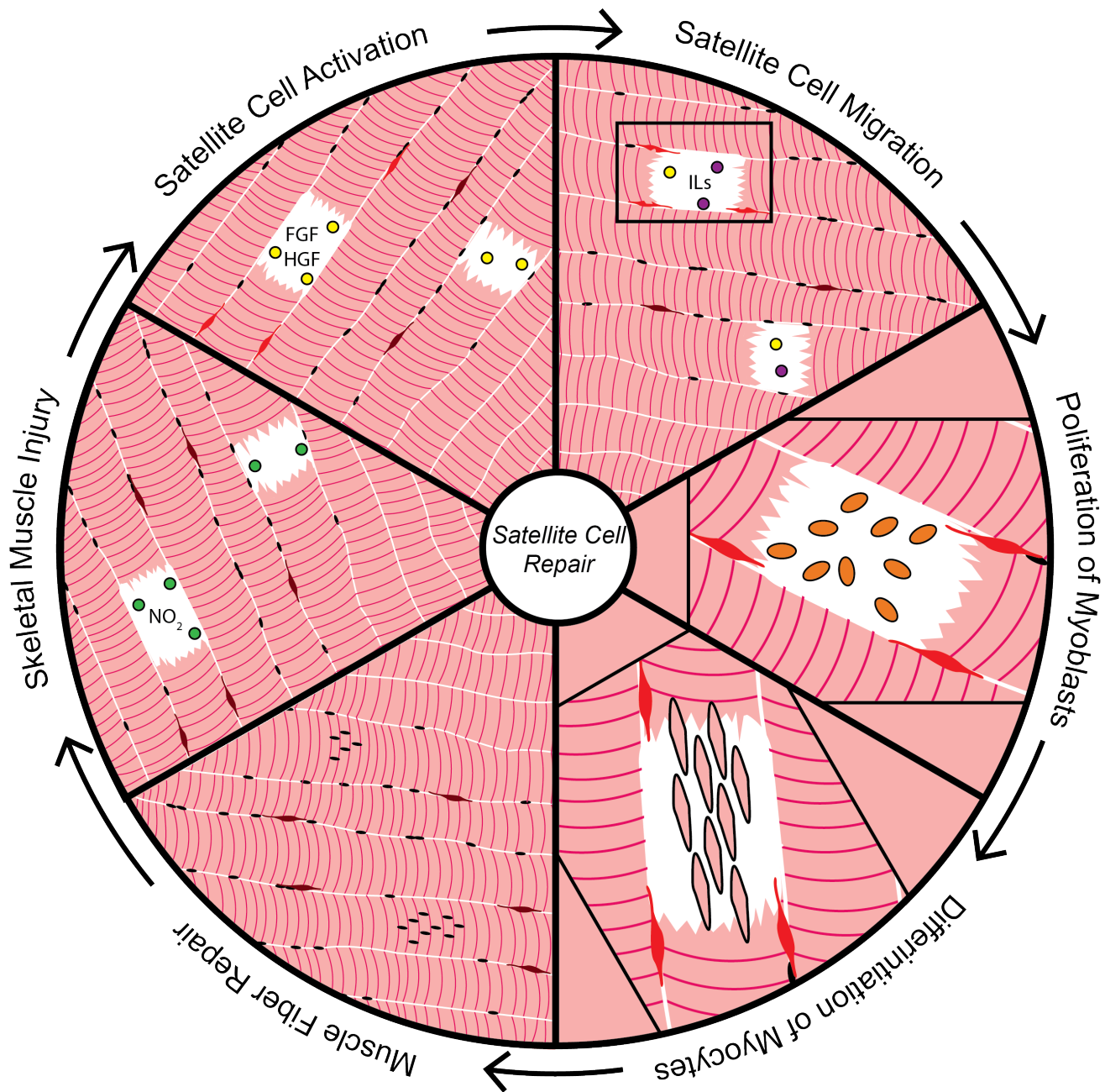
Figure 2 Satellite Cell-dependent Skeletal Muscle Repair. A graphical illustration of the progression of satellite cell-dependent skeletal muscle repair following injury. Sequential steps highlight the roles of the myogenic cell types involved at each step of repair: Burgundy, quiescent satellite cells; red, activated satellite cells, orange, proliferative myoblasts; pink, quiescent myocytes; and pink with magenta striations. multinucleated myofibers. Within damaged fiber windows examples of the many singling

factors associated with the progression of satellite cell-dependent repair between steps

are highlighted as colored spheres: green, nitric oxide (NO_2), yellow, fibroblast growth

factor and hepatocyte growth factor (FGF and HGF); and purple, a general

representation of interleukin factors (ILs). (Primary effort on figure: Whitlock, JM)

cells is complicated as there is strong evidence that committed muscle progenitor cells can undergo dedifferentiation and revert to quiescent satellite cells *in vitro* [439]. Moreover, the physiological relevance of this dedifferentiation process in maintaining repair competent satellite cells was recently bolstered with the observation of myogenic regression of committed muscle progenitors *in vivo* [440].

Regardless of their previous differentiation states, satellite cells undergo successive rounds of proliferation at the site of muscle injury. This proliferative process is partially regulated by many of the same factors that activate these cells (e.g. FGF2), however recent investigation has highlighted the role of a cascade of proinflammatory cytokines (e.g. IL-6) released in injured muscle that coincides with muscle progenitor proliferation and play major roles in regulating this process [441, 442]. Once proliferation is initiated, satellite cells can undergo two separate division processes giving rise primarily to committed satellite cells ($Pax7^+/Myf5^+$)–and to a lesser extent–maintaining an uncommitted satellite cell population ($Pax7^+/Myf5^-$) for stem cell self-renewal. $Pax7^+/Myf5^-$ cells can either undergo asymmetric (apical:basal) or symmetric (planar) division, with respect to the SL (see initial satellite cell division in Figure 3) [438]. Asymmetric division gives rise to a daughter cell that maintains $Pax7^+/Myf5^-$ attributes of the mother satellite cell and a committed $Pax7^+/Myf5^+$ cell (typically the cell that has divided toward the basal lamella and is no longer in direct contact with the SL). Symmetric division expands the $Pax7^+/Myf5^-$ satellite cell population by giving rise to two $Pax7^+/Myf5^-$ daughter cells and is likely important for the expansion of this cellular population following injury and the overall maintenance of the $Pax7^+/Myf5^-$ quiescent cell population following repair. $Pax7^+/Myf5^+$ satellite cells, while having initiated their myogenic program, are actually more proliferative than their uncommitted counterparts but only undergo symmetric cell division in order to expand this committed muscle progenitor population. These processes produce a mixed muscle precursor population

177
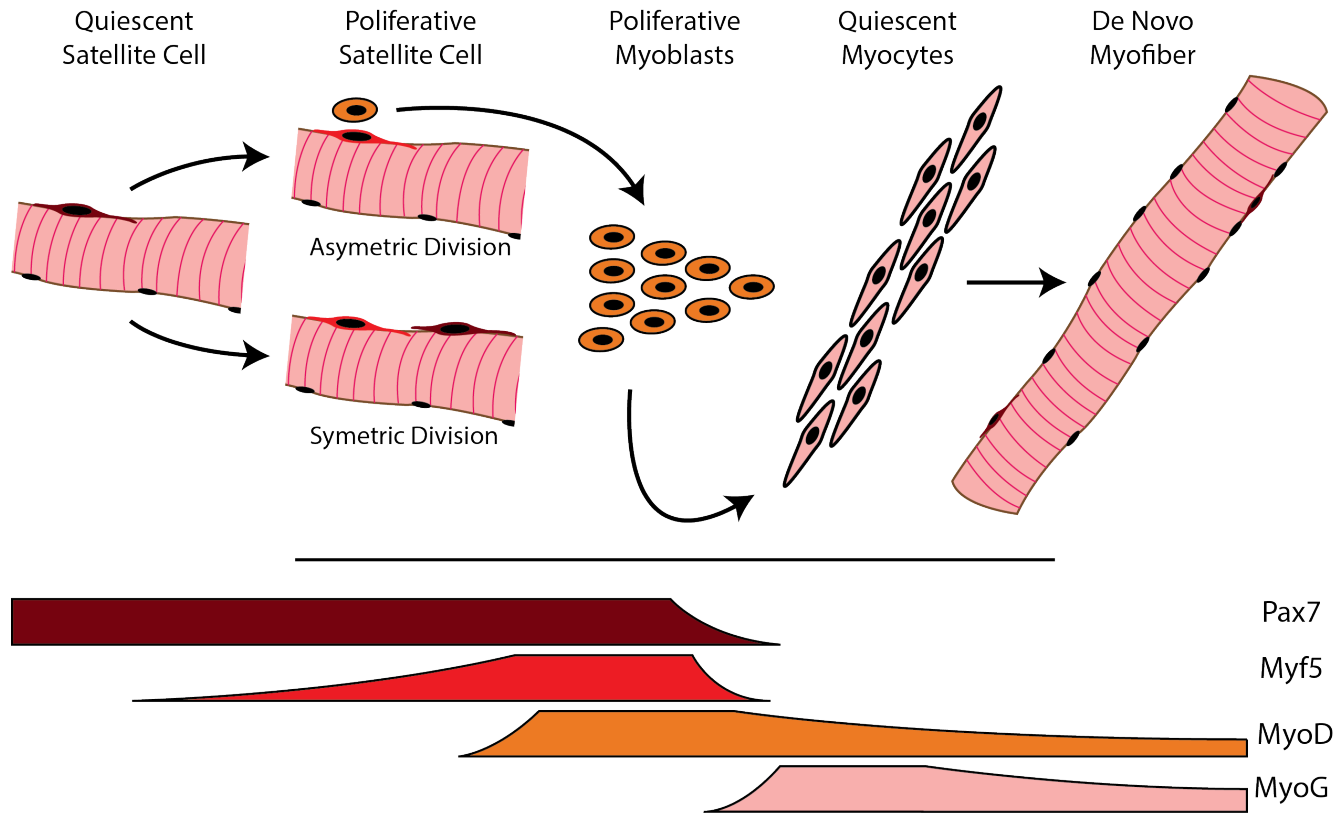
Figure 3 Myogenic progression in satellite cell-dependent skeletal muscle repair.

An illustrative model of myogenic progression associated with the activation of satellite cells and the subsequent regeneration of a skeletal muscle fiber de novo. Below is a graphical representation of the expression of the four primary myogenic factors that regulate this myogenic process and their temporal relationship to satellite cell-dependent muscle regeneration. (Primary effort on figure: Whitlock, JM)

that must further differentiate in order to contribute to the musculature and repair damage.

Satellite cell differentiation

Satellite cells are non-fusogenic and must undergo further differentiation in order to contribute to muscle tissue. Myogenic differentiation of satellite cells first begins when the majority of satellite cells start to express Myf5. Differentiation proceeds when Pax7^{+}/Myf5^{+} satellite cells begin expressing MyoD, and are then termed proliferative myoblasts. Along myogenic progression, MyoD initiates the transition from proliferation to exit of the cell cycle accompanied by further myogenic differentiation. MyoD accomplishes these further steps in myogenic progression by upregulating cell cycle inhibitors and by initiating the expression of myogenin (Fig. 3) [443, 444]. As in development, Myogenin and MRF4 both work to differentiate muscle progenitor cells by activating genes essential for muscle function (e.g. myosin heavy chain and L-type Ca^{2+} channels), as well as, activate the expression of muscle proteins required for fusion (e.g. myomaker) [445, 446]. From this point, quiescent, differentiated muscle progenitors–termed myocytes–proceed through homotypic fusion to produce nascent myofibers or through heterotypic fusion with the ends of damaged fibers to restore the muscle fiber.

Muscle fusion in fiber repair and regeneration.

Adhesion proteins in muscle fusion

Muscle progenitor cell fusion is the fundamental step by which muscle progenitor cells contribute to the repair/regeneration of skeletal muscle. Quiescent myocytes precede through myogenic fusion by recognizing a fusion partner, forming tight cell-cell adhesion with that partner, and then undergoing a complicated fusion process to form a syncytium.

Myogenic fusion is preceded by the mutual recognition of fusion partners. Fusion partner recognition is perhaps best understood in *D. melanogaster*, however muscle cell fusion is fundamentally different in fly compared to mammals (e.g. the role of founder cells, see latter subtopic: muscle by the models). In *D. melanogaster*, fusion competent myoblasts (FCMs) recognize their fusion partners (founder cells/myotubes) via immunoglobulin superfamily proteins on the surfaces of each partner. Sticks-and-stones and Hibris on FCM membranes recognize cognate immunoglobulin superfamily proteins Kin-of-IrreC and the functionally redundant Roughest on fusion partner membranes (reviewed extensively [447]). The association of these factors with their cognate partners on fusion partner membranes plays an essential role in these cells distinguishing one another from the many other cell types in the skeletal muscle tissue, in the adhesive association of fusion partners, and in activating downstream signaling required for fusion initiation (e.g. activation of cytoskeletal rearrangements discussed below).

Nephrin (vertebrate homolog of Sticks-and-stones) is the only common recognition/adhesion molecule common to both mammal and *D. melanogaster*. In mice, all myocytes are all considered equivalent, so the segregation of roles for different adhesion proteins between partners is not obvious (i.e. there are no founder cells). However, integrins $\alpha3$, $\beta1$, and $\alpha9\beta1$ have been recognized for their roles in muscle progenitor cell adhesion and fusion [448, 449]. Moreover, the muscle specific adhesion protein M-cadherin is enriched at sites of myocyte cell-cell contact and is required for the efficient fusion of immortalized rat myoblasts [450], however loss of M-cadherin expression in mice leads to no obvious perturbation in skeletal muscle development or regeneration [451]. The latter finding is hard to interpret in light of the many putative roles of M-cadherin in skeletal muscle, however this may suggest significant redundancy in adhesion/fusion machinery.

Membrane signaling in muscle recognition/fusion

180

In addition to specific adhesion proteins, the exofacial exposure of PS is a major membrane signaling process regulating muscle cell recognition, adhesion, and fusion. Its exposure is well recognized as an important signaling process regulating many physiological cell fusion events (e.g. sperm-egg, macrophage, syncytiotrophoblast, osteoclast precursor, and virus-cell fusion) [230, 233, 234, 452, 453]. Van den Eijnde *et al.* first identified non-apoptotic PS exposure on the exofacial leaflet of developing murine musculature [186]. Shortly after, they followed this observation with the description of PS exposure at sites of contact in fusing immortalized myoblasts and found that masking this PS signal inhibited fusion [187]. This transient PS exposure was not associated with the appearance of apoptotic markers and could not be blocked via inhibition of caspase activity. These findings have been confirmed in primary murine myoblasts, and exogenous PS liposomes were found to directly promote primary muscle fusion [188]. Although exposed PS regulates myocyte fusion, the exact mechanism by which this process regulates fusion is only beginning to be appreciated.

Recently, two receptors have been identified for their role in recognizing PS during myocyte fusion. BAI1 and STAB2 have both been identified as muscle PS receptors required for efficient fusion *in vitro*, and loss of either significantly perturbs satellite cell dependent muscle repair/regeneration following cardiotoxin challenge *in vivo* [190, 454]. BAI1 is a G protein-coupled receptor previously recognized for its role in mediating PS recognition on apoptotic cells through the ELMO/DOCK180/Rac1 pathway [455]. Because the ELMO/DOCK180/Rac1 pathway plays an essential role in regulating muscle fusion in fly, fish, and mouse [455-459] and PS is also implicated in muscle fusion, the role of BAI1 in muscle fusion was investigated. Although loss of BAI1, does perturb muscle repair *in vivo*, the protein's role in fusion was primarily investigated in immortalized C2C12 cells. The STAB2 receptor is also thought to mediate PS recognition through the ELMO/DOCK180/Rac1 pathway. Despite the previously

181

identified role for BAI1 in muscle fusion, investigators found that *Bai1* mRNA was barely

detectible in murine skeletal muscles or in C2C12 myoblasts during differentiation. In

contrast, high levels of *Stab2* were detected in multiple murine limb muscles, and *Stab2*

is upregulated during the differentiation of both C2C12 and primary myoblasts [454].

Stab2 steady state levels are regulated during myogenic differentiation by increases in

cytosol Ca^{2+} concentration under the regulation of NFATc, which as previously

discussed, also regulates the activation of satellite cells through FGF2 signaling upon

damage. Moreover, STAB2 can confer fusion capability to non-fusogenic fibroblasts,

suggesting that PS signaling may play a role in direct cell-cell fusion and not be

restricted to only regulating cell recognition and adhesion. In direct contrast to

Hochreiter-Hufford *et al*., Park *et al.* found apoptotic inhibition in C2C12 cells had no

effect on fusion, in control or STAB2 overexpressing conditions [454]. This finding is in

line with previous descriptions of the inhibition of caspase activity having no effect on PS

exposure or fusion in myoblasts [187]. Some of these discrepancies may be due to when

and for how long the cells were treated with caspase inhibitors. Interestingly, the loss of

either BAI1 or STAB2 has a very modest effect on skeletal muscle development despite

their obvious effects on muscle repair and in vitro muscle progenitor fusion.

Although consensus suggests myoblast PS exposure and fusion are not affected by

apoptotic inhibition, sub-apoptotic activity of caspase 2, 3, and 9 play essential roles in

myogenesis [460-462]. Recent work has convincingly demonstrated that sub-apoptotic

activity of caspase 9 is initiated in non-apoptotic C2C12 cells during myogenic

progression following differentiation. This rise in the initiator caspase 9 coincides with the

cleavage/activation of the effector caspase 3 during differentiation at levels below those

observed following apoptotic induction of C2C12 cells via staurosporine treatment [460].

This caspase 3 activity elicited in C2C12 cells was found to activate MST1, a component

of the p38 MAPK signaling pathway [461]. The p38 MAPK signaling pathway has been

highlighted previously for its role in increasing the endogenous activity of skeletal muscle transcription factors associated with myogenic progression [463, 464]. Interestingly, the inhibition of C2C12 fusion associated with caspase 3 knock-down can be rescued via MST1 overexpression, suggesting this kinase plays a integral function in the progression of myogenic progression/fusion in C2C12 cells downstream of caspase 3, which is downstream of the initiator caspase 9 [461]. Moreover, sub-apoptotic caspase 2 activity has also been highlighted for a potential role in regulating cell cycle arrest and myogenic progression upstream of C2C12 cell fusion [461]. Thus, the non-apoptotic role of caspase activity in skeletal muscle development is likely epistatic to muscle fusion and manipulating caspase activity likely perturbs these upstream signaling processes, making the effect of caspase inhibit on muscle cell fusion difficult to interpret regardless of the effect observed.

Non-apoptotic phospholipid scrambling is known to elicit the rapid exposure of exofacil PS via Ca^{2+}-dependent phospholipid scrambling (Ca^{2+}-PLS). Recently, some Anoctamin (ANO) proteins were found to function as Ca^{2+}-PLSases [66, 68, 106]. Mutations in ANO5–a close relative of the PLSase ANO6–were found to cause limb-gridle muscular dystrophy type 2L [8, 198]. We recently characterized a murine model of this MD and found that the absence of ANO5 results in significantly perturbed myoblast fusion [48]. Recent further investigation by our group has demonstrated ANO5 is essential for proper PS exposure in fusogenic primary muscle progenitors (under review). Interestingly, like loss of *Bai1* and *Stab2* loss of *Ano5* significantly perturbs muscle repair/regeneration but has a very modest effect on skeletal muscle development [48].

Other players in muscle cell fusion

Cytoskeletal regulators and rearrangement play essential roles in myogenic fusion, although the precise mechanism is still ambiguous. The essential role of actin rearrangement for muscle fusion in D. melanogaster has been discussed extensively

183

elsewhere [197]. Briefly, in D. melanogaster Arp2/3 generated actin foci are essential for the fusion of FCMs and FCs, respectively. Arp2/3 cytoskeletal rearrangement is regulated by the Scar complex, which in turn is controlled by the Rac1/2 complex. Overarching regulators of these cytoskeletal rearrangements are ELMO/Myoblast city in FCMs. All of these processes are thought to occur downstream of cell-cell adhesion under the regulation of the Sticks-and-stone/Hibris and Kin-of-IrreC/Roughest discussed earlier. Actin regulation through the ELMO/DOCK180/Rac1 pathway is also thought to be a major regulator of muscle fusion in vertebrates [190, 455-458], however the exact mechanism underlying how these changes in intracellular actin occurs is unclear. Much confusion surrounding the precise role of the cytoskeleton in muscle fusion is probably created because this system is essential for the migration required for cells to fuse. With this in mind, it is difficult to determine whether loss of these actin signaling processes perturbed actual fusion or prevent fusion by perturbing cell contact by altering cell migration.

In vitro evaluation of muscle cell fusion partner recognition from murine models commonly highlights the production of many lamellopodia and filopodia that contact potential fusion partners and are thought to sample the membranes of other cells [465, 466]. These cellular extensions are enriched in both adhesion and signaling proteins and may provide force driving the union of fusion partners during this match making process [467, 468]. Similarly, filopodial extensions are described in D. melanogaster and are essential for myogenic precursor fusion during development [469, 470]. These structures likely represent a mechanistic role for the requirement regulated actin dynamics in muscle fusion.

Finally, much recent interest has been created around the role of extracellular vesicle (EV) signaling in the regulation of muscle cell fusion. Many tissues throughout the body release EVs that play diverse cell-cell signaling roles in health and disease (extensively

184

reviewed [471]). Skeletal muscle releases EVs that are thought to function as a means of cross-talk with other tissues and may play roles in musculoskeletal disease [472, 473]. Recently, it has been shown that proliferating and differentiated myoblasts release EVs that differ in their cargo and which are endocytosed by other muscle cells [169]. Exchange of both protein and RNA cargo has been observed, and this exchange has been found to alter myogenic progression [169, 474]. Moreover, EVs from muscle appear to promote neuronal survival and neurite outgrowth, suggesting these signaling units may play an important role in the maintenance of the NMJ [475]. Much concerning the production, uptake, and regulatory role of EVs has been discovered in the past decade (reviewed extensively [471]). Interestingly, Ca^{2+}-PLS is commonly associated with the production of EVs and may play a role in the release and signaling of EVs in muscle as we have discussed previously [80].

Conclusion

Recent work investigating the mechanisms of skeletal muscle repair have highlighted the parallel roles of SL patch repair and satellite cell-dependent repair in the maintenance of skeletal muscle tissue throughout life. Significant progress has been made in elucidating the mechanisms of these repair processes over the last two decades, however the many, rapid steps that take place in each process successively have created a significant challenge in characterizing the precise contributions of molecular players to these processes. For satellite cell-dependent repair in particular it has proven difficult to demonstrate precisely what step in myogenesis/fusion a protein of interest is involved in. Many proteins have been shown to perturb muscle progenitor cell fusion, however, it is conceivable that proteins involved in myogenic differentiation, fusion partner recognition, cell-cell adhesion, or in cell-cell fusion could all lead to this outcome. Although challenging, careful evaluation of each of the processes mentioned above is important

185

for fully characterizing the role of a particular regulatory factor in satellite cell-dependent skeletal muscle repair.

In addition to the challenges of characterizing a particular molecular player's role in muscle repair, current models most commonly used to evaluate muscle progenitor cell repair competence (e.g. cultured muscle progenitor cells) likely recapitulate aspects of both embryonic muscle development as well as adult myogenic repair. Although these two processes are similar, many factors appear to have very different requirements during these two myogenic process (e.g. the different requirements for the PS signaling machinery discussed above). In the future, it may be important to employ new models where *in vivo* observation of satellite cell-dependent muscle repair is more readily observable (e.g. zebra fish larvae).

Subtopic: Muscle by the Models

Our understanding of skeletal muscle repair/regeneration is the result of employing variety of model systems that have proven essential for our understanding of this dynamic tissue. Below is a brief synopsis of those systems and their major uses in studying muscle biology. Each model system exhibits several differences in their basic muscle biology that make them ideal for the evaluation of some myogenic processes but precludes their application to the study of others. The apt understanding of these models is essential for interpreting the data their study has yielded throughout the years.

Historical use of chick and quail muscle progenitor cells

The early use of chick and quail muscle provided many foundational discoveries in the field of skeletal muscle biology despite their modest use today. Much of the original appeal of chick and quail as muscle models stems from the ease of husbandry practices and the ability to culture explants of avian embryonic muscle in simple balanced salt solutions [476]. The field of muscle biology owes several foundational discoveries to this model, including original descriptions of a myogenic cell population residing in skeletal muscle and the common origin of differentiated skeletal muscle and satellite cells [476, 477]. The latter discovery was demonstrated by the transplantation of quail somites into chick embryos. The nuclei of quail and chick cells have overtly different staining patterns using a variety of simple dyes, thus allowing for lineage tracing in transplant experiments long before the identification of specific markers or genetic techniques. Although chick and quail are not as genetically tractable as other models, chick and quail muscle are rich sources of easily enriched muscle progenitor cells that are highly amenable to the *in vitro* study of myogenesis.

The use of *C. elegans* for characterizing myofibril ultrastructure.

187

The study of *C. elegans* body wall muscle has made significant contributions to the understanding of the development, organization, and mechanistic function of the contractile apparatus in muscle. The first myosin, myosin chaperone, and giant muscle proteins were all first sequenced and characterized in *C. elegans* (reviewed [478]). The muscle community owes much of its knowledge of the organization, assembly, and protein turnover of the cytoskeletal elements of the sarcomere to *C. elegans* [479]. *C. elegans* represents an ideal model for contractile apparatus study due in part to its transparency-facilitating the visualization of fluorescently tagged proteins in live animals during muscle function. Moreover, functional muscle is non-essential in *C. elegans* and does not preclude the propagation of mutants by virtue of the model's ability to self-fertilize. This allows for the analysis of many muscle proteins that are essential in other models, precluding the evaluation of muscle in their absence. These strengths combined with the low cost of use, rapid life cycle, ease of storage, protein conservation with higher animals, and the ability to propagate genetically identical progeny via self-fertilization make *C. elegans* an ideal model system for the study of muscle. However, the worm also comes with a number of significant limitations to its use in the study of other aspects of skeletal muscle biology.

Limitations in the use of C. elegans in modeling human muscle biology

C. elegans muscle biology exhibits a number of differences from vertebrates that limit its use for evaluating many basic biological attributes of human muscle. Perhaps the greatest limitation is that *C. elegans* muscle fibers remain mononucleated and are not syncytia produced from the fusion of muscle progenitor cells, as is the case for all other models discussed. In addition, the regulation of myogenic specification and overall myogenesis is not conserved between *C. elegans* and mammals [480]. Moreover, like the fly, *C. elegans* does not possess a muscle stem cell population, precluding their use for studying stem cell dependent repair/regeneration in muscle. Thus, *C. elegans*

188

represents an excellent model for the study of the contractile apparatus and other basic muscle systems but is not useful for the evaluation of many higher order processes in vertebrate muscle biology.

D. melanogaster in *in vivo* visualization of myogenesis and muscle fusion.

D. melanogaster has become a major developmental model in the evaluation of myogenesis and the mechanistic underpinnings of skeletal muscle fusion. The fly presents a number of compelling advantages over other models for the evaluation of muscle including: a short life cycle, extreme genetic tractability, high conservation with vertebrate muscle biology, and ease of tissue imaging. For example, in contrast to mammalian muscle tissue–which typically must be dissected, fixed, sectioned, and stained for morphologic evaluation–whole muscles are easily imaged in live or fixed formats in fly larval stages. This potentially bypasses many points that commonly introduce artifacts in the study of mammalian muscle tissue. Moreover, plug and play genetic tools in the fly allow for simple tissue specific expression of fluorescently tagged proteins, allowing the investigator to evaluate tissue morphology and easily perform lineage tracing.

D. melanogaster Founder Cells in Muscle Fusion

While the many tools and simpler muscle morphology of the fly make an ideal system for the evaluation of muscle development, the fly model has a number of shortcomings that preclude its use for the reliable evaluation of some processes in mammalian muscle biology. Unlike mammalian muscle precursors that are thought to possess similar myogenic potentials and capabilities to contribute to the musculature, the fly employs a pair of muscle precursor cell types whose functions differ significantly from the former (reviewed extensively [197]) . Briefly, *D. melanogaster* muscle development relies on a population of Founder Cells (FCs) that are not themselves fusion competent and a population of Fusion Competent Myoblasts (FCMs), which are fairly similar to

mammalian myoblasts and possess the ability to fuse with FCs to form nascent

myotubes or with nascent myotubes to contribute to fiber growth. At all stages in muscle

development FCs and FCMs exhibit very different developmental progression. FCs

function primarily to organize the development of the individual muscle fibers they will

contribute to while FCMs fuse to with FCs to form the actual muscle fiber. Additionally–

unlike vertebrate models–fly muscles do not possess a resident muscle stem cell

population and therefore cannot undergo satellite cell dependent muscle repair or

regeneration. Finally, there are currently no fly cell lines of muscle origin for use in the *in

vitro* evaluation of muscle biology.

Genetic murine models and the isolation of primary fibers and muscle precursor cells

Perhaps the greatest contributor to our understanding of how human muscle functions

has been murine muscle models. Although murine models have several limitations in the

in vivo evaluation of muscle function as compared to *D. melanogaster*, they have proven

far superior translational models compared to the others discussed, due largely mouse

being a mammal. In addition to the evaluation of murine muscle tissue in adulthood and

during development, the culture of murine muscle cells have proven to be excellent

models for the study of muscle biology including: single isolated muscle fibers, isolated

primary myoblasts, and a number of immortalized myoblast cell lines.

Single isolated primary muscle fiber culture

In 1975 Richard Bischoff discovered that with simple enzymatic digestion he could

isolate single, living muscle fibers from dissected muscles and evaluate them *in vitro* for

extended periods of time. With great excitement, he recognized that satellite cells

residing on these fibers were also present and became activated, producing many

nascent myofibers in culture [481]. Isolated muscle fibers have since allowed for the

morphological evaluation of individual muscle cells, the *in vitro* study of activated satellite

cells, and a host of other forays into muscle cell biology. However, these cells cannot be cultured for more than a couple weeks and cannot be cryogenically preserved, requiring the investigator to expend an animal and undergo a laborsome isolation procedure for each experiment.

Primary muscle progenitor cell culture

Isolation and culture of primary murine muscle progenitor cells (MPCs) has proven to be an excellent tool for the *in vitro* evaluation of muscle cell fusion and myogenesis. A variety of methods are employed for the isolation of MPCs, however the most accessible relies on the mechanical/enzymatic digestion of dissected muscles followed by MPC enrichment through differential plating on ECM coated culture dishes (see methods [482]). This method routinely produces primary MPC cultures of >95% purity, that can be greatly expanded, cryogenically preserved for future use, and reliably cultured for ~15 passages. Unfortunately, satellite cells cannot be maintained in their stem cell state in long term culture, likely due to the loss of their stem cell niche. However, MPCs can be maintained in a proliferative myoblast-like state and progress through myogenesis following serum starvation, becoming highly fusogenic. The *in vitro* MPC model system has produce much of the current mechanistic understanding of how muscle cells differentiate and fuse during satellite cell dependent muscle repair/regeneration.

Immortalized myoblast cell models

In addition to primary murine MPCs, a number of immortalized myoblast lines have been produced over the years that have become useful tools for studying the processes of myogenesis and muscle cell fusion. These immortalized models–like the pioneering C2C12 line [483]–have afforded investigators increased ability to produce stable myoblast models that require increased passaging (e.g. clonal cell lines stably expressing tagged proteins and cells manipulated via CRISPR techniques). However, most immortalized myoblasts suffer from a variety of limitations compared to primary

191

MPCs including: decreased physiological relevance of some myogenic processes, poorly defined cancerous characteristics, increased difficulty/time in differentiation, and greatly reduced fusion competence.

Zebrafish as a vertebrate *in vivo* imaging model

D. rerio possesses many shared advantages with *D. melanogaster* and *C. elegans* as a model for studying muscle biology while enjoying the increased translational quality of being a vertebrate. Unlike the fly and the worm, zebrafish possess a resident satellite cell population within their musculature, permitting their use for the evaluation of post-embryonic myogenesis. For example, zebrafish were recently used to image the entire progression of post-embryonic, satellite cell dependent, muscle fiber regeneration in a living animal [420]. In this study, investigators were able to elicit skeletal muscle damage by employing a small needle attached to a micromanipulator. Following the injury of post-embryonic larval stage zebrafish the investigators imaged the satellite cell-dependent repair of that skeletal muscle in the paralyzed fish. By combining this approach with a variety of florescent tags labeling skeletal muscle, satellite cells, and MPCs the investigators observed the *de novo* regeneration of a muscle fiber in a living organism. Although historically zebrafish have been primarily used as a developmental muscle model, this novel development of the model for the evaluation of larval muscle repair bridges the gap of developmental vs post-embryonic muscle biology.

Solving previous technical issues elevates Zebrafish as a skeletal muscle model

The major limitation of zebrafish for the study of skeletal muscle has been the lack of genetic models caused by the inability to isolate embryonic stem cells from this organism. All early work has relied exclusively on morphilino knock-down or forward genetic screens. This shortcoming has largely restricted zebrafish studies to basic developmental progression and precluded their use as a model for muscle disease. However, this limitation was removed in 2013 with the introduction of the efficient

192

genomic editing ability of the CRISPR/Cas system to the zebrafish model [484, 485]. In summary, *D. rerio* represents a premier vertebrate model for the study of developmental and post-embryonic muscle biology with numerous advantages including: a short life cycle, low husbandry cost, transparent embryonic and larval stages for easy *in vivo* imaging, a resident satellite cell population, and are now highly genetically tractable.

Chapter VI

Defective membrane fusion and repair in Anoctamin5 -deficient muscular dystrophy

Summary

Limb girdle muscular dystrophies are a genetically diverse group of diseases characterized by chronic muscle wasting and weakness. Recessive mutations in *ANO5 (TMEM16E)* have been directly linked to several clinical phenotypes including limb girdle muscular dystrophy type 2L and Miyoshi myopathy type 3, although the pathogenic mechanism has remained elusive. *ANO5* is a member of the Anoctamin/TMEM16 superfamily that encodes both ion channels and regulators of membrane phospholipid scrambling. The phenotypic overlap of *ANO5* myopathies with dysferlin-associated muscular dystrophies has inspired the hypothesis that *ANO5*, like dysferlin, may be involved in the repair of muscle membranes following injury. Here we show that *Ano5*-deficient mice have reduced capacity to repair the sarcolemma following laser-induced damage, exhibit delayed regeneration after cardiotoxin injury, and defective fusion of myoblasts to form multinucleated myotubes. Together, these data suggest that ANO5 plays an important role in sarcolemmal membrane dynamics.

Introduction

The importance of muscle mass and strength for daily activities such as locomotion and breathing and for whole body metabolism is unequivocal. Deficits in muscle function produce muscular dystrophies (MDs) that are characterized by muscle weakness and wasting and have serious impacts on quality of life [486]. The most well-characterized MDs result from mutations in genes encoding members of the *dystrophin-associated protein complex* (DAPC) [487]. These MDs result from membrane fragility associated with the loss of sarcolemmal-cytoskeleton tethering by the DAPC [488, 489]. In contrast, a subset of other MDs is thought to be caused by defects in sarcolemmal repair. Due to the mechanical stress the sarcolemma experiences during contraction, even healthy muscle is in constant need of repair mechanisms to patch injured membrane [489]. Sarcolemmal patch repair relies on the fusion of membrane vesicles at sites of damage [206, 490], and the attenuation of this process is considered a putative cause of dysferlinopathies, MDs caused by mutations in dysferlin [218, 222, 491].

Recently, a new MD with features similar to dysferlinopathies and characterized by sarcolemmal lesions has been linked to recessive mutations in *ANO5 (TMEM16E)* [8, 198, 492]. *ANO5* mutations produce limb-girdle muscular dystrophy type 2L (LGMD2L) and Miyoshi myopathy dystrophy type 3 (MMD3). The phenotype associated with *ANO5* mutations is variable, but typically the disease presents in adulthood (age 20 to 50) with proximal lower limb weakness, high serum creatine kinase levels, asymmetric muscle atrophy and weakness, and is typically accompanied by sarcolemmal lesions, similar to dysferlinopathy [8, 198, 492]. To date, ~72 different *ANO5* mutations have been reported in MD patients (Supplementary Material, Fig. S1), and screens for *ANO5* mutations in LGMD patients lacking mutations in other known LGMD genes indicate that *ANO5* mutations may be one of the more common causes of LGMD [8, 198, 493].

196

The ANO/TMEM16 family is functionally split into two categories. The founding members, *ANO1 (TMEM16A)* and *ANO2 (TMEM16B)* encode calcium-activated chloride channels [58, 124, 245], while other ANOs fail to conduct chloride and have roles in phospholipid scrambling (PLS)[7, 66, 68, 494]. However, ANO5 has not been found to exhibit either of these two activities at the plasma membrane [129, 495], suggesting a novel function in skeletal muscle. This is consistent with experimental evidence placing ANO5 as a resident of internal membranes, rather than the plasma membrane [201]. Given this novelty, it remains unclear how deficiency in ANO5 function elicits a LGMD phenotype, and specifically why *Ano5* mutations manifest in a clinically similar way to dysferlin-associated MD.

 Here we report the creation of an *Ano5* knock-out mouse model that recapitulates features of human LGMD2L patients. We show that disruption of the *Ano5* gene in mice produces several dystrophic histopathologic features, exercise intolerance, dysfunction in sarcolemmal repair, and myoblast fusion defects. We hypothesize that these defects are related to changes in subcellular membrane and/or sarcolemmal membrane dynamics mediated by ANO5.

Results

Generation of an Ano5*^{-/-} *mouse model

To generate an *Ano5* knock-out model, we used a vector targeting *Ano5* from exon 8 to exon 9 to produce a truncated transcript (Fig. 1A). The targeting construct was designed as a "knock-out first" [496] so that a null allele is generated through splicing to a *lac*Z trapping element. The targeting cassette was inserted following exon 8 with flanking *FRT* and *loxP* sites present to generate a conditional allele if embryonic lethality was noted [496, 497] (Fig. 1A). Following embryonic stem cell targeting and transfer, the genotypes
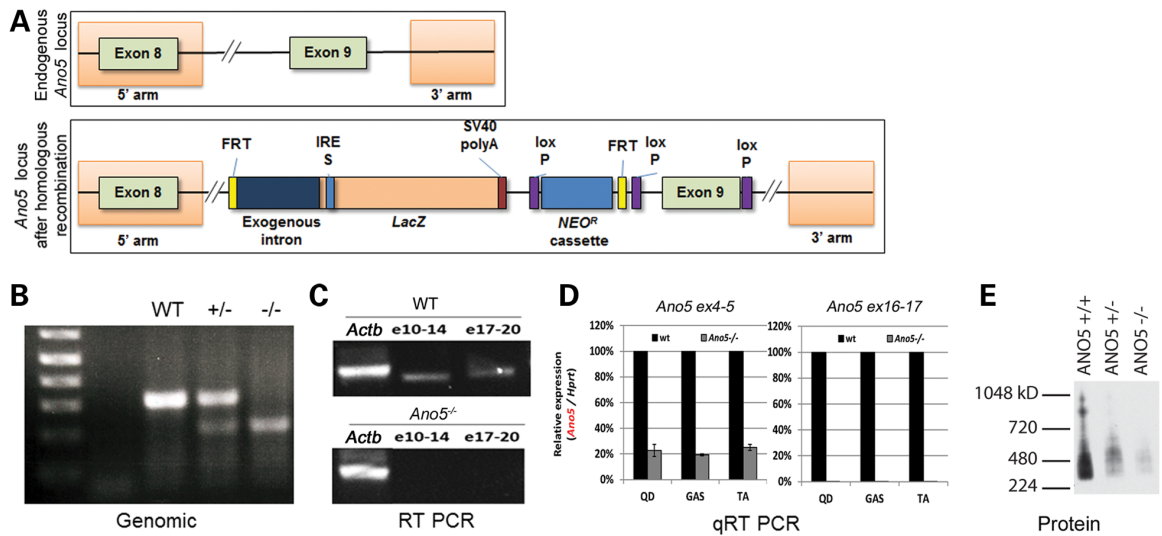
Figure 1 Generation of the *Ano5*$^{-/-}$ mouse model. (**A**) An *Ano5* targeting vector was used to include an exogenous intron and lacZ-encoding exon with a polyadenylation termination signal. The resulting mRNA terminates with exon 8. (**B**) Genomic DNA isolated from tail clippings of littermates. (Lane 1) WT mouse, (Lane 2) *Ano5*$^{+/-}$, (Lane 3) *Ano5*$^{-/-}$; WT allele: 300 bp fragment, *Ano5* allele: 200 bp fragment. (**C**) RT–PCR displaying reduced *Ano5* transcript in *Ano5*$^{-/-}$ muscle tissue using two primer sets targeting Ano5. Lane 1: β-actin control; lane 2 (e10–e14), primers spanning exons 10–14; lane 3 (e17–e20) primers spanning exons 17–20. (**D**) Approximately 80% and >99% relative reduction of Ano5 transcript, at the 5′ and 3′ end, respectively, was confirmed through qRT–PCR in quadriceps (QD), gastrocnemius (GAS) and tibialis anterior (TA) muscle extracted from the *Ano5*$^{-/-}$ mouse ($P < 0.001$). (**E**) ANO5 protein expression is absent in *Ano5*$^{-/-}$ mice. Western blot of blue native gel of muscle extracts from WT, *Ano5*$^{+/-}$ and *Ano5*$^{-/-}$ mice. WT ANO5 runs as a broad smear that centers around 400 kDa. The broad band may be explained by protein glycosylation, ubiquitination and/or multimerization. ANO5 is present, although greatly reduced in the heterozygote and is barely detectable in the knockout. (Primary effort on figure: (A-D) Rodino-Klapac Lab; (E) Whitlock, JM)

were verified by genomic PCR (Fig. 1B). RT-PCR using primers spanning exons 10-14 (e10-14) or exons 17-20 (e17-20) shows a loss of transcript distal to the *lac*Z insertion cassette (Fig. 1C). Consistent with these data, quantitative RT-PCR demonstrates ~80% reduction in pre-cassette *Ano5* transcript and >99% reduction of post-cassette *Ano5* transcript in all muscles tested (Fig. 1D). To determine whether Ano5 protein expression was reduced, muscle lysates were run on SDS-PAGE gels and western blots prepared. The presence of major muscle protein migrating at the same molecular weight as Ano5 (~107kDa) precluded a clean western blot and thus extracts were run under non-denaturing conditions on a native blue gel. Under these conditions, ANO5 migrates as a broad band around ~ 420kDa in addition to two bands of larger mass. We do not know if these bands represent oligomers of Ano5 or complexes of Ano5 with its binding partners. Regardless, no protein signal is observed in *Ano5*$^{-/-}$ muscle. Surprisingly, a greatly reduced signal is also observed in the heterozygote (Fig. 1E). No overt histological phenotypes were seen in *Ano5*$^{+/-}$ individuals, consistent with the recessive nature of muscular dystrophies due to *ANO5* mutation, No embryonic lethality noted in *Ano5*$^{-/-}$ animals. As *Ano5* shares a significant sequence homology to *Ano6*, and Ano6 is known to be expressed in skeletal muscle under some conditions [498], RT-PCR was performed to measure relative expression of *Ano6* cDNA of *Ano5*$^{-/-}$ mouse muscles. Quantitative RT-PCR demonstrates a modest, but statistically insignificant elevation of *Ano6* transcript in *Ano5* deficient muscles (Supplementary Material, Fig. S2).

Clinical and histopathological evaluation of the Ano5$^{-/-}$ *mouse*

The *Ano5*$^{-/-}$ mouse exhibits many features characteristic of human *ANO5*-myopathy including increased serum creatine kinase levels, variable weakness among muscles, altered muscle fiber diameter, and exercise intolerance [198, 495]. Serum creatine kinase is elevated approximately 2-fold in *Ano5*$^{-/-}$ mice (Fig. 2A). The specific force of muscle

199
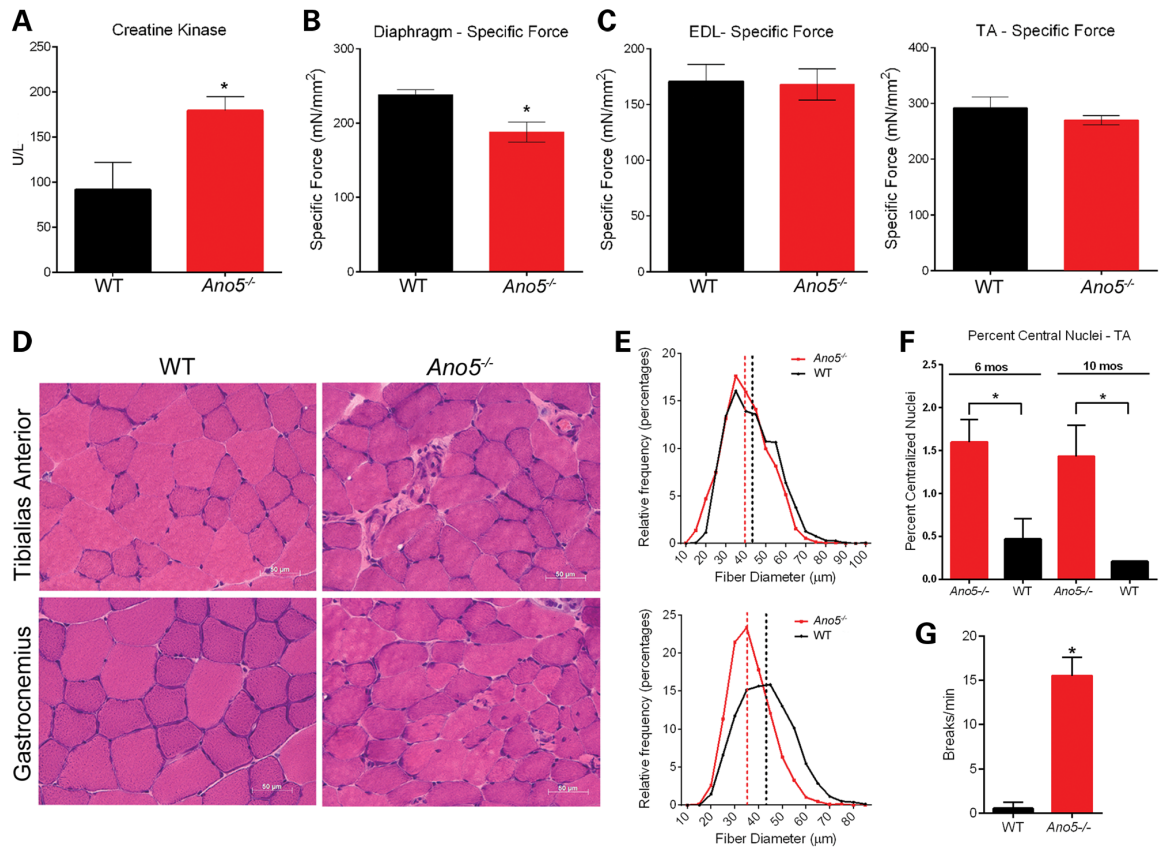
Figure 2 Characterization of Ano5$^{-/-}$ deficient mice. (**A**) Serum creatine kinase is significantly elevated in Ano5$^{-/-}$ mice 179.3 ± 15.52, n = 5 at 9 months compared with aged-matched controls 91.73 ± 30.13, n = 4 (P < 0.05). (**B**) Specific force of contraction of diaphragm strips from 10 months Ano5$^{-/-}$ mice 188.3 ± 13.52 was significantly decreased compared with controls 238.1 ± 6.770 (P < 0.01). (**C**) Specific force of contraction of EDL (9 months) and TA (4 months) muscles from Ano5$^{-/-}$ mice 168.0 ± 14.07 and 269.9 ± 8.54, respectively, were not significantly different than controls 170.5 ± 15.36 and 292.1 ± 19.59 (P > 0.05). (**D**) H&E-stained tissue sections demonstrating mild dystrophic pathology including central nuclei, fiber size variability and areas of necrosis in the TA and GAS of the Ano5$^{-/-}$mouse compared with WT controls. Scale bar = 50 μm. (**E**) Muscle fiber diameter measurements showed a reduction in Ano5$^{-/-}$ fiber diameter compared with WT especially in GAS muscle (P < 0.0001). (**F**) The number of centralized nuclei are modestly increased in Ano5$^{-/-}$muscle (P < 0.05) but remain stable

over time comparing 6- and 10-month timepoints. (**G**) *Ano5*$^{-/-}$ mice demonstrated

frequent pauses when treadmill exhaustion studies. Error bars = Mean ± SEM. (Primary

effort on figure: Rodino-Klapac Lab)

contraction is significantly decreased ~15% in diaphragm (Fig. 2B), but is essentially unaffected in extensor digitorum longus (EDL) and tibialis anterior (TA) muscles (Fig. 2C). This variability among muscles is characteristic of *ANO5* myopathies and is also observed in histological analysis of different muscles. Relative to wildtype (WT), average muscle fiber diameter is significantly smaller in gastrocnemius (GAS) muscle from *Ano5*^{-/-} mice (Ano5^{-/-}: 35.8 ± 8.3 µm, WT: 41.8 ± 11.0 µm, P<0.0001), and to a lesser extent in the TA muscle (Ano5^{-/-}: 38.1 ± 11.8 µm, WT: 44.3 ± 12.2 µm, P<0.0001) (Fig. 2D, E). *Ano5*^{-/-} muscles exhibited mild histopathology including central nuclei and occasional necrotic fibers (Fig. 2D, F). Corresponding to the adult onset of the LGMD2L, the appearance of most mouse *Ano5*^{-/-} phenotypes were typically seen at 6 months of age or later (Fig. S3). To evaluate exercise tolerance, aged-matched *Ano5*^{-/-} and WT mice were subjected to exercise regimes weekly for 1 hr for 2 mo. While WT control mice ran at a consistent speed with no breaks, *Ano5*^{-/-} mice were prone to frequent breaks on the treadmill (14 pauses/min) where they ceased running until the treadmill belt returned to the shock plate (Supplementary Material, SV1) (Fig. 2G). Needle electromyography, evoked compound muscle action potential recordings, and electrical impedance myography were performed in the hindlimbs of *Ano5*^{-/-} and WT mice but showed no significant changes, similar to the human disease (Supplementary Material, Fig. S3).

Another characteristic feature of human *ANO5* myopathy is the presence of an excessive number of muscle fibers with intramuscular deposits [499, 500]. In the *Ano5*^{-/-} mouse muscle, these structures appear as sharply-defined, irregularly-contoured areas that stain red with a modified trichrome stain [501]. Cytoplasmic aggregates were apparent beginning at 10 mo of age (Fig. 3A). Because aggregates of similar appearance have been noted in normal aged mice [501, 502], aggregate occurrence was quantified. Approximately 25% of *Ano5*^{-/-} fibers displayed irregularly-contoured red areas upon trichrome staining, while <0.02% of age-matched control fibers had these aggregates
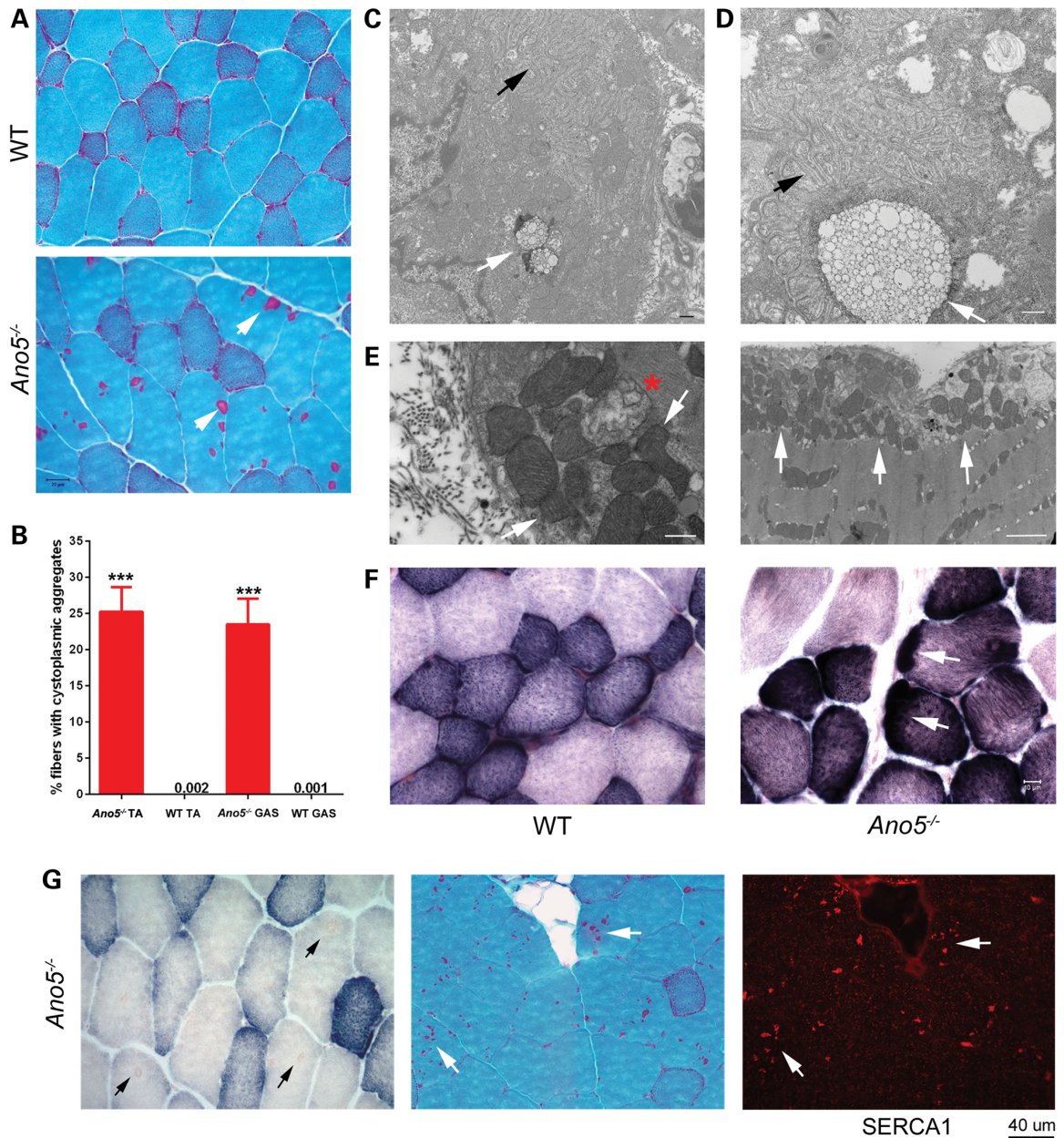
Figure 3 Subcellular histopathology in *Ano5*⁻/⁻ muscle. (**A**) Gomori Trichrome stain of 10 months *Ano5*⁻/⁻ and WT TA muscles. *Ano5*⁻/⁻ muscle contains membrane aggregates (arrows). Scale bar = 20 μm. (**B**) Quantification of the number of fibers containing aggregates in TA and GAS muscles of the *Ano5*⁻/⁻ compared with WT (*P*< 0.0001, one-way ANOVA). (**C** and **D**) Electron microscopic images demonstrating the presence of membrane aggregates in *Ano5*⁻/⁻ muscle. Aggregates were either loosely

packed, interconnecting tubular formations with fuzzy inner tubules (white arrows) or densely packed accumulations of vesicular or tubular membranes (black arrows). Scale bars = 500 nm. (**E**) Sub-sarcolemmal accumulations of mitochondria (arrows) and degenerating mitochondria (asterisk) were frequently identified by electron microscopy in *Ano5*$^{-/-}$ muscle. Scale bars = 500 nm (left) and 2 μm (right). (**F**) Succinate dehydrogenase staining of 10 months *Ano5*$^{-/-}$ TA muscle showed sarcolemmal thickening and capped fibers that were not present in WT. Scale bars = 10 μm. (**G**) Cryosections of the TA muscle from 10 months *Ano5*$^{-/-}$ mice were stained for succinate dehydrogenase (SDH). Arrows indicate reddish aggregates that do not stain for SDH (left). Serial sections from 10 months *Ano5*$^{-/-}$ mice demonstrate that many membrane aggregates (white arrows) observed with trichrome staining are positive for SERCA1 (right) suggesting they are derived from the sarcoplasmic reticulum. Scale bar = 40 μm. (Primary effort on figure: Rodino-Klapac Lab)

(Fig. 3B). Electron microscopy (EM) revealed that the aggregates were comprised of membranous material. Many *Ano5*^{-/-} muscle fibers exhibited densely packed accumulations of vesicular or tubular membranes or haphazardly oriented and loosely packed interconnecting tubular formations with fuzzy inner tubules that corresponded to the aggregates seen in light microscopy (Fig. 3C, D). *Ano5*^{-/-} mice showed similar pathology findings consistent with that of *ANO5* patients. Electron microscopy of patient muscle with compound heterozygous for two mutations [c.155A>G (p.Asn52Ser)] + [c.191dupA (p.Asn64Lysfs*15)] in the coding region of the *ANO5* gene revealed numerous aggregates and multiple sites displaying areas of degenerating mitochondria (Supplementary Material, Fig. S4). Aggregates in *Ano5*^{-/-} muscle stained positive for SERCA1 but not succinate dehydrogenase (SDH) activity, suggesting that they are derived from the sarcoplasmic reticulum and not from mitochondria (Fig. 3G) [501, 502]. However, *Ano5*^{-/-} mice did exhibit degenerating mitochondria and sub-sarcolemmal mitochondrial accumulation in addition to these membrane aggregates (Fig. 3E). The sub-sarcolemmal accumulation of mitochondria was confirmed by staining frozen sections for SDH, which was localized in dense patches near the surface of muscle fibers (Fig. 3F). To identify whether the mitochondrial degeneration observed had functional significance, we quantified citrate synthase activity as a measure of intact mitochondria and found there was a significant decrease in *Ano5*^{-/-} muscle extracts compared to WT controls (Supplementary Material, Fig. S5).

Ano5 facilitates membrane repair

In healthy individuals, normal exercise results in small lesions in the plasma membrane that are healed by two processes: (i) small tears are resealed by assembly of new plasma membrane and (ii) sites of more severe disruption are repaired by satellite cells that differentiate into myoblast-like cells and fuse to regenerate multinucleated muscle fibers

205

[197]. To test the effect of loss of *Ano5* expression on membrane repair, we first examined the effect of membrane damage produced by an intense laser pulse delivered to isolated flexor digitorum brevis (FDB) muscle fibers of 4 month old mice (Fig. 4A,B). Membrane damage was assessed by accumulation of FM1-43, a membrane-impermeant styryl cationic dye that is not fluorescent in aqueous solution but fluoresces brightly in a lipid environment and has been used extensively to study membrane repair [205, 491, 503]. A small area of fluorescence was detected at the site of damage in WT and *Ano5*$^{-/-}$ fibers immediately after laser injury (Fig. 4A). The increase in fluorescence was greater and occurred at a ~2-fold faster initial rate in *Ano5*$^{-/-}$ muscle fibers than in WT fibers. Whereas the fluorescence appeared to be leveling off at 190 sec in WT, the fluorescence continued to increase in Ano5$^{-/-}$ fibers for the duration of the experiment (Fig. 4B). To test whether the defect in membrane repair was directly related to *Ano5* expression, we expressed human *ANO5* cDNA using adeno-associated virus (AAV) in the *Ano5*$^{-/-}$ muscles. AAV.ANO5 partially restored membrane resealing in *Ano5*$^{-/-}$ muscle (Fig. 4B). Intramuscular delivery of AAV.ANO5.FLAG results in sarcolemmal ANO5 expression *Ano5*$^{-/-}$ mice (Fig. 4C).

Impaired Regeneration in Ano5 KO mice

We then asked whether muscle regeneration was also defective in *Ano5*$^{-/-}$ mice. This was done by examining the ability of the muscle to recover from injury produced by cardiotoxin injection [504] (Fig. 4D). To track temporal changes of necrosis and regeneration, TA and GAS muscles of 8 week-old mice were injected with cardiotoxin 3 times, spaced 2 weeks apart. Tissues were harvested 1, 3, 7, 14, 30, and 90 d after the final injection (Fig. 4D). The contralateral side was used as a saline-only control. The WT muscle regenerated after cardiotoxin treatment, so that by 1 mo the muscle appeared largely normal with the exception of central nuclei in newly regenerated fibers. However, in *Ano5*$^{-/-}$ mice, there was an extensive delay in regeneration and longstanding necrosis. After 3 mo, the mean
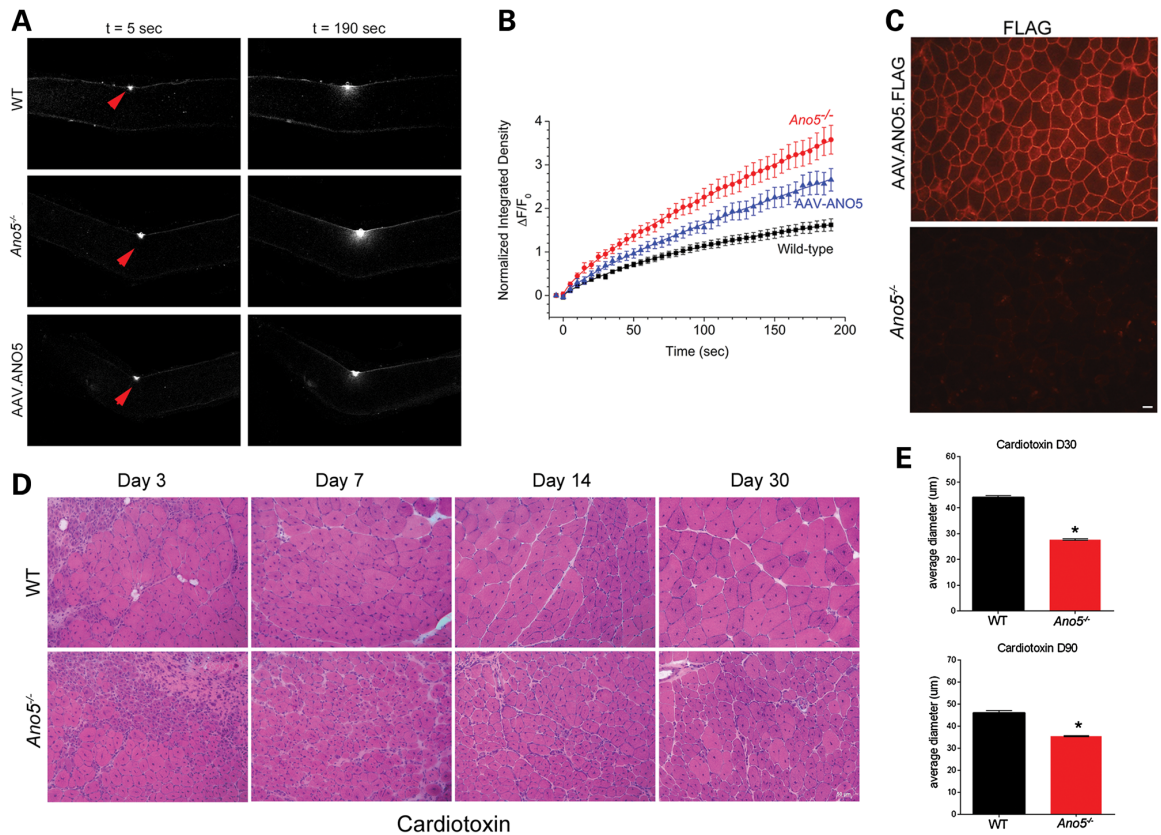
Figure 4 Membrane Repair is defective in *Ano5*$^{-/-}$ mice. (A) Images of *Ano5*$^{-/-}$ and WT muscle 4-month-old mice damaged by a laser pulse shown 5 and 190 s post-injury. Red arrows indicate the site of damage with FM1-43 dye accumulating quickly in *Ano5*$^{-/-}$ muscle compared with WT and *Ano5*$^{-/-}$ following delivery of 1 × 10^{11} vg AAV.ANO5.FLAG vector. Scale bar = 50 µm. **(B)** Measurement of fluorescence intensity after laser-induced injury. *Ano5*$^{-/-}$ muscle is statistically different from WT and AAV.ANO5 fibers at all times >100 s post-injury (two-way ANOVA, *P* < 0.001). **(C)** Expression of ANO5-FLAG in *Ano5*$^{-/-}$ uninjected TA or TA injected with 5 × 10^{10} vg AAV.ANO5.FLAG vector. Immunofluorescence with anti-FLAG antibody demonstrated ANO5-FLAG expression following intramuscular injection (top) that was absent in untreated *Ano5*$^{-/-}$ muscle (bottom). Scale bar = 40 µm. **(D)** Recovery from cardiotoxin-induced muscle damage. H&E-stained tissue sections of WT and *Ano5*$^{-/-}$ TA muscles at 1, 3, 7, 14, 30 and 90 days post-cardiotoxin injection (Days 3,7,14 and 30

shown). *Ano5*$^{-/-}$ muscle incurred more damage and showed impairment in regeneration compared with WT. (**E**) Myofiber size remains statistically smaller in *Ano5*$^{-/-}$ muscle at 30 and 90 days compared with WT at 30 days (Cardiotoxin D30) and 90 days (Cardiotoxin D90) post-cardiotoxin injection ($P < 0.05$). (Primary effort on figure: Rodino-Klapac Lab)

fiber diameter of *Ano5*$^{-/-}$ muscle remained significantly reduced compared to WT and many fibers exhibited central nuclei (Fig. 4D, E).

Loss of Ano5 Leads to a Myoblast Fusion Defect

Because cardiotoxin damages only muscle fibers but not satellite cells [504], the slow recovery of *Ano5*$^{-/-}$ muscle after cardiotoxin injection suggests that muscle regeneration is defective in *Ano5*$^{-/-}$ mice. In addition to a membrane patching mechanism to repair damaged sarcolemma*,* adult muscle requires muscle progenitor satellite cells that proliferate, differentiate, and fuse to repair/replace damaged muscle fibers *in vivo* [197]. Many LGMD2L patients first manifest clinical symptoms after a significant muscle injury that persists longer than normal [500]. This led us to hypothesize that the progenitor cell population in these individuals may have a decreased ability to repair damaged muscle fibers in addition to the sarcolemmal patch repair defect we characterized in Fig. 4. To test this, we isolated this myoblast progenitor population from 3-mo-old *Ano5*$^{-/-}$ mice and compared the fusogenic properties of these cells with age matched WT controls from the same genetic background.

First, we assessed the ability of the myoblast progenitor cell populations from *Ano5*$^{-/-}$ mice to fuse compared to WT cells. To quantify myoblast fusion, we stained cells with a marker of differentiated muscle (myosin heavy chain, MHC) and a nuclear stain to count the number of nuclei that had incorporated into multinucleated myofibers. As shown in Fig. 5A-C, after 3 d 73% of wild type cells had fused to form multinucleated MHC-positive myotubes, while only 48% of *Ano5*$^{-/-}$ cells had fused. Furthermore, we observed that the *Ano5*$^{-/-}$ myotubes were generally shorter and a large fraction exhibited an ovoid shape instead of the elongated shape seen in WT cells (Fig. 5A, B). To quantify this fusion defect further, we counted the number of nuclei in each myotube. *Ano5*$^{-/-}$ myotubes on average had fewer nuclei than WT myotubes (Fig. 5D, E). While ~50% of WT myotubes had >6 nuclei, <10% *Ano5*$^{-/-}$ myotubes had this many nuclei. Taken together, the cardiotoxin and

209
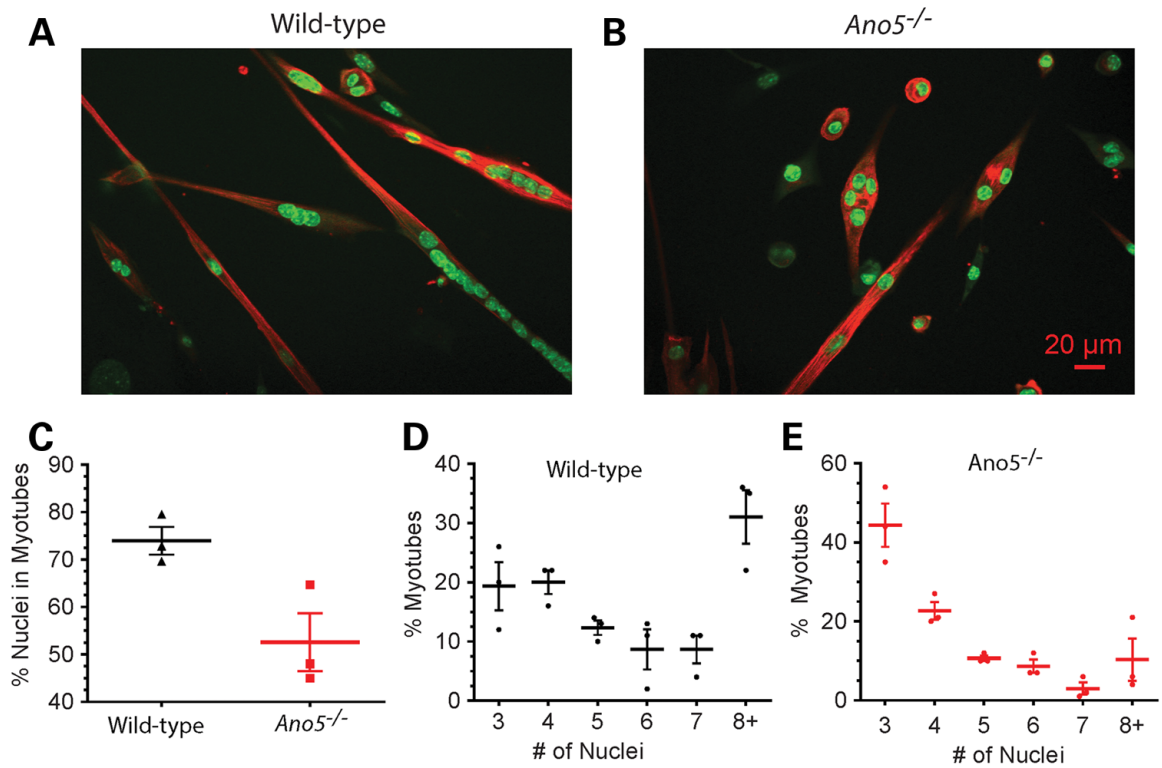
Figure 5 Loss of _Ano5_ expression impairs myoblast fusion. (**A** and **B**) Confocal images of primary myoblast cultures isolated from adult WT (**A**) and _Ano5_$^{-/-}$ (**B**) mice differentiated for 3 days on glass coverslips, fixed and stained for MHC with antibody (red) and nucleic acid (Syto24, green). (**C**) Fusion index (mean ± SEM). There was a significant reduction in fusion competence between WT (73%) and _Ano5_$^{-/-}$ (48%) myoblasts ($P < 0.03$) (**D** and **E**). The average number of nuclei per myotube was measured from the same three experiments for WT (**D**) and _Ano5_$^{-/-}$(**E**). In (**C–E**), individual data points indicate mean values for each of three independent experiments with a total of >12,000 nuclei counted. (Primary effort on figure: Whitlock, JM)

myoblast fusion assays demonstrate that both *Ano5*^{-/-} mature myocytes and myoblast progenitors are fusion defective. This defect likely contributes to the failed muscle regeneration and resultant progressive muscle wasting indicative of LGMD2L and MMD3.

Discussion

Here we demonstrate an essential role for ANO5 in muscle regeneration and repair. Loss of ANO5 causes a dystrophic phenotype in mice, reminiscent of LGMD2L patients, with mild histopathology that varies among muscles, exercise intolerance, impaired regeneration, and elevated creatine kinase levels. Mitochondrial abnormalities were observed in both young and aged *Ano5*^{-/-} mice. In addition to the structural defects the mitochondria displayed through electron microscopic imaging, we also demonstrated functional loss using quantitative enzyme analysis of citrate synthase indicating the presence of damaged mitochondria. The structural and functional mitochondrial findings may provide some clarification behind the underlying and unexplained symptoms of exercise intolerance and myalgia reported by *ANO5*^{-/-} patients [266] and replicated in *Ano5*^{-/-} mice. We also characterize an attenuation of sarcolemmal patch repair in *Ano5*^{-/-} fibers that is partially rescued by viral expression of human ANO5 and find that the disruption of *Ano5* perturbs the fusogenic quality of primary myoblasts as well as mature myocytes. The mitochondrial defects may be secondary to failed membrane repair and/or regeneration or rather represent a defect that is universal to all membranes including intracellular membrane-bound organelles.

Another noteworthy finding of this study was that the membrane aggregates observed in *Ano5-/-* knockout animals are very similar to tubular aggregates that have been reported in mice with STIM1 or ORAI1 genes disrupted [505, 506]. The mechanisms of formation of tubular aggregates remains unknown, but because STIM1 and ORAI1 are involved in store-operated Ca^{2+} signaling, it has been suggested that they are stimulated by disrupted

211

Ca^{2+} signaling. The fact that our aggregates stain for SERCA supports the idea that they are derived from SR, and supports the hypothesis that there is a defect in membrane trafficking and organization.

Disruption of *Ano5* closely phenocopies the loss of dysferlin expression in murine models [507], and dysferlin mutations cause MDs similar to ANO5 myopathies (LGMD2B and MMD1 vs LGMD2L and MMD3). The observation that many membrane repair-associated proteins, including dysferlin via its C2 domains, bind phosphatidylserine, and that some ANOs can scramble phosphatidylserine poses the intriguing possibility that defective PLS due to ANO5 loss may explain the similar disease phenotypes. Further, the reorganization of phosphatidylserine across muscle membranes is a plausible mechanism of action with respect to the repair and regeneration defects seen in ANO5 myopathies. Cardiotoxin, a neurotoxin known to cause necrosis, when injected into the hindlimb muscles of *Ano5*^{-/-} mice showed efficiency in causing necrosis in both the deficient and wild-type mouse models. However, the muscles of *Ano5*^{-/-} mice showed a delayed ability to regenerate and a decrease in size compared to wild-type muscle. The *Ano5*^{-/-} mice have a delayed muscle repair response following injury. The sequence similarity of Ano5 to Ano6 suggests strongly that Ano5 is involved in phospholipid scrambling. Although phospholipid scrambling is known to be tightly linked to membrane trafficking, it remains to be seen precisely how phospholipid scrambling may be involved in membrane repair. The apparent localization of Ano5 in the ER argues that the function of Ano5 may be more complex than simply exposure of phosphatidylserine to the external environment. Studies to examine whether ANO5 participates in some form of PLS and/or other processes of membrane dynamics are ongoing.

This *Ano5*^{-/-} mouse represents an important model for the study of *ANO5*-myopathy, sarcolemmal repair, and myogenic cell fusion. In light of the development of two recent *ano5* exon 1 deletion mouse models failing to phenocopy the human muscle disease [204,

508], our *Ano5*^{-/-} model demonstrates testable therapeutic outcomes and will allow for additional studies focused on Ano5 function and disease pathophysiology. As shown in Supplementary Figure 1, the *Ano5*^{-/-} mice we generated retain a portion of the N-terminus ending in amino acid 254 terminating the protein at exon 8. This more closely resembles that of LGMD2L patients with pathogenic mutations identified only in exon 4 or later and the most frequent mutation (founder) located at the 5' splice site of exon 5 [266]. Future studies will explore the impact of this N-terminal fragment. Here we have developed proof of principle for gene replacement therapy as a treatment strategy for *ANO5*-myopathy by partially rescuing the membrane repair phenotype via AAV.ANO5 treatment of *Ano5*^{-/-} mice. Additionally, we believe that this model will be important for further refinement of the ANO5 mechanism of action in sarcolemmal repair and myoblast fusion which will greatly inform the mechanistic understanding of *ANO5*-myopathy, as well as inform patient treatment strategies in the future.

Materials and Methods

Ethical Statement

This study has been approved by the Animal Care and Use Committee of The Research Institute at Nationwide Children's Hospital (RINCH). All animal handling was performed in accordance with the Guidelines for Animal Experiments at RINCH. All injections were performed under anesthesia. Efforts were made to eliminate pain and suffering.

Generation of anoctamin5-deficient mice

To generate the *Ano5*$^{-/-}$ mouse, the knockout first, conditional ready, lacZ-tagged mutant allele *Ano5*:tm1a(KOMP)Wtsi targeting vector was obtained from the UC Davis KOMP Repository (PG00097_Z_1_G0) [497]. This targeting vector was submitted to the Transgenic and Embryonic Stem Cell Core at RINCH for electroporation into ES cells. Clones were screened by PCR using the following primer sets, which produce a 300bp amplicon from the endogenous *Ano5* locus and a 200bp amplicon from the *Ano5* cassette insertion locus:

genotyping F   5'-AGTCCTTTTCAGCACAGTCTTTG-3'

genotyping R   5'-TGAGGCAGTGTGGAGTGAGTA-3'

DF38700   5'-GCCAATCATATGGTCTCAGT-3'   LR-loxp R 5'-ACTGATGGCGAGCTCAGACC-3'

Successfully targeted ES cells were then injected into blastocysts of C57BL/6 mice, and embryos transferred to generate chimeras for germline transmission. Transgenic heterozygotes were verified by genotyping and were backcrossed four times to C57BL/6 wild type, before breeding to homozygosity.

Stocks of *Ano5*^{-/-} and C57BL/6mice were bred and maintained as homozygous animals in standardized conditions in the Vivarium at the RINCH. They were maintained on Teklad Global Rodent Diet (3.8% Fiber, 18.8% Protein, 5% fat chow) with a 12:12 h dark:light cycle. Procedures used in the experiments were approved by the Institutional Animal Care and Use Committee at Nationwide Children's Hospital (AR12-00004).

RT-PCR

For both semi-quantitative and quantitative transcript measurements, total RNA was isolated from fresh-frozen muscle shavings using Trizol (Life Technologies, Carslbad, CA), according to the manufacturer's protocol. RNA was then column-purified using the RNAEasy method (Qiagen, Valencia, CA), and quantified by spectrophotometry using a NanoDropLite (Thermo Fisher Scientific, Waltham, MA). cDNA was generated with the High Capactiy cDNA Reverse Transcription Kit (Thermo Fisher Scientific), using equivalent amounts of sample RNA per reaction (200-500 ng), isolated from 3 individual mice per genotype. For semi-quantitative PCR, equal volumes of cDNA were subjected to 30 PCR cycles, followed by agarose gel electrophoresis. Primers used were: mβAct-rt-5', CCTGGCCGTCAGGCAGAT; mβAct-rt-3', GACATGGAGAAGATCTGGCACC; mAno5-rt-F1,CCAACAGAATGAGAACCT; mAno5-rt-R1,GACAGGGGTGGGTACTTTGG; mAno5-rt-F3 , CGTTGGCAGCAAGATCAT; mAno5-rt-R3 GGGTACCTATAATCTCTGTACCTGC. Quantitative PCR was performed and analyzed on a Fast Real-Time PCR System (Thermo Fisher Scientific). Reactions were run with Applied Biosystems primer- FAM probe cocktails for *Ano5* (Mm00624629_m1, Mm01335981_m1), *Ano6* (Mm00614693_m1), *Gapdh* (Mm99999915_g1), and *Hprt* (Mm03024075_m1) in triplicate for each sample. The ΔΔCt method was used to calculate normalized fold-change reductions of *Ano5* and *Ano6* mRNA in *Ano5*^{-/-} muscles as compared to wild type. *Hprt* and *Gapdh* were each

215

tested with respect to invariance between test groups, and *Hprt* was chosen based upon better stability as a reference gene.

Blue Native Gel Electrophoresis Western Blotting

Hind limb muscles were dissected from genotyped *Ano5*$^{+/+}$, *Ano5*$^{+/-}$ and *Ano5*$^{-/-}$ mice and homogenized in 50mM BisTris, 6N HCl, 50 mM NaCl, 10% w/v glycerol, 0.001% ponceau S, pH 7.2 supplemented with protease inhibitor cocktail III (Calbiochem). Samples were tumbled end over end for 30 minutes at 4°C and centrifuged at 20,000 xg for 30 min. Soluble protein was collected and protein concentration was measured using the BCA assay. Proteins were separated using blue native polyacrylamide electrophoresis (NativePAGE™ Novex® Bis-Tris Gel System Invitrogen) and transferred to a PVDF membrane. Excess Coomassie Blue dye was washed by agitation over night with PBST. The membrane was blocked for 1 hr in 5% non-fat dry milk and stained over night at 4°C with Anti-Ano5 antibody (NeuroMab clone N421A/85) at a 1:100 dilution in PBST + 1% milk. HRP conjugated goat anti-mouse secondary antibody (Biorad) was incubated with membrane for 1 h at room temperature and chemiluminescent signal was measured using ECL and radiographic film. In preliminary experiments 20 µg protein of each muscle extract was loaded and equal loading was verified by Ponceau-S staining. To facilitate detection of protein in the heterozygote and knockout, the amount of protein loaded in the 3 lanes was unequal: *Ano5*$^{+/+}$*:* 6 µg, *Ano5*$^{+/-}$: 10 µg, *Ano5*$^{-/-}$: 16 µg.

Electron Microscopy

Segments of tibialis anterior (TA) muscle from 4 and 10 mo old *Ano5*$^{-/-}$ and control mice were removed, stretched to their *in situ* length across a wooden tongue depressor and immersed in 3% glutaraldehyde in 0.1 M phosphate buffer pH 7.0 for 4 hr. The muscle was dissected into 2-mm-long tissue blocks, stored in 0.1 M phosphate buffer pH 7.4 overnight, followed by post-fixation in 1% osmium tetroxide for 2 hr and dehydration in graded ethanol solutions before plastic embedding. 1 µm-thick cross sections were

stained with toluidine blue, examined by light microscopy, and tissue sections from selected blocks were examined under a Hitachi H-7650 TEM electron microscope utilizing an Advanced Microscopy Techniques camera and software.

Immunofluorescence

12 µm cryosections were placed onto Fisher Superfrost microscope slides and blocked with 10% goat serum and 0.1% Tween-20 in PBS for 1 hr at room temperature. Slides were incubated in primary antibody for 1 hr at room temperature (Anti-FLAG F7425 Sigma-Aldrich, 1:175; Serca1 CaF2-5D2 (Developmental Studies Hybridoma Bank, 1:50). Slides were then rinsed 3 times with PBS for 1 hr at room temperature followed by a 30 min block. Goat-anti-mouse conjugated to Alexa Fluor 594 (A21125, Life Technologies) or goat-anti-rabbit conjugated to Alexa Fluor 568 (A11011, Life Technologies) secondary antibodies were diluted at 1:250 in blocking solution and incubated for 45 min followed by 3 PBS rinses for 1 hr. The sections were mounted with Vectashield (Vector Labs, Burlingame, CA) mounting media and analyzed with a Zeiss Axioskop 2 microscope using a Cy5 filter (excitation, 578 nm-590 nm; emission 603 nm-671 nm) (Zeiss, Thornwood, NY). Image exposure time was standardized using the positive control for each antibody, each day. Images were taken using the Axiovision 4.5 software.

Morphometrics

Fiber Diameters: Muscle cross-sectional fiber diameters were determined from TA and gastrocnemius (GAS) muscles from 6 mo old *Ano5*$^{-/-}$ and WT strain control mice (n=3 mice per strain). Muscles were sectioned and stained with hematoxylin and eosin (H&E). 4 random 20x images per section per animal were taken with a Zeiss AxioCam MRC5 camera. Fiber diameters were determined by measuring the shortest distance

217

across the muscle fiber using Zeiss Axiovision LE4 software. Fiber diameter histograms were generated from an average of 500-600 fibers per TA and 600-700 fibers per GAS.

Aggregate quantification: Muscle sections from TA and GAS muscles of 10 mo old *Ano5$^{-/-}$* and WT mice (n=3 mice per tissue and strain) were stained with Gomori Trichrome. Four 20X images were taken and the number of fibers with one or more aggregates were counted using Image J software and expressed as a percentage of the total number of fibers.

Central Nuclei quantification: Muscle sections from TA and GAS muscles of 10 mo old *Ano5$^{-/-}$* and WT mice (n=3 mice per tissue and strain) were stained with hematoxylin and eosin. Four 20X images were taken and the number of fibers with centralized nuclei were counted using Image J software and expressed as a percentage of the total number of fibers.

Succinate Dehydrogenase Staining (SDH): TA and quadriceps muscles were sectioned at 18 µm and stained with SDH solution consisting of 0.2% nitro blue tetrazolium (NBT) dissolved in 0.1 M succinic acid and 0.1 M phosphate buffer pH 7.4 and incubated at 37°C for 3 hrs. Following incubation, slides were rinsed with water and dehydrated in serial alcohols then cleared with xylene. Slides were imaged on Zeiss AxioCam MRC5 camera.

rAAV production

The human *ANO5* cDNA was cloned into an AAV2 ITR plasmid using Not1 restriction sites between the MHCK7 promoter and polyadenlylation signal. rAAV vectors were produced by a modified cross-packaging approach whereby the AAV type 2 ITRs can be packaged into multiple AAV capsid serotypes [509]. Production was accomplished using a standard 3-plasmid DNA CaPO$_4$ precipitation method using HEK293 cells. HEK293 cells were maintained in DMEM supplemented with 10% Cosmic calf serum (CCS, Hyclone). The production plasmids were: (i) pAAV.MHCK7.ANO5, (ii) rep2-cap8

modified AAV helper plasmids encoding cap serotype 8-like isolate rh.74, and (iii) an adenovirus type 5 helper plasmid (pAdhelper) expressing adenovirus E2A, E4 ORF6, and VA I/II RNA genes. Vectors were purified from clarified HEK293 cell lysates by sequential iodixanol gradient purification and anion-exchange column chromatography using a linear NaCl salt gradient as previously described [510]. A quantitative PCR-based titration method was used to determine an encapsidated vector genome (vg) titer utilizing a Prism 7500 Taqman detector system (PE Applied Biosystems, Carlsbad, CA) [510].

AAV vector delivery through intramuscular injection to mouse muscle

1-2 month old $Ano5^{-/-}$ mice were treated by intramuscular injection of $5x10^{10}$ vg and $1x10^{11}$ vg of rAAVrh.74.MHCK7.huANO5.FLAG into TA (n=4) or FDB (n=4) muscles, respectively. For each mouse, the contralateral muscles (right TA and FDB) were used as untreated controls. TA muscles were harvested 4 weeks post injection and processed for viral potency which included histological and ANO5.FLAG expression. Flexor digitorum brevis (FDB) muscle fibers were harvested 10 weeks post treatment and processed for membrane repair assay.

Membrane Repair

$Ano5^{-/-}$ mice were injected with $1x10^{11}$vg of AAV.ANO5 into the FDB muscle at 4-5 weeks of age. Muscles were harvested 10 weeks post injection and subjected to a laser-induced injury. Membrane repair assay was performed on left (treated) and right (untreated) FDB muscles of $Ano5^{-/-}$ (n=4) and age-matched C57BL6 (n=4) mice as previously described when the mice were 4 months of age [503]. Briefly, FDB fibers were isolated using a solution containing 2% w/v collagenase type I suspended in DMEM. Following dissociation of the muscle, fibers were placed in a glass bottom dish holding 2.5 μM FM1-43 dye in Dulbecco's PBS (no Ca/Mg) supplemented with 1.5 mM Ca^{2+}. Fibers were subjected to laser injury using a FluoView® FV1000 two-photon

219

confocal laser-scanning microscope (Olympus). Fibers were damaged with an 850 nm laser-guided spot of 4.479 µm at 20% power and imaged every 5 sec for 190 s to visualize FM1-43 dye uptake. An average of 7-10 fibers were imaged per muscle per mouse, (total 31 WT, 39 *Ano5*$^{-/-}$, and 30 AAV-ANO5 rescued *Ano5*$^{-/-}$ fibers). Fluorescence intensity of dye infiltration surrounding the damage site on the membrane was analyzed with Image J software by measuring integrated density of pixel intensity within the defined area. To do so, under a 2X zoom setting on ImageJ, a rectangular box measuring 7.5 µm by 10 µm region of interest (ROI) is drawn and used to measure the intensity of dye in that region. In the analysis, measured fluorescent intensity at an individual time point was normalized to initial intensity measured at t = -5s (pre-injury) using the equation: $NI = \frac{(I - I_0)}{I_0}$, where NI is the normalized intensity, I is the measured intensity and I_0 is the intensity at t = -5s. When fluorescence intensity was analyzed, values from all fibers from each strain were averaged together. A 2-way ANOVA was performed to determine statistical significance between treated and untreated fibers at each time point (p<0.001). *Ano5*$^{-/-}$ fibers, WT fibers, and AAV.ANO5 treated *Ano5*$^{-/-}$ fibers were significantly different beginning at 100 seconds post-injury.

Cardiotoxin injections

Mice were anesthetized with inhaled isoflurane and injected with cardiotoxin (diluted to 10 µM with sterile saline) every two weeks, for a total of 3 rounds. 30 µL and 50 µL of cardiotoxin was injected into the left TA and left GAS muscles respectively of 8 week old *Ano5*$^{-/-}$ and aged-matched controls. Sterile saline was injected into contralateral muscle as a sham control. Groups of mice were euthanized and their muscles harvested at 1, 3, 7, 14, 30 and 90 days post final injection of cardiotoxin (n=3 mice per strain per timepoint). Four 20X images per TA were imaged and fiber diameter was measured on

220

H&E-stained cryosections 1 and 3 mo after the final cardiotoxin injection using Axio Vision 4.8. An average of 500-600 muscle fibers per animal was measured.

Behavioral (treadmill) study

7.5 mo *Ano5*^{-/-} and aged matched C57BL6 mice were run once a week until the age of 9.5 mo at a -10° decline with a speed of 15 m/min and increased by 1 m every minute until exhaustion was reached (n=3 mice per strain). Each individual test was stopped when the mouse remained on the shock plate (Columbus Instruments) with electrical stimulus set to 20V for more than 10 s without attempting to engage in exercise. Breaks were defined as the times where the mice ceased running and rested while the treadmill belt returned to the shock plate.

Force generation

Tetanic force measurements were obtained from extensor digitorum longus (EDL) of 10 mo old mice (n=6 mice per strain), TA from 4 mo old mice (n=5 mice per strain), and diaphragm muscles of 10 mo old *Ano5*^{-/-} and WT mice (n=4 mice per strain). The EDLs were dissected at the tendons and subjected to a physiology protocol to assess function as previously described by our lab and others [511, 512] with modifications. During the eccentric contraction protocol, a 5% stretch-re-lengthening procedure executed between 500 and 700 ms (5% stretch over 100 ms, followed by return to optimal length in 100 ms). Following the tetanus and eccentric contraction protocol, the muscle was removed, wet-weighed, mounted on chuck using gum tragacanth, and then frozen in methyl-butane cooled in liquid nitrogen. Force measurements in the TA were performed as previously described [513, 514]. After the eccentric contractions, the mice were then euthanized and the TA muscle was dissected out, weighed and frozen for analysis. For diaphragm force measurements, mice were euthanized and the diaphragm was dissected with rib attachments and central tendon intact, and placed in Krebs-Henselet

(K-H) buffer as previously described [515-517]. A 2-4 mm wide section of diaphragm was isolated. Diaphragm strips were tied firmly with braided surgical silk (6/0; Surgical Specialties, Reading, PA) at the central tendon, and sutured through a portion of rib bone affixed to the distal end of the strip. Each muscle was transferred to a water bath filled with oxygenated K-H solution that was maintained at 37°C. The muscles were aligned horizontally and tied directly between a fixed pin and a dual-mode force transducer-servomotor (305C; Aurora Scientific, Aurora, Ontario, Canada). Two platinum plate electrodes were positioned in the organ bath so as to flank the length of the muscle. The muscle was stretched to optimal tension of 1 g, and then allowed to rest for 10 min before initiation of the tetanic protocol. Once the muscle was stabilized, the muscle was subjected to a warm-up consisting of three 1 Hz twitches every 30 sec followed by three 150 Hz twitches every minute. After a 3 min rest period, the diaphragm was stimulated at 20, 50, 80, 120, 150, 180 Hz, allowing a 2 min rest period between each stimulus, each with a duration of 250 ms to determine maximum tetanic force. Muscle length and weight was measured. The force was normalized for muscle weight and length [CSA: muscle mass (mg)/{Lf(mm) x muscle density ($1.06mg/mm^3$)}]. Statistical significance was assessed using an unpaired Student's T-test for specific force and 2-way ANOVA with repeated measurements for resistance to eccentric contraction protocol.

EMG/EIM

Electrophysiology was performed on 6-8 mo $Ano5^{-/-}$ and control muscles using methods similar to those previously published [518]. Mice were anesthetized using inhaled isoflurane and placed in the prone position with the hind limbs extended at 45° away from the body of the animal. Compound muscle action potential (CMAP) amplitudes were measured from bilateral triceps surae muscles following supramaximal sciatic

222

nerve stimulation in mutant (n=6 animals, 12 hind limbs) and control (n=7 animals, 14 hind limbs) mice. Needle electromyography was performed in the right GAS muscle to assess for the presence or absence of fibrillation potentials.[518] Localized impedance measures, or electrical impedance myography (EIM), was performed in bilateral GAS muscles at frequencies from 1000 Hz-10 MHz using a Skulpt Inc EIM1103 system (San Francisco, CA) using methods similar to those previously reported in mouse models of amyotrophic lateral sclerosis and muscular dystrophy [519, 520]. A fixed electrode array with four 26 gauge insulated electromyography needle electrodes (Natus, Middleton, WI) spaced 1 mm apart was used in place of surface electrodes. The electrode array was inserted into the belly of bilateral gastrocnemius muscles in a longitudinal configuration in respect to muscle fiber direction, and two trials of impedance measurements were obtained in each muscle and averaged for a single value in each limb (n=6 animals, 12 hind limbs for each group). Using the convention from previously published EIM studies and for simplicity, we analyzed reactance, resistance, and phase at two current frequencies, 50 kHz and 100 kHz. CMAP amplitudes and impedance characteristics were compared using a two-tailed t test.

Primary muscle cell culture

Primary myoblasts were derived from the hindlimb muscles of 3 month old $Ano5^{-/-}$ mice and age matched C57BL/6 mice [521, 522]. Hindlimb muscle was dissected from individual mice and subjected to pronase digestion. The digest was then mechanically dissociated by repeated trituration followed by filtration through a 100-µm vacuum filter (Millipore). Mononucleated cells were resuspended in Ham's F-10 supplemented with 20% fetal bovine serum, 5 ng/ml basic FGF, 100 U/ml penicillin G, and 100 µg/ml streptomycin (Growth Media) and were cultured on collagen-coated dishes (Bovine Collagen I Gibco). During the first several passages of the primary cultures, myoblasts were enriched by preplating [523].

Primary muscle cell differentiation and fusion index

Cells were differentiated on glass cover slips coated with Entactin-Collagen IV-Laminin (Millipore) at a density of $2x10^5$ cells per well in 12-well culture dishes. Myogenic differentiation was induced by culturing the cells in low-glucose DMEM supplemented with 1% Insulin-Selenium-Transferin (Gibco), 100 μg/ml penicillin and 100 μg/ml streptomycin (Differentiation Media) for a period of three days. Cells were fixed with 4% paraformaldehyde and stained for myosin heavy chain (Sigma) to identify differentiated muscle cells and with SYTO 24 Green to visualize nuclei. The fusion index was calculated as the number of nuclei located in cells having more than one nucleus (myotubes) divided by the total number of nuclei. Measurements were done using Image J and >1100 nuclei were counted for each experiment. Fusion experiments were done in triplicate with primary isolates from three different mice. Statistical significance was assessed using an unpaired two-tailed Student's T-test.

Statistical analysis

Data were expressed as the mean ± SEM and analyzed using unpaired two-tailed T-tests using GraphPad Prism 5 (Graphpad Software, La Jolla, CA) unless otherwise specified.

225

Supplementary Figure 1. *ANO5* mutations associated with myopathy. Topology model of ANO5 protein with all known *ANO5* patient mutations associated with myopathy and mutation used in this mouse study. Green: point mutation, Red: frame shift leading to a premature stop codon, Pink: predicted splice site mutation [8, 106, 200, 499, 524-530], Blue: final ANO5 amino acid encoded by mouse *Ano5⁻ᐟ⁻* locus. (Primary effort on figure: Hartzell, HC)
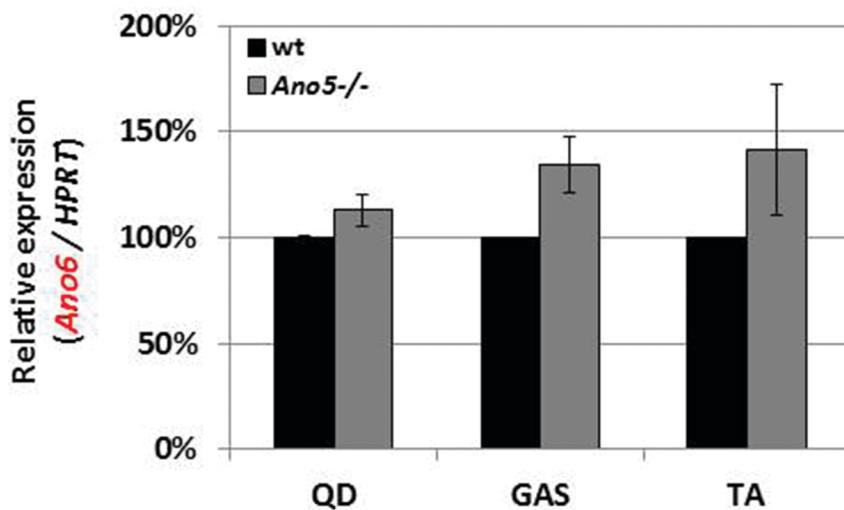
Supplementary Figure 2. Relative expression of *Ano6* in *Ano5⁻ᐟ⁻* muscles. Relative *Ano6* expression at the RNA level was assessed through qRT-PCR in quadriceps (QD), gastrocnemius (GAS) and tibialis anterior (TA) muscle extracted from BL6 wildtype and *Ano5⁻ᐟ⁻* mice. Expression was increased to 113-142% of wildtype levels, although due to a high degree of variability, none of these changes were found to be statistically significant (QD, P=0.15, GAS, P=0.06, TA, P=0.25). (Primary effort on figure: Rodino-Klapac Lab)

226
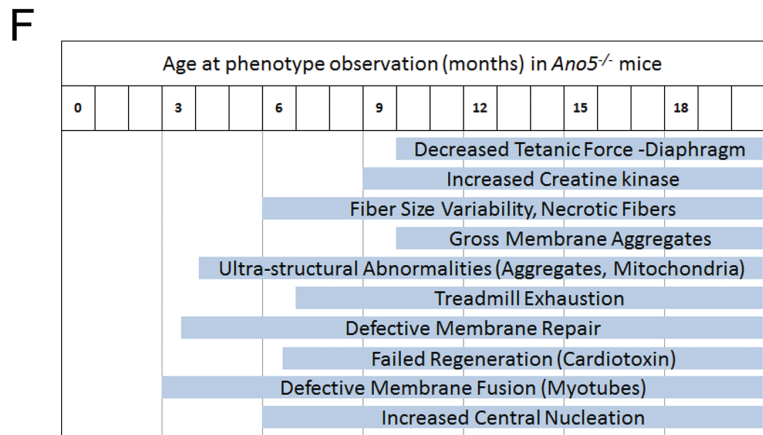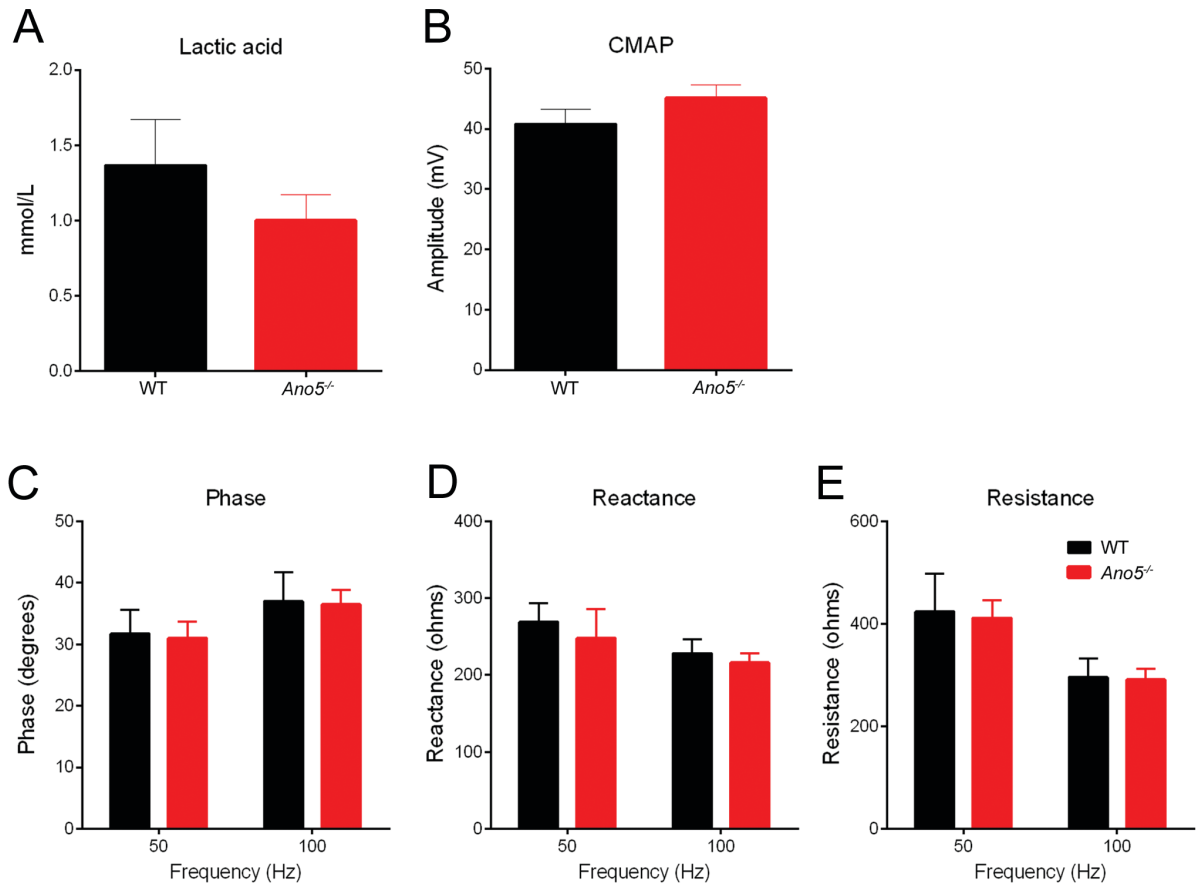
Supplementary Figure 3. Physiological Characterization of *Ano5* mice

(A) Lactic acid levels were slightly reduced in *Ano5* mice compared to WT controls

following treadmill running (P=0.15). (B) Electrophysiological characteristics of the

muscle. CMAP amplitude was not significantly difference between *Ano5* (45.1±2.2 mV)

and WT (40.8±2.4 mV) (p=0.22). No $Ano5^{-/-}$ or WT animal demonstrated fibrillation

potentials. (C-E) Impedance characteristics of muscle at 50 kHz (phase; reactance;

resistance, respectively). There were no differences between $Ano5^{-/-}$ (31.0±2.7;

248.1±37.8 Ω; 411.4±34.6 Ω) and WT fibers (31.7±3.9; 269.0±83.9 Ω; 424.3±73.9 Ω)

(phase: P=0.59; reactance: P=0.44; resistance: P=0.59). No differences were observed

at 100 kHz between $Ano5^{-/-}$ (36.5±2.4; 216.2±27.3 Ω; 290.7±22.0 Ω) and WT fibers

(37.0±4.8; 228.4±63.9 Ω; 295.8±36.1 Ω) (phase: P=0.77; reactance: P=0.55; resistance:

P=0.68) (Primary effort on figure: Rodino-Klapac Lab)
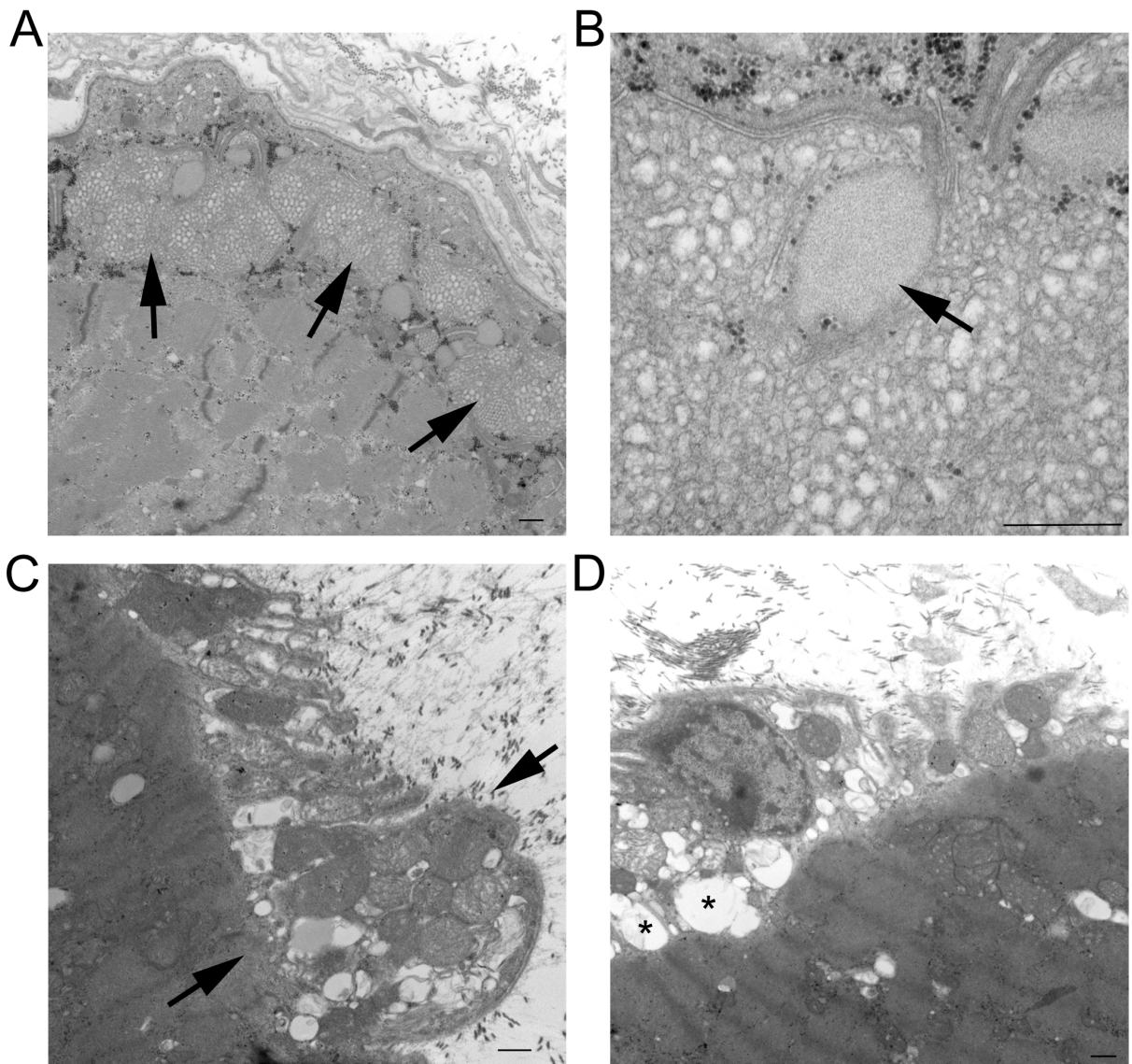
Supplementary Figure 4. *Ano5* [-/-] **mouse histologically phenocopies LGMD2L patient**

Patient compound heterozygous for two mutations [c.155A>G (p.Asn52Ser)] + [c.191dupA (p.Asn64Lysfs*15)] in the coding region of the *ANO5* gene. (A) Image demonstrating aggregates. (B) High magnification image of aggregates and filamentous structure surrounded by fuzzy inner tubules. (C, D) degenerating (arrows) and necrotic (asterisks) mitochondria. Scale bars = 500nm. (Primary effort on figure: Rodino-Klapac Lab)
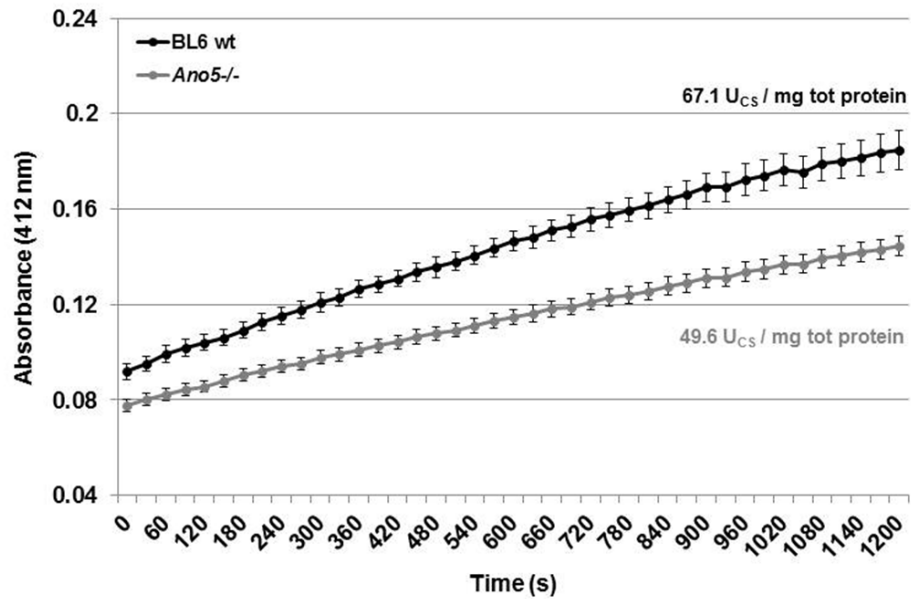
Supplementary Figure 5. Loss of *Ano5* alters citrate synthase activity. Citrate Synthase Assay Plot of absorbance at 412nm over 20 minute time-course marking citrate synthase activity in BL6 wildtype and *Ano5*^{-/-} gastrocnemius muscle. *Ano5*^{-/-} muscle lysate exhibited reduced citrate synthase activity relative to WT that was statistically significant at every time point ($P < 0.01$). Specific activity of the enzyme, as determined by reaction rate, noted adjacent to absorbance curves. (Primary effort on figure: Rodino-Klapac Lab)

229

Supplementary Video. Abnormal running pattern observed in *Ano5*^{-/-} mice

9 mo old *Ano5*^{-/-} mice (bottom 2 lanes) showed inconsistencies in ability to run on the treadmill compared to WT (top 2 lanes) mice. Every time a mouse ceased running until the treadmill belt returned to the shock plate was considered a break. Exhaustion was met when mice stopped on shocker plate for a minimum of 10 sec without engaging in exercise. (Primary effort on figure: Rodino-Klapac Lab)

Chapter VII

Anoctamin 5/TMEM16E Ca^{2+}-dependent phospholipid scrambling facilitates muscle precursor cell fusion.

Summary

Limb-girdle muscular dystrophy Type 2L (LGMD2L) is a myopathy arising from mutations in *ANO5,* however, information concerning how ANO5 contributes to muscle physiology is lacking. We find that exogenous ANO5 confers Ca^{2+}-dependent phospholipid scrambling to cells. Moreover, like other Anoctamin/TMEM16 homologs that elicit scrambling, ANO5 scrambling is associated with the simultaneous development of ionic current. To explain the role of ANO5 in LGMD2L, we hypothesized that ANO5-mediated phospholipid scrambling facilitates fusion of mononucleated muscle progenitor cells (MPCs) required for muscle repair. We previously reported that, MPCs isolated from adult *Ano5*$^{-/-}$ mice exhibit defective cell fusion and produce muscle fibers with significantly fewer nuclei in culture as compared to controls. We find that this defective fusion is associated with a decrease of Ca^{2+}-dependent phosphatidylserine exposure in isolated MPCs and a decrease in the amplitude of Ca^{2+}-dependent outwardly rectifying ionic currents. Viral introduction of *ANO5* in *Ano5*$^{-/-}$ MPCs restores MPC fusion competence, ANO5-dependent phospholipid scrambling, and Ca^{2+}-dependent outwardly rectifying ionic currents. *ANO5* rescued MPCs produce myotubes having numbers of nuclei similar to wild-type controls. This work highlights the role of ANO proteins in physiologically relevant lipid signaling and the role of phosphatidylserine signaling in muscle health.

Introduction

During the past several decades, advances in molecular genetics have greatly accelerated our capacity to identify variants linked to genetic diseases. However, elucidating the processes that lead to pathology lags significantly behind our diagnostic abilities. The limb-girdle muscular dystrophies (LGMD) are a case-in-point. In the last decade, 15 new genes have been linked to LGMDs, but how mutations in these genes contribute to their associated diseases remains incompletely understood.

Muscular dystrophies encompass a heterogeneous group of pathologies characterized by progressive skeletal muscle weakness and atrophy. There are now at least 34 genes that have been linked to LGMDs that affect mainly hip or shoulder, girdle, and limb muscles. Here we focus on LGMD type 2L, an autosomal recessive LGMD that is characterized by late onset (onset range 11 – 50 years) with myalgia that is commonly associated with exercise intolerance, progressive muscle weakness/atrophy, and elevated serum creatine kinase [531]. LGMD2L was linked to mutations in *ANO5 (TMEM16E)* in 2010 [8, 199, 532], but how ANO5 participates in muscle function remains a mystery.

Many LGMD genes encode proteins that are involved in maintaining muscle structural integrity. For example, the most common LGMDs, the α-dystroglycanopathies (ten LGMD2 linked genes), are caused by defects in proteins linking the muscle cytoskeleton to the extracellular matrix through the sarcolemma, thus rendering the muscle sarcolemma more susceptible to mechanical damage [533]. Other LGMD genes, such as those encoding dysferlin (LGMD2B) and caveolin (LGMD1C), are thought to play roles in membrane repair [534, 535]. Because muscle is subjected to immense physical stress during activity, highly sophisticated processes exist to repair damage and regenerate injured muscle [427, 491]. Previous work has suggested that mutations in ANO5 alter muscle repair processes [8, 202, 223]. For example, we previously

characterized an *Ano5*^{-/-} knockout mouse which recapitulates many of the phenotypes of LGMD2L patients and demonstrated that this mouse exhibits defective muscle repair processes, both *in vivo* and *in vitro* [202]. One mechanism by which muscle fibers are repaired involves fusion of mononucleated muscle precursor cells (MPCs) with damaged muscle. Just as multinucleated muscle fibers are formed during embryogenesis by the fusion of hundreds to thousands of MPCs [197], this process is recapitulated during muscle repair and regeneration as MPCs are recruited to fuse with and repair torn fibers or to form a new muscle fiber [222, 420, 421]. We suggest that ANO5 plays a role in regulating/coordinating the fusion of MPCs during regenerative muscle repair.

Initially, it was thought that ANO5 was an ion channel because the founding members of the 10-gene ANO/TMEM16 family are Ca^{2+}-activated Cl^- channels [9, 49-51, 124, 245]. However, it is now recognized that many ANO paralogs are not Cl^- channels but have other functions, most notably Ca^{2+}-activated phospholipid scrambling (Ca^{2+}-PLS) [7, 9, 66, 68]. ANO6 was the first ANO found to exhibit PLSase activity, but more recently two ANO homologs from fungi were found to be PLSases when purified and reconstituted into liposomes [66, 68, 110]. One of these scramblases has been crystallized [68], which has greatly informed efforts to elucidate how it functions [114, 115]. While initial reports suggested that ANO5 was not a phospholipid scramblase [129], other evidence suggests that it might elicit Ca^{2+}-PLS in certain biological contexts [536]. Moreover, during the preparation of this manuscript additional evidence has suggested that ANO5-dependent PLS might play a role in the development of gnathodiaphyseal dysplasia [537].

Phospholipid scrambling (PLS) is utilized by many cells as a means of cell-cell communication during a variety of biological processes, including cell fusion [260]. The plasma membrane (PM) is composed of two lipid monolayers that exhibit tightly regulated asymmetric lipid organization, with the extracellular leaflet enriched in

234

phosphatidylcholine and sphingomyelin and an intracellular leaflet enriched in phosphatidylserine (PtdSer), phosphatidylinositides, and phosphatidylethanolamine (PtdEt) (reviewed [88]). When activated by increases in cytosolic Ca^{2+}, PLSases form a hydrophilic pathway through the membrane, facilitating the diffusion of polar lipid head groups non-selectively between membrane leaflets, resulting in the loss of leaflet asymmetry [111, 538]. The loss of this asymmetry has a variety of biophysical consequences, including altering lipid packing and lateral pressure between lipid head groups [9]. In addition, PLS exposes PtdSer and PtdEt to the extracellular face, where they are recognized by a variety of both soluble and membrane-bound receptors that elicit diverse intracellular signaling cascades in neighboring cells [95]. PtdSer exposure via PLS is a signal thought to regulate muscle fusion [187, 188, 539], both during development and regeneration, and several PtdSer receptors have recently been identified for their role in regulating the fusion of muscle progenitor cells (MPCs) [189, 190, 454, 540] .

Here we investigate the function of the ANO5/TMEM16E protein and explore how loss of *Ano5* affects muscle cell biology. We find that exogenous ANO5 confers Ca^{2+}-PLS to HEK2 cells. Moreover, we find that ANO5-dependent PLS is associated with the development of an ionic conductance. This conductance, like that described for ANO6 and the fungal ANO scramblases afTMEM16 and nhTMEM16, is largely ion non-selective. Next, we investigated the Ca^{2+}-PLS activity of fusogenic, primary MPCs and demonstrate that the loss of *Ano5* perturbs both the Ca^{2+}-dependent exposure of PtdSer and PLS-associated ionic currents. Finally, we further explore our previous discovery that loss of *Ano5* expression manifests in a MPC fusion defect that severely decreases the number of nuclei per myofiber *in vitro*. We find that introducing exogenous *ANO5* restores Ca^{2+}-PLS and rescues fusion of $Ano5^{-/-}$ MPCs. We believe this work highlights a role for ANO5 in muscle regeneration, and emphasizes a role for ANO5-dependent

235

Ca^{2+}-PLS in the upstream regulator of proper MPC fusion to produce multinucleated skeletal muscle fibers.

Abstracts of this work have been published previously [541-543].

Results

ANO5 elicits phospholipid scrambling.

ANO5 is the most closely related paralog of ANO6 with 48% identity in amino acid sequence [544]. Because ANO6 elicits Ca^{2+}-PLS [7, 106], we hypothesized that ANO5 also activates Ca^{2+}-PLS, and that perturbations in this activity may be associated with changes in skeletal muscle function that contribute to the progression of LGMD2L. First, we aimed to evaluate the ability of ANO5 to confer Ca^{2+}-PLS. To do so we evaluated the ability of ANO5 to confer Ca^{2+}-PLS to HEK cells. We employed HEK cells because 1) they do not natively express ANO5, 2) they exhibit low endogenous Ca^{2+}-PLS activity, as we have described previously [106], and 3) they represent and ideal model for evaluating an ion channel conductance associated with potential Ca^{2+}-PLS.

We first evaluated ANO5's ability to confer Ca^{2+}-dependent PtdSer exposure in stable cell lines expressing ANO5. ANO5-eGFP expression conferred robust surface exposure of PtdSer monitored by binding of annexinV-Alexa568 when intracellular Ca^{2+} was elevated by ionophore-stimulated store-operated Ca^{2+} entry (SOCE, see Methods) (Fig. 1a). Ca^{2+} stimulation proved to elicit Ca^{2+}-dependent PtdSer exposure in the vast majority of cells expressing exogenous ANO5 in contrast to parental HEK cells that do not exhibit this activity (Fig. 1b). ANO5-mediated PLS developed at a rate slightly slower than that produced by ANO6-eGFP, however both elicited maximal PtdSer exposure in ~10mins (Fig. 1d). We confirmed that the observed PS exposure was in fact Ca^{2+}-dependent by employing the PtdSer probe LactC2-Clover, which unlike annexinV does

236

not require exogenous Ca^{2+} as a cofactor for PtdSer binding. Treating transiently

transfected ANO5-3xFLAG cells in the same manner as Figure 1a, but omitting Ca^{2+}, we

found that the cells were not bound by LactC2-Clover and therefore did not expose

PtdSer via Ca^{2+}-PLS (Fig. 1e). Perfusion of Ca^{2+} rapidly elicit PtdSer in these transfected

cells demonstrating ANO5-dependent PtdSer exposure requires Ca^{2+}.

  Previous studies have suggested that ANO5 is located in intracellular organelles [76,

201] and does not mediate plasma membrane scrambling [129]. Some of these

discrepancies with our observations may be due to the use of vastly different cells

models, our use of codon optimized human ANO5 vs the murine ANO5 used previously,

and our selection of stable cells lines with high ANO5 expression. To confirm ANO5 is

present on the cell surface, surface proteins on HEK cells expressing ANO5-3XFLAG

were biotinylated using membrane-impermeant NHS-biotin. Biotinylated surface proteins

were captured on streptavidin beads, run on SDS-PAGE gels, and western blots were

probed with anti-FLAG antibody (Fig. 1b). We found that a small fraction of ANO5

trafficked to the PM in our HEK cells, which afforded us the opportunity to evaluate

ANO5's functional properties at the PM. Because HEK cells do not endogenously

express ANO5, we would assume that ANO5 trafficking in these cells is not

representative of native ANO5 trafficking, but instead provides us a model to investigate

ANO5's exogenous function.

ANO5 phospholipid scrambling is associated with non-selective ionic currents.

We have previously shown that ANO6 generates ionic currents that develop in parallel

with phospholipid scrambling [106] and have argued that this current represents ions

that are conducted through the same pathway that conducts lipids [9, 115, 544]. To

determine whether ANO5 also generates ionic currents, we performed whole-cell patch

clamp evaluation of ANO5-expressing HEK cells while simultaneously measuring

phospholipid scrambling by annexinV-Alexa568 binding. Pipet (intracellular) solutions
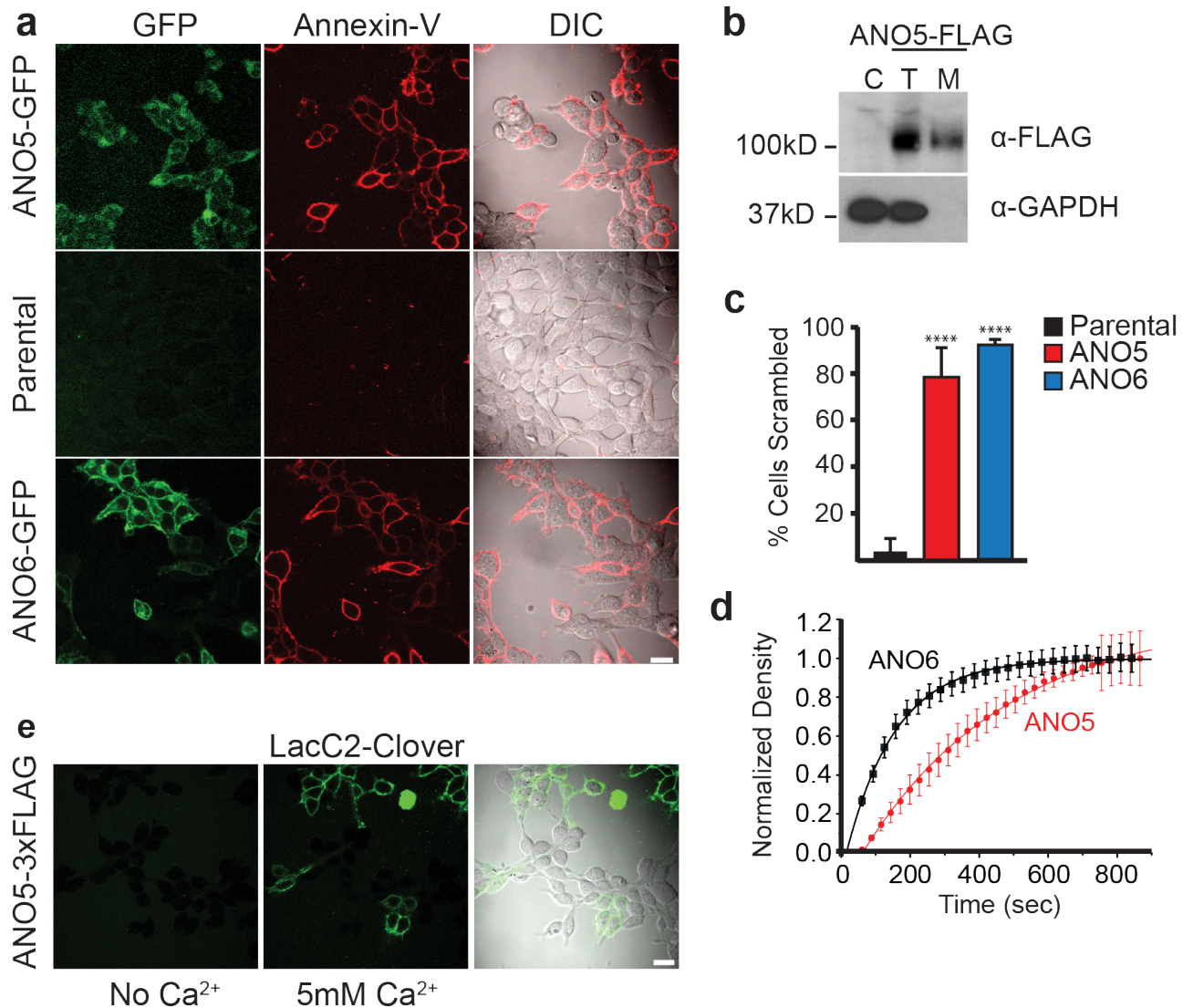
Figure 1. ANO5 expression activates Ca^{2+}-PLS. (a) HEK cell lines stably expressing

eGFP tagged ANOs were stimulated using the store operated Ca^{2+} entry assay for

10mins and PtdSer exposure was monitored via annexin-Alexa568 binding. (b) Western

blot of HEK293 cells expressing ANO5-3xFLAG. Cells were surface biotinylated and the

biotinylated surface membrane fraction was isolated using streptavidin beads. C=control

untransfected lysate, T=total ANO5-3xFLAG transfected lysate, and M=anti-FLAG

isolated surface biotinylated fraction from ANO5-3xFLAG transfected lysate. GAPDH

was used as a loading control and to show no cytoplasmic proteins are biotinylated

238

(lower blot). (c) Quantification of the fraction of cells, expressing Clover tagged ANOs, that were bound by the PtdSer probe LactC2-Cherry when stimulated using the store operated Ca^{2+} entry assay for 10mins. 3 independent experiments totaling >250 cells per condition. Error bars indicate SEM. Significance was evaluated via one-way ANOVA with Dunnett's correction, P = 0.0001 (****) for both. (d) Time course of annexin-V binding to HEK cells expressing ANO5-eGFP and ANO6-eGFP. Images of the same field of 30–100 cells were acquired at ~20 s intervals. Annexin-V: mean ± SEM of >3 independent experiments. Means at the end of the recordings were normalized to 1. (e) Binding of the PtdSer probe LactC2-Clover to HEK cells where some express ANO5-3xFLAG. In the first panel, HEK cells were incubated with A23187 in the absence of Ca^{2+} for 10 min. In the second panel, Ca^{2+} was added. (Primary effort on figure: (a, c, and e) Whitlock, JM; (b) Yu, K; (d) Hartzell, HC and Whitlock, JM)

containing 200 µM free Ca^{2+} were used to activate ANO5. Both phospholipid scrambling and ionic currents developed slowly after elevation of cytosolic Ca^{2+} (Fig. 2a). In general, both current and annexin-V binding began to increase several minutes after establishing whole-cell recording and reached a plateau within 15 min. This is very similar to our previous observations of ANO6 [106]. Under these patch clamp conditions, ~90% of ANO5-expressing cells scramble, while 25% of untransfected cells scramble (Fig. 2b). Currents generally exhibited linear current-voltage relationships (Fig. 2c) with slow activation at positive voltages and some deactivation at very negative voltages. Moreover, we evaluated ANO5 and ANO6 Ca^{2+} sensitivity and found that 200 µM free Ca^{2+} was the ideal Ca^{2+} concentration to evaluate the Ca^{2+}-PLS of each (Fig. 2d). However, we found that both ANO5 and ANO6 confer Ca^{2+}-dependent PtdSer exposure at lower Ca^{2+} concentrations, despite these Ca^{2+} concentrations being non-ideal to elicit Ca^{2+}-dependent PtdSer exposure in the maximal percentage of cells. Increasing free Ca^{2+} concentration did not increase the fraction of cells exhibiting Ca^{2+}-PLS in either ANO5 or ANO6 expressing cells.

Ionic selectivity of ANO5 currents was determined by changing extracellular [CsCl], measuring the shift in reversal potential, and calculating the relative ionic permeabilities with the Goldmann-Hodgkin-Katz equation [545]. ANO5 currents are slightly cation-selective. For example, in Figure 3a a switch from symmetrical CsCl solutions on both sides of the membrane to a 10-fold lower concentration of extracellular CsCl results in only a modest ~10 mV negative shift in the current's reversal potential. This corresponds to a P_{Cs}/P_{Cl} permeability ratio of 1.6 (Fig. 3b). A similar value was found for P_{Na}/P_{Cl}. The ANO5 pore appears to be relatively large because it is also permeable to the large organic cation $NMDG^+$, which has a mean diameter of >7 Å. These results are in sharp contrast to ANO1, which is highly Cl^- -selective (Fig. 3b).
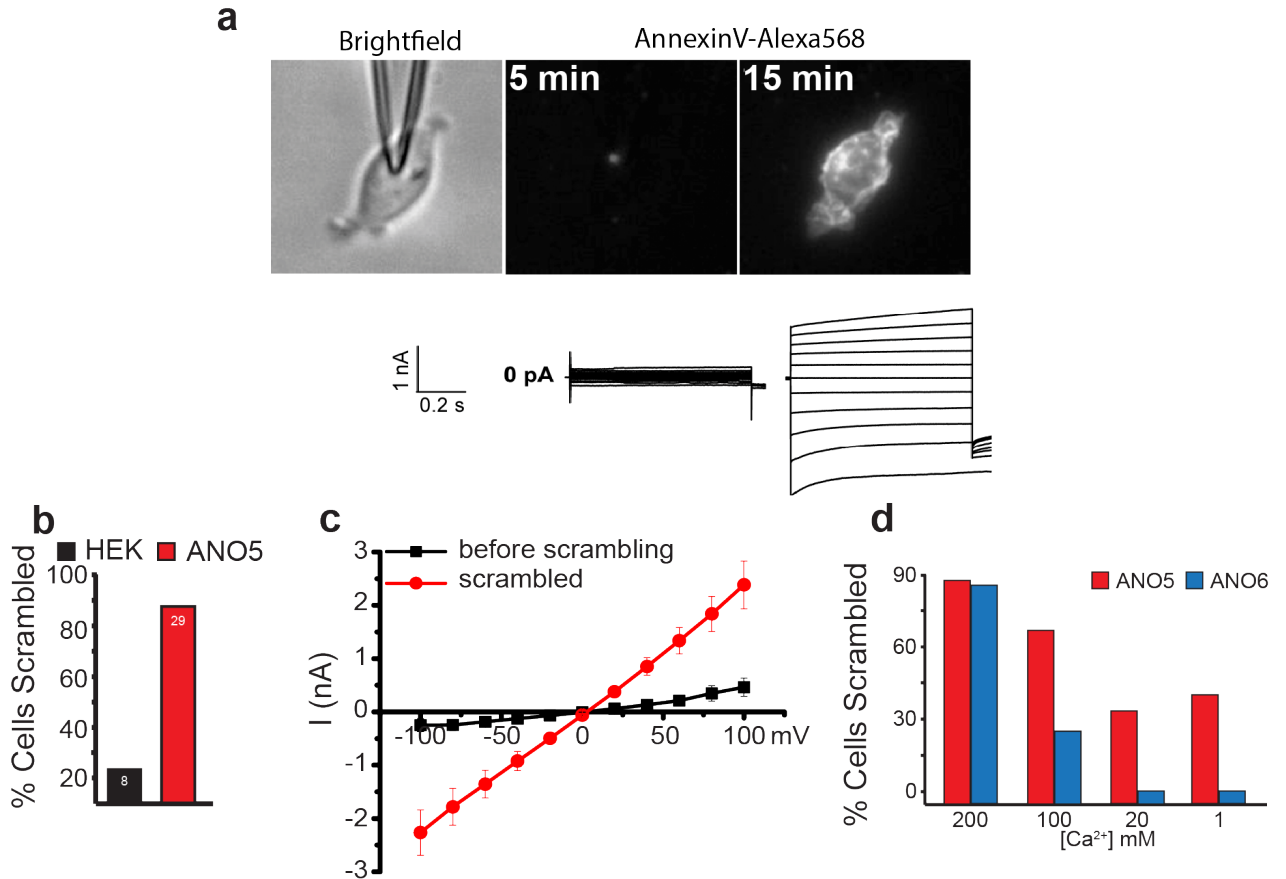
Figure 2. ANO5-dependent Ca^{2+}-PLS is associated with an ionic current. (a) Simultaneous measurement of annexinV-Alexa568 binding and whole cell patch clamp recording of ANO5-Clover HEK cells. Cells were patch clamped with 200 μM free Ca^{2+} in the intracellular (pipette) solution and currents were measured from a holding potential of 0 mV by voltage steps from -100 mV to +100 mV in 20 mV increments. Representative images (top) and corresponding currents (bottom) show typical one of 29 experiments. The first panel is a brightfield image of the cell, the second two images show fluorescence of bound annexin-V. (b) Number of cells scrambled during patch clamp experiments. White numbers indicate the number of cells. (c) Mean current-voltage (I-V) relationships before (black squares) and after (red circles) cells showed significant annexin-V binding. (d) Quantification of the percentage of cells bound by annexinV-Alexa568 in ANO5-Clover or ANO6-Clover HEK cells when stimulated via whole cell

241

patch clamp as in part a but with different concentrations of free Ca^{2+} in the intracellular

(pipette) solution. Each condition represents data from >10 cells. (Primary effort on

figure: Yu, K)
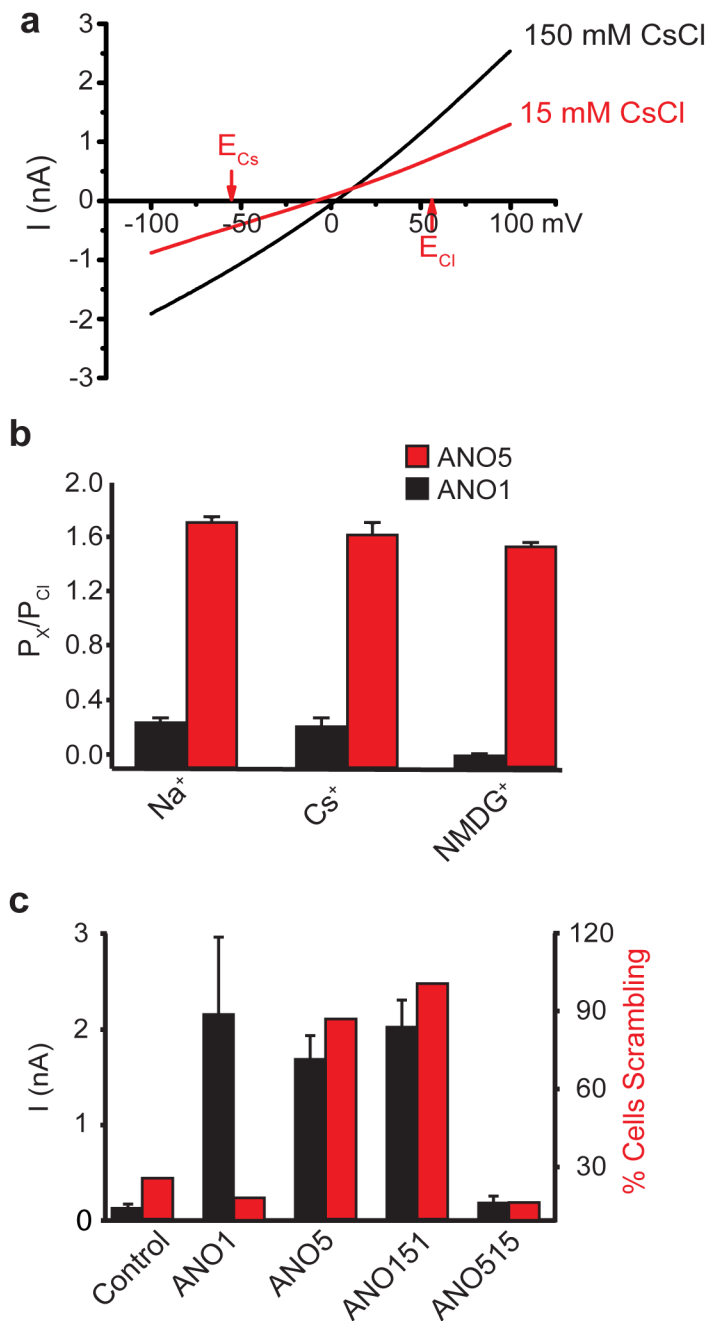
Figure 3. ANO5-PLS associated ionic currents are non-selective. (a) Representative

whole-cell current traces recorded from ANO5- expressing HEK293 cells with 200 μM

free Ca^{2+} in the pipette with external solutions containing 150 mM (black) or 15 mM (red) CsCl. Currents were generated by ramps from -100 to +100 mV. (b) Cation permeability of ANO5 and ANO1 currents relative to Cl$^-$ (P_x/P_{Cl}) calculated by changes in reversal potential as shown in (a). (c) Ionic current amplitudes and phospholipid scrambling of HEK cells expressing ANO1, ANO5, ANO1 harboring the ANO5 scrambling domain (ANO151), and ANO5 harboring the ANO1 scrambling domain ANO515. (Primary effort on figure: Kuai, K)

To verify that currents and phospholipid scrambling were mediated by ANO5 and not caused by up-regulation of another endogenous scramblase, we mutated the scramblase domain of ANO5. We previously identified a 34-amino acid sequence we call the scrambling domain (SCRD) in ANO6 that is necessary for Ca^{2+}-PLS [106]. The SCRD sequences of ANO5 and ANO6 are highly conserved. When the SCRD domain of ANO5 was replaced with the homologous domain from ANO1 ("ANO515"), phospholipid scrambling and the development of non-selective, scrambling-associated currents were greatly reduced (Fig. 3c). In contrast, when the ANO5 SCRD was swapped into ANO1 ("ANO151"), it gave ANO1 the ability to scramble lipids and was associated with the development of non-selective, scrambling-associated currents. These results confirm that scrambling in ANO5-transfected HEK cells is mediated by ANO5 and preclude the possibility that phospholipid scrambling is caused by the upregulation of another phospholipid scramblase.

Muscle progenitor cell (MPC) fusion and phosphatidylserine exposure is defective in an Ano5-/- MPCs.

Previously, we characterized an *Ano5-/-* mouse model [202] that was created by inserting a "gene trap" exogenous splice acceptor site followed by a premature stop codon between exons 8 and 9 (Fig. 4a). A similar premature termination of *ANO5* is associated with most LGMD2L patients (c.190dupA) and is considered a LGMD2L founder mutation [532]. This mouse model recapitulates many aspects of LGMD2L and demonstrates defective cell-cell fusion of isolated MPCs [202]. This model exhibits a loss of ANO5 protein in two tissues that typically express high levels of steady state ANO5, skeletal muscle and testis (Fig. 4b).

To investigate the function of ANO5 in skeletal muscle, MPCs were isolated from the hindlimbs of adult animals and patch clamped with an internal (pipet) solution containing
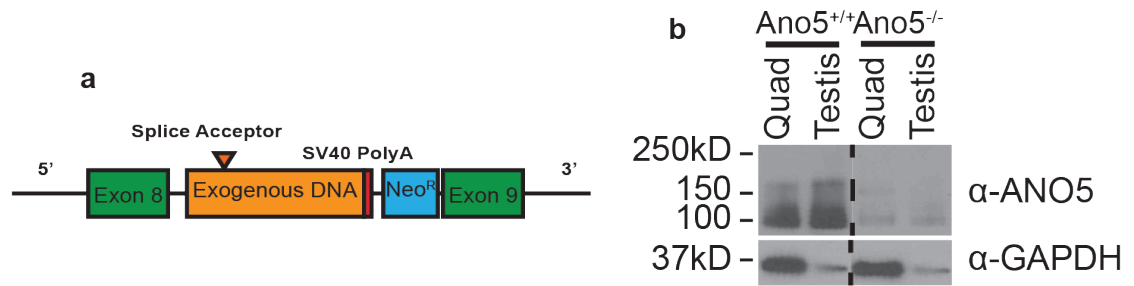
Figure 4. Exogenous "gene trap" knock-in results in loss of ANO5. (a) *Ano5* knockout construct. Briefly, a "gene trapping" element was inserted between exons 8 and 9 consisting of an exogenous splice acceptor followed by stop codons [202]. (b) Western blot of SDS-PAGE gel from lysates of quadriceps (Quad) or testis from 3-month-old wild type or *Ano5* knockout mice. (Primary effort on figure: Whitlock, JM)

200 μM free Ca^{2+} (Fig. 5a). Ionic currents were measured by voltage steps and PtdSer

exposure was measured by annexinV-Alexa568 binding, simultaneously. A majority

(>90%) of differentiated wild type $Ano5^{+/+}$ MPCs expose PtdSer on the external surface

and develop ionic currents characteristic of ANO5 currents after elevating cytosolic Ca^{2+}

by establishing whole-cell recording (Fig. 5a,b). Current amplitude and annexinV-

Alexa568 binding increased in parallel. The currents had similar biophysical properties to

currents in ANO5-transfected HEK cells (Fig. 1): they had linear current-voltage

relationships and exhibited slow activation at positive voltages and some deactivation at

very negative voltages. In contrast, the majority of $Ano5^{-/-}$ cells (~75%) did not expose

PtdSer when patch-clamped with Ca^{2+} in the patch pipet and did not develop PLS-

associated ionic currents (Fig. 5a,b).

ANO5 is not the only scramblase expressed in MPCs. Most notably, MPCs also express

significant levels of ANO6. We wondered whether the absence of phospholipid

scrambling in $Ano5^{-/-}$ MPCs might be explained by down-regulation of ANO6 in addition

to loss of ANO5 expression. However, western blot showed that ANO6 levels were

comparable in differentiated $Ano5^{+/+}$ and $Ano5^{-/-}$ MPCs (Fig. 5c). This result

demonstrates that the absence of scrambling in $Ano5^{-/-}$ cells is not explained by changes

in ANO6 steady state levels. However, it raises the question why the ANO6 that is

present does not mediate scrambling (see Discussion).

***MPC Phospholipid Scrambling and Fusion Are Rescued by infection with ANO5-
virus.***

If our hypothesis that ANO5 elicits Ca^{2+}-PLS that plays an important role in MPC fusion

is correct, it should be possible to rescue the defective fusion of $Ano5^{-/-}$ MPCs by over-

expressing the human *ANO5* we characterized in figures 1-3. We chose culture

conditions that generated robust myotube development following ~36 hours of $Ano5^{+/+}$

246
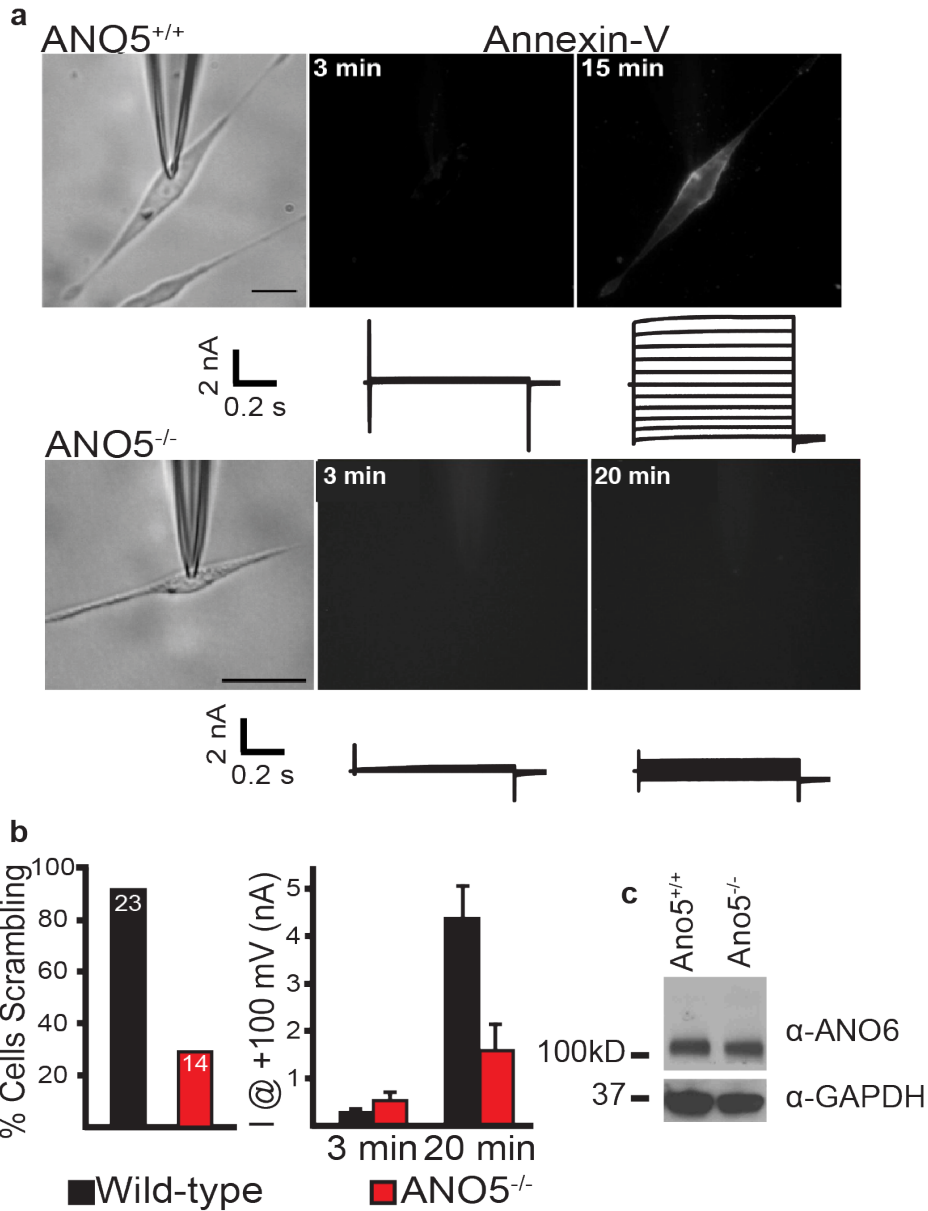
Figure 5. *Ano5^-/-* muscle cells exhibit perturbed Ca^{2+}-PLS and PLS-associated ionic current.

(a) Simultaneous whole cell patch clamp and annexinV-Alexa568 binding as an indicator of Ca^{2+}-PLS of primary MPCs differentiated for ~24hrs. Images on the left show brightfield micrographs of patched MPCs. Images on the right show annexinV-Alexa568 binding. Scale bar = 10µm. Below the images are ionic currents recorded using voltage steps between +100 and -100 mV in 20 mV increments from a holding potential of 0 mV.

(b) Quantification of Ca^{2+}-PLS in MPCs (left), and average current of differentiated myoblasts at +100 mV (right). (c) Western blot of native ANO6 levels in wild type and *Ano5* knockout MPCs differentiated for ~24hrs. (Primary effort on figure: (a and b) Yu, K; (c) Whitlock, JM)

MPC differentiation to highlight the discrepancy between $Ano5^{+/+}$ and $Ano5^{-/-}$ MPCs to contribute to developed myofibers with high nuclear number that we have reported previously (Fig. 6a) [202]. The ability of cells to form multinucleated myotubes was measured by counting the number of nuclei (DAPI stained) per myotube (phalloidin-stained) in $Ano5^{+/+}$, $Ano5^{-/-}$, $Ano5^{-/-}$ knockout treated with lentivirus expressing a scrambled sequence or the $hANO5$ we characterized in figures 1-3 (Fig. 6b). The lentiviral introduction of $hANO5$ did not increase the steady state level of $Ano6$ transcript, so that effects of $hANO5$ rescue are not the result of simply upregulating $Ano6$ (Fig. 6c). The lentivirus expressed our codon-optimized h$ANO5$ under the control of the PGK promotor. Previous investigations have demonstrated that lentivirus is robust in introducing stably integrated transgenes in MPCs. Additionally, unlike common promotors which are readily silenced via methylation in muscle (e.g. CMV), the PGK promotor produces reliable, consistent expression of virally introduced transgenes in muscle cells [546, 547]. The images (Fig. 6a), cumulative frequency plot (Fig. 6d), and frequency histogram (Fig. 6e) show that $Ano5^{+/+}$ MPCs formed myotubes having far more nuclei compared to $Ano5^{-/-}$ and that $hANO5$ significantly rescues this breakdown in fusion regulation/coordination. For example, where in $Ano5^{+/+}$ conditions only ~25% of the nuclei were found in myotubes having ≤5 nuclei, loss of $Ano5$ results in ~50% of the population being halted at the ≤5 nuclei stage (Fig. 6e,). $hANO5$ significantly rescues the percentage of nuclei in myotubes with ≤5 nuclei from 50% to 26% (v1.3 IFU) or 30% (v13 IFU), very close to the wild type value.

Exogenous $hANO5$ also rescued ANO5-dependent Ca^{2+}-PLS in $Ano5^{-/-}$ MPCs. Although only ~25% of $Ano5^{-/-}$ MPCs exhibit PtdSer when stimulated with 200 µM free intracellular Ca^{2+}, >80% of $Ano5^{-/-}$ has this activity restored upon $hANO5$ rescue (Fig 7a&b). Moreover, $hANO5$ PLS rescue is accompanied by the restoration of ANO5-depdendent, non-selective ionic current when stimulated with 200 µM free intracellular Ca^{2+} (Fig. 7c).

249
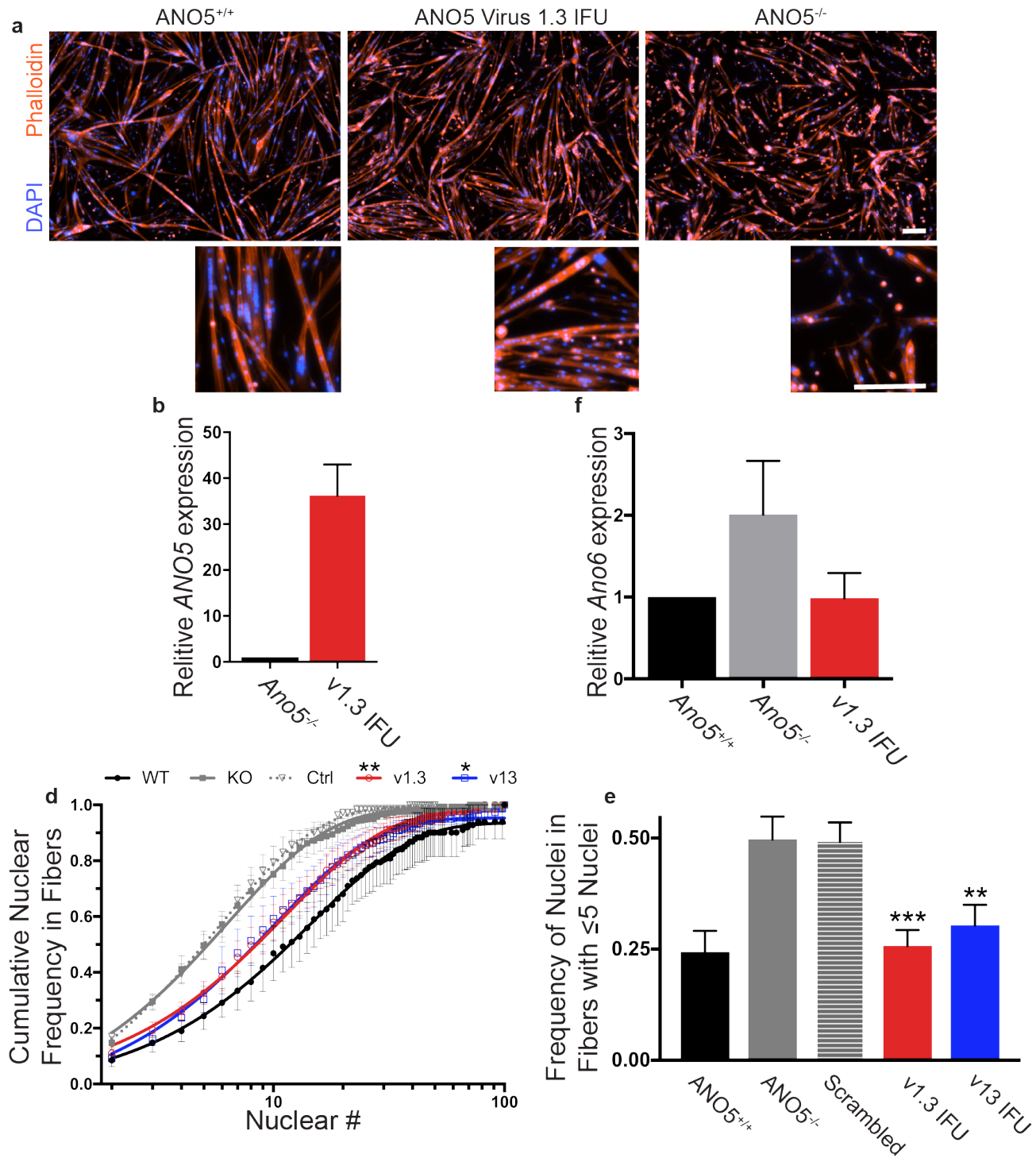
Figure 6. Exogenous ANO5 expression rescues Ano5$^{-/-}$ MPC fusion. (a) Comparison of representative images of MPC fusion after ~36hrs differentiation for *Ano5$^{+/+}$*, *Ano5$^{-/-}$*, and *Ano5$^{-/-}$* rescued with 1.3 IFUs of ANO5 virus. Scale bar = 300μm. (b) qPCR

evaluation of steady state *ANO5* transcript levels, following viral infection, normalized to *Gapdh.* (c) qPCR evaluation of steady state, endogenous *Ano6* levels normalized to *G*apdh. (d) Cumulative frequency of nuclei per fiber size for *Ano5$^{+/+}$*, *Ano5$^{-/-}$*, *Ano5$^{-/-}$* rescued with scrambled virus, *Ano5$^{-/-}$* rescued with 1.3 IFUs of ANO5 virus, and *Ano5$^{-/-}$* rescued with 13 IFUs of ANO5 virus. Nuclei per fiber distributions were evaluated by fitting the data for each replicate in each condition to a single exponential. Ano5$^{+/+}$ represents 3 independent experiments with 3 independently isolated cell lines (>6,500 nuclei). *Ano5$^{-/-}$*, *ANO5* 1.3 IFU, and ANO5 13 IFU represent 5 independent experiments, with 3 independently isolated cell lines (>7,000 nuclei per condition). Error bars = SEM. The exponential constants for each replicate of conditions were statistically compared to evaluate differences in the distributions of nuclei in fibers. Statistical significance for the difference from knockout was $P = 0.0095$ (**) for ANO5 virus 1.3 IFU and $P = 0.04$ (*) for ANO5 virus 13 IFU, one-way ANOVA with Dunett's correction. (e) Comparison of the frequency of nuclei in fibers containing ≤ 5 nuclei from d. $P = 0.0003$ (***) for ANO5 virus 1.3 IFU and 0.0013 (**) for ANO5 virus 13 IFU, one-way ANOVA with Dunett's correction. (Primary effort on figure: Whitlock, JM)

251
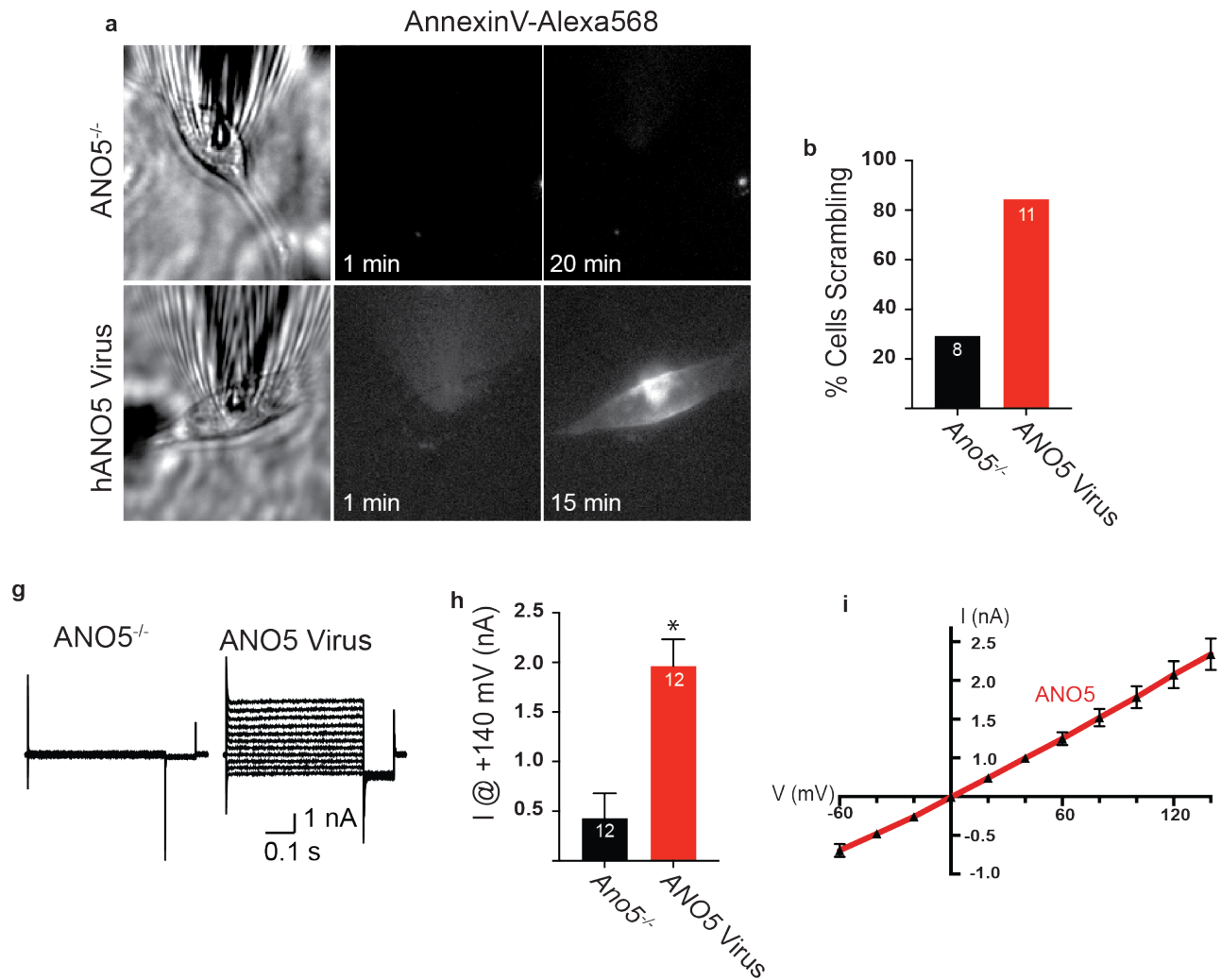
Figure 7. Exogenous ANO5 expression rescues Ano5$^{-/-}$ MPC Ca^{2+}-PLS. (a) Simultaneous whole cell patch clamp and annexin-V-Alexa568 binding as an indicator of Ca^{2+}-PLS of primary MPCs differentiated for ~24hrs. Images on the left show brightfield micrographs of patched MPCs. Images on the right show annexin-V binding. (b) Quantification of Ca^{2+}-PLS in MPCs. (c) Representative traces of ionic currents from MPCs isolated from the same mouse with or without ANO5 virus rescue following 10 mins of whole cell patch clamp with 200μM Ca^{2+} intracellular solution. Voltage steps from -60 to 140 mV. (h) Quantification of ionic currents from cell lines isolated from two 3-month-old mice with and without viral rescue. P = 0.027 (*), paired t-test. (i) Current

voltage relationship *ANO5* rescued *Ano5*^{-/-} MPCs from h. (Primary effort on figure:

Whitlock, JM)

Supplemental Figure 1. ANO5 expression rescues Ano5^{-/-} MPC fusion. Frequency

histogram representation of data from Figure 6d. Number of nuclei per fiber in bins,

center of bins represented along x-axis. Error bars = SEM. (Primary effort on figure:

Whitlock, JM)
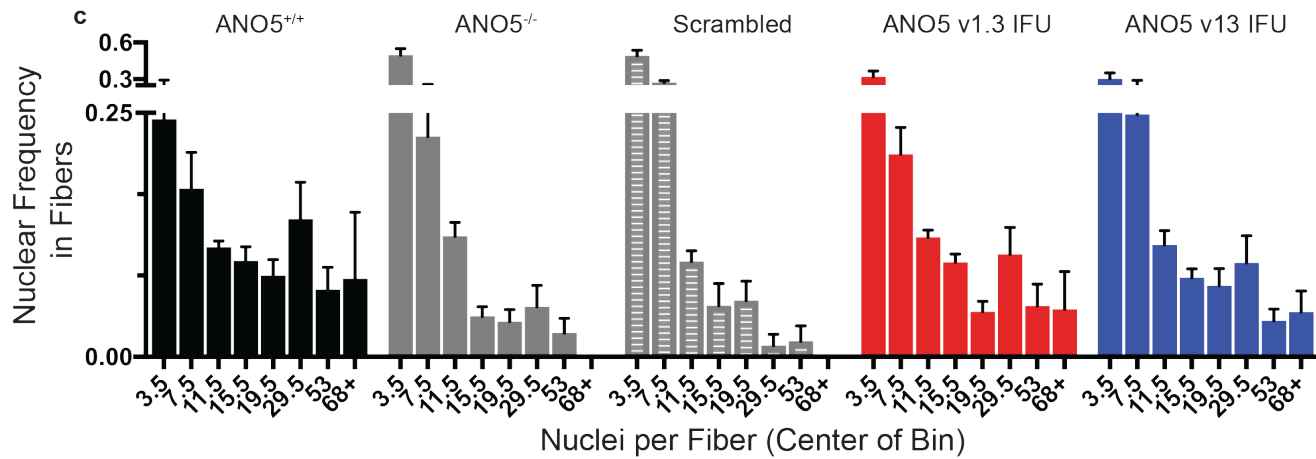
These Ca^{2+} stimulated currents were significantly larger at +140mV when compared to currents in *Ano5*$^{-/-}$ MPCs (P=0.027) (Fig. 7d). Similar to ANO5-dependent currents in wild-type MPCs, ANO5 rescued currents exhibited a linear current/voltage relationship (Fig. 7e).

Discussion

Here we demonstrate that ANO5 elicits Ca^{2+}-PLS, and that this ANO5 activity is associated with proper MPC fusion to produce myofibers. ANO5 expression in HEK cells elicits Ca^{2+}-PLS, supporting the hypothesis that ANO5 like ANO6 elicits Ca^{2+}-PLS [7, 106, 129]. This observation is bolstered by the ability of the mutations in the ANO5 scrambling domain to destroy its scrambling activity, while this same region confers Ca^{2+}-PLS to the CaCC ANO1. Moreover, MPCs isolated from mice lacking ANO5 exhibit a significant loss of Ca^{2+}-PLS.

A previous report suggested that transient transfection of cells with *Ano5* did not support phospholipid scrambling [129]. This previous investigation into ANO5's ability to confer Ca^{2+}-PLS may be confounded by the low ANO5 expression achieved or a consequence of the thymocyte model where ANO5 was evaluated [129]. Moreover, this previous investigation evaluated the Ca^{2+}-PLS competence of murine ANO5, where we evaluate a synthetic, codon optimized human ANO5 (see methods). In addition, this previous report did not evaluate the ability of ANO5 to traffic to the PM, where Ca^{2+}-PLS was evaluated. As has previously been described for other ANO scramblases (nhTMEM16, afTMEM16, and ANO6) [7, 66, 68, 106, 115], ANO5-dependent Ca^{2+}-PLS is associated with the simultaneous development of non-selective ionic currents that we believe are a consequence of membrane disturbances created by lipid translocation. The loss of ANO5-dependent Ca^{2+}-PLS and PLS-associated ionic currents is associated with a significant decrease in the ability of MPCs to fuse and produce myotubes with high nuclear multiplicity. These data provide additional insights into our previous observation

254

that the ability of muscle to regenerate *in vivo* in response to cardiotoxin injury is greatly

diminished in this *Ano5*$^{-/-}$ knockout model [202]. Although it is possible that ANO5 has

other functions within the cell, the fact that the loss of ANO5-dependent Ca^{2+}-PLS and

associated currents is correlated with diminished MPC fusion competence strongly

suggests that these functions of ANO5 contribute to the perturbed muscle repair and

ANO5 myopathy phenotype observed in our model. Although we have focused on the

role of ANO5 in MPC fusion, it is possible that ANO5 also facilitates muscle repair in

other ways. In particular, repair of isolated muscle fibers after laser damage, a process

that does not rely on progenitor cell fusion [489], is diminished in the *Ano5* knockout

mouse [202]. Nevertheless, our observations here, our previous characterization of a

LGMD2L-like phenotype in this model, and data from other investigators highlighting the

role of PtdSer exposure in MPC fusion [187, 190, 454, 539], support the conclusion that

the loss of ANO5-dependent Ca^{2+}-PLS likely contributes to the development and/or

progression of LGMD2L by perturbing MPC fusion regulation.

Are PLS-associated currents simply a consequence of PLS or are they biologically

significant?

In addition to numerous transcription factors, adhesion/migration proteins, signaling

proteins, and fusion machinery that are involved in the fusion of myoblasts to form

multinucleated muscle fibers [197, 548], PtdSer plays an integral role. Almost 20 years

ago, van den Eijnde and coworkers observed exposure of PtdSer on the outer leaflet of

the plasma membrane in differentiating muscle *in vivo* [539], and PtdSer's transient

exposure at sites of contact between fusing myoblasts [187]. Moreover, prolonged

exposure (5 days) to the PtdSer binding protein, annexin-V or PtdSer-antibody during

myoblast fusion significantly inhibits the formation of myotubes. Additionally, liposomes

of PtdSer, but not PtdCho, stimulate myoblast fusion [187, 188].

255

Recently, it has been reported that the PtdSer receptors BAI1 and STAB2 play roles in myoblast fusion [190, 454]. These data support the suggestion that PLS is a factor in MPC fusion, but because PLS is consistently associated with a simultaneous ionic current, we cannot assume that the ionic current plays no role in fusion. Nor can we exclude the possibility that ionic currents are necessary for proper PLS. Ionic currents could contribute to cell fusion in various ways. One very speculative idea involves the release of extracellular vesicles. ANO-dependent Ca^{2+}-PLS is associated with the release of extracellular vesicles (EVs) [101, 156, 174], and it has been suggested that extracellular vesicles play a role in muscle development and regeneration [549, 550]. ANO5-dependent currents could conceivably play a role in osmotic forces involved in the production of shed vesicles. Perhaps the non-selective ionic conductance associated with ANO5-PLS elicits changes in the osmotic pressure at the PM along with the PLS alterations in lipid packing simultaneously promoting vesiculation of the membrane.

Why is Ca-PLS defective in Ano5$^{-/-}$ MPCs despite ANO6 expression?

It has now been suggested that ANOs 3, 4, 5, 6, 7, and 9 are phospholipid scramblases [129]. This raises the question why this level of redundancy exists. Certainly, there is good evidence that different ANOs are expressed in a tissue-specific manner, but most tissues express multiple ANO scramblases [129]. ANO6 seems to be expressed ubiquitously, while ANOs 3-7 and 9 are more restricted in their distribution. Muscle expresses both ANO5 and ANO6 (in addition to ANO8 and ANO10), but surprisingly *Ano5$^{-/-}$* MPCs exhibit defective Ca^{2+}-PLS despite the presence of ANO6. These data suggest that despite their similar functions, ANO5 and ANO6 play different roles in primary muscle cells. Another possibility is that ANO5 is not itself a scramblase, but a scramblase regulator, possibly forming a complex with ANO6. Regardless, knockdown or rescue of *Ano5* does not seem to have major effects on *Ano6* expression or endogenous ANO6 steady state level. Thus, changes in Ca^{2+}-PLS do not stem from

altered levels of ANO6. Our mutagenesis shows that ANO5 is required to elicit Ca^{2+}-PLS and that this activity does not stem from exogenous ANO5 upregulating an endogenous scramblase like ANO6, but it does not exclude the possibility that ANO5 is part of a complex that includes ANO6. The differential role of ANO5 and ANO6 in MPCs and their fusion further highlights the merit of elucidating how the functions of ANO PLSases differ between homologs and how these differences regulate the function of biological membranes in cells.

It is important to note that two other laboratories have reported *Ano5* knockout mouse models that have no muscle phenotype [204, 536]. Recently, the Sui *et al.* has produced a rabbit *Ano5$^{-/-}$* model by disrupting *Ano5* later in the coding sequence, similar to our murine model, and this model exhibits dystrophic phenotypes similar to our murine model [551]. We are unable to determine why our mouse has a noticeable-yet mild-skeletal muscle phenotype, as described previously [202], and exhibits significantly perturbed myogenic fusion described here while other murine models do not. These discrepancies may be the result of genetic differences in the murine models, the different approaches to disrupt *Ano5*, or other outside factors. However, the ability of our *ANO5* lentivirus to rescue Ca^{2+}-PLS, PLS-associated ion currents, and fusion in *Ano5* knockout MPCs suggests that the defects we describe here result from the loss of ANO5.

Methods

Surface Biotinylation: Surface proteins were covalently biotinylated by 0.5mg/ml Sulfo-NHS-LC biotin (Pierce) for 40 mins on ice. The reaction was quenched with 20mM glycine for 30 min on ice. Protein lysates were collected in RIPA buffer (TEKNOVA) with protease inhibitors and 1/5th soluble protein lysate was reserved to evaluate "total" protein. The remaining lysate was incubated with streptavidin conjugated beads

overnight at 4 °C to capture biotinylated proteins. Total vs membrane protein pools were evaluated via western blot.

Western Blot: Steady state protein levels were evaluated via SDS-PAGE followed by immunoblot. Antibodies used were mouse anti-ANO5 clone 85.1 (1:250, UC-Davis Neuromab, Antibodies Inc.), mouse anti-FLAG (1:1,000, Sigma), anti-ANO6 (1:1,000, Invitorgen), and mouse anti-GAPDH (1:1,000, Millipore).

Cell Culture: T-REx™-293 cells (Invitrogen) were maintained in modified, high-glucose DMEM (supplemented with 10% FBS, 100 U/ml penicillin G and 100 μg/ml streptomycin). Primary mouse myoblasts were isolated as described previously [48] from 3-month-old Ano5$^{-/-}$ or age matched wild-type C57BL/6J mice. Myoblasts were maintained in growth media (Ham's F10 media (Invitrogen) supplemented with 20% FBS, 5 ng/ml basic FGF, 100 U/ml penicillin G and 100 μg/ml streptomycin) on bovine collagen coated plates (Gibco).

cDNA Constructs: mANO6 (Uniprot Q6P9J9) as tagged on the C-terminus with Clover and inserted into the pcDNA™5/TO plasmid (Invitrogen). A codon-optimized cDNA for hANO5 (Uniprot Q75V66) was synthesized by DNA2.0 (Newark, CA) and tagged on the C-terminus with Clover or 3XFLAG and inserted into the pcDNA™5/TO plasmid (Invitrogen). For designing chimeras, mANO1 and hANO5 cDNAs were aligned using MUSCLE (McWilliam et al., 2013). Chimeras were constructed using overlap extension PCR (Pont-Kingdon, 1997). Chimeras are named X-Y-X, where X is the ANO paralog template whose amino acids numbered are replaced with the aligned amino acids from ANO paralog Y. For ANO151 amino acids 554-588 of ANO1 were replaced with amino acids from ANO5, and for ANO515 amino acids 530-564 of ANO5 were replaced with amino acids from ANO1. PCR primers were designed to engineer complementary overlapping sequences onto the junction-forming ends of PCR products that were subsequently assembled by PCR. PCR-based mutagenesis was used to generate mutations in one or a few amino acids. The protein coding region of all chimeras and mutants

258

were sequenced. Plasmids were introduced into T-REx™-293 cells using Lipofectamine 2000, and stable incorporation was selected for in the cells using hygromycin B (Invitrogen) and blasticidin (Sigma) according to the manufacturer's protocol. Protein expression was induced by supplementing cell culture media with 2 μM tetracycline (Sigma) overnight.

PLS Assay: PLS was assessed in control HEK cells and cells expressing eGFP, Clover, and 3XFLAG tagged ANOS by live-cell imaging using the PtdSer binding proteins annexin-V-A568 or LactC2-mCherry and -Clover as described previously [106]. Briefly, cells were washed in nominally Ca^{2+}-free PLS solution (in mM: 140 NaCl, 5 KCl, 10 Tris-HCl pH 7.4, mOsm 360), treated for 5 min with PLS solution + 10μM A23187, then washed, and stimulated by the addition of Ca^{2+} (typically 5mM). A23187 in nominally zero-Ca^{2+} depletes ER stores and activates store operated Ca^{2+} entry that elevates cytosolic Ca^{2+} upon addition of extracellular Ca^{2+}. PLS and simultaneous patch-clamp recording was conducted by elevating intracellular $[Ca^{2+}]$ via the pipet solution as described previously [106].

MPC Fusion Assay: Primary MPCs were plated on ECL (Milipore) coated 12-well plates (Sigma) and allowed to adhere to the dish overnight in growth media. Cells were switched to differintiation media (DMEM, 1g/L glucose), supplemented with 1% horse serum (Gibco)) the following morning and cultured for ~36hrs. Cells were fixed (4% PFA) and stained with DAPI (Invitrogen) and Phalloidin (Invitrogen). Two collections of 3x3 images were taken of each well for each condition. Each collection of images was stitched together and evaluated for the number of fibers/nuclei represented.

Electrophysiology: Single cells expressing ANO5-Clover, ANO1-EGFP, or ANO6-EGFP were identified by fluorescence on a Zeiss Axiovert microscope and voltage-clamped using conventional whole-cell patch-clamp techniques with an EPC-7 amplifier (HEKA, Germany). Fire-polished borosilicate patch pipettes were 3-5 MΩ. Experiments were conducted at ambient temperature (24-26°C). Because liquid junction potentials

259

calculated using pClamp were predicted to be <2 mV, no correction was made. Solutions (in mM) were as follows. Zero intracellular Ca^{2+}: 146 CsCl, 2 $MgCl_2$, 5 EGTA, 10 sucrose, 10 HEPES pH 7.3 adjusted with NMDG. 20μM intracellular Ca^{2+}: 146 CsCl, 2 $MgCl_2$, 5 Ca^{2+}-EGTA, 10 sucrose, 10 HEPES pH 7.3 adjusted with NMDG. 0.2mM intracellular Ca^{2+}: 0.2 $CaCl_2$ was added to the 20μM Ca^{2+}solution. Standard extracellular solution: 140 NaCl, 5 KCl, 2 $CaCl_2$,1 $MgCl_2$, 15 glucose, 10 HEPES pH 7.4. For determining ionic selectivity, 140 mM NaCl in the standard extracellular solution was replaced with the indicated concentrations of NaCl, CsCl, or NMDG-Cl as indicated and the internal solution contained 150 NaCl (or CsCl), 1$MgCl_2$, 5 Ca-EGTA, 0.2 $CaCl_2$, 1-HEPES pH 7.4. The osmolarity of each solution was adjusted to 300 mOsm by addition of mannitol. Relative permeabilities of cations relative to Cl^- were determined by measuring the changes in zero-current E_{rev} using the Goldman-Hodgkin-Katz equation when the concentration of extracellular ions were changed ('dilution potential' method) as previously described (Yu et al 2012).

$$\Delta E_{rev} = 25.7\ln [(X_0 + Cl_i * P_{Cl}/P_{Na}) / (X_i + Cl_0 * P_{Cl}/P_{Na})]$$

Where X is the cation and ΔE_{rev} is the difference between E_{rev} with the test solution XCl and that observed with symmetrical solutions.

MPCs were evaluated in the same manner as HEK cells with an intracellular solution: 146 CsCl, 2 $MgCl_2$, 5 Ca^{2+}-EGTA, 10 sucrose, 10 HEPES and 0.2mM $CaCl_2$ and an extracellular solution: 140 NaCl, 5 KCl, 2 $CaCl_2$,1 $MgCl_2$, 15 glucose, 10 HEPES pH 7.4.

Imaging: PLS was measured in populations of intact HEK293 cells grown on glass coverslips mounted in Attofluor chambers (Invitrogen, CA) and imaged at ambient temperature with a Zeiss confocal microscope using a 63× Plan-Aprochromat NA 1.4 objective. Binding of annexin-V-Alexa-568 to patch-clamped cells during voltage-clamp recording was imaged with a wide-field Zeiss Axiovert 100 microscope using a 40× NA

0.6 LD-Acroplan objective. Images were acquired with an Orca-FLASH 4.0 digital CMOS camera (C11440, Hamamatsu, Japan) controlled by Metamorph 7.8 software (Molecular Devices, CA). Images were analyzed using Fiji Image-J 1.49.

RNA Expression Analysis: To characterize the ANO5 KO mouse in more detail, RT-PCR was performed with RNA isolated from leg muscle of wild type and ANO5$^{-/-}$ mice. RT-PCR was performed using primer pairs designed by NCBI Primer-BLAST using accession number NM_177694 with at least one primer that spanned an exon-exon boundary. 0.125 µg RNA in 12.5µl Superscript-III one-step RT-PCR with Platinum Taq for 35 cycles at 55° C annealing temperature.

Primers and expected product size (in parenthesis) were:

Exon1/2F:AGCAGGAAGGCTTAACAGCCA, Exon4R:AGACGCCTCCTCAGGAACAAA (145)

Exon5/6F:GCTGAAGGCAGAAAGAAGACGAG,

Exon7R:ACAGGGGTGGGTACTTTGGC (215)

Exon8/9F:TCCATGATGGCCAGTATTGGAAAC,

Exon10R:CAGAGCCGCAAACAACAGCA (200)

Exon9F:GGAGCAACCTTTTCATTTGATTCGG,

Exon11/12R:GGGAGAACTTTGAATGCAAACACG (272)

Exon12F:TGCGCTCTTCATGGGGATCT,

Exon14/15R:GGAGAGCCATCCCAAAGGTCA (260)

Exon14/15F:ACAGTGACCTTTGGGATGGCT,

Exon16R:AGGCTGCTCTCATACTCCTGG (275)

Exon16/17F:AGCGAAGAGTGTGGTCCTGC, Exon19R:CAAACAGGGGTGCCAGAGGA (298)

Exon19/20F:ATCGTTTCTGTTGCAACTAATGCCT,

Exon21R:TGGCAGCAAGAACATGCCAG (280)

261

For real-time PCR, total RNA was collected from MPCs using PureLink RNA kit following manufactures instruction (Invitrogen). All RNA sample were treated with DNAse I (Invitrogen) according to manufactures protocol to ensure purity. cDNA was generated from total RNA via reverse transcriptase reaction using SuperScript III reverse transcriptase (Invitrogen) and random hexamer primers. cDNA was then amplified using the SYBR Select Master Mix reagent (Applied Biosystems) and 2.5μM of each primer. Real-Time PCR reactions were preformed and analyzed with StepOnePlus Real Time PCR System (Applied Biosystems), using GAPDH as an internal control. Fold change of gene expression was determined using the $\Delta\Delta$Ct method [552]. Multiple independent experiments were performed and analyzed in duplicate. qPCR primers were:

synANO5: Fwd: CATGGAGCACAACACCTCCT, Rvs: TTGAGTTCAGCCGCCAGTAG

mAno6: Fwd: CTTATCAGGAAGTATTACGGC, Rvs: AGATATCCATAGAGGAAGCAG

mGapdh: Fwd: GGGTCCCAGCTTAGGTTCAT, RVS: TACGGCCAAATCCGTTCACA

Lentivirus: Synthetic hANO5 was subcloned into a modified version of the lentiviral transfer plasmid LJM1 (Addgene #19319)[553] under control of the PGK promoter and flanked by a viral 2A site and eGFP to mark infected cells. The PAX2 (Addgene # 12260) packaging plasmid and pMD2.G envelope plasmid (Addgene #12259) were co-transfected into HEK293T cells using Lipofectamine 3000 (Invitrogen, manufacturer's protocol) along with *ANO5* transfer plasmid or Scrambled transfer plasmid (Addgene #1864) [554], and viral supernatants were collected at 24, 48, and 72 hours post transfection. Viral supernatants were filtered (0.45 μm) and lentiviral particles were concentrated using ultracentrifugation. Viral concentrations were estimated by ELISA for p24 to control for consistent infections between experiments and to calculate infectious units (IFUs) (Takara Bio #632200). MPCs were infected at low passage overnight in the presence of 8μg/ml polybrene in growth media using indicated IFUs.

262

Acknowledgements:

Chapter VIII

Conclusion

Overview

The first observation of Ca^{2+}-PLS was first reported by Bevers *et al.* >35 years ago, but decades passed in the pursuit of the elusive PLSase without success. In 2010 an elegant expression cloning approach highlighted the ANO protein family for the role of some family members in regulating the Ca^{2+}-PLS, however the precise function of the original ANO PLSase, ANO6, was controversial to say the least (reviewed in chapters I, II, and IV). Prior to my own work investigating the role of ANOs in Ca^{2+}-PLS and the physiological consequences of this activity, several additional ANOs were highlighted for their potential roles in Ca^{2+}-PLS. However, others had claimed that ANO proteins did not elicit Ca^{2+}-PLS themselves but were cation channels regulating Ca^{2+}-PLS upstream of some PLSase that remained to be identified. The work presented herein supports a direct role for some ANOs as Ca^{2+}-PLSases, investigates the ANO structure and function that facilitates this activity, and demonstrates a novel physiological role for ANO Ca^{2+}-PLS in regulating skeletal muscle repair. The primary findings include:

5. ANO5 and ANO6 elicit Ca^{2+}-PLS, while the CaCC ANO1 does not.

6. ANO5 and ANO6 possess a discrete domain necessary and sufficient for Ca^{2+}-PLS in ANO proteins.

7. ANO5 and ANO6 Ca^{2+}-PLS is associated with non-selective ionic conductance that is likely a consequence of lipid movement during PLS.

8. ANO5 is responsible for coordinating Ca^{2+}-PLS in MPCs essential for proper skeletal muscle repair.

In this closing chapter I will briefly discuss the significance of these findings, discuss important ventures in future investigation of ANO PLSases, and will speculate on the physiological processes potentially associated with Ca^{2+}-PLS.

Summary and Significance

ANO6 in Ca^{2+}-PLS and the identification of the ANO SCRD.

In chapter IV my co-authors and I demonstrated the ability of ANO6 to confer Ca^{2+}-PLS

to cells, identified a domain both necessary and sufficient for ANO Ca^{2+}-PLS, and

concluded that the hotly debated ionic conductance associated with ANO6 was likely a

consequence of Ca^{2+}-PLS, was non-selective among ions, proved inseparable from

ANO6 Ca^{2+}-PLS, and activated concurrently with ANO6-dependent Ca^{2+}-PLS. Closely

preceding this work, two fungal ANO homologs were demonstrated to be Ca^{2+}-PLSases

in reconstitution experiments (reviewed in chapters I and II). Our demonstration that

ANO6 itself conferred Ca^{2+}-PLS, was not an ion channel regulating this activity, and did

not simply upregulate an unidentified PLSase settled the controversy of whether ANO6

was a bona fide ion channel that regulated Ca^{2+}-PLS or elicited Ca^{2+}-PLS itself. This

work strongly supported the recognition of ANO6 as the first identified Ca^{2+}-PLSase.

Moreover, recent work has demonstrated that the majority of mammalian ANOs-

including ANO3, ANO4, ANO5, ANO7, and ANO9-possess a region similar to the SCRD

of ANO6 that can confer Ca^{2+}-PLS to the CaCC ANO1, demonstrating that this region

we identified in ANO6 is a general feature of mammalian ANO PLSases [555].

Realizing the role of ANO5 in skeletal muscle repair and fusion.

In Chapter VI I contributed to the characterization of an ANO5 knockout mouse model

that partially recapitulates hallmarks of human LGMD2L and discovered perturbations in

the fusion competence of MPCs isolated from these mice. Prior to this work little

concerning the mechanism of LGMD2L was known. LGMD2L was first linked to

mutations in ANO5 in 2010 (discussed in chapters V, VI, and VII), but previous work

consisted almost exclusively of clinical reports describing patient phenotypes. Little work

investigating the physiological function of ANO5 existed, and no functional investigation

had been performed in skeletal muscle cells. This study produced the first murine model

of this disease and demonstrated that the phenotypes associated with a loss of ANO5

were associated with significantly perturbed muscle repair processes. There I characterized an antibody we employed as a tool to evaluated steady state ANO5 protein levels and characterized a MPC fusion defect in cells from these animals resulting from the loss of ANO5. As discussed in chapter V, MPC fusion is partially regulated by PS exposure on the surface of MPCs, and this initial characterization served as the foundation for my continued investigation into the role of ANO5 in skeletal muscle function.

ANO5-dependent Ca^{2+}-PLS in coordinating skeletal muscle fusion.

In chapter VII, my co-authors and I demonstrated that ANO5 confers Ca^{2+}-PLS, investigated the non-selective ionic conductance associated with ANO5 Ca^{2+}-PLS, and found that the loss of ANO5 in MPCs we previously showed resulted in altered MPC fusion was also associated with a loss of MPC Ca^{2+}-PLS competence. Moreover, I demonstrated human ANO5 was sufficient to rescue Ca^{2+}-PLS, PLS-associated ionic conductance, and MPC fusion coordination. Interestingly, upon closer investigation we found that ANO5 Ca^{2+}-PLS was not essential for MPC fusion itself, but the coordination of MPC fusion to produce large myofibers containing of many myonuclei. As a result, loss of ANO5 precluded the production of large myofibers with many nuclei and instead resulted in the production of many smaller myofibers with fewer nuclei. Based on these findings we concluded that loss of ANO5-dependent Ca^{2+}-PLS perturbs MPC fusion coordination and likely contributes to the development of LGMD2L, as coordinated MPC fusion is essential for the maintenance of skeletal muscle. These descriptions, along with a paper published during the preparation of our manuscript, represent the first characterization of ANO5 function in cells, ours the first in physiologically relevant, primary muscle cells.

A Look Forward

My work on ANO Ca^{2+}-PLS and the physiological functions of this activity has led to the development of a series of hypotheses that I believe merit future investigation. Some of these hypotheses are supported by current investigation into the topic while others are highly speculative in nature. In the next section I will briefly outline these hypotheses and discuss their links to current knowledge of Ca^{2+}-PLS.

EVs as long range signals of Ca^{2+}-PLS

Discussions in chapter II highlight the role of Ca^{2+}-PLS in the production of EVs and recent presentation of unpublished data links ANO6 to the production of chemically induced giant membrane vesicles shed from the PM (Jan laboratory 2018). Because of the discussion of this topic in chapter II, I will not labor the point here on the association of Ca^{2+}-PLS with EV production. However, I hypothesize that the release of EVs during Ca^{2+}-PLS function as physiologically relevant, long distances messengers that coordinate the function of Ca^{2+}-PLS in physiological systems. In the future, investigation into the contents of EVs release during Ca^{2+}-PLS, their uptake into neighboring cells, and how EVs released during scrambling effect neighboring cells may shed light on the biological significance of these messengers. In our previous HEK experiments we noticed that while cells with high ANO5 or 6 expression began robust PS exposure when stimulated with Ca^{2+}, often neighboring cells that did not exhibit obvious exogenous ANO expression within a close radius of the PLS cells would begin exposing PS on their own membranes as well. With this in mind, it would be interesting to evaluate whether EVs collected from Ca^{2+}-PLS cells might stimulate uninduced cells to activate Ca^{2+}-PLS. EV activation of Ca^{2+}-PLS may be a method cells use to propagate this membrane signal through tissues.

The role of PS exposure during skeletal muscle fusion

As covered extensively in chapter V, PS exposure has been associated with promoting skeletal muscle precursor fusion for decades, however, while loss of the currently

recognized machinery associated with PS recognition and exposure in skeletal muscle perturbs regenerative skeletal muscle fusion, it has little to no effect on the development of skeletal muscle tissue. Loss of *Ano5* does not appear to effect skeletal muscle development during embryogenesis, either in humans or in our mouse model [202]. How the loss of *Ano5* perturbs MPC fusion during regeneration but has no effect on muscle fiber development remains an open question. Although PtdSer exposure regulates MPC fusion, the importance and molecular machinery associated with PtdSer exposure during embryonic development compared to post-natal growth and regeneration is ill-defined. Recently two different PtdSer-receptors have been recognized for their roles in MPC fusion, BAI1 and STAB2 [190, 454]. Although the progression of myogenesis seems to be highly conserved in embryonic development vs post-natal growth and repair/regeneration (discussed extensively in chapter V), the fusion machinery operating during development and during regeneration or its regulation must be quite different. Muscle fibers develop in both *Bai1*^{-/-} and *Stab2*^{-/-} murine models, however like *Ano5*^{-/-}, both models exhibit significant deficits in muscle recovery following injury and in MPC fusion [190, 454]. I hypothesize that the machinery that elicits and recognizes PS exposure is different in embryonic development vs postnatal development and muscle regeneration. Further understanding of the differences in the regulation of muscle fusion during and after embryonic development is essential in understanding LGMD2L and other diseases of muscle repair. In particular, a more thorough investigation of the role of PS exposure and recognition and the machinery regulating this process during embryonic development vs regeneration is essential for creating a full understanding of the regulation of skeletal muscle fusion.

References

1. Tsutsumi, S., et al., *The novel gene encoding a putative transmembrane protein is mutated in gnathodiaphyseal dysplasia (GDD).* Am J Hum Genet, 2004. **74**(6): p. 1255-61.
2. Feenstra, B., et al., *Common variants associated with general and MMR vaccine-related febrile seizures.* Nat Genet, 2014. **46**(12): p. 1274-82.
3. Balreira, A., et al., *ANO10 mutations cause ataxia and coenzyme Q(1)(0) deficiency.* J Neurol, 2014. **261**(11): p. 2192-8.
4. Liu, F., et al., *TMEM16A overexpression contributes to tumor invasion and poor prognosis of human gastric cancer through TGF-beta signaling.* Oncotarget, 2015. **6**(13): p. 11585-99.
5. Jun, I., et al., *ANO9/TMEM16J promotes tumourigenesis via EGFR and is a novel therapeutic target for pancreatic cancer.* Br J Cancer, 2017. **117**(12): p. 1798-1809.
6. Chang, Z., et al., *Anoctamin5 regulates cell migration and invasion in thyroid cancer.* Int J Oncol, 2017. **51**(4): p. 1311-1319.
7. Suzuki, J., et al., *Calcium-dependent phospholipid scrambling by TMEM16F.* Nature, 2010. **468**(7325): p. 834-8.
8. Bolduc, V., et al., *Recessive mutations in the putative calcium-activated chloride channel Anoctamin 5 cause proximal LGMD2L and distal MMD3 muscular dystrophies.* Am J Hum Genet, 2010. **86**(2): p. 213-21.
9. Whitlock, J.M. and H.C. Hartzell, *Anoctamins/TMEM16 Proteins: Chloride Channels Flirting with Lipids and Extracellular Vesicles.* Annu Rev Physiol, 2017. **79**: p. 119-143.
10. Huang, X., et al., *High-resolution mapping of the 11q13 amplicon and identification of a gene, TAOS1, that is amplified and overexpressed in oral cancer cells.* Proc Natl Acad Sci U S A, 2002. **99**(17): p. 11369-74.
11. Katoh, M. and M. Katoh, *FLJ10261 gene, located within the CCND1-EMS1 locus on human chromosome 11q13, encodes the eight-transmembrane protein homologous to C12orf3, C11orf25 and FLJ34272 gene products.* Int J Oncol, 2003. **22**(6): p. 1375-81.
12. West, R.B., et al., *The novel marker, DOG1, is expressed ubiquitously in gastrointestinal stromal tumors irrespective of KIT or PDGFRA mutation status.* Am J Pathol, 2004. **165**(1): p. 107-13.
13. Huang, X., et al., *Comprehensive genome and transcriptome analysis of the 11q13 amplicon in human oral cancer and synteny to the 7F5 amplicon in murine oral carcinoma.* Genes Chromosomes Cancer, 2006. **45**(11): p. 1058-69.
14. Carles, A., et al., *Head and neck squamous cell carcinoma transcriptome analysis by comprehensive validated differential display.* Oncogene, 2006. **25**(12): p. 1821-31.
15. Bae, J.S., et al., *Expression of ANO1/DOG1 is associated with shorter survival and progression of breast carcinomas.* Oncotarget, 2018. **9**(1): p. 607-621.

16. Vallejo-Benitez, A., et al., *Expression of dog1 in low-grade fibromyxoid sarcoma: A study of 19 cases and review of the literature.* Ann Diagn Pathol, 2017. **30**: p. 8-11.

17. Said-Al-Naief, N., et al., *Combined DOG1 and Mammaglobin Immunohistochemistry Is Comparable to ETV6-breakapart Analysis for Differentiating Between Papillary Cystic Variants of Acinic Cell Carcinoma and Mammary Analogue Secretory Carcinoma.* Int J Surg Pathol, 2017. **25**(2): p. 127-140.

18. Ng, W., et al., *DOG1 Expression in Soft Tissue Tumors.* Int J Surg Pathol, 2016. **24**(3): p. 274-6.

19. Friedrich, R.E., et al., *Expression of DOG1 (Using SP31) in Poorly Differentiated Carcinoma of the Head and Neck.* Anticancer Res, 2016. **36**(6): p. 3117-22.

20. Creytens, D. and J. Van Dorpe, *DOG1 expression in phosphaturic mesenchymal tumour.* J Clin Pathol, 2016.

21. Cleven, A.H., et al., *DOG1 expression in giant-cell-containing bone tumours.* Histopathology, 2016. **68**(6): p. 942-5.

22. Abd Raboh, N.M. and S.A. Hakim, *Diagnostic role of DOG1 and p63 immunohistochemistry in salivary gland carcinomas.* Int J Clin Exp Pathol, 2015. **8**(8): p. 9214-22.

23. Sah, S.P. and W.G. McCluggage, *DOG1 immunoreactivity in uterine leiomyosarcomas.* J Clin Pathol, 2013. **66**(1): p. 40-3.

24. Akpalo, H., C. Lange, and J. Zustin, *Discovered on gastrointestinal stromal tumour 1 (DOG1): a useful immunohistochemical marker for diagnosing chondroblastoma.* Histopathology, 2012. **60**(7): p. 1099-106.

25. Liegl, B., et al., *Monoclonal antibody DOG1.1 shows higher sensitivity than KIT in the diagnosis of gastrointestinal stromal tumors, including unusual subtypes.* Am J Surg Pathol, 2009. **33**(3): p. 437-46.

26. Espinosa, I., et al., *A novel monoclonal antibody against DOG1 is a sensitive and specific marker for gastrointestinal stromal tumors.* Am J Surg Pathol, 2008. **32**(2): p. 210-8.

27. Wu, H., et al., *Cell-specific regulation of proliferation by Ano1/TMEM16A in breast cancer with different ER, PR, and HER2 status.* Oncotarget, 2017. **8**(49): p. 84996-85013.

28. Guan, L., et al., *Inhibition of calcium-activated chloride channel ANO1 suppresses proliferation and induces apoptosis of epithelium originated cancer cells.* Oncotarget, 2016. **7**(48): p. 78619-78630.

29. Mazzone, A., et al., *Inhibition of cell proliferation by a selective inhibitor of the Ca(2+)-activated Cl(-) channel, Ano1.* Biochem Biophys Res Commun, 2012. **427**(2): p. 248-53.

30. Stanich, J.E., et al., *Ano1 as a regulator of proliferation.* Am J Physiol Gastrointest Liver Physiol, 2011. **301**(6): p. G1044-51.

31. Britschgi, A., et al., *Calcium-activated chloride channel ANO1 promotes breast cancer progression by activating EGFR and CAMK signaling.* Proc Natl Acad Sci U S A, 2013. **110**(11): p. E1026-34.

32.	Liu, W., et al., *Inhibition of Ca(2+)-activated Cl(-) channel ANO1/TMEM16A expression suppresses tumor growth and invasiveness in human prostate carcinoma.* Cancer Lett, 2012. **326**(1): p. 41-51.

33.	Jia, L., et al., *Inhibition of Calcium-Activated Chloride Channel ANO1/TMEM16A Suppresses Tumor Growth and Invasion in Human Lung Cancer.* PLoS One, 2015. **10**(8): p. e0136584.

34.	Duvvuri, U., et al., *TMEM16A induces MAPK and contributes directly to tumorigenesis and cancer progression.* Cancer Res, 2012. **72**(13): p. 3270-81.

35.	Ayoub, C., et al., *ANO1 amplification and expression in HNSCC with a high propensity for future distant metastasis and its functions in HNSCC cell lines.* Br J Cancer, 2010. **103**(5): p. 715-26.

36.	Riss, T.L., et al., *Cell Viability Assays*, in *Assay Guidance Manual*, G.S. Sittampalam, et al., Editors. 2004: Bethesda (MD).

37.	Qu, Z., et al., *The Ca(2+) -activated Cl(-) channel, ANO1 (TMEM16A), is a double-edged sword in cell proliferation and tumorigenesis.* Cancer Med, 2014. **3**(3): p. 453-61.

38.	Rock, J.R., et al., *Identification of genes expressed in the mouse limb using a novel ZPA microarray approach.* Gene Expr Patterns, 2007. **8**(1): p. 19-26.

39.	Rock, J.R., et al., *Transmembrane protein 16A (TMEM16A) is a Ca2+-regulated Cl-secretory channel in mouse airways.* J Biol Chem, 2009. **284**(22): p. 14875-80.

40.	Rock, J.R. and B.D. Harfe, *Expression of TMEM16 paralogs during murine embryogenesis.* Dev Dyn, 2008. **237**(9): p. 2566-74.

41.	Rock, J.R., C.R. Futtner, and B.D. Harfe, *The transmembrane protein TMEM16A is required for normal development of the murine trachea.* Dev Biol, 2008. **321**(1): p. 141-9.

42.	Gritli-Linde, A., et al., *Expression patterns of the Tmem16 gene family during cephalic development in the mouse.* Gene Expr Patterns, 2009. **9**(3): p. 178-91.

43.	He, M., et al., *Cytoplasmic Cl(-) couples membrane remodeling to epithelial morphogenesis.* Proc Natl Acad Sci U S A, 2017. **114**(52): p. E11161-E11169.

44.	Ruppersburg, C.C. and H.C. Hartzell, *The Ca2+-activated Cl- channel ANO1/TMEM16A regulates primary ciliogenesis.* Mol Biol Cell, 2014. **25**(11): p. 1793-807.

45.	Gerdes, J.M., E.E. Davis, and N. Katsanis, *The vertebrate primary cilium in development, homeostasis, and disease.* Cell, 2009. **137**(1): p. 32-45.

46.	Ousingsawat, J., et al., *Anoctamin-6 controls bone mineralization by activating the calcium transporter NCX1.* J Biol Chem, 2015. **290**(10): p. 6270-80.

47.	Gyobu, S., et al., *A Role of TMEM16E Carrying a Scrambling Domain in Sperm Motility.* Mol Cell Biol, 2016. **36**(4): p. 645-59.

48.	Griffin, D.A., et al., *Defective membrane fusion and repair in Anoctamin5-deficient muscular dystrophy.* Hum Mol Genet, 2016.

49.	Caputo, A., et al., *TMEM16A, a membrane protein associated with calcium-dependent chloride channel activity.* Science, 2008. **322**(5901): p. 590-4.

50.	Schroeder, B.C., et al., *Expression cloning of TMEM16A as a calcium-activated chloride channel subunit.* Cell, 2008. **134**(6): p. 1019-29.

51.   Yang, Y.D., et al., *TMEM16A confers receptor-activated calcium-dependent chloride conductance.* Nature, 2008. **455**(7217): p. 1210-5.

52.   Hartzell, C., I. Putzier, and J. Arreola, *Calcium-activated chloride channels.* Annu Rev Physiol, 2005. **67**: p. 719-58.

53.   Bader, C.R., D. Bertrand, and E.A. Schwartz, *Voltage-activated and calcium-activated currents studied in solitary rod inner segments from the salamander retina.* J Physiol, 1982. **331**: p. 253-84.

54.   Barish, M.E., *A transient calcium-dependent chloride current in the immature Xenopus oocyte.* J Physiol, 1983. **342**: p. 309-25.

55.   Miledi, R., *A calcium-dependent transient outward current in Xenopus laevis oocytes.* Proc R Soc Lond B Biol Sci, 1982. **215**(1201): p. 491-7.

56.   Galietta, L.J., et al., *IL-4 is a potent modulator of ion transport in the human bronchial epithelium in vitro.* J Immunol, 2002. **168**(2): p. 839-45.

57.   Humphrey, R.R., G.M. Malacinski, and H.M. Chung, *Developmental studies on an apparent cell-lethal mutant gene-ut-in the Mexican axolotl, Ambystoma mexicanum.* Cell Differ, 1978. **7**(1-2): p. 47-59.

58.   Hartzell, H.C., et al., *Anoctamin/TMEM16 family members are Ca2+-activated Cl-channels.* J Physiol, 2009. **587**(Pt 10): p. 2127-39.

59.   Schwappach, B., *An overview of trafficking and assembly of neurotransmitter receptors and ion channels (Review).* Mol Membr Biol, 2008. **25**(4): p. 270-8.

60.   Sheridan, J.T., et al., *Characterization of the oligomeric structure of the Ca(2+)-activated Cl- channel Ano1/TMEM16A.* J Biol Chem, 2011. **286**(2): p. 1381-8.

61.   Fallah, G., et al., *TMEM16A(a)/anoctamin-1 shares a homodimeric architecture with CLC chloride channels.* Mol Cell Proteomics, 2011. **10**(2): p. M110 004697.

62.   Peckys, D.B., et al., *The stoichiometry of the TMEM16A ion channel determined in intact plasma membranes of COS-7 cells using liquid-phase electron microscopy.* J Struct Biol, 2017. **199**(2): p. 102-113.

63.   Lim, N.K., A.K. Lam, and R. Dutzler, *Independent activation of ion conduction pores in the double-barreled calcium-activated chloride channel TMEM16A.* J Gen Physiol, 2016. **148**(5): p. 375-392.

64.   Jeng, G., et al., *Independent activation of distinct pores in dimeric TMEM16A channels.* J Gen Physiol, 2016. **148**(5): p. 393-404.

65.   Franz, A., K. Maass, and M. Seedorf, *A complex peptide-sorting signal, but no mRNA signal, is required for the Sec-independent transport of Ist2 from the yeast ER to the plasma membrane.* FEBS Lett, 2007. **581**(3): p. 401-5.

66.   Malvezzi, M., et al., *Ca2+-dependent phospholipid scrambling by a reconstituted TMEM16 ion channel.* Nat Commun, 2013. **4**: p. 2367.

67.   Suzuki, T., J. Suzuki, and S. Nagata, *Functional swapping between transmembrane proteins TMEM16A and TMEM16F.* J Biol Chem, 2014. **289**(11): p. 7438-47.

68.   Brunner, J.D., et al., *X-ray structure of a calcium-activated TMEM16 lipid scramblase.* Nature, 2014. **516**(7530): p. 207-12.

69.	Tien, J., et al., *Identification of a dimerization domain in the TMEM16A calcium-activated chloride channel (CaCC).* Proc Natl Acad Sci U S A, 2013. **110**(16): p. 6352-7.

70.	Paulino, C., et al., *Structural basis for anion conduction in the calcium-activated chloride channel TMEM16A.* Elife, 2017. **6**.

71.	Paulino, C., et al., *Activation mechanism of the calcium-activated chloride channel TMEM16A revealed by cryo-EM.* Nature, 2017. **552**(7685): p. 421-425.

72.	Dang, S., et al., *Cryo-EM structures of the TMEM16A calcium-activated chloride channel.* Nature, 2017. **552**(7685): p. 426-429.

73.	Flores, C.A., et al., *TMEM16 proteins: the long awaited calcium-activated chloride channels?* Braz J Med Biol Res, 2009. **42**(11): p. 993-1001.

74.	Galietta, L.J., *The TMEM16 protein family: a new class of chloride channels?* Biophys J, 2009. **97**(12): p. 3047-53.

75.	Schreiber, R., et al., *Expression and function of epithelial anoctamins.* J Biol Chem, 2010. **285**(10): p. 7838-45.

76.	Duran, C., et al., *ANOs 3-7 in the anoctamin/Tmem16 Cl- channel family are intracellular proteins.* Am J Physiol Cell Physiol, 2012. **302**(3): p. C482-93.

77.	Huang, F., et al., *TMEM16C facilitates Na(+)-activated K+ currents in rat sensory neurons and regulates pain processing.* Nat Neurosci, 2013. **16**(9): p. 1284-90.

78.	Wolf, W., et al., *Yeast Ist2 recruits the endoplasmic reticulum to the plasma membrane and creates a ribosome-free membrane microcompartment.* PLoS One, 2012. **7**(7): p. e39703.

79.	Manford, A.G., et al., *ER-to-plasma membrane tethering proteins regulate cell signaling and ER morphology.* Dev Cell, 2012. **23**(6): p. 1129-40.

80.	Whitlock, J.H., HC, *Anoctamins/TMEM16 proteins: Chloride channels flirting with lipids and extracellular vesicles.* Annu Rev Physiol, 2017. **79**.

81.	Wong, X.M., et al., *Subdued, a TMEM16 family Ca(2)(+)-activated Cl(-)channel in Drosophila melanogaster with an unexpected role in host defense.* Elife, 2013. **2**: p. e00862.

82.	Edidin, M., *Lipids on the frontier: a century of cell-membrane bilayers.* Nat Rev Mol Cell Biol, 2003. **4**(5): p. 414-8.

83.	Gorter, E. and F. Grendel, *On Bimolecular Layers of Lipoids on the Chromocytes of the Blood.* J Exp Med, 1925. **41**(4): p. 439-43.

84.	Bretscher, M.S., *Asymmetrical lipid bilayer structure for biological membranes.* Nat New Biol, 1972. **236**(61): p. 11-2.

85.	Singer, S.J. and G.L. Nicolson, *The fluid mosaic model of the structure of cell membranes.* Science, 1972. **175**(4023): p. 720-31.

86.	Finkelstein, A., *Water and nonelectrolyte permeability of lipid bilayer membranes.* J Gen Physiol, 1976. **68**(2): p. 127-35.

87.	Andersen, O.S. and R.E. Koeppe, 2nd, *Bilayer thickness and membrane protein function: an energetic perspective.* Annu Rev Biophys Biomol Struct, 2007. **36**: p. 107-30.

88.	van Meer, G., D.R. Voelker, and G.W. Feigenson, *Membrane lipids: where they are and how they behave.* Nat Rev Mol Cell Biol, 2008. **9**(2): p. 112-24.

89.   Marx, U., et al., *Rapid flip-flop of phospholipids in endoplasmic reticulum membranes studied by a stopped-flow approach.* Biophys J, 2000. **78**(5): p. 2628-40.

90.   Devaux, P.F., P. Fellmann, and P. Herve, *Investigation on lipid asymmetry using lipid probes: Comparison between spin-labeled lipids and fluorescent lipids.* Chem Phys Lipids, 2002. **116**(1-2): p. 115-34.

91.   Daleke, D.L., *Regulation of transbilayer plasma membrane phospholipid asymmetry.* J Lipid Res, 2003. **44**(2): p. 233-42.

92.   Williamson, P., et al., *Phospholipid scramblase activation pathways in lymphocytes.* Biochemistry, 2001. **40**(27): p. 8065-72.

93.   Suzuki, J., et al., *Xk-related protein 8 and CED-8 promote phosphatidylserine exposure in apoptotic cells.* Science, 2013. **341**(6144): p. 403-6.

94.   Fadok, V.A., et al., *Loss of phospholipid asymmetry and surface exposure of phosphatidylserine is required for phagocytosis of apoptotic cells by macrophages and fibroblasts.* J Biol Chem, 2001. **276**(2): p. 1071-7.

95.   Bevers, E.M. and P.L. Williamson, *Getting to the Outer Leaflet: Physiology of Phosphatidylserine Exposure at the Plasma Membrane.* Physiol Rev, 2016. **96**(2): p. 605-45.

96.   Luo, K.Q., et al., *Application of the fluorescence resonance energy transfer method for studying the dynamics of caspase-3 activation during UV-induced apoptosis in living HeLa cells.* Biochem Biophys Res Commun, 2001. **283**(5): p. 1054-60.

97.   Goldstein, J.C., et al., *Cytochrome c is released in a single step during apoptosis.* Cell Death Differ, 2005. **12**(5): p. 453-62.

98.   Dudgeon C., Q.W., Sun Q., Zhang L., Yu J., *Transcriptional Regulation of Apoptosis. In: Dong Z., Yin XM. (eds) Essentials of Apoptosis.* Humana Press, Totowa, NJ, 2009.

99.   Weiss, H.J., *Scott syndrome: a disorder of platelet coagulant activity.* Semin Hematol, 1994. **31**(4): p. 312-9.

100.   Yang, H., et al., *TMEM16F forms a Ca2+-activated cation channel required for lipid scrambling in platelets during blood coagulation.* Cell, 2012. **151**(1): p. 111-22.

101.   Fujii, T., et al., *TMEM16F is required for phosphatidylserine exposure and microparticle release in activated mouse platelets.* Proc Natl Acad Sci U S A, 2015. **112**(41): p. 12800-5.

102.   Castoldi, E., et al., *Compound heterozygosity for 2 novel TMEM16F mutations in a patient with Scott syndrome.* Blood, 2011. **117**(16): p. 4399-400.

103.   Brooks, M.B., et al., *A TMEM16F point mutation causes an absence of canine platelet TMEM16F and ineffective activation and death-induced phospholipid scrambling.* J Thromb Haemost, 2015. **13**(12): p. 2240-52.

104.   Boisseau, P., et al., *A new mutation of ANO6 in two familial cases of Scott syndrome.* Br J Haematol, 2018. **180**(5): p. 750-752.

105.   Zwaal, R.F., P. Comfurius, and E.M. Bevers, *Scott syndrome, a bleeding disorder caused by defective scrambling of membrane phospholipids.* Biochim Biophys Acta, 2004. **1636**(2-3): p. 119-28.

106.   Yu, K., et al., *Identification of a lipid scrambling domain in ANO6/TMEM16F.* Elife, 2015. **4**: p. e06901.

107.   Lee, B.C., A.K. Menon, and A. Accardi, *The nhTMEM16 Scramblase Is Also a Nonselective Ion Channel.* Biophys J, 2016. **111**(9): p. 1919-1924.

108.   Bevers, E.M., P. Comfurius, and R.F. Zwaal, *Platelet procoagulant activity: physiological significance and mechanisms of exposure.* Blood Rev, 1991. **5**(3): p. 146-54.

109.   Li, Z., et al., *Necrotic Cells Actively Attract Phagocytes through the Collaborative Action of Two Distinct PS-Exposure Mechanisms.* PLoS Genet, 2015. **11**(6): p. e1005285.

110.   Pelz, T., et al., *An ancestral TMEM16 homolog from Dictyostelium discoideum forms a scramblase.* PLoS One, 2018. **13**(2): p. e0191219.

111.   Pomorski, T. and A.K. Menon, *Lipid flippases and their biological functions.* Cell Mol Life Sci, 2006. **63**(24): p. 2908-21.

112.   Baldridge, R.D. and T.R. Graham, *Identification of residues defining phospholipid flippase substrate specificity of type IV P-type ATPases.* Proc Natl Acad Sci U S A, 2012. **109**(6): p. E290-8.

113.   Baldridge, R.D. and T.R. Graham, *Two-gate mechanism for phospholipid selection and transport by type IV P-type ATPases.* Proc Natl Acad Sci U S A, 2013. **110**(5): p. E358-67.

114.   Bethel, N.P. and M. Grabe, *Atomistic insight into lipid translocation by a TMEM16 scramblase.* Proc Natl Acad Sci U S A, 2016. **113**(49): p. 14049-14054.

115.   Jiang, T., et al., *Lipids and ions traverse the membrane by the same physical pathway in the nhTMEM16 scramblase.* Elife, 2017. **6**.

116.   Uhlen, M., et al., *Proteomics. Tissue-based map of the human proteome.* Science, 2015. **347**(6220): p. 1260419.

117.   Thul, P.J., et al., *A subcellular map of the human proteome.* Science, 2017. **356**(6340).

118.   Eggermont, J., *Calcium-activated chloride channels: (un)known, (un)loved?* Proc Am Thorac Soc, 2004. **1**(1): p. 22-7.

119.   Duran, C. and H.C. Hartzell, *Physiological roles and diseases of Tmem16/Anoctamin proteins: are they all chloride channels?* Acta Pharmacol Sin, 2011. **32**(6): p. 685-92.

120.   Duran, C., et al., *Chloride channels: often enigmatic, rarely predictable.* Annu Rev Physiol, 2010. **72**: p. 95-121.

121.   Huang, F., X. Wong, and L.Y. Jan, *International Union of Basic and Clinical Pharmacology. LXXXV: calcium-activated chloride channels.* Pharmacol Rev, 2012. **64**(1): p. 1-15.

122.   Milenkovic, V.M., et al., *Evolution and functional divergence of the anoctamin family of membrane proteins.* BMC Evol Biol, 2010. **10**: p. 319.

123.   Pajcini, K.V., et al., *Myoblasts and macrophages share molecular components that contribute to cell-cell fusion.* J Cell Biol, 2008. **180**(5): p. 1005-19.

124.   Pedemonte, N. and L.J. Galietta, *Structure and function of TMEM16 proteins (anoctamins).* Physiol Rev, 2014. **94**(2): p. 419-59.

125.   Wanitchakool, P., et al., *Role of anoctamins in cancer and apoptosis.* Philos Trans R Soc Lond B Biol Sci, 2014. **369**(1638): p. 20130096.

126.   Wang, Y., et al., *Phylogenetic, expression, and functional analyses of anoctamin homologs in Caenorhabditis elegans.* Am J Physiol Regul Integr Comp Physiol, 2013. **305**(11): p. R1376-89.

127.   Ehlen, H.W., et al., *Inactivation of anoctamin-6/Tmem16f, a regulator of phosphatidylserine scrambling in osteoblasts, leads to decreased mineral deposition in skeletal tissues.* J Bone Miner Res, 2013. **28**(2): p. 246-59.

128.   Ousingsawat, J., et al., *Anoctamin 6 mediates effects essential for innate immunity downstream of P2X7 receptors in macrophages.* Nat Commun, 2015. **6**: p. 6245.

129.   Suzuki, J., et al., *Calcium-dependent phospholipid scramblase activity of TMEM16 protein family members.* J Biol Chem, 2013. **288**(19): p. 13305-16.

130.   Coleman, J.A., F. Quazi, and R.S. Molday, *Mammalian P4-ATPases and ABC transporters and their role in phospholipid transport.* Biochim Biophys Acta, 2013. **1831**(3): p. 555-74.

131.   Hankins, H.M., et al., *Role of flippases, scramblases and transfer proteins in phosphatidylserine subcellular distribution.* Traffic, 2015. **16**(1): p. 35-47.

132.   van Meer, G., *Dynamic transbilayer lipid asymmetry.* Cold Spring Harb Perspect Biol, 2011. **3**(5).

133.   Kay, J.G. and S. Grinstein, *Phosphatidylserine-mediated cellular signaling.* Adv Exp Med Biol, 2013. **991**: p. 177-93.

134.   Ruggiero, L., et al., *Diurnal, localized exposure of phosphatidylserine by rod outer segment tips in wild-type but not Itgb5-/- or Mfge8-/- mouse retina.* Proc Natl Acad Sci U S A, 2012. **109**(21): p. 8145-8.

135.   Bratton, D.L., et al., *Appearance of phosphatidylserine on apoptotic cells requires calcium-mediated nonspecific flip-flop and is enhanced by loss of the aminophospholipid translocase.* J Biol Chem, 1997. **272**(42): p. 26159-65.

136.   Orrenius, S., B. Zhivotovsky, and P. Nicotera, *Regulation of cell death: the calcium-apoptosis link.* Nat Rev Mol Cell Biol, 2003. **4**(7): p. 552-65.

137.   van Kruchten, R., et al., *Both TMEM16F-dependent and TMEM16F-independent pathways contribute to phosphatidylserine exposure in platelet apoptosis and platelet activation.* Blood, 2013. **121**(10): p. 1850-7.

138.   Williamson, P., et al., *Continuous analysis of the mechanism of activated transbilayer lipid movement in platelets.* Biochemistry, 1995. **34**(33): p. 10448-55.

139.   Whitlock, J.M. and H.C. Hartzell, *A Pore Idea: the ion conduction pathway of TMEM16/ANO proteins is composed partly of lipid.* Pflugers Arch, 2016.

140.   Tien, J., et al., *A comprehensive search for calcium binding sites critical for TMEM16A calcium-activated chloride channel activity.* Elife, 2014. **3**.

277

141. Yu, K., et al., *Explaining calcium-dependent gating of anoctamin-1 chloride channels requires a revised topology.* Circ Res, 2012. **110**(7): p. 990-9.

142. Yu, K., et al., *Activation of the Ano1 (TMEM16A) chloride channel by calcium is not mediated by calmodulin.* J Gen Physiol, 2014. **143**(2): p. 253-67.

143. Kmit, A., et al., *Calcium-activated and apoptotic phospholipid scrambling induced by Ano6 can occur independently of Ano6 ion currents.* Cell Death Dis, 2013. **4**: p. e611.

144. Moller-Tank, S. and W. Maury, *Phosphatidylserine receptors: enhancers of enveloped virus entry and infection.* Virology, 2014. **468-470**: p. 565-580.

145. Murakami, Y., et al., *CD300b regulates the phagocytosis of apoptotic cells via phosphatidylserine recognition.* Cell Death Differ, 2014. **21**(11): p. 1746-57.

146. Zenarruzabeitia, O., et al., *The Biology and Disease Relevance of CD300a, an Inhibitory Receptor for Phosphatidylserine and Phosphatidylethanolamine.* J Immunol, 2015. **194**(11): p. 5053-60.

147. Toda, S., R. Hanayama, and S. Nagata, *Two-step engulfment of apoptotic cells.* Mol Cell Biol, 2012. **32**(1): p. 118-25.

148. Segawa, K., J. Suzuki, and S. Nagata, *Constitutive exposure of phosphatidylserine on viable cells.* Proc Natl Acad Sci U S A, 2011. **108**(48): p. 19246-51.

149. Simhadri, V.R., et al., *Human CD300a binds to phosphatidylethanolamine and phosphatidylserine, and modulates the phagocytosis of dead cells.* Blood, 2012. **119**(12): p. 2799-809.

150. Frolov, V.A., A.V. Shnyrova, and J. Zimmerberg, *Lipid polymorphisms and membrane shape.* Cold Spring Harb Perspect Biol, 2011. **3**(11): p. a004747.

151. Bigay, J. and B. Antonny, *Curvature, lipid packing, and electrostatics of membrane organelles: defining cellular territories in determining specificity.* Dev Cell, 2012. **23**(5): p. 886-95.

152. Suetsugu, S., S. Kurisu, and T. Takenawa, *Dynamic shaping of cellular membranes by phospholipids and membrane-deforming proteins.* Physiol Rev, 2014. **94**(4): p. 1219-48.

153. Chernomordik, L.V., G.B. Melikyan, and Y.A. Chizmadzhev, *Biomembrane fusion: a new concept derived from model studies using two interacting planar lipid bilayers.* Biochim Biophys Acta, 1987. **906**(3): p. 309-52.

154. van den Brink-van der Laan, E., J.A. Killian, and B. de Kruijff, *Nonbilayer lipids affect peripheral and integral membrane proteins via changes in the lateral pressure profile.* Biochim Biophys Acta, 2004. **1666**(1-2): p. 275-88.

155. Allan, D. and R.H. Michell, *Accumulation of 1,2-diacylglycerol in the plasma membrane may lead to echinocyte transformation of erythrocytes.* Nature, 1975. **258**(5533): p. 348-9.

156. Comfurius, P., et al., *Loss of membrane phospholipid asymmetry in platelets and red cells may be associated with calcium-induced shedding of plasma membrane and inhibition of aminophospholipid translocase.* Biochim Biophys Acta, 1990. **1026**(2): p. 153-60.

157. Heijnen, H.F., et al., *Activated platelets release two types of membrane vesicles: microvesicles by surface shedding and exosomes derived from exocytosis of multivesicular bodies and alpha-granules.* Blood, 1999. **94**(11): p. 3791-9.

158. Allan, D. and P. Thomas, *Ca2+-induced biochemical changes in human erythrocytes and their relation to microvesiculation.* Biochem J, 1981. **198**(3): p. 433-40.

159. Abels, E.R. and X.O. Breakefield, *Introduction to Extracellular Vesicles: Biogenesis, RNA Cargo Selection, Content, Release, and Uptake.* Cell Mol Neurobiol, 2016. **36**(3): p. 301-12.

160. Cocucci, E. and J. Meldolesi, *Ectosomes and exosomes: shedding the confusion between extracellular vesicles.* Trends Cell Biol, 2015. **25**(6): p. 364-72.

161. Colombo, M., G. Raposo, and C. Thery, *Biogenesis, secretion, and intercellular interactions of exosomes and other extracellular vesicles.* Annu Rev Cell Dev Biol, 2014. **30**: p. 255-89.

162. de Souza, P.S., et al., *Membrane microparticles: shedding new light into cancer cell communication.* J Cancer Res Clin Oncol, 2016. **142**(7): p. 1395-406.

163. Ibrahim, A. and E. Marban, *Exosomes: Fundamental Biology and Roles in Cardiovascular Physiology.* Annu Rev Physiol, 2016. **78**: p. 67-83.

164. Machtinger, R., L.C. Laurent, and A.A. Baccarelli, *Extracellular vesicles: roles in gamete maturation, fertilization and embryo implantation.* Hum Reprod Update, 2016. **22**(2): p. 182-93.

165. Raposo, G. and W. Stoorvogel, *Extracellular vesicles: exosomes, microvesicles, and friends.* J Cell Biol, 2013. **200**(4): p. 373-83.

166. Sadallah, S., C. Eken, and J.A. Schifferli, *Ectosomes as modulators of inflammation and immunity.* Clin Exp Immunol, 2011. **163**(1): p. 26-32.

167. Suades, R., T. Padro, and L. Badimon, *The Role of Blood-Borne Microparticles in Inflammation and Hemostasis.* Semin Thromb Hemost, 2015. **41**(6): p. 590-606.

168. Boilard, E., A.C. Duchez, and A. Brisson, *The diversity of platelet microparticles.* Curr Opin Hematol, 2015. **22**(5): p. 437-44.

169. Forterre, A., et al., *Proteomic analysis of C2C12 myoblast and myotube exosome-like vesicles: a new paradigm for myoblast-myotube cross talk?* PLoS One, 2014. **9**(1): p. e84153.

170. Gong, J., et al., *Microparticles in cancer: A review of recent developments and the potential for clinical application.* Semin Cell Dev Biol, 2015. **40**: p. 35-40.

171. Varon, D. and E. Shai, *Platelets and their microparticles as key players in pathophysiological responses.* J Thromb Haemost, 2015. **13 Suppl 1**: p. S40-6.

172. Bianco, F., et al., *Acid sphingomyelinase activity triggers microparticle release from glial cells.* EMBO J, 2009. **28**(8): p. 1043-54.

173. Dachary-Prigent, J., et al., *Aminophospholipid exposure, microvesiculation and abnormal protein tyrosine phosphorylation in the platelets of a patient with Scott syndrome: a study using physiologic agonists and local anaesthetics.* Br J Haematol, 1997. **99**(4): p. 959-67.

174. Sims, P.J., et al., *Assembly of the platelet prothrombinase complex is linked to vesiculation of the platelet plasma membrane. Studies in Scott syndrome: an*

isolated defect in platelet procoagulant activity. J Biol Chem, 1989. **264**(29): p. 17049-57.

175.   Toti, P., et al., *Celiac disease with cerebral calcium and silica deposits: x-ray spectroscopic findings, an autopsy study.* Neurology, 1996. **46**(4): p. 1088-92.

176.   Brooks, M.B., et al., *Evaluation of platelet function screening tests to detect platelet procoagulant deficiency in dogs with Scott syndrome.* Vet Clin Pathol, 2009. **38**(3): p. 306-15.

177.   Thouverey, C., et al., *Matrix vesicles originate from apical membrane microvilli of mineralizing osteoblast-like Saos-2 cells.* J Cell Biochem, 2009. **106**(1): p. 127-38.

178.   Laffont, B., et al., *Activated platelets can deliver mRNA regulatory Ago2*microRNA complexes to endothelial cells via microparticles.* Blood, 2013. **122**(2): p. 253-61.

179.   Brill, A., et al., *Platelet-derived microparticles induce angiogenesis and stimulate post-ischemic revascularization.* Cardiovasc Res, 2005. **67**(1): p. 30-8.

180.   Dashevsky, O., D. Varon, and A. Brill, *Platelet-derived microparticles promote invasiveness of prostate cancer cells via upregulation of MMP-2 production.* Int J Cancer, 2009. **124**(8): p. 1773-7.

181.   Jy, W., et al., *Platelet microparticles bind, activate and aggregate neutrophils in vitro.* Blood Cells Mol Dis, 1995. **21**(3): p. 217-31; discussion 231a.

182.   Sprague, D.L., et al., *Platelet-mediated modulation of adaptive immunity: unique delivery of CD154 signal by platelet-derived membrane vesicles.* Blood, 2008. **111**(10): p. 5028-36.

183.   Familari, M., et al., *Placenta-derived extracellular vesicles: their cargo and possible functions.* Reprod Fertil Dev, 2017. **29**(3): p. 433-447.

184.   Huynh, N., et al., *Characterization of Regulatory Extracellular Vesicles from Osteoclasts.* J Dent Res, 2016.

185.   Willkomm, L. and W. Bloch, *State of the art in cell-cell fusion.* Methods Mol Biol, 2015. **1313**: p. 1-19.

186.   Van den Eijnde, S.M., et al., *Phosphatidylserine plasma membrane asymmetry in vivo: a pancellular phenomenon which alters during apoptosis.* Cell Death Differ, 1997. **4**(4): p. 311-6.

187.   van den Eijnde, S.M., et al., *Transient expression of phosphatidylserine at cell-cell contact areas is required for myotube formation.* J Cell Sci, 2001. **114**(Pt 20): p. 3631-42.

188.   Jeong, J. and I.M. Conboy, *Phosphatidylserine directly and positively regulates fusion of myoblasts into myotubes.* Biochem Biophys Res Commun, 2011. **414**(1): p. 9-13.

189.   Hamoud, N., et al., *G-protein coupled receptor BAI3 promotes myoblast fusion in vertebrates.* Proc Natl Acad Sci U S A, 2014. **111**(10): p. 3745-50.

190.   Hochreiter-Hufford, A.E., et al., *Phosphatidylserine receptor BAI1 and apoptotic cells as new promoters of myoblast fusion.* Nature, 2013. **497**(7448): p. 263-7.

191.   Leikina, E., et al., *Annexin A1 Deficiency does not Affect Myofiber Repair but Delays Regeneration of Injured Muscles.* Sci Rep, 2015. **5**: p. 18246.

192. Leikina, E., et al., *Extracellular annexins and dynamin are important for sequential steps in myoblast fusion.* J Cell Biol, 2013. **200**(1): p. 109-23.

193. Gerke, V., C.E. Creutz, and S.E. Moss, *Annexins: linking Ca2+ signalling to membrane dynamics.* Nat Rev Mol Cell Biol, 2005. **6**(6): p. 449-61.

194. Rintala-Dempsey, A.C., A. Rezvanpour, and G.S. Shaw, *S100-annexin complexes--structural insights.* FEBS J, 2008. **275**(20): p. 4956-66.

195. Lee, G. and H.B. Pollard, *Highly sensitive and stable phosphatidylserine liposome aggregation assay for annexins.* Anal Biochem, 1997. **252**(1): p. 160-4.

196. Meers, P., T. Mealy, and A.I. Tauber, *Annexin I interactions with human neutrophil specific granules: fusogenicity and coaggregation with plasma membrane vesicles.* Biochim Biophys Acta, 1993. **1147**(2): p. 177-84.

197. Abmayr, S.M. and G.K. Pavlath, *Myoblast fusion: lessons from flies and mice.* Development, 2012. **139**(4): p. 641-56.

198. Hicks, D., et al., *A founder mutation in Anoctamin 5 is a major cause of limb-girdle muscular dystrophy.* Brain, 2011. **134**(Pt 1): p. 171-82.

199. Mahjneh, I., et al., *A new distal myopathy with mutation in anoctamin 5.* Neuromuscul Disord, 2010. **20**(12): p. 791-5.

200. Savarese, M., et al., *Next generation sequencing on patients with LGMD and nonspecific myopathies: Findings associated with ANO5 mutations.* Neuromuscul Disord, 2015.

201. Mizuta, K., et al., *Molecular characterization of GDD1/TMEM16E, the gene product responsible for autosomal dominant gnathodiaphyseal dysplasia.* Biochem Biophys Res Commun, 2007. **357**(1): p. 126-32.

202. Griffin, D.A., et al., *Defective membrane fusion and repair in Anoctamin5-deficient muscular dystrophy.* Hum Mol Genet, 2016. **25**(10): p. 1900-1911.

203. Xu, P., et al., *Phosphatidylserine flipping enhances membrane curvature and negative charge required for vesicular transport.* J Cell Biol, 2013. **202**(6): p. 875-86.

204. Xu, J., et al., *Genetic disruption of Ano5 in mice does not recapitulate human ANO5-deficient muscular dystrophy.* Skelet Muscle, 2015. **5**: p. 43.

205. McDade, J.R., A. Archambeau, and D.E. Michele, *Rapid actin-cytoskeleton-dependent recruitment of plasma membrane-derived dysferlin at wounds is critical for muscle membrane repair.* FASEB J, 2014. **28**(8): p. 3660-70.

206. McNeil, P.L. and T. Kirchhausen, *An emergency response team for membrane repair.* Nat Rev Mol Cell Biol, 2005. **6**(6): p. 499-505.

207. Sonnemann, K.J. and W.M. Bement, *Wound repair: toward understanding and integration of single-cell and multicellular wound responses.* Annu Rev Cell Dev Biol, 2011. **27**: p. 237-63.

208. Idone, V., C. Tam, and N.W. Andrews, *Two-way traffic on the road to plasma membrane repair.* Trends Cell Biol, 2008. **18**(11): p. 552-9.

209. Jimenez, A.J., et al., *ESCRT machinery is required for plasma membrane repair.* Science, 2014. **343**(6174): p. 1247136.

210. Bansal, D., et al., *Defective membrane repair in dysferlin-deficient muscular dystrophy.* Nature, 2003. **423**(6936): p. 168-72.

211. Gerasimenko, J.V., O.V. Gerasimenko, and O.H. Petersen, *Membrane repair: Ca(2+)-elicited lysosomal exocytosis.* Curr Biol, 2001. **11**(23): p. R971-4.

212. Lai, A.L., et al., *Synaptotagmin 1 modulates lipid acyl chain order in lipid bilayers by demixing phosphatidylserine.* J Biol Chem, 2011. **286**(28): p. 25291-300.

213. Marty, N.J., et al., *The C2 domains of otoferlin, dysferlin, and myoferlin alter the packing of lipid bilayers.* Biochemistry, 2013. **52**(33): p. 5585-92.

214. Murray, D. and B. Honig, *Electrostatic control of the membrane targeting of C2 domains.* Mol Cell, 2002. **9**(1): p. 145-54.

215. Shahin, V., et al., *Synaptotagmin perturbs the structure of phospholipid bilayers.* Biochemistry, 2008. **47**(7): p. 2143-52.

216. Andrews, N.W., *Membrane resealing: synaptotagmin VII keeps running the show.* Sci STKE, 2005. **2005**(282): p. pe19.

217. Fuson, K., et al., *Alternate splicing of dysferlin C2A confers Ca(2)(+)-dependent and Ca(2)(+)-independent binding for membrane repair.* Structure, 2014. **22**(1): p. 104-15.

218. Lennon, N.J., et al., *Dysferlin interacts with annexins A1 and A2 and mediates sarcolemmal wound-healing.* J Biol Chem, 2003. **278**(50): p. 50466-73.

219. Roostalu, U. and U. Strahle, *In vivo imaging of molecular interactions at damaged sarcolemma.* Dev Cell, 2012. **22**(3): p. 515-29.

220. Swaggart, K.A., et al., *Annexin A6 modifies muscular dystrophy by mediating sarcolemmal repair.* Proc Natl Acad Sci U S A, 2014. **111**(16): p. 6004-9.

221. Rahimov, F. and L.M. Kunkel, *The cell biology of disease: cellular and molecular mechanisms underlying muscular dystrophy.* J Cell Biol, 2013. **201**(4): p. 499-510.

222. Glover, L. and R.H. Brown, Jr., *Dysferlin in membrane trafficking and patch repair.* Traffic, 2007. **8**(7): p. 785-94.

223. Jaiswal, J.K., et al., *Patients with a non-dysferlin Miyoshi myopathy have a novel membrane repair defect.* Traffic, 2007. **8**(1): p. 77-88.

224. Jarry, J., et al., *A novel autosomal recessive limb-girdle muscular dystrophy with quadriceps atrophy maps to 11p13-p12.* Brain, 2007. **130**(Pt 2): p. 368-80.

225. Monjaret, F., et al., *The phenotype of dysferlin-deficient mice is not rescued by adeno-associated virus-mediated transfer of anoctamin 5.* Hum Gene Ther Clin Dev, 2013. **24**(2): p. 65-76.

226. Avalos-Rodriguez, A., et al., *Fluorometric study of rabbit sperm head membrane phospholipid asymmetry during capacitation and acrosome reaction using Annexin-V FITC.* Arch Androl, 2004. **50**(4): p. 273-85.

227. Davis, B.K., R. Byrne, and K. Bedigian, *Studies on the mechanism of capacitation: albumin-mediated changes in plasma membrane lipids during in vitro incubation of rat sperm cells.* Proc Natl Acad Sci U S A, 1980. **77**(3): p. 1546-50.

228. Ensslin, M.A. and B.D. Shur, *Identification of mouse sperm SED1, a bimotif EGF repeat and discoidin-domain protein involved in sperm-egg binding.* Cell, 2003. **114**(4): p. 405-17.

229. Miyado, K., et al., *The fusing ability of sperm is bestowed by CD9-containing vesicles released from eggs in mice.* Proc Natl Acad Sci U S A, 2008. **105**(35): p. 12921-6.

230. Helming, L. and S. Gordon, *Molecular mediators of macrophage fusion.* Trends Cell Biol, 2009. **19**(10): p. 514-22.

231. Helming, L., J. Winter, and S. Gordon, *The scavenger receptor CD36 plays a role in cytokine-induced macrophage fusion.* J Cell Sci, 2009. **122**(Pt 4): p. 453-9.

232. Das, M., et al., *Phosphatidylserine efflux and intercellular fusion in a BeWo model of human villous cytotrophoblast.* Placenta, 2004. **25**(5): p. 396-407.

233. Riddell, M.R., et al., *Pleiotropic actions of forskolin result in phosphatidylserine exposure in primary trophoblasts.* PLoS One, 2013. **8**(12): p. e81273.

234. Adler, R.R., A.K. Ng, and N.S. Rote, *Monoclonal antiphosphatidylserine antibody inhibits intercellular fusion of the choriocarcinoma line, JAR.* Biol Reprod, 1995. **53**(4): p. 905-10.

235. Huppertz, B. and M. Gauster, *Trophoblast fusion.* Adv Exp Med Biol, 2011. **713**: p. 81-95.

236. Rand, J.H., et al., *The annexin A5-mediated pathogenic mechanism in the antiphospholipid syndrome: role in pregnancy losses and thrombosis.* Lupus, 2010. **19**(4): p. 460-9.

237. Rodriguez-Garcia, V., et al., *Examining the prevalence of non-criteria anti-phospholipid antibodies in patients with anti-phospholipid syndrome: a systematic review.* Rheumatology (Oxford), 2015. **54**(11): p. 2042-50.

238. Lavieu, G., et al., *Induction of cortical endoplasmic reticulum by dimerization of a coatomer-binding peptide anchored to endoplasmic reticulum membranes.* Proc Natl Acad Sci U S A, 2010. **107**(15): p. 6876-81.

239. Kralt, A., et al., *Intrinsically disordered linker and plasma membrane-binding motif sort Ist2 and Ssy1 to junctions.* Traffic, 2015. **16**(2): p. 135-47.

240. Fischer, M.A., et al., *Binding of plasma membrane lipids recruits the yeast integral membrane protein Ist2 to the cortical ER.* Traffic, 2009. **10**(8): p. 1084-97.

241. Quon, E. and C.T. Beh, *Membrane Contact Sites: Complex Zones for Membrane Association and Lipid Exchange.* Lipid Insights, 2015. **8**(Suppl 1): p. 55-63.

242. MacKinnon, R., *Nobel Lecture. Potassium channels and the atomic basis of selective ion conduction.* Biosci Rep, 2004. **24**(2): p. 75-100.

243. Hartzell, C., I. Putzier, and J. Arreola, *Calcium-activated chloride channels.* Annual Reviews of Physiology, 2005. **67**: p. 719-758.

244. Hartzell, H.C., et al., *Anoctamin / TMEM16 family members are Ca^{2+}-activated Cl^- channels.* The Journal of Physiology, 2009. **587.10**: p. 2127-2139.

245. Picollo, A., M. Malvezzi, and A. Accardi, *TMEM16 proteins: unknown structure and confusing functions.* J Mol Biol, 2015. **427**(1): p. 94-105.

246. Duran, C., et al., *ANOs 3-7 in the anoctamin/tmem16 Cl^- channel family are intracellular proteins.* Am J Physiol Cell Physiol, 2012. **302**: p. C482-93.

247. Kunzelmann, K., et al., *Molecular functions of anoctamin 6 (TMEM16F): a chloride channel, cation channel, or phospholipid scramblase?* Pflugers Arch, 2014. **466**(3): p. 407-14.

248. Li, W., et al., *The EMBL-EBI bioinformatics web and programmatic tools framework.* Nucleic Acids Res, 2015. **43**(W1): p. W580-4.

249.   Capella-Gutierrez, S., J.M. Silla-Martinez, and T. Gabaldon, *trimAl: a tool for automated alignment trimming in large-scale phylogenetic analyses.* Bioinformatics, 2009. **25**(15): p. 1972-3.

250.   Virtanen, J.A., K.H. Cheng, and P. Somerharju, *Phospholipid composition of the mammalian red cell membrane can be rationalized by a superlattice model.* Proc Natl Acad Sci U S A, 1998. **95**(9): p. 4964-9.

251.   Marinetti, G.V. and R. Love, *Extent of cross-linking of amino-phospholipid neighbors in the erythrocyte membrane as influenced by the concentration of difluorodinitrobenzene.* Biochem Biophys Res Commun, 1974. **61**(1): p. 30-7.

252.   Whiteley, N.M. and H.C. Berg, *Amidination of the outer and inner surfaces of the human erythrocyte membrane.* J Mol Biol, 1974. **87**(3): p. 541-61.

253.   Zwaal, R.F., et al., *Organization of phospholipids in human red cell membranes as detected by the action of various purified phospholipases.* Biochim Biophys Acta, 1975. **406**(1): p. 83-96.

254.   Yeagle, P.L., *Lipid regulation of cell membrane structure and function.* FASEB J, 1989. **3**(7): p. 1833-42.

255.   Holthuis, J.C. and A.K. Menon, *Lipid landscapes and pipelines in membrane homeostasis.* Nature, 2014. **510**(7503): p. 48-57.

256.   Koller, D. and K. Lohner, *The role of spontaneous lipid curvature in the interaction of interfacially active peptides with membranes.* Biochim Biophys Acta, 2014. **1838**(9): p. 2250-9.

257.   Leonard, T.A. and J.H. Hurley, *Regulation of protein kinases by lipids.* Curr Opin Struct Biol, 2011. **21**(6): p. 785-91.

258.   Bevers, E.M., P. Comfurius, and R.F. Zwaal, *Changes in membrane phospholipid distribution during platelet activation.* Biochim Biophys Acta, 1983. **736**(1): p. 57-66.

259.   Fadok, V.A., et al., *Exposure of phosphatidylserine on the surface of apoptotic lymphocytes triggers specific recognition and removal by macrophages.* J Immunol, 1992. **148**(7): p. 2207-16.

260.   Bevers, E.M. and P.L. Williamson, *Phospholipid scramblase: an update.* FEBS Lett, 2010. **584**(13): p. 2724-30.

261.   Suzuki, J., E. Imanishi, and S. Nagata, *Exposure of phosphatidylserine by Xk-related protein family members during apoptosis.* J Biol Chem, 2014. **289**(44): p. 30257-67.

262.   Kodigepalli, K.M., et al., *Roles and regulation of phospholipid scramblases.* FEBS Lett, 2015. **589**(1): p. 3-14.

263.   Bevers, E.M., et al., *Generation of prothrombin-converting activity and the exposure of phosphatidylserine at the outer surface of platelets.* Eur J Biochem, 1982. **122**(2): p. 429-36.

264.   Lhermusier, T., H. Chap, and B. Payrastre, *Platelet membrane phospholipid asymmetry: from the characterization of a scramblase activity to the identification of an essential protein mutated in Scott syndrome.* J Thromb Haemost, 2011. **9**(10): p. 1883-91.

265. Tian, Y., R. Schreiber, and K. Kunzelmann, *Anoctamins are a family of Ca2+-activated Cl- channels.* J Cell Sci, 2012. **125**(Pt 21): p. 4991-8.

266. Savarese, M., et al., *Next generation sequencing on patients with LGMD and nonspecific myopathies: Findings associated with ANO5 mutations.* Neuromuscul Disord, 2015. **25**(7): p. 533-41.

267. Penttila, S., J. Palmio, and B. Udd, *ANO5-Related Muscle Diseases*, in *GeneReviews(R)*, R.A. Pagon, et al., Editors. 1993: Seattle (WA).

268. Tsutsumi, S., et al., *Molecular cloning and characterization of the murine gnathodiaphyseal dysplasia gene GDD1.* Biochem Biophys Res Commun, 2005. **331**(4): p. 1099-106.

269. Mohsenzadegan, M., et al., *Study of NGEP expression pattern in cancerous tissues provides novel insights into prognostic marker in prostate cancer.* Biomark Med, 2015. **9**(4): p. 391-401.

270. Das, S., et al., *Topology of NGEP, a prostate-specific cell:cell junction protein widely expressed in many cancers of different grade level.* Cancer Res, 2008. **68**(15): p. 6306-12.

271. Das, S., et al., *NGEP, a prostate-specific plasma membrane protein that promotes the association of LNCaP cells.* Cancer Res, 2007. **67**(4): p. 1594-601.

272. Balreira, A., et al., *ANO10 mutations cause ataxia and coenzyme Q10 deficiency.* J Neurol, 2014. **261**(11): p. 2192-8.

273. Malvezzi, M., et al., *Ca^{2+}-dependent phospholipid scrambling by a reconstituted TMEM16 ion channel.* Nat. Commun., 2013. **4**: p. 2367.

274. Stefan, C.J., A.G. Manford, and S.D. Emr, *ER-PM connections: sites of information transfer and inter-organelle communication.* Curr Opin Cell Biol, 2013. **25**(4): p. 434-42.

275. Grubb, S., et al., *TMEM16F (Anoctamin 6), an anion channel of delayed Ca(2+) activation.* J Gen Physiol, 2013. **141**(5): p. 585-600.

276. Martins, J.R., et al., *Anoctamin 6 is an essential component of the outwardly rectifying chloride channel.* Proc Natl Acad Sci U S A, 2011. **108**(44): p. 18168-72.

277. Shimizu, T., et al., *TMEM16F is a component of a Ca2+-activated Cl- channel but not a volume-sensitive outwardly rectifying Cl- channel.* Am J Physiol Cell Physiol, 2013. **304**(8): p. C748-59.

278. Sahu, S.K., et al., *Phospholipid scramblases: an overview.* Arch Biochem Biophys, 2007. **462**(1): p. 103-14.

279. Martin, D.W. and J. Jesty, *Calcium stimulation of procoagulant activity in human erythrocytes. ATP dependence and the effects of modifiers of stimulation and recovery.* J Biol Chem, 1995. **270**(18): p. 10468-74.

280. Kelley, L.A. and M.J. Sternberg, *Protein structure prediction on the Web: a case study using the Phyre server.* Nat Protoc, 2009. **4**(3): p. 363-71.

281. Stansfeld, P.J., et al., *MemProtMD: Automated Insertion of Membrane Protein Structures into Explicit Lipid Membranes.* Structure, 2015. **23**(7): p. 1350-61.

282. Jordan, I.K., et al., *Evolutionary and functional divergence between the cystic fibrosis transmembrane conductance regulator and related ATP-binding cassette transporters.* Proc Natl Acad Sci U S A, 2008. **105**(48): p. 18865-70.

285

283. Miller, C., *CFTR: break a pump, make a channel.* Proc Natl Acad Sci U S A, 2010. **107**(3): p. 959-60.

284. Gadsby, D.C., P. Vergani, and L. Csanady, *The ABC protein turned chloride channel whose failure causes cystic fibrosis.* Nature, 2006. **440**(7083): p. 477-83.

285. Lisal, J. and M. Maduke, *The ClC-0 chloride channel is a 'broken' Cl-/H+ antiporter.* Nat.Struct.Mol.Biol., 2008. **15**(8): p. 805-810.

286. Miller, C., *ClC chloride channels viewed through a transporter lens.* Nature, 2006. **440**(7083): p. 484-489.

287. Adomaviciene, A., et al., *Putative pore-loops of TMEM16/anoctamin channels affect channel density in cell membranes.* J Physiol, 2013. **591**(Pt 14): p. 3487-505.

288. Almaca, J., et al., *TMEM16 proteins produce volume-regulated chloride currents that are reduced in mice lacking TMEM16A.* J Biol Chem, 2009. **284**(42): p. 28571-8.

289. Juul, C.A., et al., *Anoctamin 6 differs from VRAC and VSOAC but is involved in apoptosis and supports volume regulation in the presence of Ca2+.* Pflugers Arch, 2014. **466**(10): p. 1899-910.

290. Szteyn, K., et al., *Expression and functional significance of the Ca(2+)-activated Cl(-) channel ANO6 in dendritic cells.* Cell Physiol Biochem, 2012. **30**(5): p. 1319-32.

291. Bobkov, Y.V., E.A. Corey, and B.W. Ache, *The pore properties of human nociceptor channel TRPA1 evaluated in single channel recordings.* Biochim Biophys Acta, 2011. **1808**(4): p. 1120-8.

292. Eisenman, G. and R. Horn, *Ionic selectivity revisited: the role of kinetic and equilibrium processes in ion permeation through channels.* Journal of Membrane Biology, 1983. **76**: p. 197-225.

293. Scudieri, P., et al., *Ion channel and lipid scramblase activity associated with expression of TMEM16F/ANO6 isoforms.* J Physiol, 2015. **593**(17): p. 3829-48.

294. Peters, C.J., et al., *Four basic residues critical for the ion selectivity and pore blocker sensitivity of TMEM16A calcium-activated chloride channels.* Proc Natl Acad Sci U S A, 2015. **112**(11): p. 3547-52.

295. Xiao, Q., et al., *Voltage- and calcium-dependent gating of TMEM16A/Ano1 chloride channels are physically coupled by the first intracellular loop.* Proc Natl Acad Sci U S A, 2011. **108**(21): p. 8891-6.

296. Xiao, Q., et al., *Voltage- and calcium-dependent gating of TMEM16A/Ano1 chloride channels are physically coupled by the first intracellular loop.* Proc. Natl. Acad. Sci., 2011. **108**(21): p. 8891-8896.

297. Ferrera, L., et al., *Regulation of TMEM16A chloride channel properties by alternative splicing.* J Biol Chem, 2009. **284**(48): p. 33360-8.

298. Qu, Z. and H.C. Hartzell, *Anion permeation in Ca^{2+} -activated Cl^- channels.* Journal of General Physiology, 2000. **116**(6): p. 825-844.

299. Terashima, H., A. Picollo, and A. Accardi, *Purified TMEM16A is sufficient to form Ca2+-activated Cl- channels.* Proceedings of the National Academy of Sciences of the United States of America, 2013. **110**(48): p. 19354-19359.

300. Kuruma, A. and H.C. Hartzell, *Dynamics of calcium regulation of chloride currents in Xenopus oocytes.* American Journal of Physiology, 1999. **276**(1 Pt 1): p. C161-C175.

301. Betto, G., et al., *Interactions between permeation and gating in the TMEM16B/anoctamin2 calcium-activated chloride channel.* J Gen Physiol, 2014. **143**(6): p. 703-18.

302. Sagheddu, C., et al., *Calcium concentration jumps reveal dynamic ion selectivity of calcium-activated chloride currents in mouse olfactory sensory neurons and TMEM16b-transfected HEK 293T cells.* J Physiol, 2010. **588**(Pt 21): p. 4189-204.

303. Kuruma, A. and H.C. Hartzell, *Bimodal control of a Ca^{2+} -activated Cl$^-$ channel by different Ca^{2+} signals.* Journal of General Physiology, 2000. **115**(1): p. 59-80.

304. Boton, R., et al., *Two calcium-activated chloride conductances in Xenopus laevis oocytes permeabilized with the ionophore A23187.* J Physiol, 1989. **408**: p. 511-34.

305. Boton, R., D. Singer, and N. Dascal, *Inactivation of calcium-activated chloride conductance in Xenopus oocytes: roles of calcium and protein kinase C.* Pflugers Archiv - European Journal of Physiology, 1990. **416**(1-2): p. 1-6.

306. Hartzell, H.C., *Activation of different Cl currents in Xenopus oocytes by Ca liberated from stores and by capacitative Ca influx.* Journal of General Physiology, 1996. **108**(3): p. 157-175.

307. Namkung, W., P.W. Phuan, and A.S. Verkman, *TMEM16A inhibitors reveal TMEM16A as a minor component of calcium-activated chloride channel conductance in airway and intestinal epithelial cells.* J Biol Chem, 2011. **286**(3): p. 2365-74.

308. De La Fuente, R., et al., *Small-molecule screen identifies inhibitors of a human intestinal calcium-activated chloride channel.* Mol Pharmacol, 2008. **73**(3): p. 758-68.

309. Oh, S.J., et al., *MONNA, a potent and selective blocker for transmembrane protein with unknown function 16/anoctamin-1.* Mol Pharmacol, 2013. **84**(5): p. 726-35.

310. Namkung, W., et al., *Inhibition of Ca2+-activated Cl- channels by gallotannins as a possible molecular basis for health benefits of red wine and green tea.* FASEB J, 2010. **24**(11): p. 4178-86.

311. Liu, Y., et al., *Characterization of the effects of Cl(-) channel modulators on TMEM16A and bestrophin-1 Ca(2)(+) activated Cl(-) channels.* Pflugers Arch, 2015. **467**(7): p. 1417-30.

312. Qu, Z. and H.C. Hartzell, *Functional geometry of the permeation pathway of Ca2+-activated Cl-channels inferred from analysis of voltage-dependent block.* Journal of Biological Chemistry, 2001. **276**(21): p. 18423-18429.

313. Schneider, I., et al., *Limb girdle muscular dystrophy type 2L presenting as necrotizing myopathy.* Acta Myol, 2014. **33**(1): p. 19-21.

314. Bradley, E., et al., *Pharmacological characterization of TMEM16A currents.* Channels (Austin), 2014. **8**(4): p. 308-20.

315. Namkung, W., et al., *Small-molecule activators of TMEM16A, a calcium-activated chloride channel, stimulate epithelial chloride secretion and intestinal contraction.* FASEB J, 2011. **25**: p. 4048-4062.

316. Verstraeten, S.V., C.G. Fraga, and P.I. Oteiza, *Interactions of flavan-3-ols and procyanidins with membranes: mechanisms and the physiological relevance.* Food Funct, 2015. **6**(1): p. 32-41.

317. Furlan, A.L., et al., *Red wine tannins fluidify and precipitate lipid liposomes and bicelles. A role for lipids in wine tasting?* Langmuir, 2014. **30**(19): p. 5518-26.

318. Takahashi, T., E. Neher, and B. Sakmann, *Rat brain serotonin receptors in Xenopus oocytes are coupled by intracellular calcium to endogenous channels.* Proceedings of the National Academy of Sciences of the United States of America, 1987. **84**(14): p. 5063-5067.

319. Davis, A.J., et al., *Potent vasorelaxant activity of the TMEM16A inhibitor T16A(inh) -A01.* Br J Pharmacol, 2012.

320. Burris, S.K., et al., *9-Phenanthrol inhibits recombinant and arterial myocyte TMEM16A channels.* Br J Pharmacol, 2015. **172**(10): p. 2459-68.

321. Yang, Y.D., et al., *TMEM16A confers receptor-activated calcium-dependent chloride conductance.* Nature, 2008. **455**: p. 1210-1215.

322. Taberner, F.J., et al., *TRP channels interaction with lipids and its implications in disease.* Biochim Biophys Acta, 2015. **1848**(9): p. 1818-27.

323. Baenziger, J.E., et al., *Nicotinic acetylcholine receptor-lipid interactions: Mechanistic insight and biological function.* Biochim Biophys Acta, 2015. **1848**(9): p. 1806-17.

324. Hille, B., et al., *Phosphoinositides regulate ion channels.* Biochim Biophys Acta, 2015. **1851**(6): p. 844-56.

325. Levitan, I., D.K. Singh, and A. Rosenhouse-Dantsker, *Cholesterol binding to ion channels.* Front Physiol, 2014. **5**: p. 65.

326. Poveda, J.A., et al., *Lipid modulation of ion channels through specific binding sites.* Biochim Biophys Acta, 2014. **1838**(6): p. 1560-7.

327. Hansen, S.B., *Lipid agonism: The PIP2 paradigm of ligand-gated ion channels.* Biochim Biophys Acta, 2015. **1851**(5): p. 620-8.

328. Anishkin, A., et al., *Feeling the hidden mechanical forces in lipid bilayer is an original sense.* Proc Natl Acad Sci U S A, 2014. **111**(22): p. 7898-905.

329. Mosgaard, L.D. and T. Heimburg, *Lipid ion channels and the role of proteins.* Acc Chem Res, 2013. **46**(12): p. 2966-76.

330. Heimburg, T., *Lipid ion channels.* Biophys Chem, 2010. **150**(1-3): p. 2-22.

331. Gilbert, R.J., et al., *Membrane pore formation at protein-lipid interfaces.* Trends Biochem Sci, 2014. **39**(11): p. 510-6.

332. Metkar, S.S., et al., *Perforin oligomers form arcs in cellular membranes: a locus for intracellular delivery of granzymes.* Cell Death Differ, 2015. **22**(1): p. 74-85.

333. Praper, T., et al., *Human perforin employs different avenues to damage membranes.* J Biol Chem, 2011. **286**(4): p. 2946-55.

334. Prieto, L., Y. He, and T. Lazaridis, *Protein arcs may form stable pores in lipid membranes.* Biophys J, 2014. **106**(1): p. 154-61.

335.   Sonnen, A.F., J.M. Plitzko, and R.J. Gilbert, *Incomplete pneumolysin oligomers form membrane pores.* Open Biol, 2014. **4**: p. 140044.

336.   Rosado, C.J., et al., *The MACPF/CDC family of pore-forming toxins.* Cell Microbiol, 2008. **10**(9): p. 1765-74.

337.   Urrea Moreno, R., et al., *Functional assessment of perforin C2 domain mutations illustrates the critical role for calcium-dependent lipid binding in perforin cytotoxic function.* Blood, 2009. **113**(2): p. 338-46.

338.   Sokolov, Y., et al., *Membrane channel formation by antimicrobial protegrins.* Biochim Biophys Acta, 1999. **1420**(1-2): p. 23-9.

339.   Sobko, A.A., et al., *Lipid dependence of the channel properties of a colicin E1-lipid toroidal pore.* J Biol Chem, 2006. **281**(20): p. 14408-16.

340.   Bullock, J.O., *Ion selectivity of colicin E1: modulation by pH and membrane composition.* J Membr Biol, 1992. **125**(3): p. 255-71.

341.   Anderluh, G., et al., *Pore formation by equinatoxin II, a eukaryotic protein toxin, occurs by induction of nonlamellar lipid structures.* J Biol Chem, 2003. **278**(46): p. 45216-23.

342.   Valcarcel, C.A., et al., *Effects of lipid composition on membrane permeabilization by sticholysin I and II, two cytolysins of the sea anemone Stichodactyla helianthus.* Biophys J, 2001. **80**(6): p. 2761-74.

343.   Metkar, S.S., et al., *Perforin rapidly induces plasma membrane phospholipid flip-flop.* PLoS One, 2011. **6**(9): p. e24286.

344.   Garcia-Saez, A.J., et al., *Peptides corresponding to helices 5 and 6 of Bax can independently form large lipid pores.* FEBS J, 2006. **273**(5): p. 971-81.

345.   Hotop, H. and W.C. Lineberger, *Binding energies in atomic negative ions.* Journal of Physical and Chemical Reference Data, 1975. **4**(3): p. 539-576.

346.   Andersen, T., H.K. Haugen, and H. Hotop, *Binding Energies in Atomic Negative Ions: III.* Journal of Physical and Chemical Reference Data, 1999. **28**(6): p. 1511-1533.

347.   Fadeel, B. and D. Xue, *The ins and outs of phospholipid asymmetry in the plasma membrane: roles in health and disease.* Crit Rev Biochem Mol Biol, 2009. **44**(5): p. 264-77.

348.   Panatala, R., H. Hennrich, and J.C. Holthuis, *Inner workings and biological impact of phospholipid flippases.* J Cell Sci, 2015.

349.   Borst, P., N. Zelcer, and A. van Helvoort, *ABC transporters in lipid transport.* Biochim Biophys Acta, 2000. **1486**(1): p. 128-44.

350.   Suh, B.C. and B. Hille, *PIP2 is a necessary cofactor for ion channel function: how and why?* Annu Rev Biophys, 2008. **37**: p. 175-95.

351.   Fairn, G.D., et al., *Phosphatidylserine is polarized and required for proper Cdc42 localization and for development of cell polarity.* Nat Cell Biol, 2011. **13**(12): p. 1424-30.

352.   Hosseini, A.S., H. Zheng, and J. Gao, *Understanding Lipid Recognition by Protein-Mimicking Cyclic Peptides.* Tetrahedron, 2014. **70**(42): p. 7632-7638.

353.   Graham, T.R. and M.M. Kozlov, *Interplay of proteins and lipids in generating membrane curvature.* Curr Opin Cell Biol, 2010. **22**(4): p. 430-6.

354. Emoto, K., et al., *Exposure of phosphatidylethanolamine on the surface of apoptotic cells.* Exp Cell Res, 1997. **232**(2): p. 430-4.

355. Verhoven, B., R.A. Schlegel, and P. Williamson, *Mechanisms of phosphatidylserine exposure, a phagocyte recognition signal, on apoptotic T lymphocytes.* J Exp Med, 1995. **182**(5): p. 1597-601.

356. Kay, J.G., et al., *Phosphatidylserine dynamics in cellular membranes.* Mol Biol Cell, 2012. **23**(11): p. 2198-212.

357. Zwaal, R.F., P. Comfurius, and E.M. Bevers, *Lipid-protein interactions in blood coagulation.* Biochim Biophys Acta, 1998. **1376**(3): p. 433-53.

358. Harre, U., et al., *Moonlighting osteoclasts as undertakers of apoptotic cells.* Autoimmunity, 2012. **45**(8): p. 612-9.

359. Shin, N.Y., et al., *Dynamin and endocytosis are required for the fusion of osteoclasts and myoblasts.* J Cell Biol, 2014. **207**(1): p. 73-89.

360. Verma, S.K., et al., *Late stages of the synchronized macrophage fusion in osteoclast formation depend on dynamin.* Biochem J, 2014. **464**(3): p. 293-300.

361. Huppertz, B., C. Bartz, and M. Kokozidou, *Trophoblast fusion: fusogenic proteins, syncytins and ADAMs, and other prerequisites for syncytial fusion.* Micron, 2006. **37**(6): p. 509-17.

362. Sanyal, S. and A.K. Menon, *Flipping lipids: why an' what's the reason for?* ACS Chem Biol, 2009. **4**(11): p. 895-909.

363. Schoenwaelder, S.M., et al., *Two distinct pathways regulate platelet phosphatidylserine exposure and procoagulant function.* Blood, 2009. **114**(3): p. 663-6.

364. Basse, F., et al., *Isolation of an erythrocyte membrane protein that mediates Ca2+-dependent transbilayer movement of phospholipid.* J Biol Chem, 1996. **271**(29): p. 17205-10.

365. Comfurius, P., et al., *Reconstitution of phospholipid scramblase activity from human blood platelets.* Biochemistry, 1996. **35**(24): p. 7631-4.

366. Acharya, U., et al., *Drosophila melanogaster Scramblases modulate synaptic transmission.* J Cell Biol, 2006. **173**(1): p. 69-82.

367. Ory, S., et al., *Phospholipid scramblase-1-induced lipid reorganization regulates compensatory endocytosis in neuroendocrine cells.* J Neurosci, 2013. **33**(8): p. 3545-56.

368. Goren, M.A., et al., *Constitutive phospholipid scramblase activity of a G protein-coupled receptor.* Nat Commun, 2014. **5**: p. 5115.

369. Yang, H., et al., *TMEM16F Forms a Ca(2+)-Activated Cation Channel Required for Lipid Scrambling in Platelets during Blood Coagulation.* Cell, 2012. **151**(1): p. 111-22.

370. Schroeder, B.C., et al., *Expression Cloning of TMEM16A as a Calcium-Activated Chloride Channel Subunit.* Cell, 2008. **134**: p. 1019-1029.

371. Caputo, A., et al., *TMEM16A, A Membrane Protein Associated With Calcium-Dependent Chloride Channel Activity.* Science, 2008. **322**: p. 590-594.

372. Yang, H., et al., *Scan: A Novel Small-Conductance Ca2+-Activated Non-Selective Cation Channel Encoded by TMEM16F.* Biophysical Journal, 2011. **100**(3): p. 259a.

373. Shi, J., et al., *Lactadherin detects early phosphatidylserine exposure on immortalized leukemia cells undergoing programmed cell death.* Cytometry A, 2006. **69**(12): p. 1193-201.

374. Hou, J., et al., *Lactadherin functions as a probe for phosphatidylserine exposure and as an anticoagulant in the study of stored platelets.* Vox Sang, 2011. **100**(2): p. 187-95.

375. Kay, J.G. and S. Grinstein, *Sensing phosphatidylserine in cellular membranes.* Sensors (Basel), 2011. **11**(2): p. 1744-55.

376. Tyurin, V.A., et al., *Oxidative lipidomics of programmed cell death.* Methods Enzymol, 2008. **442**: p. 375-93.

377. Harper, M.T. and A.W. Poole, *Chloride channels are necessary for full platelet phosphatidylserine exposure and procoagulant activity.* Cell Death Dis, 2013. **4**: p. e969.

378. Kastl, K., et al., *Kinetics and thermodynamics of annexin A1 binding to solid-supported membranes: a QCM study.* Biochemistry, 2002. **41**(31): p. 10087-94.

379. Gu, X., *A simple statistical method for estimating type-II (cluster-specific) functional divergence of protein sequences.* Mol Biol Evol, 2006. **23**(10): p. 1937-45.

380. Bill, A., et al., *Variomics Screen Identifies the Re-entrant Loop of the Calcium-activated Chloride Channel ANO1 That Facilitates Channel Activation.* J Biol Chem, 2015. **290**(2): p. 889-903.

381. Lopez-Marques, R.L., et al., *P4-ATPases: lipid flippases in cell membranes.* Pflugers Arch, 2014. **466**(7): p. 1227-40.

382. Dawson, D.C., S.S. Smith, and M.K. Mansoura, *CFTR: mechanism of anion conduction.* Physiological Reviews, 1999. **79**(1 Suppl): p. S47-S75.

383. Liu, X., S.S. Smith, and D.C. Dawson, *CFTR: what's it like inside the pore?. [Review] [37 refs].* Journal of Experimental Zoology, 2003. **Part A, Comparative Experimental Biology. 300**(1): p. 69-75.

384. Breen, M.S., et al., *Epistasis as the primary factor in molecular evolution.* Nature, 2012. **490**(7421): p. 535-8.

385. Bridgham, J.T., E.A. Ortlund, and J.W. Thornton, *An epistatic ratchet constrains the direction of glucocorticoid receptor evolution.* Nature, 2009. **461**(7263): p. 515-9.

386. Stefan, C.J., et al., *Osh proteins regulate phosphoinositide metabolism at ER-plasma membrane contact sites.* Cell, 2011. **144**(3): p. 389-401.

387. McWilliam, H., et al., *Analysis Tool Web Services from the EMBL-EBI.* Nucleic Acids Res, 2013. **41**(Web Server issue): p. W597-600.

388. Pont-Kingdon, G., *Creation of chimeric junctions, deletions, and insertions by PCR.* Methods Mol Biol, 1997. **67**: p. 167-72.

389. Barry, P., *The reliability of relative anion-cation permeabilities deduced from reversal (Dilution) potential measurements in ion channel studies.* Cell Biochemistry and Biophysics, 2006. **46**(2): p. 143-154.

390. Gu, X., et al., *An update of DIVERGE software for functional divergence analysis of protein family.* Mol Biol Evol, 2013. **30**(7): p. 1713-9.

391. Adams, P.D., et al., *PHENIX: a comprehensive Python-based system for macromolecular structure solution.* Acta Crystallogr D Biol Crystallogr, 2010. **66**(Pt 2): p. 213-21.

392. Proctor, D.N., et al., *Comparison of techniques to estimate total body skeletal muscle mass in people of different age groups.* Am J Physiol, 1999. **277**(3 Pt 1): p. E489-95.

393. Yang, D., S.F. Morris, and L. Sigurdson, *The sartorius muscle: anatomic considerations for reconstructive surgeons.* Surg Radiol Anat, 1998. **20**(5): p. 307-10.

394. White, R.B., et al., *Dynamics of muscle fibre growth during postnatal mouse development.* BMC Dev Biol, 2010. **10**: p. 21.

395. Spalding, K.L., et al., *Dynamics of hippocampal neurogenesis in adult humans.* Cell, 2013. **153**(6): p. 1219-1227.

396. Calderon, J.C., P. Bolanos, and C. Caputo, *The excitation-contraction coupling mechanism in skeletal muscle.* Biophys Rev, 2014. **6**(1): p. 133-160.

397. Andrews, N.W., P.E. Almeida, and M. Corrotte, *Damage control: cellular mechanisms of plasma membrane repair.* Trends Cell Biol, 2014. **24**(12): p. 734-42.

398. Gozen, I. and P. Dommersnes, *Pore dynamics in lipid membranes.* Eur. Phys. J. Spec. Top., 2014. **223**(9): p. 1813–1829.

399. Cooper, S.T. and P.L. McNeil, *Membrane Repair: Mechanisms and Pathophysiology.* Physiol Rev, 2015. **95**(4): p. 1205-40.

400. Miyake, K. and P.L. McNeil, *Vesicle accumulation and exocytosis at sites of plasma membrane disruption.* J Cell Biol, 1995. **131**(6 Pt 2): p. 1737-45.

401. Bi, G.Q., J.M. Alderton, and R.A. Steinhardt, *Calcium-regulated exocytosis is required for cell membrane resealing.* J Cell Biol, 1995. **131**(6 Pt 2): p. 1747-58.

402. Terasaki, M., K. Miyake, and P.L. McNeil, *Large plasma membrane disruptions are rapidly resealed by Ca2+-dependent vesicle-vesicle fusion events.* J Cell Biol, 1997. **139**(1): p. 63-74.

403. Togo, T., et al., *The mechanism of facilitated cell membrane resealing.* J Cell Sci, 1999. **112 (Pt 5)**: p. 719-31.

404. Reddy, A., E.V. Caler, and N.W. Andrews, *Plasma membrane repair is mediated by Ca(2+)-regulated exocytosis of lysosomes.* Cell, 2001. **106**(2): p. 157-69.

405. Detrait, E., et al., *Axolemmal repair requires proteins that mediate synaptic vesicle fusion.* J Neurobiol, 2000. **44**(4): p. 382-91.

406. Chakrabarti, S., et al., *Impaired membrane resealing and autoimmune myositis in synaptotagmin VII-deficient mice.* J Cell Biol, 2003. **162**(4): p. 543-9.

407. McNeil, P.L. and R.A. Steinhardt, *Loss, restoration, and maintenance of plasma membrane integrity.* J Cell Biol, 1997. **137**(1): p. 1-4.

408. McNeil, P.L. and R. Khakee, *Disruptions of muscle fiber plasma membranes. Role in exercise-induced damage.* Am J Pathol, 1992. **140**(5): p. 1097-109.

409. Corbalan-Garcia, S. and J.C. Gomez-Fernandez, *Signaling through C2 domains: more than one lipid target.* Biochim Biophys Acta, 2014. **1838**(6): p. 1536-47.

410. Johnson, C.P. and E.R. Chapman, *Otoferlin is a calcium sensor that directly regulates SNARE-mediated membrane fusion.* J Cell Biol, 2010. **191**(1): p. 187-97.

411. Cai, C., et al., *MG53 nucleates assembly of cell membrane repair machinery.* Nat Cell Biol, 2009. **11**(1): p. 56-64.

412. Cai, C., et al., *Zinc Binding to MG53 Protein Facilitates Repair of Injury to Cell Membranes.* J Biol Chem, 2015. **290**(22): p. 13830-9.

413. Defour, A., et al., *Annexin A2 links poor myofiber repair with inflammation and adipogenic replacement of the injured muscle.* Hum Mol Genet, 2017. **26**(11): p. 1979-1991.

414. Mauro, A., *Satellite cell of skeletal muscle fibers.* J Biophys Biochem Cytol, 1961. **9**: p. 493-5.

415. Sambasivan, R., et al., *Pax7-expressing satellite cells are indispensable for adult skeletal muscle regeneration.* Development, 2011. **138**(17): p. 3647-56.

416. Lepper, C., T.A. Partridge, and C.M. Fan, *An absolute requirement for Pax7-positive satellite cells in acute injury-induced skeletal muscle regeneration.* Development, 2011. **138**(17): p. 3639-46.

417. Snow, M.H., *Myogenic cell formation in regenerating rat skeletal muscle injured by mincing. II. An autoradiographic study.* Anat Rec, 1977. **188**(2): p. 201-17.

418. Reznik, M., *Thymidine-3H uptake by satellite cells of regenerating skeletal muscle.* J Cell Biol, 1969. **40**(2): p. 568-71.

419. Allen, R.E. and L.K. Boxhorn, *Regulation of skeletal muscle satellite cell proliferation and differentiation by transforming growth factor-beta, insulin-like growth factor I, and fibroblast growth factor.* J Cell Physiol, 1989. **138**(2): p. 311-5.

420. Gurevich, D.B., et al., *Asymmetric division of clonal muscle stem cells coordinates muscle regeneration in vivo.* Science, 2016. **353**(6295): p. aad9969.

421. Collins, C.A., et al., *Stem cell function, self-renewal, and behavioral heterogeneity of cells from the adult muscle satellite cell niche.* Cell, 2005. **122**(2): p. 289-301.

422. Rosenblatt, J.D., et al., *Culturing satellite cells from living single muscle fiber explants.* In Vitro Cell Dev Biol Anim, 1995. **31**(10): p. 773-9.

423. Corona, B.T., et al., *Autologous minced muscle grafts: a tissue engineering therapy for the volumetric loss of skeletal muscle.* Am J Physiol Cell Physiol, 2013. **305**(7): p. C761-75.

424. Gros, J., et al., *A common somitic origin for embryonic muscle progenitors and satellite cells.* Nature, 2005. **435**(7044): p. 954-8.

425. Tajbakhsh, S., et al., *Redefining the genetic hierarchies controlling skeletal myogenesis: Pax-3 and Myf-5 act upstream of MyoD.* Cell, 1997. **89**(1): p. 127-38.

426. Bober, E., et al., *Pax-3 is required for the development of limb muscles: a possible role for the migration of dermomyotomal muscle progenitor cells.* Development, 1994. **120**(3): p. 603-12.

427. Dumont, N.A., et al., *Satellite Cells and Skeletal Muscle Regeneration.* Compr Physiol, 2015. **5**(3): p. 1027-59.

428. Cheung, T.H. and T.A. Rando, *Molecular regulation of stem cell quiescence.* Nat Rev Mol Cell Biol, 2013. **14**(6): p. 329-40.

429. Mansouri, A., et al., *Dysgenesis of cephalic neural crest derivatives in Pax7-/-mutant mice.* Development, 1996. **122**(3): p. 831-8.

430. Anderson, J.E., *A role for nitric oxide in muscle repair: nitric oxide-mediated activation of muscle satellite cells.* Mol Biol Cell, 2000. **11**(5): p. 1859-74.

431. Tatsumi, R., *Mechano-biology of skeletal muscle hypertrophy and regeneration: possible mechanism of stretch-induced activation of resident myogenic stem cells.* Anim Sci J, 2010. **81**(1): p. 11-20.

432. Liu, Y. and M.F. Schneider, *FGF2 activates TRPC and Ca(2+) signaling leading to satellite cell activation.* Front Physiol, 2014. **5**: p. 38.

433. Tatsumi, R., et al., *HGF/SF is present in normal adult skeletal muscle and is capable of activating satellite cells.* Dev Biol, 1998. **194**(1): p. 114-28.

434. Allen, R.E., et al., *Hepatocyte growth factor activates quiescent skeletal muscle satellite cells in vitro.* J Cell Physiol, 1995. **165**(2): p. 307-12.

435. Bischoff, R., *Chemotaxis of skeletal muscle satellite cells.* Dev Dyn, 1997. **208**(4): p. 505-15.

436. Siegel, A.L., et al., *3D timelapse analysis of muscle satellite cell motility.* Stem Cells, 2009. **27**(10): p. 2527-38.

437. Neuhaus, P., et al., *Reduced mobility of fibroblast growth factor (FGF)-deficient myoblasts might contribute to dystrophic changes in the musculature of FGF2/FGF6/mdx triple-mutant mice.* Mol Cell Biol, 2003. **23**(17): p. 6037-48.

438. Kuang, S., et al., *Asymmetric self-renewal and commitment of satellite stem cells in muscle.* Cell, 2007. **129**(5): p. 999-1010.

439. Zammit, P.S., et al., *Muscle satellite cells adopt divergent fates: a mechanism for self-renewal?* J Cell Biol, 2004. **166**(3): p. 347-57.

440. Shea, K.L., et al., *Sprouty1 regulates reversible quiescence of a self-renewing adult muscle stem cell pool during regeneration.* Cell Stem Cell, 2010. **6**(2): p. 117-29.

441. Wang, X., et al., *Effects of interleukin-6, leukemia inhibitory factor, and ciliary neurotrophic factor on the proliferation and differentiation of adult human myoblasts.* Cell Mol Neurobiol, 2008. **28**(1): p. 113-24.

442. Cantini, M., et al., *Human satellite cell proliferation in vitro is regulated by autocrine secretion of IL-6 stimulated by a soluble factor(s) released by activated monocytes.* Biochem Biophys Res Commun, 1995. **216**(1): p. 49-53.

443. Hollenberg, S.M., P.F. Cheng, and H. Weintraub, *Use of a conditional MyoD transcription factor in studies of MyoD trans-activation and muscle determination.* Proc Natl Acad Sci U S A, 1993. **90**(17): p. 8028-32.

444. Halevy, O., et al., *Correlation of terminal cell cycle arrest of skeletal muscle with induction of p21 by MyoD.* Science, 1995. **267**(5200): p. 1018-21.

445. Millay, D.P., et al., *Myomaker is a membrane activator of myoblast fusion and muscle formation.* Nature, 2013. **499**(7458): p. 301-5.

446. Davie, J.K., et al., *Target gene selectivity of the myogenic basic helix-loop-helix transcription factor myogenin in embryonic muscle.* Dev Biol, 2007. **311**(2): p. 650-64.

447. Rochlin, K., et al., *Myoblast fusion: when it takes more to make one.* Dev Biol, 2010. **341**(1): p. 66-83.

448. Schwander, M., et al., *Beta1 integrins regulate myoblast fusion and sarcomere assembly.* Dev Cell, 2003. **4**(5): p. 673-85.

449. Lafuste, P., et al., *ADAM12 and alpha9beta1 integrin are instrumental in human myogenic cell differentiation.* Mol Biol Cell, 2005. **16**(2): p. 861-70.

450. Zeschnigk, M., et al., *Involvement of M-cadherin in terminal differentiation of skeletal muscle cells.* J Cell Sci, 1995. **108 (Pt 9)**: p. 2973-81.

451. Hollnagel, A., et al., *The cell adhesion molecule M-cadherin is not essential for muscle development and regeneration.* Mol Cell Biol, 2002. **22**(13): p. 4760-70.

452. Zaitseva, E., et al., *Fusion Stage of HIV-1 Entry Depends on Virus-Induced Cell Surface Exposure of Phosphatidylserine.* Cell Host Microbe, 2017. **22**(1): p. 99-110 e7.

453. Verma, S.K., et al., *Cell-surface phosphatidylserine regulates osteoclast precursor fusion.* J Biol Chem, 2018. **293**(1): p. 254-270.

454. Park, S.Y., et al., *Stabilin-2 modulates the efficiency of myoblast fusion during myogenic differentiation and muscle regeneration.* Nat Commun, 2016. **7**: p. 10871.

455. Park, D., et al., *BAI1 is an engulfment receptor for apoptotic cells upstream of the ELMO/Dock180/Rac module.* Nature, 2007. **450**(7168): p. 430-4.

456. Vasyutina, E., et al., *The small G-proteins Rac1 and Cdc42 are essential for myoblast fusion in the mouse.* Proc Natl Acad Sci U S A, 2009. **106**(22): p. 8935-40.

457. Moore, C.A., et al., *A role for the Myoblast city homologues Dock1 and Dock5 and the adaptor proteins Crk and Crk-like in zebrafish myoblast fusion.* Development, 2007. **134**(17): p. 3145-53.

458. Laurin, M., et al., *The atypical Rac activator Dock180 (Dock1) regulates myoblast fusion in vivo.* Proc Natl Acad Sci U S A, 2008. **105**(40): p. 15446-51.

459. Geisbrecht, E.R., et al., *Drosophila ELMO/CED-12 interacts with Myoblast city to direct myoblast fusion and ommatidial organization.* Dev Biol, 2008. **314**(1): p. 137-49.

460. Murray, T.V., et al., *A non-apoptotic role for caspase-9 in muscle differentiation.* J Cell Sci, 2008. **121**(Pt 22): p. 3786-93.

461. Fernando, P., et al., *Caspase 3 activity is required for skeletal muscle differentiation.* Proc Natl Acad Sci U S A, 2002. **99**(17): p. 11025-30.

462. Boonstra, K., D. Bloemberg, and J. Quadrilatero, *Caspase-2 is required for skeletal muscle differentiation and myogenesis.* Biochim Biophys Acta, 2018. **1865**(1): p. 95-104.

463. Ornatsky, O.I., et al., *Post-translational control of the MEF2A transcriptional regulatory protein.* Nucleic Acids Res, 1999. **27**(13): p. 2646-54.

464. Lechner, C., et al., *ERK6, a mitogen-activated protein kinase involved in C2C12 myoblast differentiation.* Proc Natl Acad Sci U S A, 1996. **93**(9): p. 4355-9.

465. Stadler, B., T.M. Blattler, and A. Franco-Obregon, *Time-lapse imaging of in vitro myogenesis using atomic force microscopy.* J Microsc, 2010. **237**(1): p. 63-9.

466. Segal, D., et al., *Adhesion and Fusion of Muscle Cells Are Promoted by Filopodia.* Dev Cell, 2016. **38**(3): p. 291-304.

467. Mukai, A., et al., *Dynamic clustering and dispersion of lipid rafts contribute to fusion competence of myogenic cells.* Exp Cell Res, 2009. **315**(17): p. 3052-63.

468. Abramovici, H. and S.H. Gee, *Morphological changes and spatial regulation of diacylglycerol kinase-zeta, syntrophins, and Rac1 during myoblast fusion.* Cell Motil Cytoskeleton, 2007. **64**(7): p. 549-67.

469. Yoon, S., et al., *C6ORF32 is upregulated during muscle cell differentiation and induces the formation of cellular filopodia.* Dev Biol, 2007. **301**(1): p. 70-81.

470. Murphy, D.A. and S.A. Courtneidge, *The 'ins' and 'outs' of podosomes and invadopodia: characteristics, formation and function.* Nat Rev Mol Cell Biol, 2011. **12**(7): p. 413-26.

471. van Niel, G., G. D'Angelo, and G. Raposo, *Shedding light on the cell biology of extracellular vesicles.* Nat Rev Mol Cell Biol, 2018. **19**(4): p. 213-228.

472. Whitham, M., et al., *Extracellular Vesicles Provide a Means for Tissue Crosstalk during Exercise.* Cell Metab, 2018. **27**(1): p. 237-251 e4.

473. Murphy, C., et al., *Emerging role of extracellular vesicles in musculoskeletal diseases.* Mol Aspects Med, 2018. **60**: p. 123-128.

474. De Gasperi, R., et al., *Denervation-related alterations and biological activity of miRNAs contained in exosomes released by skeletal muscle fibers.* Sci Rep, 2017. **7**(1): p. 12888.

475. Madison, R.D., et al., *Extracellular vesicles from a muscle cell line (C2C12) enhance cell survival and neurite outgrowth of a motor neuron cell line (NSC-34).* J Extracell Vesicles, 2014. **3**.

476. Lewis, W.H. and M.R. Lewis, *Behavior of cross striated muscle in tissue cultures.* American Journal of Anatomy, 1917. **22**(2): p. 169-194.

477. Armand, O., et al., *Origin of Satellite Cells in Avian Skeletal-Muscles.* Archives D Anatomie Microscopique Et De Morphologie Experimentale, 1983. **72**(2): p. 163-181.

478. Gieseler, K., H. Qadota, and G.M. Benian, *Development, structure, and maintenance of C. elegans body wall muscle.* WormBook, 2017. **2017**: p. 1-59.

479. Ono, S., *Regulation of structure and function of sarcomeric actin filaments in striated muscle of the nematode Caenorhabditis elegans.* Anat Rec (Hoboken), 2014. **297**(9): p. 1548-59.

480. Baugh, L.R. and C.P. Hunter, *MyoD, modularity, and myogenesis: conservation of regulators and redundancy in C. elegans.* Genes Dev, 2006. **20**(24): p. 3342-6.

481. Bischoff, R., *Regeneration of single skeletal muscle fibers in vitro.* Anat Rec, 1975. **182**(2): p. 215-35.

482. Mitchell, P.O. and G.K. Pavlath, *Skeletal muscle atrophy leads to loss and dysfunction of muscle precursor cells.* Am J Physiol Cell Physiol, 2004. **287**(6): p. C1753-62.

483. Yaffe, D. and O. Saxel, *Serial passaging and differentiation of myogenic cells isolated from dystrophic mouse muscle.* Nature, 1977. **270**(5639): p. 725-7.

484. Hwang, W.Y., et al., *Efficient genome editing in zebrafish using a CRISPR-Cas system.* Nat Biotechnol, 2013. **31**(3): p. 227-9.

485. Burger, A., et al., *Maximizing mutagenesis with solubilized CRISPR-Cas9 ribonucleoprotein complexes.* Development, 2016. **143**(11): p. 2025-37.

486. Guiraud, S., et al., *The Pathogenesis and Therapy of Muscular Dystrophies.* Annu Rev Genomics Hum Genet, 2015. **16**: p. 281-308.

487. Constantin, B., *Dystrophin complex functions as a scaffold for signaling proteins.* Biochim Biophys Acta, 2014. **1838**(2): p. 635-42.

488. Lapidos, K.A., R. Kakkar, and E.M. McNally, *The dystrophin glycoprotein complex: signaling strength and integrity for the sarcolemma.* Circ Res, 2004. **94**(8): p. 1023-31.

489. Cooper, S.T. and S.I. Head, *Membrane Injury and Repair in the Muscular Dystrophies.* Neuroscientist, 2015. **21**(6): p. 653-68.

490. McNeil, P.L. and M.M. Baker, *Cell surface events during resealing visualized by scanning-electron microscopy.* Cell Tissue Res, 2001. **304**(1): p. 141-6.

491. Han, R. and K.P. Campbell, *Dysferlin and muscle membrane repair.* Curr Opin Cell Biol, 2007. **19**(4): p. 409-16.

492. Bouquet, F., et al., *Miyoshi-like distal myopathy with mutations in anoctamin 5 gene.* Rev Neurol (Paris), 2012. **168**(2): p. 135-41.

493. Penttila, S., et al., *Eight new mutations and the expanding phenotype variability in muscular dystrophy caused by ANO5.* Neurology, 2012. **78**(12): p. 897-903.

494. Yu, K., et al., *Identification of a lipid scrambling domain in ANO6/TMEM16F.* Elife, 2015. **4**.

495. Tran, T.T., et al., *TMEM16E (GDD1) exhibits protein instability and distinct characteristics in chloride channel/pore forming ability.* J Cell Physiol, 2014. **229**(2): p. 181-90.

496. Testa, G., et al., *A reliable lacZ expression reporter cassette for multipurpose, knockout-first alleles.* Genesis, 2004. **38**(3): p. 151-8.

497. Skarnes, W.C., et al., *A conditional knockout resource for the genome-wide study of mouse gene function.* Nature, 2011. **474**(7351): p. 337-42.

498. Zhao, P., et al., *Anoctamin 6 regulates C2C12 myoblast proliferation.* PLoS One, 2014. **9**(3): p. e92749.

499. Liewluck, T., et al., *ANO5-muscular dystrophy: clinical, pathological and molecular findings.* Eur J Neurol, 2013. **20**(10): p. 1383-9.

500. Milone, M., et al., *Amyloidosis and exercise intolerance in ANO5 muscular dystrophy.* Neuromuscul Disord, 2012. **22**(1): p. 13-5.

501. Pavlovicova, M., M. Novotova, and I. Zahradnik, *Structure and composition of tubular aggregates of skeletal muscle fibres.* Gen Physiol Biophys, 2003. **22**(4): p. 425-40.

502. Agbulut, O., et al., *Age-related appearance of tubular aggregates in the skeletal muscle of almost all male inbred mice.* Histochem Cell Biol, 2000. **114**(6): p. 477-81.

503. Sondergaard, P.C., et al., *AAV.Dysferlin Overlap Vectors Restore Function in Dysferlinopathy Animal Models.* Ann Clin Transl Neurol, 2015. **2**(3): p. 256-70.

297

504.   Harris, J.B., *Myotoxic phospholipases A2 and the regeneration of skeletal muscles.* Toxicon, 2003. **42**(8): p. 933-45.

505.   Endo, Y., et al., *Dominant mutations in ORAI1 cause tubular aggregate myopathy with hypocalcemia via constitutive activation of store-operated Ca(2)(+) channels.* Hum Mol Genet, 2015. **24**(3): p. 637-48.

506.   Bohm, J., et al., *Constitutive activation of the calcium sensor STIM1 causes tubular-aggregate myopathy.* Am J Hum Genet, 2013. **92**(2): p. 271-8.

507.   Krahn, M., et al., *A naturally occurring human minidysferlin protein repairs sarcolemmal lesions in a mouse model of dysferlinopathy.* Sci Transl Med, 2010. **2**(50): p. 50ra69.

508.   Gyobu, S., et al., *A role of TMEM16E carrying a scrambling domain in sperm motility.* Mol Cell Biol, 2015.

509.   Rabinowitz, J.E., et al., *Cross-packaging of a single adeno-associated virus (AAV) type 2 vector genome into multiple AAV serotypes enables transduction with broad specificity.* J Virol, 2002. **76**(2): p. 791-801.

510.   Clark, K.R., et al., *Highly purified recombinant adeno-associated virus vectors are biologically active and free of detectable helper and wild-type viruses.* Hum Gene Ther, 1999. **10**(6): p. 1031-9.

511.   Rodino-Klapac, L.R., et al., *A translational approach for limb vascular delivery of the micro-dystrophin gene without high volume or high pressure for treatment of Duchenne muscular dystrophy.* J Transl Med, 2007. **5**: p. 45.

512.   Liu, M., et al., *Adeno-associated virus-mediated microdystrophin expression protects young mdx muscle from contraction-induced injury.* Mol Ther, 2005. **11**(2): p. 245-56.

513.   Hakim, C.H., R.W. Grange, and D. Duan, *The passive mechanical properties of the extensor digitorum longus muscle are compromised in 2- to 20-mo-old mdx mice.* J Appl Physiol (1985), 2011. **110**(6): p. 1656-63.

514.   Wein, N., et al., *Translation from a DMD exon 5 IRES results in a functional dystrophin isoform that attenuates dystrophinopathy in humans and mice.* Nat Med, 2014. **20**(9): p. 992-1000.

515.   Beastrom, N., et al., *mdx((5)cv) mice manifest more severe muscle dysfunction and diaphragm force deficits than do mdx Mice.* Am J Pathol, 2011. **179**(5): p. 2464-74.

516.   Rafael-Fortney, J.A., et al., *Early treatment with lisinopril and spironolactone preserves cardiac and skeletal muscle in Duchenne muscular dystrophy mice.* Circulation, 2011. **124**(5): p. 582-8.

517.   Grose, W.E., et al., *Homologous recombination mediates functional recovery of dysferlin deficiency following AAV5 gene transfer.* PLoS One, 2012. **7**(6): p. e39233.

518.   Arnold, W.D., et al., *Electrophysiological Biomarkers in Spinal Muscular Atrophy: Preclinical Proof of Concept.* Ann Clin Transl Neurol, 2014. **1**(1): p. 34-44.

519.   Li, J., M. Sung, and S.B. Rutkove, *Electrophysiologic Biomarkers for Assessing Disease Progression and the Effect of Riluzole in SOD1 G93A ALS Mice.* PLoS ONE, 2013. **8**(6): p. e65976.

520. Li, J., et al., *Electrical impedance myography for the in vivo and ex vivo assessment of muscular dystrophy (mdx) mouse muscle.* Muscle Nerve, 2014. **49**(6): p. 829-35.

521. Bondesen, B.A., et al., *The COX-2 pathway is essential during early stages of skeletal muscle regeneration.* American Journal of Physiology-Cell Physiology, 2004. **287**(2): p. C475-C483.

522. Mitchell, P.O. and G.K. Pavlath, *A muscle precursor cell-dependent pathway contributes to muscle growth after atrophy.* Am J Physiol Cell Physiol, 2001. **281**(5): p. C1706-15.

523. Rando, T.A. and H.M. Blau, *Primary mouse myoblast purification, characterization, and transplantation for cell-mediated gene therapy.* J Cell Biol, 1994. **125**(6): p. 1275-87.

524. Aartsma-Rus, A., et al., *Entries in the Leiden Duchenne muscular dystrophy mutation database: an overview of mutation types and paradoxical cases that confirm the reading-frame rule.* Muscle Nerve, 2006. **34**(2): p. 135-44.

525. Joshi, P.R., et al., *Anoctamin 5 muscular dystrophy associated with a silent p.Leu115Leu mutation resulting in exon skipping.* Neuromuscul Disord, 2014. **24**(1): p. 43-7.

526. Lahoria, R., et al., *Novel ANO5 homozygous microdeletion causing myalgia and unprovoked rhabdomyolysis in an Arabic man.* Muscle Nerve, 2014. **50**(4): p. 610-3.

527. Neusch, C., et al., *Late-onset myopathy of the posterior calf muscles mimicking Miyoshi myopathy unrelated to dysferlin mutation: a case report.* J Med Case Rep, 2012. **6**: p. 345.

528. Penisson-Besnier, I., et al., *Myopathy caused by anoctamin 5 mutations and necrotizing vasculitis.* J Neurol, 2012. **259**(9): p. 1988-90.

529. Wahbi, K., et al., *Dilated cardiomyopathy in patients with mutations in anoctamin 5.* Int J Cardiol, 2013. **168**(1): p. 76-9.

530. Witting, N., et al., *Anoctamin 5 muscular dystrophy in Denmark: prevalence, genotypes, phenotypes, cardiac findings, and muscle protein expression.* J Neurol, 2013. **260**(8): p. 2084-93.

531. Liewluck, T. and M. Milone, *Untangling the complexity of limb-girdle muscular dystrophies.* Muscle Nerve, 2018.

532. Hicks, D., et al., *A founder mutation in Anoctamin 5 is a major cause of limb-girdle muscular dystrophy.* Brain, 2011. **134**(Pt 1): p. 171-182.

533. Endo, T., *Glycobiology of alpha-dystroglycan and muscular dystrophy.* J Biochem, 2015. **157**(1): p. 1-12.

534. Corrotte, M., et al., *Caveolae internalization repairs wounded cells and muscle fibers.* Elife, 2013. **2**: p. e00926.

535. Bansal, D. and K.P. Campbell, *Dysferlin and the plasma membrane repair in muscular dystrophy.* Trends Cell Biol, 2004. **14**(4): p. 206-13.

536. Gyobu, S., et al., *A Role of TMEM16E Carrying a Scrambling Domain in Sperm Motility.* Mol Cell Biol, 2015. **36**(4): p. 645-59.

537.   Di Zanni, E., et al., *Gain of function of TMEM16E/ANO5 scrambling activity caused by a mutation associated with gnathodiaphyseal dysplasia.* Cell Mol Life Sci, 2017.

538.   Brunner, J.D., S. Schenck, and R. Dutzler, *Structural basis for phospholipid scrambling in the TMEM16 family.* Curr Opin Struct Biol, 2016. **39**: p. 61-70.

539.   van den Eijnde, S.M., et al., *In situ detection of apoptosis during embryogenesis with annexin V: from whole mount to ultrastructure.* Cytometry, 1997. **29**(4): p. 313-20.

540.   Kim, G.W., S.Y. Park, and I.S. Kim, *Novel function of stabilin-2 in myoblast fusion: the recognition of extracellular phosphatidylserine as a "fuse-me" signal.* BMB Rep, 2016. **49**(6): p. 303-4.

541.   Whitlock, J.M., et al., *The role of TMEM16E/Anoctamin 5 in muscular dystrophy and phospholipid scramlbing* Journal of General Physiology, 2015. **146**(3): p. 16A-16A.

542.   Whitlock, J.M., et al., *Limb-girldle muscular dystrophy 2L is associated with a defect in phospholipid scrambling mediated by ANO5.* Molecular Biology of the Cell, 2016. **27**.

543.   Whitlock, J.M., et al., *Limb-girdle muscular dystrophy 2L is caused by a defect in phospholipid scramling mediated by ANO5.* Journal of General Physiology, 2016. **148**(2): p. 35A-35A.

544.   Whitlock, J.M. and H.C. Hartzell, *A Pore Idea: the ion conduction pathway of TMEM16/ANO proteins is composed partly of lipid.* Pflugers Arch, 2016. **468**(3): p. 455-73.

545.   Barry, P.H., *The reliability of relative anion-cation permeabilities deduced from reversal (dilution) potential measurements in ion channel studies.* Cell Biochem Biophys, 2006. **46**(2): p. 143-54.

546.   Jackson, M.F., et al., *Genetic manipulation of myoblasts and a novel primary myosatellite cell culture system: comparing and optimizing approaches.* FEBS J, 2013. **280**(3): p. 827-39.

547.   Brooks, A.R., et al., *Transcriptional silencing is associated with extensive methylation of the CMV promoter following adenoviral gene delivery to muscle.* J Gene Med, 2004. **6**(4): p. 395-404.

548.   Chen, E.H. and E.N. Olson, *Towards a molecular pathway for myoblast fusion in Drosophila.* Trends Cell Biol, 2004. **14**(8): p. 452-60.

549.   Guescini, M., et al., *Extracellular Vesicles Released by Oxidatively Injured or Intact C2C12 Myotubes Promote Distinct Responses Converging toward Myogenesis.* Int J Mol Sci, 2017. **18**(11).

550.   Demonbreun, A.R. and E.M. McNally, *Muscle cell communication in development and repair.* Curr Opin Pharmacol, 2017. **34**: p. 7-14.

551.   Sui, T., et al., *Development of muscular dystrophy in a CRISPR-engineered mutant rabbit model with frame-disrupting ANO5 mutations.* Cell Death Dis, 2018. **9**(6): p. 609.

552.	Livak, K.J. and T.D. Schmittgen, *Analysis of relative gene expression data using real-time quantitative PCR and the 2(-Delta Delta C(T)) Method.* Methods, 2001. **25**(4): p. 402-8.

553.	Sancak, Y., et al., *The Rag GTPases bind raptor and mediate amino acid signaling to mTORC1.* Science, 2008. **320**(5882): p. 1496-501.

554.	Sarbassov, D.D., et al., *Phosphorylation and regulation of Akt/PKB by the rictor-mTOR complex.* Science, 2005. **307**(5712): p. 1098-101.

555.	Gyobu, S., et al., *Characterization of the scrambling domain of the TMEM16 family.* Proc Natl Acad Sci U S A, 2017. **114**(24): p. 6274-6279.